

AD-A090 838

MOORE SCHOOL OF ELECTRICAL ENGINEERING PHILADELPHIA PA  
SUPER-RESOLUTION IMAGERY BY FREQUENCY SWEEPING.(U)

F/G 17/9

AUG 80 N H FARHAT, C WERNER

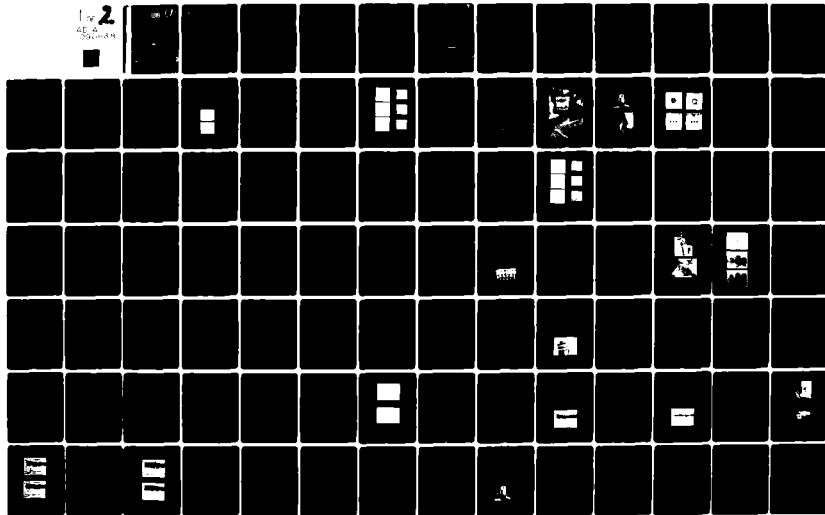
AFOSR-77-3256

UNCLASSIFIED

AFOSR-TR-80-1068

NL

For 2  
AD-A090 838

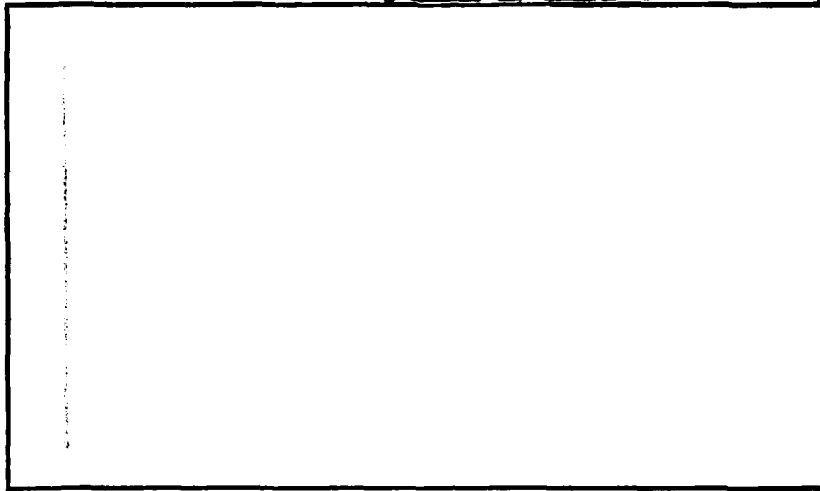


AFOSR-TR- 80 - 1068

LEVEL II

9

AD A090838



DDC FILE COPY

UNIVERSITY of PENNSYLVANIA  
*The Moore School of Electrical Engineering*  
PHILADELPHIA, PENNSYLVANIA 19104

DTIC  
ELECTE  
OCT 23 1980  
S D D

Approved for public release;  
distribution unlimited.

80 10 21 054

UNCLASSIFIED

(12) 1791

SECURITY CLASSIFICATION OF THIS PAGE (When Data Entered)

1. REPORT DOCUMENTATION PAGE		READ INSTRUCTIONS BEFORE COMPLETING FORM	
AFOSR-TR-80-1068		2. GOVT ACCESSION NO.	3. RECIPIENT'S CATALOG NUMBER
AD-A090838			5-22277
4. TITLE (and Subtitle)		5. TYPE OF REPORT & PERIOD COVERED	
6 Super-Resolution Imagery by Frequency Sweeping		9 FINAL rept.	
7. AUTHOR(s)		8. CONTRACT OR GRANT NUMBER(s)	
10 N.H. Farhat C./Werner		15 AFOSR-77-3256	
9. PERFORMING ORGANIZATION NAME AND ADDRESS		10. PROGRAM ELEMENT, PROJECT, TASK AREA & WORK UNIT NUMBERS	
University of Pennsylvania The Moore School of Electrical Engineering 200 S. 33rd St., Phila., Pa. 19104		16 61102F 2305 B1	
11. CONTROLLING OFFICE NAME AND ADDRESS		12. REPORT DATE	
United States Air Force Air Force Office of Scientific Research Bldg. 410, Bolling AFB, D.C. 20332		15 August 1980	
13. MONITORING AGENCY NAME & ADDRESS (if different from Controlling Office)		14. NUMBER OF PAGES	
Office of Research Administration 3451 Walnut St. Phila., Pa. 19104		76	
17 B1		15. SECURITY CLASS. (of this report)	
		UNCLASSIFIED	
		15a. DECLASSIFICATION/DOWNGRADING SCHEDULE	

DISTRIBUTION STATEMENT (of this Report)

Approved for public release;  
distribution unlimited.

DISTRIBUTION STATEMENT (of the abstract entered in Block 20, if different from Report)

SUPPLEMENTARY NOTES

KEY WORDS (Continue on reverse side if necessary and identify by block number)

Microwave 3-D imaging, frequency diversity, holography, inverse scattering, aperture synthesis, Fourier domain projection, target derived reference, network analysis, radar cross-section, projection hologram, tomographic radar.

ABSTRACT (Continue on reverse side if necessary and identify by block number)

A longstanding problem in radar and electromagnetic scattering measurements is the reconstruction of object shape and detail, i.e. an image, from far field scatter data to be used in object identification and classification. During the period covered by this report we have been able to demonstrate in a feasibility study the first reconstruction of a 3-D image of a perfectly reflecting object from its wave-vector diversity (multifrequency and multi-aspect) scatter data making use of a new Weighted Fourier Domain Projection

UNCLASSIFIED

SECURITY CLASSIFICATION OF THIS PAGE (When Data Entered)

Theorem (WFDPT) and establish a relationship between holography with wavelength diversity and inverse scattering. Coherent wave vector diversity radar techniques are used to access a finite volume of the 3-D Fourier space (also known as reciprocal space or  $\bar{p}$ -space) of the scattering object. The WFDPT permits the use of hybrid (digital/optical) computing that enables the retrieval and display of 3-D image information in parallel slices or cross-sectional outlines. The major attributes of this approach as compared to totally digital computing are its potential for displaying a true 3-D image in real-time. Wave-vector diversity methods appear suitable for the imaging of two classes of practical objects namely non-dispersive perfectly reflecting objects of the type often encountered in radar (and sonar) and semitransparent weakly scattering objects such as certain ultrasound and light scattering objects encountered in biology and medicine. The method has several unique characteristics. It furnishes true super-resolution, i.e. resolution exceeding the classical Rayleigh Limit of the available recording aperture, in this case a highly thinned (widely dispersed) broad-band coherent receiver array. True super-resolution is achieved because of an inherent aperture synthesis due to frequency diversity (frequency scanning, stepping or comb illumination) and conversion of spectral degrees of freedom into spatial image detail. Accordingly, when applied to the imaging of a dispersive object, a *target signature* rather than a geometrical image should be expected. Such a target signature could still be useful in object identification and classification since it contains information pertaining to the material composition of the object intermixed with geometrical image detail. The use of frequency diversity was found to lead to a unipolar impulse response. This is very useful in suppressing coherent noise (speckle) which is known to be the major drawback of coherent imaging.

Preliminary work on 3-D image display has yielded encouraging results on 3-D display from a series of weighted projection holograms of various slices of a test object. The projection holograms were viewed in rapid succession using the virtual Fourier transform.

To identify optimal and practical approaches to wave-vector diversity data acquisition a unique microwave measurement system has been assembled, installed and tested in our anechoic chamber facility. The system was used also in the study of TDR (target derived reference) methods in which a reference for phase measurement can be furnished by the scattering object eliminating thus the need for costly local oscillator distribution networks and eliminating at the same time undesirable range phase ambiguities from the collected data. The measurement facility is computer aided furnishing thereby semi-automatic control of object positioning or orientation, frequency stepping, data acquisition and storage, and final data correction and analysis. A high resolution CRT display enables the display of *weighted projection holograms* computed from the  $\bar{p}$ -space data making use of the WFDPT. Preliminary results of this measurement system capabilities included in this report confirm its tremendous versatility. At this stage, the program strongly suggests the practical feasibility of a new generation of cost effective, real-time, super-resolving 3-D imaging radars that can because of their 3-D image slicing characteristic be appropriately referred to as *Tomographic Radars* (Tomos=slice in Greek).

Finally, a study of 3-D imaging using other forms of broadband radiation such as impulsive, random noise and particularly thermal emission for passive 3-D wavelength diversity imaging has been also initiated.

UNCLASSIFIED

The findings in this report are those of the authors and are not to be interpreted as the official position of the Air Force Office of Scientific Research or the U.S. Government.

## TABLE OF CONTENTS

	<u>Page</u>
1. Introduction	1
2. Summary of Important Results	2
3. Conclusions	7
4. List of Publications	8
5. Appendices	19
I. The Frequency Displaced Target Derived Reference.	
II. Holography, Wavelength Diversity and Inverse Scattering.	
III. The Virtual Fourier Transform and its Application in Three Dimensional Display.	
IV. An Automated Frequency Response and Radar Cross-Section Measure- ment Facility for Microwave Imaging.	

**LEVEL II**

**9**

UNIVERSITY OF PENNSYLVANIA  
PHILADELPHIA, PENNSYLVANIA 19104

FINAL REPORT

SUPER RESOLUTION IMAGERY  
BY FREQUENCY SWEEPING

AIR FORCE OFFICE OF SCIENTIFIC RESEARCH/NE  
BUILDING 410 BOLLING AIR FORCE BASE  
WASHINGTON, D.C. 20332

AUGUST 15, 1980

GRANT NUMBER **[REDACTED]**  
**AFOSR-77-3256**

Accession For		
NTIS GRA&I	<input checked="checked" type="checkbox"/>	
DTIC TAB	<input type="checkbox"/>	
Unannounced	<input type="checkbox"/>	
Justification		
By		
Distribution/		
Availability Codes		
Dist Special		
<b>A</b>		

PREPARED BY  
N.H. FARHAT AND C. WERNER

**DTIC**  
**ELECTE**  
**S** **D**  
OCT 25 1980  
**D**

AIR FORCE OFFICE OF SCIENTIFIC RESEARCH (AFSC)  
NOTICE OF TRANSMITTAL TO DDC  
This technical report has been reviewed and is  
approved for public release IAW AFR 190-12 (7b).  
Distribution is unlimited.  
A. D. BLOSE  
Technical Information Officer

## HIGH RESOLUTION FREQUENCY SWEPT IMAGING

### 1. Introduction

The aim of the research work outlined in this final report was the analysis and investigation of methods by which frequency or wavelength diversity techniques can be employed to impart to a highly thinned, and therefore cost-effective, longwave (microwave or ultrasound) imaging aperture resolution capabilities better than its monochromatic classical (Rayleigh) limit achieving thereby super-resolution by means of frequency synthesized apertures. This approach to longwave imaging gains practical significance when one considers the current highly developed state of the art of broadband microwave gear suitable for use in a new generation of cost-effective high resolution microwave imaging radars utilizing frequency diversity techniques.

It is well known that the development of longwave holographic imaging systems possessing resolution and image quality approaching those of optical systems is hampered by three factors: (a) prohibitive cost and size of longwave imaging apertures, (b) rapid deterioration of longitudinal resolution with range, (c) inability to view a 3-D image as with optical Fresnel holograms because of a wavelength scaling problem and (d) degradation of image quality by speckle or coherent noise because of the low numerical apertures attainable with present techniques. For example, a longwave imaging aperture operating at a wavelength of 3 cm should be about 3 km in size in order to achieve image resolution comparable to an ordinary photographic camera. In addition to inconvenient size, the cost of filling such a large aperture with suitable coherent sensors is clearly prohibitive. Furthermore, recall that in conventional longwave holography when optical image retrieval is utilized, it is necessary to store the longwave hologram data (fringe pattern) in an optical transparency suitable for processing on the optical bench using laser light. In order to avoid longitudinal distortion\* of the reconstructed image, the size of the optical hologram replica must be  $m (= \lambda_{\text{long}} / \lambda_{\text{laser}})$  times smaller than the longwave recording aperture. For the example cited earlier, this means an optical hologram replica of less than a millimeter in size. It is certainly not possible to view a virtual 3-D image through such a minute hologram even with optical aids since these tend to introduce their own longitudinal distortion. As a result, longwave holographers have long learned to forgo 3-D imagery and settled instead for 2-D imagery obtained by projecting the reconstructed real image on a screen. This permits lowering of the reduction factor  $m$  and consequently relaxing the resolution requirements of the photographic film which allows in turn the use of highly convenient Polaroid transparency film for preparation of the optical hologram replica. Because of the small size (measured in wavelength) of longwave apertures attainable in practice and the above methods of viewing the real image, speckle noise is always present leading to degradation in image quality.

\* Longitudinal distortion causes for example the image of a sphere to appear elongated in the range direction like a very long ellipsoid.



In this report we summarize the main results of our investigation under this grant. Our findings show that frequency diversity techniques not only circumvent the limitations discussed above but provide a means of viewing true 3-D images of distant objects such as satellites and aircraft. It is worthwhile to point out that our studies of wave-vector diversity imaging (or frequency swept imaging) were motivated to some extent by evidence of super-resolved "imaging" capabilities in the dolphin and the bat which are known to use frequency swept (chirp) signals in their "sonar" to discern small objects in their environment.

## 2. Summary of Important Results

The main findings of the study, details of which are given in the appendices and our publications (see list of publications), are outlined next.

(a) Wave-vector diversity (multifrequency and multiaspect) techniques can be used to enhance the amount of object information collected by a broadband coherent aperture deployed in the far field of the scattering object. Thus the data collected by a highly thinned array of coherent receivers intercepting the wavefield scattered from a distant 3-D reflecting object, as the frequency of its illumination (and/or its direction of incidence) are changed (see Fig. 1-a for example), can be stored as a 3-D data manifold in  $\bar{p}$ -space (Fig. 2) from which an image of the object can be retrieved by means of a 3-D Fourier Transform. The size and shape of the 3-D data manifold, and therefore the resolution, depend on the relative positions of the object, the transmitter (illuminator), and the receiving array and on the spectral width of the illumination utilized.

(b) The data collected must be corrected for a quadratic phase factor  $F$  (caused by the unequal distances between the object and the receiving stations forming the widely dispersed imaging array) before it is stored in a 3-D manifold in  $\bar{p}$ -space and an undistorted image of the 3-D reflecting object reconstructed through the 3-D Fourier transform operation. A bothersome range-azimuth ambiguity is also avoided through elimination of this quadratic phase term.

The most promising methods for data acquisition and correction is that which utilizes a target derived reference (TDR) at the synchronous detectors of the various receivers to correct for the unequal phase shifts or propagation time delays from the object to each receiver. In this approach the data furnished by the various receivers of the recording array is free of the undesired factor  $F$ . Therefore no additional processing by a computer will be necessary before filing the data at the appropriate locations in  $\bar{p}$ -space. The TDR method has several advantages which include:

(i) Elimination of the need for a costly and unreliable central local oscillator distribution network.

(ii) Because TDR results in a recording configuration similar to that of a lensless Fourier Transform hologram, the resolution requirements from the recording device are greatly relaxed\*.

\*A. Macovski, "Hologram Information Capacity", J. Opt. Soc. Am., Vol. 60, Jan. 1970, pp. 21-29.

In longwave holography this fact is translated into a significant reduction of the number of receiving elements in the recording aperture. In addition the use of TDR allows us to place all the resolving power of the recording aperture on the target. This means that high resolution images of distant isolated targets should be feasible with array apertures consisting of tens of elements. The ability to synthesize a 2-D receiving aperture with a Wells array† consisting of two orthogonal linear arrays one of transmitters and the other of receivers provides further means of reducing the number of stations needed for data acquisition without sacrifice in resolution. A frequency swept Wells array of 10 transmitters and 10 receivers using a (2-4) GHz sweep should be able to easily furnish  $10^4$  3-D distinguishable resolution cells on the target which is more than sufficient for discerning the scattering centers on practical targets.

(iv) Greater immunity to phase fluctuations arising from turbulence and inhomogeneities in the propagation medium because both the reference and imaging signals arriving at each receiving element of the aperture travel roughly over the same path.

(v) TDR eliminates the range azimuth ambiguity and excessive bandwidth problems that arise in fast frequency swept imaging when the reference signal for the array aperture is distributed instead from the illumination source or a centrally located local oscillator phase locked to it.

Two TDR methods have been considered to some extent in our work to date. In one method which we term LFTDR (*Low Frequency Target Derived Reference*), the object is assumed to be illuminated simultaneously with a high frequency imaging signal and a low frequency signal that is a subharmonic of the illuminating frequency. The subharmonic reference frequency  $\omega_r$  is chosen such that  $k_r l \ll 1$ ,  $l$  being the maximum linear dimension of the object and  $k_r = \omega_r / c$ ,  $c$  being the velocity of light. This places scattering from the object in the Rayleigh region where the object behaves as point scatterer with zero phase contribution. The far field phase of the reference signal at any receiver is therefore entirely due to propagation between a reference point formed at the object to the receiver. A method for measuring this reference signal phase and using it to correct the imaging signal phase due to propagation has been proposed by Porter\* and analyzed for a one-dimensional object geometry. The reference signal phase and the imaging signal phase are measured separately at each receiving station with the aid of two receivers whose local oscillators (L.O)'s, one at the reference frequency and one at the imaging frequency, are phase-locked only to each other and not to a central local oscillator as would be the case were we to use a conventional receiver array. Phase locking of the two L.O's can be accomplished by simply making the imaging L.O a harmonic of the

†C.N. Nilsen and D.N. Swingler, "Quasi-Real-Time Inertialess Microwave Holography", Proc. IEEE (Letters), Vol. 65, March 1975, pp. 491-492.

\*R.P. Porter, "A Radar Imaging System Using the Object as Reference", Proc. IEEE (Letters), Vol. 59, Feb. 1971, pp. 307-308.

reference L.O. This would eliminate the difficulties encountered in the implementation of large or giant thinned coherent receiving arrays of the type required here, namely the distribution of a central local oscillator signal. A great reduction in cost and effort associated with installation of a central L.O. distribution network can thus be achieved. This cost reduction should be compared however with the cost of implementing a LFTDR. Because of the large difference between the high frequency imaging frequencies and the low frequency reference frequency required for the high resolution imaging of practical objects, the same microwave gear can not be used for both frequencies. This could increase system cost. In addition since the measured reference phase must be multiplied by a factor  $\beta$  equal to the ratio of the imaging to the reference frequency before being used as a reference phase in the imaging signal measurement, any errors in the reference phase measurement will also be amplified by this ratio. The precision of the reference phase measurement and phase error analysis are important and will have therefore to be examined further.

Another TDR methods which we call the *Frequency Displaced Target Derived Reference* (FDTDR) also shows promise. In this method, the analytical details of which are outlined in appendix I, the object is illuminated simultaneously during the sweep with two phase locked imaging frequencies  $\omega_1$  and  $\omega_2 = \omega_1 + \Delta\omega$ ,  $\Delta\omega$  being a small incremental frequency. This can be realized also by single side band modulation of the swept signal or by phase locking two sweep oscillators. Measurement of the differential phase between the signals scattered from the target at these frequencies yields  $\frac{\Delta\omega}{c} (R_T + R_R)$ ,  $R_T$  being

the distance from the transmitter to the object and  $R_R$  being the distance from the object to the receiver. Multiplication of this phase by  $\omega_1/\Delta\omega$  yields the phase factor  $F$  at frequency  $\omega_1$  which would be used to correct the phase measured at  $\omega_1$ . At first look this method would appear to still require a reference local oscillator. This however is not so since the procedure outlined above need not involve explicit phase measurements and multiplications. For example by mixing the two received signals at  $\omega_1$  and  $\omega_1 + \Delta\omega$  in a square law detector at each receiver a beat signal at frequency  $\Delta\omega$  is derived whose phase is equal to  $\frac{\Delta\omega}{c} (R_R + R_T)$ . The phase shift of

this signal due to the object is effectively zero because the wavelength at  $\Delta\omega$  is much larger than the object extent making it behave effectively as a point scatterer. Harmonic mixing of the signal  $\omega_1$  received at each receiver with this beat signal should yield the corrected  $\bar{p}$ -space data at  $\omega_1$ . Because of the small difference  $\Delta\omega$  between the two frequencies  $\omega_1$  and  $\omega_2$  utilized, the effect of phase errors due to system and atmospheric propagation could be more completely cancelled in this method than in the low frequency TDR methods. The small difference  $\Delta\omega$  means also that unlike the LFTDR case the same microwave gear (antennas, transmission lines and other microwave circuit components) can be utilized in the handling of the reference and imaging signals. A variation of the TDR technique involving double side-band modulation is also possible and appears to be more simple to implement than the single side-band method.

(c) Because in addition to being dependent on geometry, the dimensions of the 3-D data in  $\bar{p}$ -space shown in Fig. 2 are dependent on the spectral range of the illumination, super-resolution (i.e. resolution beyond the classical limit of the available physical aperture) is achieved. This aperture synthesis by wave-vector or frequency diversity helps cut down array cost (since a thinned array can be used to frequency synthesize a large array with higher filling factor).

(d) *Fourier Domain Projection Theorems* (see appendixes II and III for details) enable the generation of two dimensional holograms from projections (or weighted projections) of the corrected  $\bar{p}$ -space 3-D data manifold of Fig. 2 permitting thereby optical image retrieval of the 3-D object in slices parallel to the projection plane one at a time. For example, Fig. 1-b shows the projection hologram for the  $\bar{p}$ -space data obtained in a computer simulation of the arrangement shown in Fig. 1-a. The central cross-sectional outline of the object (the two 1 m diameter reflecting spheres of Fig. 1-a) retrieved from this projection hologram by means of a 2-D Fourier transform carried out on the optical bench is shown in Fig. 1-c. A similar example is shown in Figs. 3 and 4. Figure 3 shows a second test object consisting of 3-D distribution of a set of 8 point scatterers with locations and spacings given in the Figure. Figure 4 shows the projection holograms corresponding to the three slices of the object containing the point scatterers and the image retrieved from each. The sweep width in this example, as in the previous example, was (2-4) GHz however the number of receivers in the recording array has been reduced from 50 to 16. These computer simulations demonstrate that a 3-D (lateral and longitudinal) resolution of the order of twenty centimeters\* is easily achieved with a frequency sweep covering only (2-4) GHz using a broad-band array of 16 receivers and one transmitter. Wider-spectral windows should yield better resolution. It is worthwhile to note in this respect that commercial microwave sweepers and synthesizers are available with a spectral coverage of (.1-25) GHz indicating a potential for practical resolutions of the order of possibility few centimeters with cost-effective broad-band apertures consisting of tens of receivers operating with one central illuminator.

(e) The viewing or the display of a true 3-D image of the various slices or cross-sectional outlines should be possible by reconstruction of the various projection holograms in rapid succession while projecting the reconstructed real images of the corresponding slices on a rapidly moving projection screen. The screen would be displaced rapidly (together with the Fourier transforming lens) on the optical bench in the axial directions by small amounts proportional to the distances between the various slices. In another approach we have found that the 2-D *virtual Fourier transform* of a projection hologram can be carried out by simply viewing (with the unaided eye) a transparency containing an array of reduced replicas of the projection hologram arranged side-by-side with a point source. The image retrieved in this fashion would lie in the plane of the point source. This approach has the potential for 3-D display by viewing the virtual images retrieved from a series of projection holograms corresponding to different slices or cross-sectional outlines

\*This means  $10^3$  distinguishable 3-D resolution cells in the  $(2 \times 2 \times 2)\text{m}^3$  volume of the assumed object.

of the object passed in front of the eye in rapid succession while moving the reconstruction point source axially back and forth at a suitable rate of incremental axial displacements. A proposed electro-optical scheme that permits carrying out this procedure in real-time using a rapidly recyclable spatial light modulator (SLM) operating in a reflection mode is shown in Fig. 5. The computer, the high resolution CRT and the projection optics are used to project reduced noncoherent images of the various projection holograms in rapid succession on the SLM while the axial position of the reconstruction point sources is altered rapidly also under computer control. The point source need not be derived from a laser in order to yield an image but could also be a miniature "grain of wheat" light bulb. Details of this task are found in Appendix III.

(f) As seen in (e), unlike monochromatic longwave holographic imaging, there is no specific scaling requirements imposed on the projection holograms in order to avoid longitudinal distortion in the optical reconstruction circumventing thus the wavelength scaling problem.

(g) Because of the broad spectral extent of the illumination used and ability to display the reconstructed image in separate slices, speckle or coherent noise, which is known to plague coherent imaging systems, is suppressed making the system behave in as far as image noise is concerned like a noncoherent imaging system but at the same time enjoy the superior detection characteristics associated with synchronous detection techniques.

(h) The broad-band nature of the imaging process also helps suppress undesirable image detail that could arise from object resonances, which could seriously degrade image quality in a monochromatic imaging system.

(i) The data collected at every receiver, represents after correction, essentially the frequency response of the scattering object measured from a different aspect angle. Assuming the scattering process is linear, this frequency response is related to the impulse response of the object by a Fourier transform (see ref. 5 in List of publications). This suggests that impulse illumination can be utilized instead of frequency swept illumination. When this is done, the 3-D data manifold in  $p$ -space may be generated by Fourier transforming the impulse response at each receiver, correcting the data for the Factor  $F$  mentioned in (b), and storing the result in the appropriate  $p$ -space locations for each receiver. The resulting  $p$ -space volume accessed in this fashion can then be employed as described earlier to yield 3-D image information. Impulse illumination is desirable in certain instances of rapid target motion but may be more difficult to implement than frequency swept illumination. Since the impulse response of a time invariant linear system can also be deduced from white noise excitation and correlation of the output response with the input as described elsewhere in more detail (see 5 in list of publications), it follows that the techniques described in this report for coherent broadband radiation should be equally applicable with minor signal processing modification to noise-like broadband

radiation including passive black-body radiation.

(j) Experimental verification for both the principle of frequency diversity imaging and the TDR concept were obtained with the aid of a semi-automated network analyzer configured and installed in a recently refurbished anechoic chamber within the scope of this program (see Figs. 6 and 7). This versatile system is capable of vector (amplitude and phase) measurements of wavefields scattered from test objects situated in the anechoic chamber over any frequency range lying in the (.1-18)GHz range for a variety of polarizations. A test object consisting of two parallel cylinders 25 cm apart each 5 cm in diameter and 50 cm long was mounted on a rotating styrofoam pedestal that is under computer control and illuminated as shown in Fig. 8. The distance from the center of the object to the illuminating parabolic antenna to the left and the receiving horn feeding the network analyzer was 2.5 m. The complex frequency response of this object was measured in the (5-14)GHz range and the data stored for 128 object orientation covering  $360^\circ$ . The stored data was corrected for range-phase with a synthetic TDR generated in the computer and the corrected data displayed and photographed yielding the frequency swept hologram shown in Fig. 9 (c). The image retrieved from this hologram via an optical Fourier transform carried out on the optical bench is shown in Fig. 9 (d). For reasons of comparison a computer simulation of this experiment assuring a (2-18)GHz sweep was performed. The resultant range-phase corrected hologram and the image retrieved from it optically are shown in Fig. 9 (a) and (b). Further detail on this phase of the program were reported in an MSc. thesis made part of this report in Appendix IV. This part of the program is being continued with the aim of further enhancing measurement accuracy and demonstrating imaging of a nonsimple 3-D test object such as a model aircraft utilizing polarization diversity to further enhance image quality.

### 3. Conclusions.

The primarily analytical and numerical study of frequency diversity imaging performed under this grant demonstrates conclusively the feasibility of a new generation of coherent broadband imaging radars capable of furnishing 3-D image detail of distant target with cost effective giant apertures and efficient digital/optical signal processing.

Future work in this area will focus more on the analysis and identification of optimal methods for data acquisition, processing and 3-D display. The ultimate aim is the generation of design criteria for a prototype system and its assessment in the 3-D imaging of low flying aircraft passing within range of our facilities on route for landing at the Philadelphia Airport.

### List of Publications

1. N.H. Farhat, "Frequency Synthesized Imaging Apertures", Proc. 1976, International Optical Computing Conference, IEEE Cat. #76 CH 1100-7C, pp. 19-24.
2. N.H. Farhat, M.S. Chang, J.D. Blackwell and C.K. Chan, "Frequency Swept Imaging of a Strip", Proc. 1976, Ultrasonics Symposium, IEEE Cat. #76 CH 1120-5SU.
3. J.D. Blackwell and N.H. Farhat, "Image Enhancement in Longwave Holography by Electronic Differentiation", Optics Communications, Vol. 20, Jan. 1977, pp. 76-80.
4. C.K. Chan, N.H. Farhat, M.S. Chang and J.D. Blackwell, "New Results in Computer Simulated Frequency Swept Imaging", Proc. IEEE (Letters), Vol. 65, pp. 1214-1215, Aug. 1977.
5. N.H. Farhat, "Principles of Broad-Band Coherent Imaging", J. Opt. Soc. Am., Vol. 67, pp. 1015-1020, Aug. 1977.
6. N.H. Farhat, "Comment on Computer Simulation of Frequency Swept Imaging", Proc. IEEE, Vol. 65, pp. 1223-1226, Aug. 1977.
7. N.H. Farhat, "Comment on a New Imaging Principle", Proc. IEEE (Letters), Vol. 66, pp. 609-700, May 1978.
8. N.H. Farhat, "Microwave Holographic Imaging - Prospects For a Real-Time Camera", SPIE, Vol. 180, *Real-Time Signal Processing II*, (1979).
9. N.H. Farhat and C.K. Chan, "Three-Dimensional Imaging by Wave-Vector Diversity", *Acoustical Imaging*, Vol. 8, A. Metherell (ed.), Plenum Press, New York (1980), pp. 499-515.
10. C.K. Chan and N.H. Farhat, "Frequency Swept Imaging of Three Dimensional Perfectly Reflecting Objects", IEEE Trans. on Antennas and Propagation - Special Issue on Inverse Scattering. (Accepted for publication.)
11. C.K. Chan, "Analytical and Numerical Studies of Frequency Swept Imaging", University of Pennsylvania, Ph.D. Dissertation (1978).
12. N.H. Farhat, "Microwave Holography and Coherent Tomography", (Invited paper). Presented at 1980 IEEE/MTT's International Microwave Symposium, Electromagnetic Dosimetric Imaging. (To be published in special conference proceedings).

### Related Publications

1. N.H. Farhat, "New Imaging Principle", Proc. IEEE (Letters), Vol. 64, pp. 379-380, March 1976.
2. N.H. Farhat, T. Dzekov and E. Ledet, "Computer Simulation of Frequency Swept Imaging", Proc. IEEE (Letters), Vol. 64, pp. 1453-1454, Jan. 1977.
3. G. Tricoles and N.H. Farhat, "Microwave Holography: Applications and Techniques", Invited paper, Proc. IEEE, Vol. 65, pp. 108-121, Jan. 1977.
4. M.A. Kujoory and N.H. Farhat, "Microwave Holographic Substraction for Imaging of Buried Objects", Proc. IEEE (Letters), Vol. 66, pp. 94-96, Jan. 1978.
5. M.A. Kujoory and N.H. Farhat, "Format Generation For Double Circular Scanners For Use in Longwave Holography", Acoustical Imaging and Holography, Vol. 1, No. 2, pp. 133-141 (1979).
6. N.H. Farhat and J. Bordogna, "An Electro-Optics and Microwave-Optics Program In Electrical Engineering", IEEE Trans. on Education - Special Issue on Optics Education (accepted for publication).
7. N.H. Farhat, "Holographically Steered Millimeter Wave Antennas", IEEE Trans. on Antennas and Propagation, Vol. AP-28, July 1980, pp. 476-480.



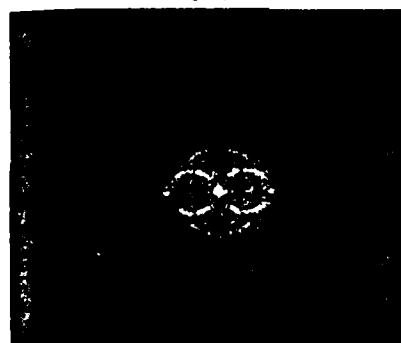
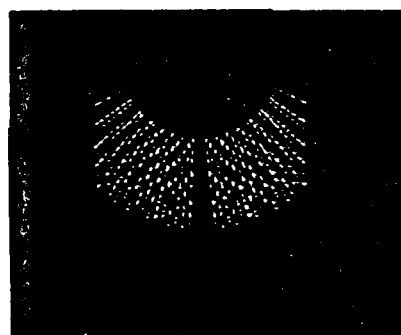
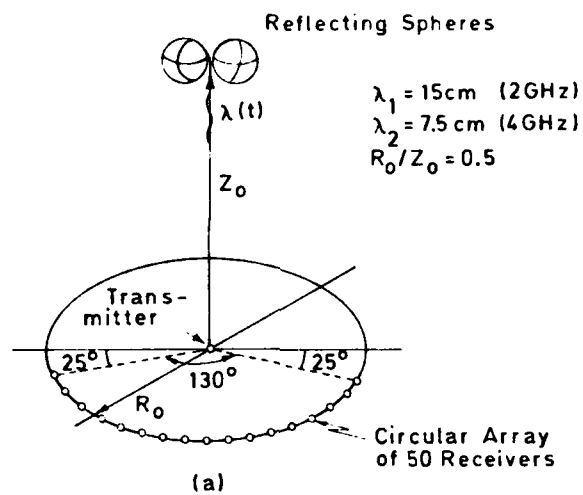


Fig. 1. Computer Simulation of Wave-vector Diversity Imaging,  
 (a) Geometry, (b) Projection Hologram, (c) Retrieved  
 Central Cross-sectional Image.

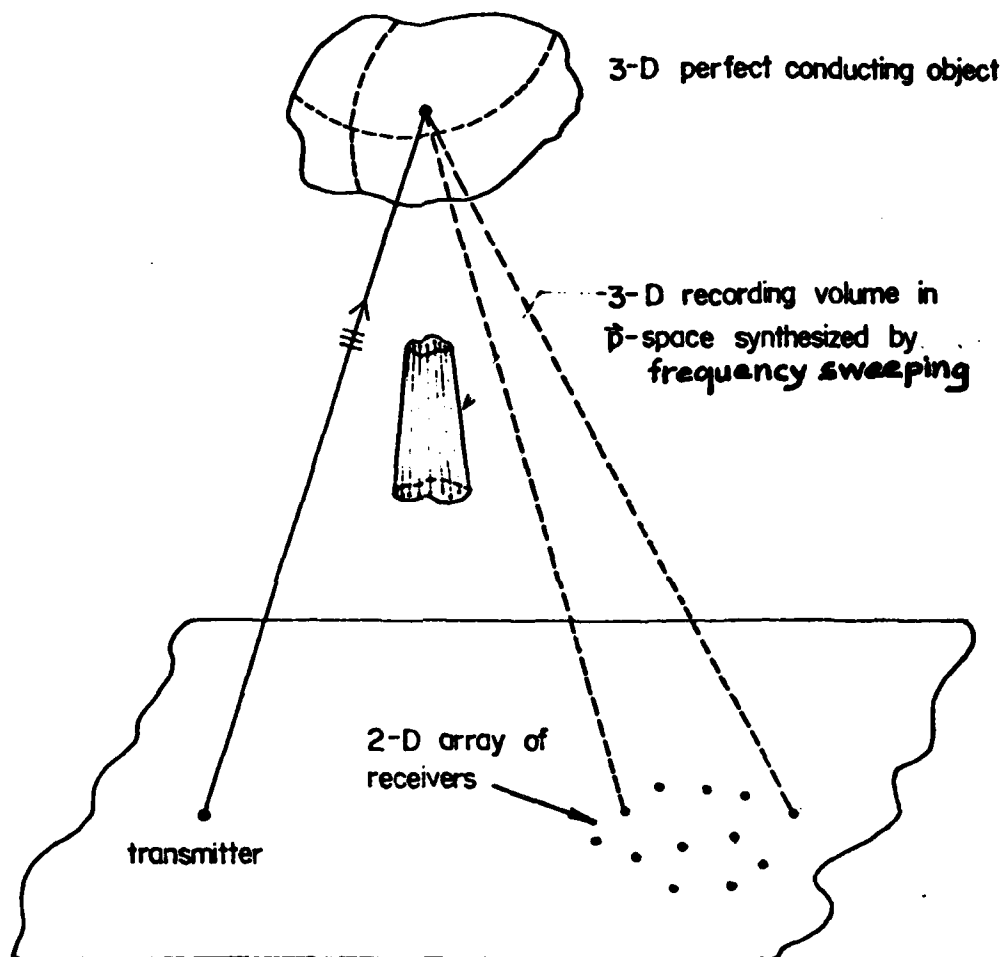


Fig.2 Three dimensional  $\tilde{p}$ -space data generated by frequency sweeping and collected by a 2-D array of receivers.

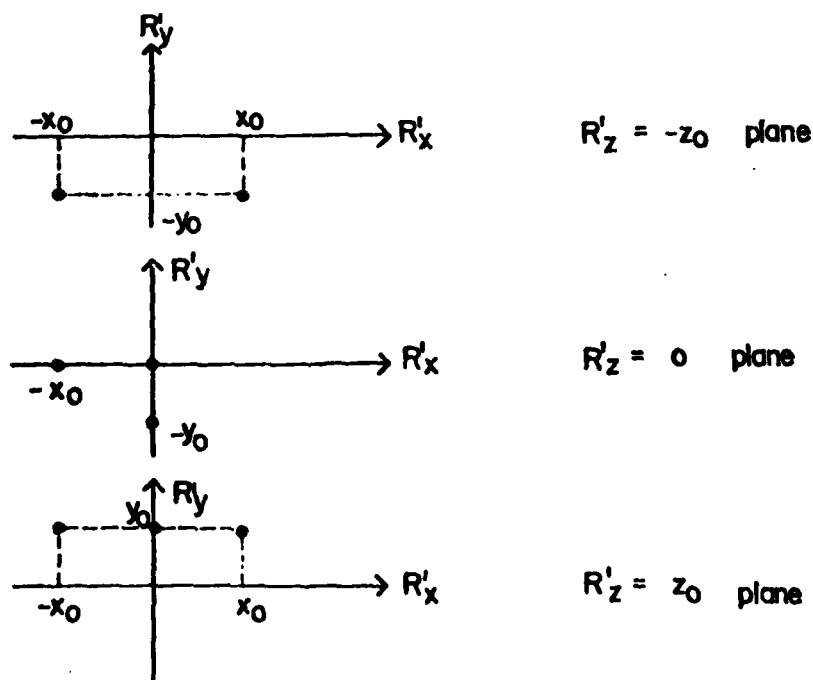
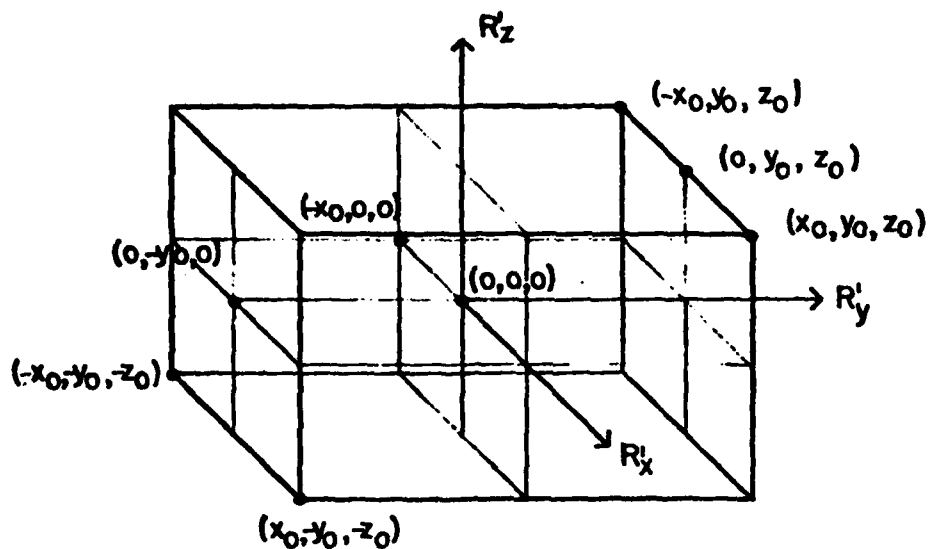


Fig. 3. 3-D object consisting of a set of eight point scatterers shown in isometric and  $R'_x$ - $R'_y$  plane views at  $R'_z = -z_0, 0, z_0$ .  $x_0 = y_0 = z_0 = 100^x \text{ cm}^y$ .

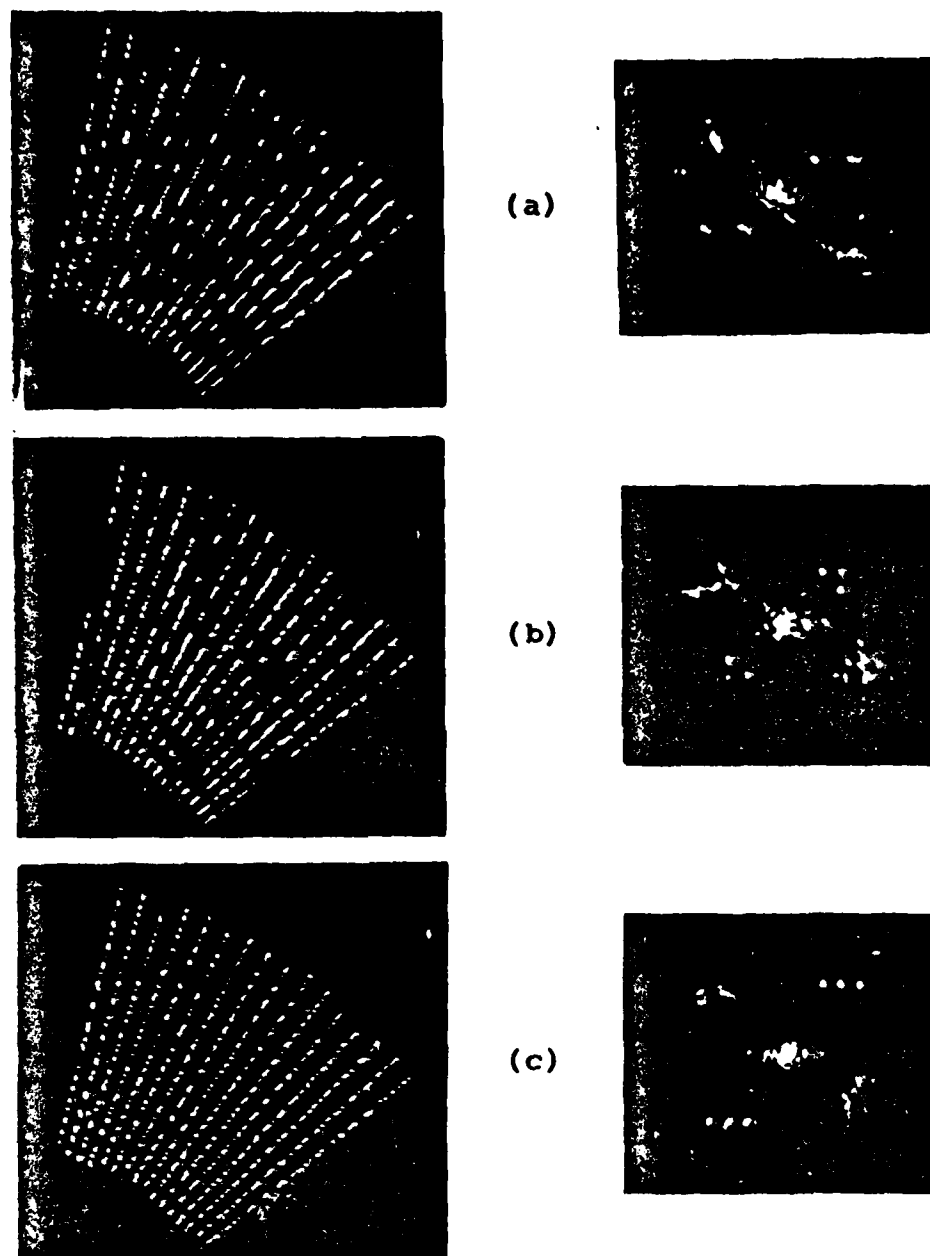


Fig. 4. Projection holograms and their optical reconstructions for the set of point scatterers in Fig.7.10 at different  $R'_z$  planes. (a) Hologram and reconstructed image of  $z$  scatterers at  $R'_z = -z_0$  plane. (b) Hologram and image at  $R'_z = 0$  plane. (c) Hologram and image at  $R'_z = z_0$  plane.  $x_0 = y_0 = z_0 = 100\text{cm}$ .

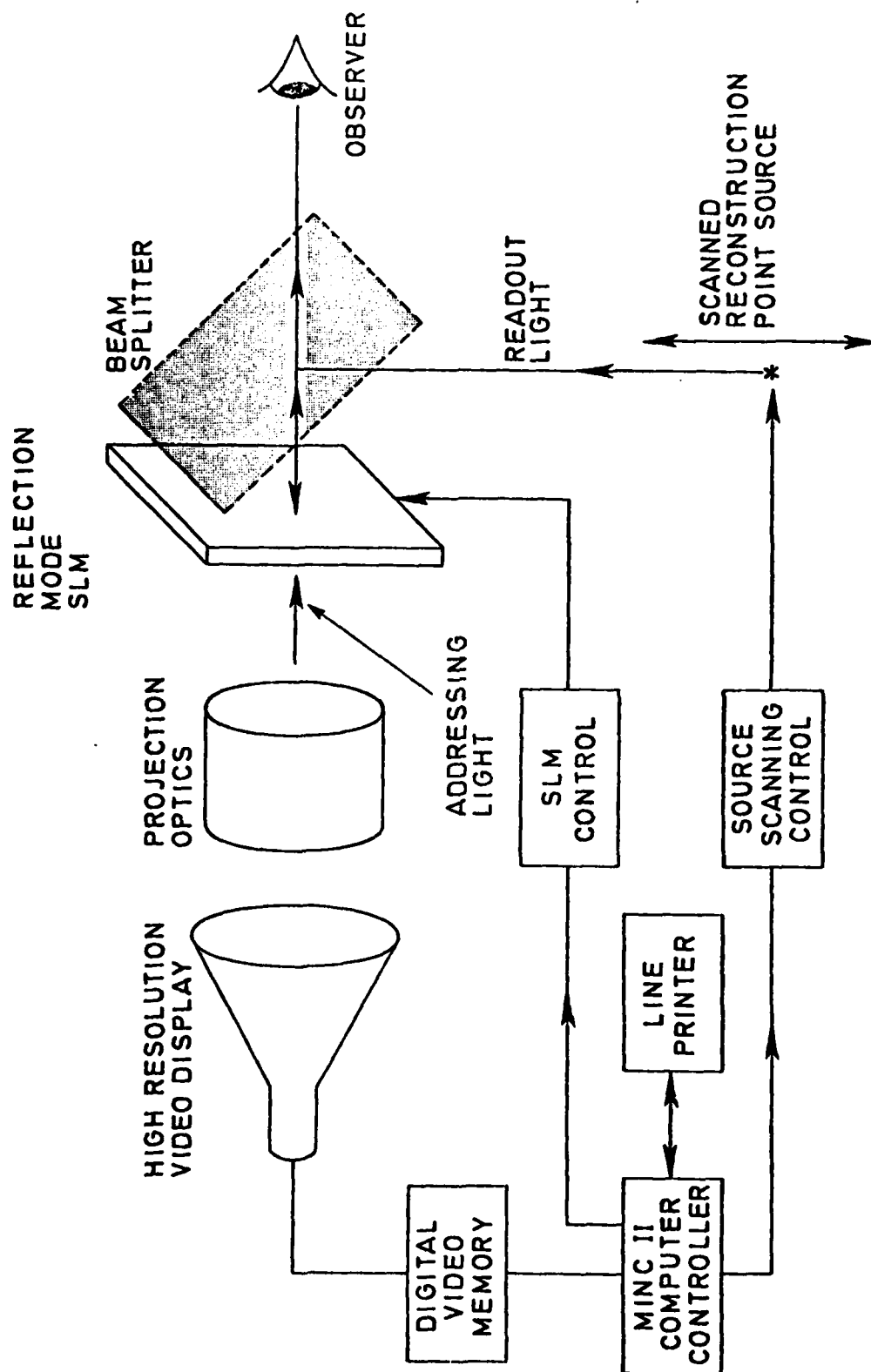


Fig. 5. True 3-D image reconstruction based on the virtual Fourier transform.

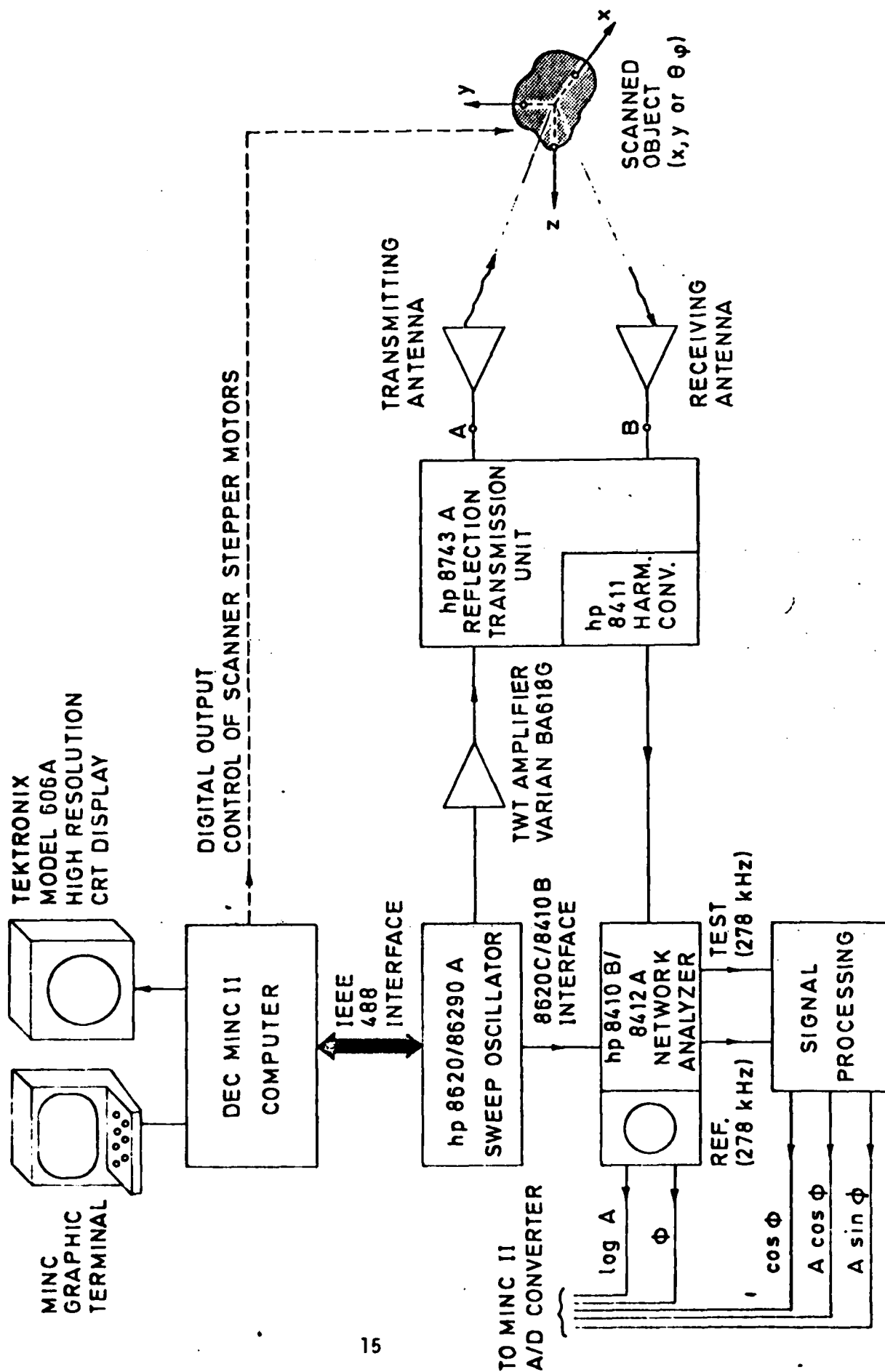


Fig. 6. Block Diagram of Automated Microwave Network Analyzer Showing Interface to MINC II Computer via IEEE 488 Standard Interface Bus.

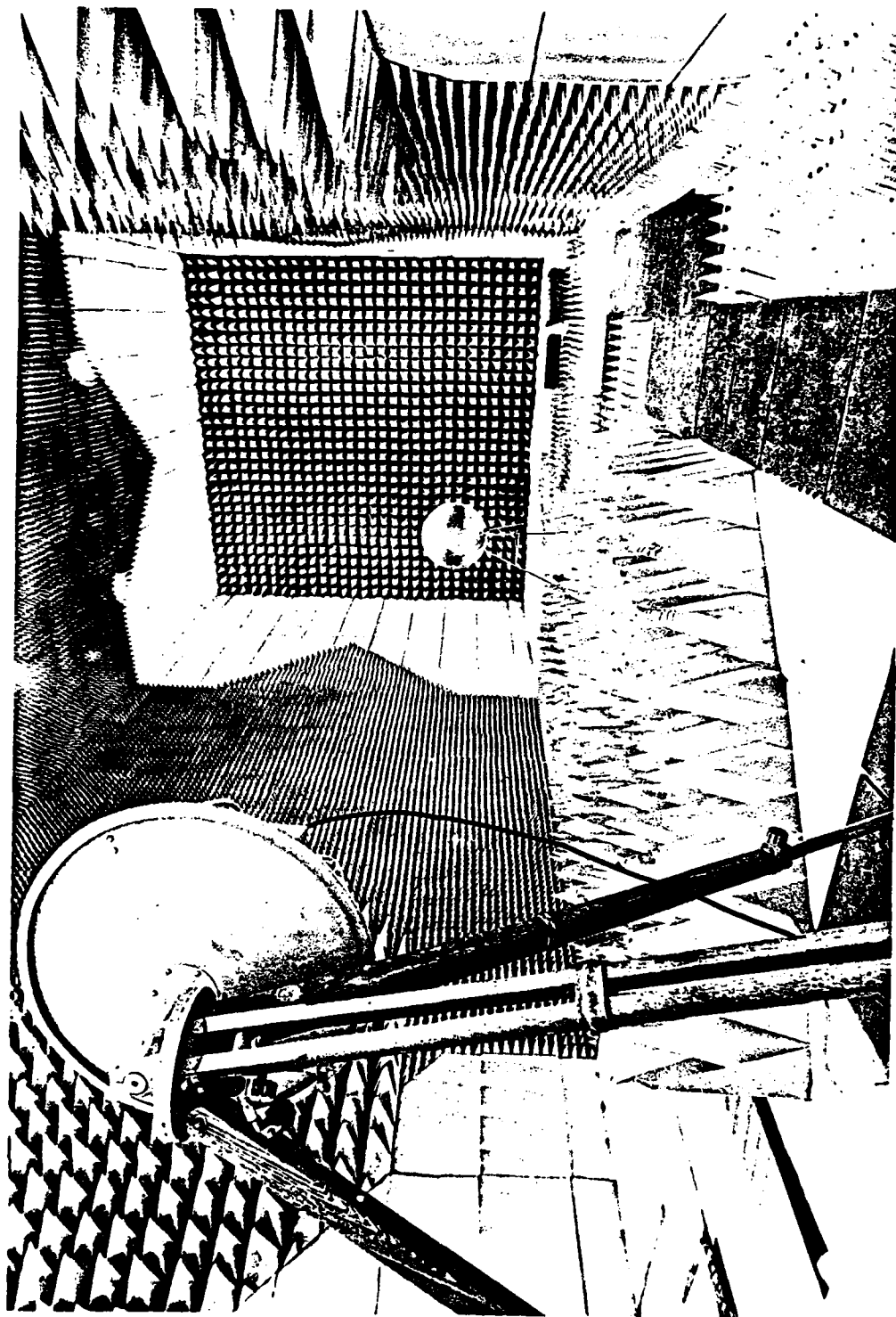
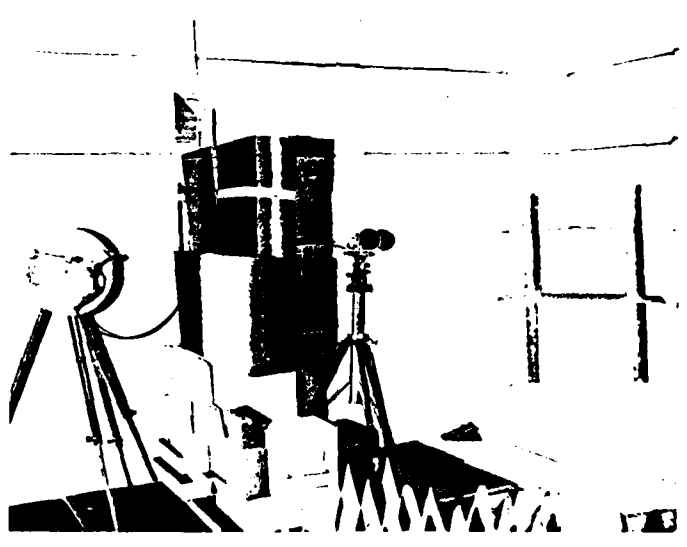
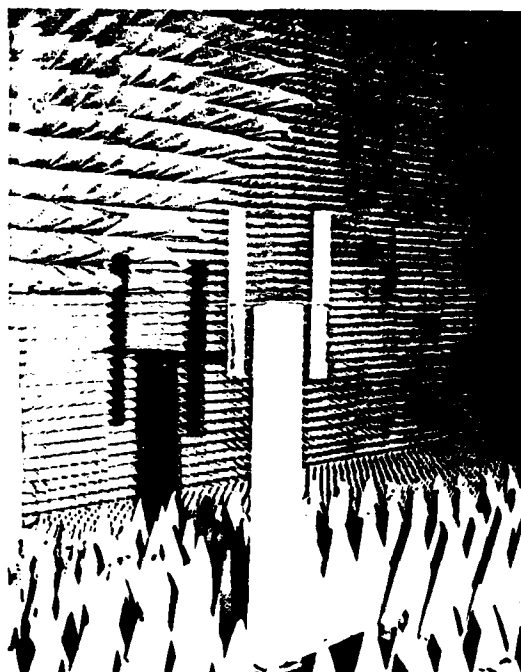


Fig. 7. View of Microwave Anechoic chamber showing illuminator antenna and a calibration sphere in background.



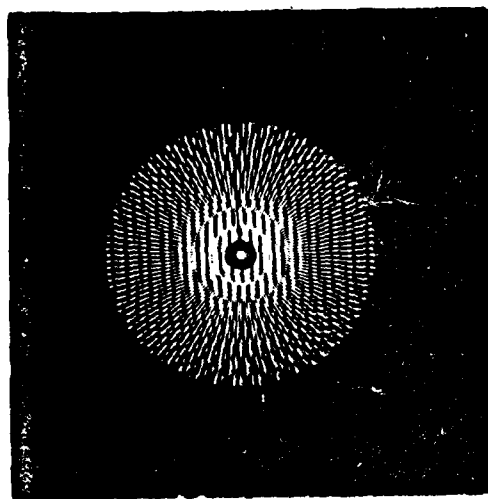
(a)



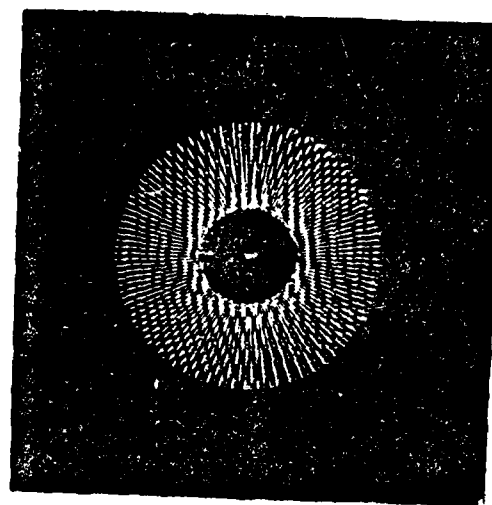
(b)

Fig. 8. Two views of dual-cylinder test object in Anechoic chamber. (a) View showing illuminator to the left and the receiving horn on the right separated by absorbing barrier. (b) View showing test object mounted on rotating styrofoam pedestal. Cylinders are 5 cm in diameter, 50 cm long, 25 cm apart.

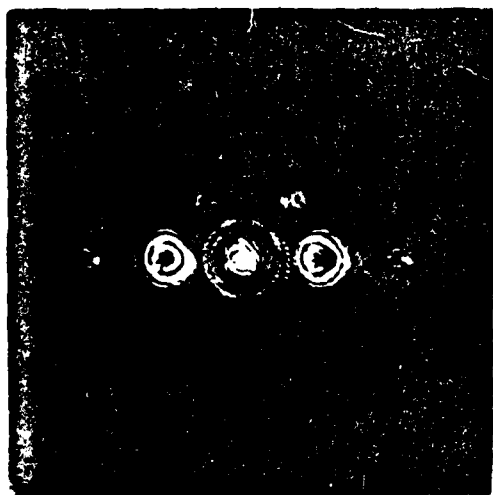




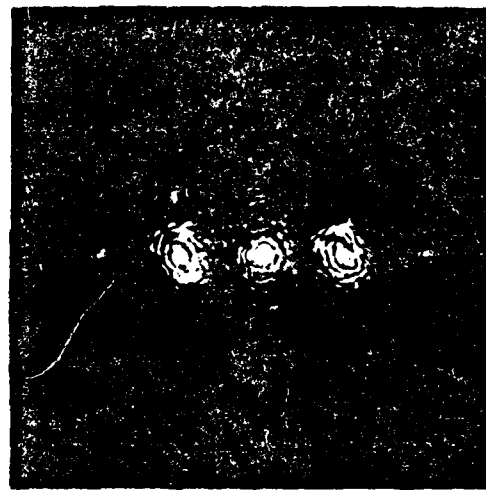
(a)



(c)



(b)



(d)

Fig. 9. Frequency swept holograms and retrieved images for a dual-cylinder test object. (a) Computed frequency swept hologram for a (2-18)GHz sweep and (b) retrieved image; (c) measured frequency swept hologram for a (5-14)GHz sweep and (d) retrieved image.

APPENDICES

## APPENDIX I

### The Frequency Displaced Target Derived Reference

A second TDR method which we refer to as a *Frequency Displaced Target Derived Reference* (FDTDR) method also shows promise. This method involves simultaneous illumination of the object with two phase locked imaging frequencies  $\omega_1$  and  $\omega_2 = \omega_1 + \Delta\omega$  that differ by a small frequency increment  $\Delta\omega$ . Referring to eq. (9) of ref. 10 (see list of publications) we can write for the far field at a given receiver location  $R_R$ ,

$$\psi_1(k_1, R_R) = \frac{jk_1}{2\pi R_R} e^{-jk_1(R_T+R_R)} \int U(\vec{r}) e^{-j\vec{p}_1 \cdot \vec{r}} d\vec{r} \quad (1)$$

$$\begin{aligned} \psi_2(k_2, R_R) = \frac{j(k_1+\Delta k)}{2\pi R_R} e^{-jk_1(R_T+R_R)} e^{-j\Delta k(R_T+R_R)} \\ \times \int U(\vec{r}) e^{-j\vec{p}_1 \cdot \vec{r}} \left(1 + \frac{\Delta\omega}{\omega_1}\right) \cdot \vec{r} d\vec{r} \end{aligned} \quad (2)$$

where  $k_{1,2} = \omega_{1,2}/c$  and  $\Delta k = \Delta\omega/c$ .

By making  $\Delta\omega/\omega \ll 1$  the integral in (2) will approach that in (1). The only difference between the far fields  $\psi_1$  and  $\psi_2$  at the receivers is then the phase term  $\Delta k(R_T + R_R)$ . Measurement of this phase difference yields  $(R_T + R_R)$  since  $\Delta k$  is known. This information can be used to correct the phase of either the  $\psi_1$  or  $\psi_2$  signals to obtain the required  $\vec{p}$ -space information.

$$\Gamma(\vec{p}) = \int U(\vec{r}) e^{j\vec{p} \cdot \vec{r}} d\vec{r} \quad (3)$$

## Appendix II

### HOLOGRAPHY, WAVE-LENGTH DIVERSITY AND INVERSE SCATTERING

#### ABSTRACT

The use of wavelength diversity to enhance the performance of thinned coherent imaging apertures is discussed. It is shown that wavelength diversity lensless Fourier transform recording arrangements that utilize a reference point source in the vicinity of the object can be used to access the three-dimensional Fourier space of non-dispersive perfectly reflecting or weakly scattering objects. Hybrid (opto-digital) computing applied to the acquired 3-D Fourier space data is shown to yield tomographic reconstruction of 3-D image detail either in parallel or meridional (central) slices. Because of an inherent ability of converting spectral degrees of freedom into spatial 3-D image detail true super-resolution is achieved together with suppression of coherent noise. The similarity of the key equations derived to those of inverse scattering theory is pointed out and the feasibility of using other forms of broadband radiation such as impulsive, noise and thermal is discussed. Finally, the potential of utilizing wavelength diversity imaging in microscopy and telescopy are discussed.

#### INTRODUCTION

A frequently encountered question in the science of image formation is how to make an available aperture collect more information about the scene or object being imaged in order to enhance its resolving power beyond the classical Rayleigh limit. This process is known as super-resolution and is relevant to all imaging systems whether holographic or conventional. There are five known methods for achieving super-resolution. These include: weighting or apodization of the aperture data<sup>1,2</sup>; analytic continuation of the wavefield measured over the aperture<sup>3,4</sup>; use of evanescent wave illumination<sup>5</sup>; maximum entropy method<sup>6</sup>; and use of the time channel<sup>7</sup>. Weighting and analytical continuation techniques are known to become rapidly ineffective as the signal to noise ratio of the data collected decreases. Maximum entropy techniques are known to be more robust as far as noise is concerned but involve usually extensive computation. Illumination with evanescent waves is practical in limited situations where full control of the recording arrangement exists as in microscopy for example.

This leaves the time channel approach in which one can collect in time more information about the object through the available recording aperture by altering the object aspect relative to the aperture by means of rotation or linear motion<sup>8,9</sup> or by altering the parameters of the illumination such as directions of incidence, wavelength and/or polarization. These latter operations are known to increase the degrees of freedom of the wavefields impinging on the recording aperture enhancing thereby their ability to convey information about the nature of the scattering object. Sophisticated imaging systems endeavour to convert the nonspatial degrees of freedom of the wavefield, e.g., angular, spectral and polarization to spatial image detail enhancing thereby the resolution capability beyond the classical Rayleigh limit of the available physical aperture. Obviously such procedures involve more signal processing than that performed by conventional imaging with lens systems or holography.

In this paper we consider generalizing the holographic concept to include wavelength diversity as a means of enhancing resolution. A quick examination of the basic equations of holography reveals that the lensless Fourier transform hologram recording arrangement is amenable to this generalization. This conclusion is used then as a starting point for a Fourier optics formulation of wavelength diversity imaging of 3-D (three dimensional) nondispersive objects. The results show that measurement of the multiaspect or multistatic frequency (or wavelength) response of the 3-D object permits accessing its 3-D Fourier space. The resulting formulas are identical to those obtained from a multistatic generalization of inverse scattering<sup>10,11,12</sup> establishing thus a clear connection between holography and the inverse scattering imaging problem. The inclusion of wavelength diversity in holography is shown to have several important features: (a) the availability of the 3-D Fourier space data permits 3-D image retrieval tomographically in parallel or meridional (central) slices or cross-sectional outlines by the application of Fourier domain projection theorems, (b) suppression of coherent noise and speckle in the retrieved image, (c) removal of several longstanding constraints on longwave (microwave and acoustical) holography such as the impractically high cost of the apertures needed, the inability to view a true 3-D image as in optical holography because of a wavelength scaling problem, and minimization of the effects of resonances on the object.

#### WAVELENGTH DIVERSITY

We start by inquiring into the conditions under which the data from  $N$  holograms of the same nondispersive object recorded over the same aperture, each at a different wavelength, can be combined to yield a single image superior in quality to the image retrieved from any of the individual holograms.

One approach to answering the question posed above would be to determine the conditions under which the well known formulas<sup>13</sup> for the focusing condition, magnification and image location in holography can be made independent of wavelength. This quickly leads to the conclusion that wavelength independence can be met if a reference point source centered on the object is used and proper scaling of the individual holograms by the ratio of recording to the reconstruction wavelength is performed before super-position<sup>15,24</sup>. The former condition is that for recording a lensless Fourier transform hologram<sup>14</sup> where the presence of the reference point source in the object plane leads to the recording of a Fraunhofer diffraction pattern of the object rather than its Fresnel diffraction pattern because of the elimination of a quadratic phase term in the object wavefield in the recorded hologram. This is known to result in a highly desirable reduction in the resolution required from the hologram recording medium and is therefore of practical importance especially in nonoptical holography. More detail of the processing involved in combining the data in multi wavelength hologram can be found elsewhere<sup>15</sup>.

Additional insight into the process of attaining super-resolution by wavelength diversity is obtained by considering the concept of wavelength or frequency synthesized aperture<sup>16-20</sup>. The synthesis of a one dimensional aperture by wavelength diversity is based on the simple fact that the Fraunhofer or far field diffraction pattern of a nondispersive planar object changes its scale, i.e. it "breathes", but does not change its shape (functional dependence), as the wavelength is changed. A stationary array of broadband sensors capable of measuring the complex field variations deployed in this breathing diffraction pattern at suitably chosen locations would sense different parts of the diffraction pattern as the wavelength is altered collecting thereby more information on the nature of the diffraction pattern and therefore on the object that gave rise to it than if the wavelength was fixed (stationary diffraction pattern). Each stationary sensor in the array is thus able to collect as the wavelength is changed, and the breathing diffraction pattern sweeps over it, the same set of data or information collected by a movable sensor mechanically scanned over the appropriate part of the diffraction pattern when it is kept stationary by fixing the wavelength. Hence the term wavelength or frequency synthesized aperture.

The orientation and location of the wavelength synthesized aperture for any planar distribution of sensors deployed in the Fraunhofer diffraction pattern of a planar object and the retrieval of an image from the data collected has been treated earlier<sup>16,17</sup>. It was clear, however, that extension of the wavelength diversity concept to the case of 3-D objects is necessary before its generality and practical use could be established.

For this purpose we considered<sup>20</sup> as shown in Fig. 1(a) an isolated planar object of finite extent with reflectivity  $D(\bar{\rho}_0)$ , where  $\bar{\rho}_0$  is a two dimensional position vector in the object plane  $(x_0, y_0)$ . The object is illuminated by a coherent plane wave of unit-amplitude and of wave vector  $\bar{k}_i = k \bar{I}_{k_i}$  produced for example by a distant source located at  $\bar{R}_T$ . The wavefield scattered by the object is monitored at a receiving point designated by position vector  $\bar{R}_R$  belonging to a recording aperture lying in the far field region of the object. The receiving point will henceforth be referred to as the receiver and the source point at the transmitter. The position vectors  $\bar{\rho}_0$ ,  $\bar{R}_T$  and  $\bar{R}_R$  are measured from the origin of a cartesian coordinate system  $(x_0, y_0, z_0)$  centered in the object. The object is assumed to be nondispersive i.e.,  $D$  is independent of  $k$ . However, when the object is dispersive such that  $D(\bar{\rho}_0, k) = D_1(\bar{\rho}_0)D_2(k)$  and  $D_2(k)$  is known, the analysis presented here can easily be modified to account for such object dispersion by correcting the data collected for  $D_2(k)$  as  $k$  is changed.

Referring to Figure 1(a) and ignoring polarization effects, the field amplitude at  $\bar{R}_R$  caused by the object scattered wavefield may be expressed as,

$$\psi(k, \bar{R}_R) = \frac{jk}{2\pi} \int D(\bar{\rho}_0) e^{-j\bar{k}_i \cdot \bar{r}_T} \frac{e^{-jk r_R}}{r_R} d\bar{\rho}_0 \quad (1)$$

where  $d\bar{\rho}_0$  is an abbreviation for  $dx_0 dy_0$  and the integration is carried out over the extent of the object. Noting that  $\bar{r}_T = \bar{\rho}_0 - \bar{R}_T$ ,  $\bar{R}_T = -R_T \bar{I}_{k_i}$  and using the usual approximations valid here:  $r_R \simeq R_R + \rho_0^2/2R_R - \bar{I}_R \cdot \bar{\rho}_0$  for the exponential in (1) and  $r_R \simeq R_R$  for the denominator in (1) where  $\bar{I}_R = \bar{R}_R/R_R$  and  $\bar{I}_{k_i} = \bar{k}_i/k$  are unit vectors in the  $\bar{R}_R$  and  $\bar{k}_i$  directions respectively, one can write eq. (1) as,

$$\psi(k, \bar{R}_R) = \frac{jk}{2\pi R_R} e^{-jk(R_T + R_R)} \int D(\bar{\rho}_0) e^{-j\bar{p} \cdot \bar{\rho}_0} d\bar{\rho}_0, \quad (2)$$

where we have used the fact that the observation point is in the far field of the object so that  $\exp(-jk \rho_0^2/2R_R)$  under the integral sign can be replaced by unity. In eq. (2),  $\bar{p} = k(\bar{I}_{k_i} - \bar{I}_R) \triangleq p_x \bar{I}_x + p_y \bar{I}_y + p_z \bar{I}_z$  is a three dimensional vector whose length and orientation depend

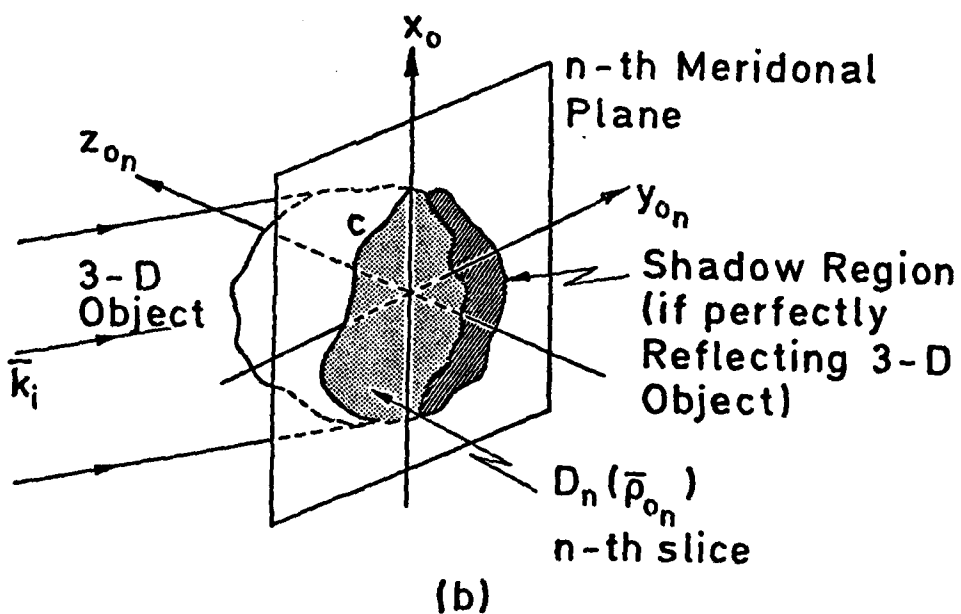
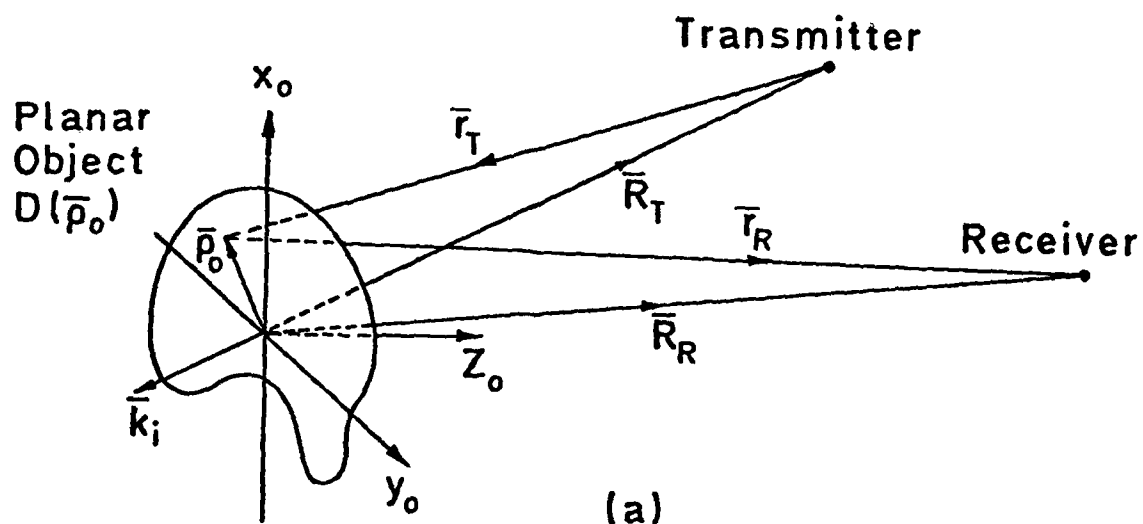


Fig. 1. Geometries for wavelength diversity imaging. (a) Two dimensional object, (b) Three dimensional object with the  $n$ -th meridional (central) slice and cross sectional outline  $c$  shown.



on the wavenumber  $k$  and the angular positions of the transmitter and the receiver. For each receiver and/or transmitter present,  $\bar{p}$  indicates the position vector for data storage. An array of receivers for example would yield therefore as  $k$  is changed (frequency diversity) or as  $\bar{k}$  ( $=k\bar{l}_{k_i}$ ) is changed (wave-vector diversity) a 3-D data manifold.

The projection of this 3-D data manifold on the object plane yields  $\psi(k, R_T)$  because  $\bar{p} \cdot \bar{p}_0 = \bar{p}_t \cdot \bar{p}_0 = p_x x_0 + p_y y_0$  where  $p_x = k(\bar{l}_{k_i} - \bar{l}_R)_x$  and  $p_y = k(\bar{l}_{k_i} - \bar{l}_R)_y$  are the cartesian components of the projection  $\bar{p}_t$  of  $\bar{p}$  on the object plane. Accordingly eq. (2) can be expressed as,

$$\psi(k, R_R) = \frac{jk}{2\pi R_R} e^{-jk(R_T + R_R)} \int D(x_0, y_0) e^{-j(p_x x_0 + p_y y_0)} dx_0 dy_0 \quad (3)$$

Because of the finite extent of the object, the limits on the integral can be extended to infinity without altering the result. The integral in (3) is recognized then as the two dimensional Fourier transform  $\tilde{D}(p_x, p_y)$  of  $D(x_0, y_0)$ . It is seen to be dependent on the object reflectivity function, the angular positions of the transmitter and the receiver and on the values assumed by the wavenumber  $k$  but is entirely independent of range. Information about  $D$  can thus be collected by varying these parameters. Note that the range information is contained solely in the factor  $F = jk \exp [-jk(R_T + R_R)]/2\pi R_R$  preceeding the integral. The field observed at  $\bar{R}_R$  has thus been separated into two terms one of which, the integral  $\tilde{D}$ , contains the lateral object information and the other  $F$ , contains the range information. The presence of  $F$  in eq. (3) hinders the imaging process since it complicates data acquisition and if not removed, gives rise to image distortion because  $R_R$  is generally not the same for all receivers. To retrieve an image of the object via a 2-D Fourier transform of eq. (3), the factor  $F$  must first be eliminated. Holographic recording of the complex field amplitude given in (3) using a reference point source located at the center of the object will result in the elimination of the factor  $F$  and the recording of a Fourier transform hologram. This operation yields  $\tilde{D}$  over a two dimensional region in the  $p_x, p_y$  plane.

The size of this region, which determines the resolution of the retrieved image depends on the angular positions of the transmitter and the receiver and on the values assumed by  $k$ , i.e. the extent of the spectral window used. The later dependence on  $k$  implies super-resolution imaging capability because of the frequency synthesized dimension of the 2-D data manifold generated. Because of the dependence of resolution on the relative positions of the object, the transmitter, and receiving aperture, the impulse response is clearly spatially variant. In fact a receiver point situated at  $\bar{R}_R$  for which  $\bar{p}$  is normal to the object

plane can not collect any lateral object information because for this condition ( $\bar{p} \cdot \bar{\rho}_0 = 0$ ) the integrals in (2) and (3) yield a constant.

Such receiving point is located in the direction of specular reflection from the object where the diffraction pattern is stationary i.e. does not change with  $k$ . In this case the observed field is solely proportional to  $F$  containing thus range information only. Obviously this case can easily be avoided through the use of more than one receiver which is required anyway when 2-D or 3-D object resolution is sought<sup>20,21</sup>.

The analysis presented above can be extended to three dimensional objects by viewing a 3-D object as a collection of thin meridional or central slices as depicted in Fig. 1(b) each of which representing a two dimensional object of the type analyzed above. With the  $n$ -th slice we associate a cartesian coordinate system  $x_{0n}, y_{0n}, z_{0n}$  that

differ from other slices by rotation about the common  $x_0$  axis. Since the vectors  $\bar{p}$ ,  $\bar{R}_T$  and  $\bar{R}_R$  are the same in all  $n$ -coordinate systems, eq. (3) holds.  $\psi_n(k, \bar{R}_R)$  is then obtained from projection of the three dimensional data manifold collected for the 3-D object on the  $x_{0n}, y_{0n}$  plane associated with the  $n$ -th slice. An image for each slice can then be obtained as described before. An inherent assumption in this argument is that all slices are illuminated by the same plane wave. This is a reasonable approximation when the 3-D object is weakly scattering and the Born approximation is applicable or when the 3-D object is perfectly reflecting and does not give rise to multiple reflections between its parts. In the later case the two dimensional meridional slices  $D_n(\bar{\rho}_{0n})$  deteriorate into contours, such as  $C$  in

Fig. 1(b) defined by the intersection of the meridional planes with the illuminated portion of the surface of the object. Accordingly we can write for the  $n$ -th meridional slice or contour,

$$\psi_n(k, \bar{R}_R) = F \int D_n(\bar{\rho}_{0n}) e^{-j\bar{p} \cdot \bar{\rho}_{0n}} d\bar{\rho}_{0n} \quad (4)$$

We can regard  $D_n(\bar{\rho}_{0n})$  as the  $n$ -th meridional slice or contour of a three dimensional object of reflectivity  $U(\bar{r})$  where  $\bar{r}$  is a three dimensional position vector in object space. This means that  $D_n(\bar{\rho}_{0n}) = U(\bar{r}) \delta(z_{0n})$  where  $\delta$  is the Dirac delta "function".

Consequently eq. (4) becomes,

$$\begin{aligned}
 \psi_n(k, R_R) &= F \int U(\vec{r}) \delta(z_{o_n}) e^{-j\vec{p} \cdot \vec{\rho}_{o_n}} d\vec{\rho}_{o_n} \\
 &= F \int U(\vec{r}) \delta(z_{o_n}) e^{-j\vec{p} \cdot \vec{r}} d\vec{r}
 \end{aligned} \tag{5}$$

where  $d\vec{r}$  designated an element of volume in object space and where the last equation is obtained by virtue of the sifting property of the delta function.

Summing up the data from all slices or contours of the object we obtain,

$$\sum_n \psi_n = F \int U(\vec{r}) e^{-j\vec{p} \cdot \vec{r}} d\vec{r} = \psi(\vec{p}) \tag{6}$$

because

$$\sum_n U(\vec{r}) \delta(z_{o_n}) = U(\vec{r}).$$

Assuming that the Factor F in eq. (6) is eliminated as before, equation (6) reduces to

$$\psi(\vec{p}) = \int U(\vec{r}) e^{-j\vec{p} \cdot \vec{r}} d\vec{r} \tag{7}$$

which is the 3-D Fourier transform of the object reflectivity  $U(\vec{r})$ . Wavelength diversity permits therefore accessing the 3-D Fourier space of a nondispersive object providing thereby the basis for 3-D Lensless Fourier transform holography. An alternate formulation to that given above of super-resolved wave-vector diversity imaging of 3-D perfectly conducting objects is possible<sup>22</sup> by extending the formulation of the inverse scattering imaging problem<sup>10,11</sup> to the multistatic case, along lines that are similar but somewhat different than those given by Raz<sup>12</sup>. The resulting scalarized formulas are identical to (7) establishing thus the connection between the holographic and the inverse scattering approaches to the imaging problem.

### THREE DIMENSIONAL IMAGE RETRIEVAL

The above considerations of multiwavelength holography have lead us to determining a means by which the 3-D Fourier space of the object can be accessed employing synchroneous detection. It is clear that once the 3-D Fourier space data is available, 3-D image detail can be retrieved by means of an inverse 3-D Fourier transform which can be carried out digitally. Alternately, holographic techniques

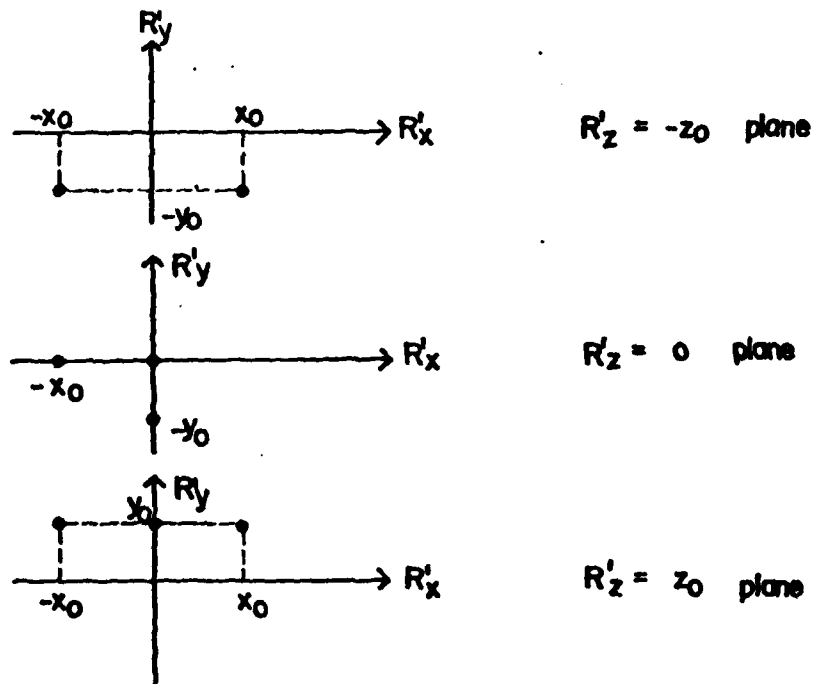
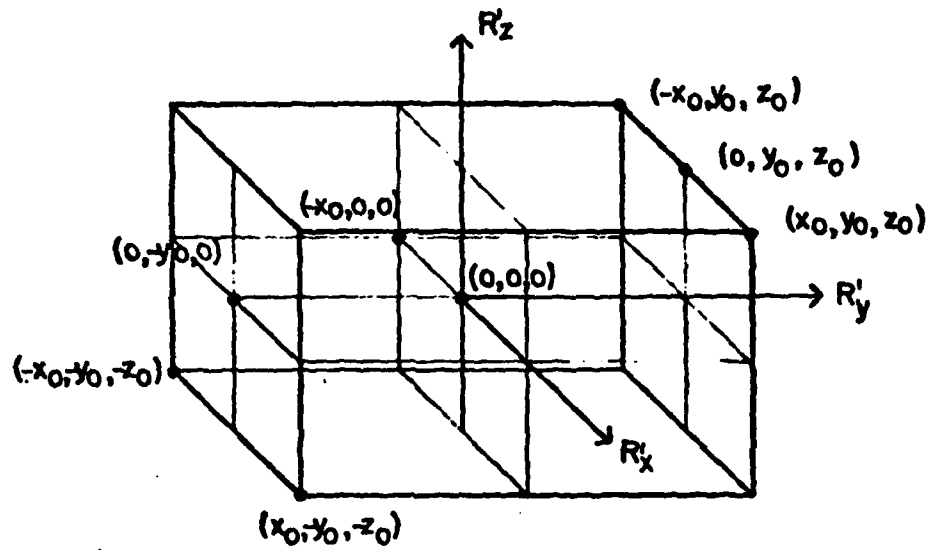


Fig. 2. 3-D object consisting of a set of eight point scatterers shown in isometric and  $R'_x$ - $R'_y$  plane views at  $R'_z = -z_0, 0, z_0$ .  $x_0 = y_0 = z_0 = 100$  cm.

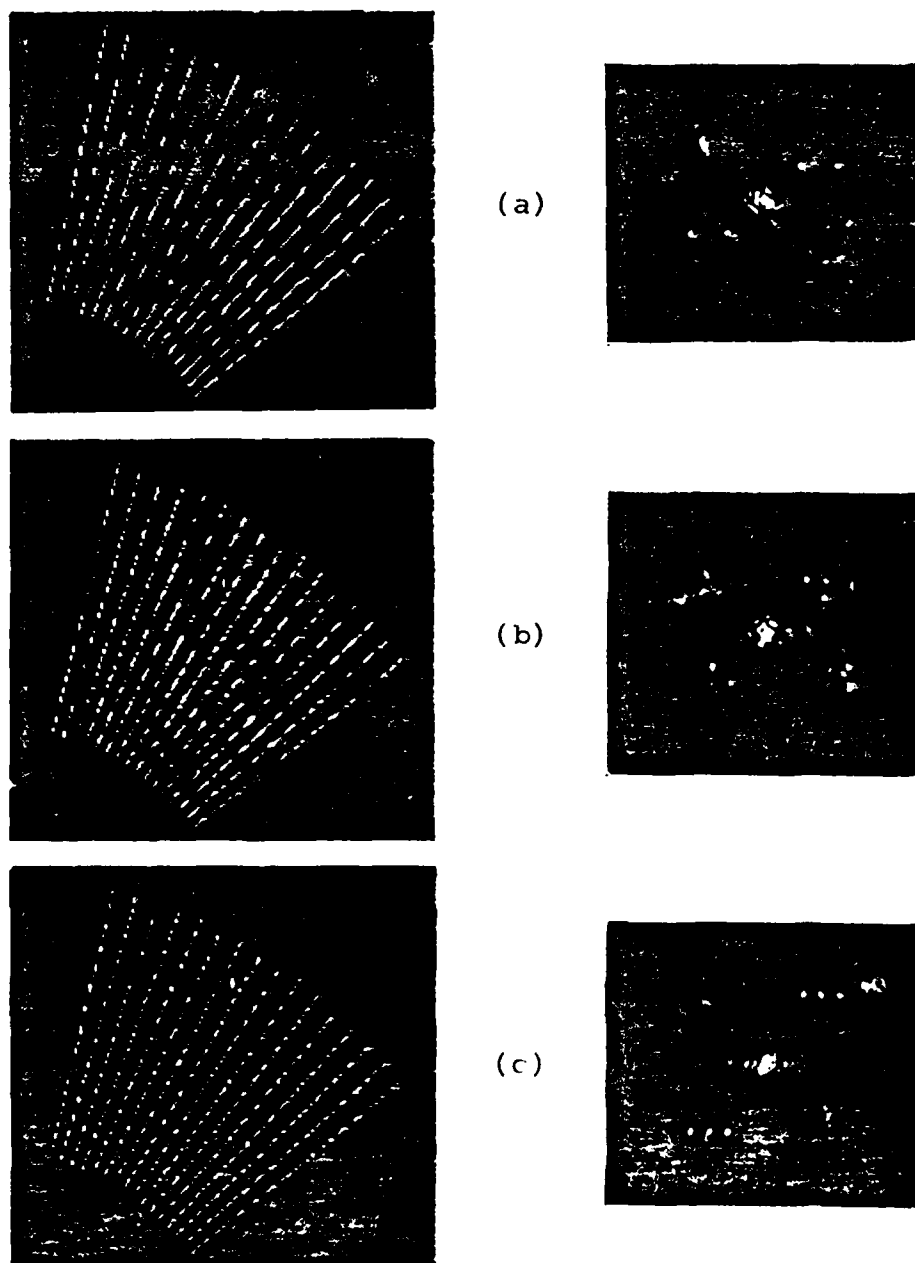


Fig. 3. Projection holograms and their optical reconstructions for the set of point scatterers in Fig. 2 at different  $R'_z$  planes. (a) Hologram and reconstructed image of scatterers at  $R'_z = -z_0$  plane. (b) Hologram and image at  $R'_z = 0$  plane. (c) Hologram and image at  $R'_z = z_0$  plane.  $x_0 = y_0 = z_0 = 100$  cm.

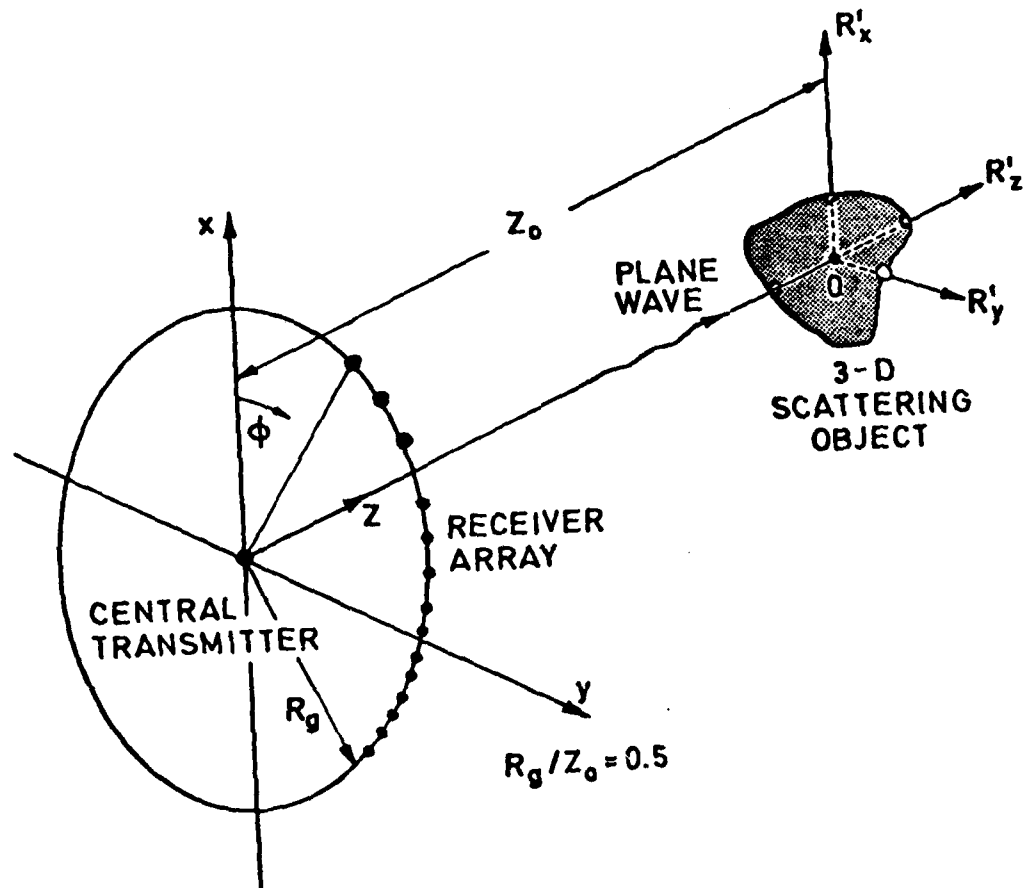


Fig. 4. Arrangement used in computer simulation of wavelength diversity imaging.

can be invoked again. Fourier domain projection theorems<sup>23</sup> that are dual to the spatial domain projection theorem<sup>25,26</sup> can be applied to the Fourier space data to produce a series of projection holograms from which 2-D images of meridional or parallel slices of the object can be retrieved on the optical bench<sup>20</sup>. This procedure does not involve any specific scaling of the size of the optical hologram transparency relative to the size of the original recording aperture by the ratio of the recording to the reconstruction wavelengths as in longwave holography where the scaling necessary for viewing a 3-D image free of longitudinal distortion usually leads to an impractically minute equivalent hologram transparency that cannot be readily viewed by an observer. The lateral and longitudinal resolutions in the retrieved image depend now on the dimensions of the volume in Fourier space accessed by wavelength diversity. This volume depends on the wavelength range and on the recording geometry. Thus the longitudinal resolution does not deteriorate now as rapidly with range as in conventional monochromatic imaging systems.

An example of computer simulations of frequency diversity holographic imaging of a 3-D object consisting of eight point scatterers distributed as shown in Fig. 2 is given in Fig. 3. Shown in Fig. 3 are three weighted Fourier domain projection holograms and the corresponding optically retrieved images for three equally spaced parallel slices of the object containing distinguishable 2-D distributions of scatterers. The simulated recording arrangement shown in Fig. 4 consisted of an array of 16 receivers equally distributed on an arc extending from  $\phi = 40^\circ$  to  $\phi = 77.5^\circ$  surrounding a central transmitter capable of providing plane wave illumination of the object. The results shown were obtained with microwave imaging in mind assuming a frequency sweep of (2-4)GHz. They clearly indicate a lateral and longitudinal resolution capability of the order of 25 cm. Wider sweep widths yield better resolution. For example a (1-18)GHz sweep would yield a 3-D resolution of the order of 1.5 cm.

## DISCUSSION AND CONCLUSIONS

Seeking means by which the information content in a hologram can be increased for example by wavelength diversity we have arrived at a formulation of 3-D Lensless Fourier transform holography capable of furnishing 3-D image detail tomographically. This ability of producing 3-D images in slices from coherently detected wavefields enable us to regard the method also as coherent tomography. The Fourier space accessed in the above fashion by wavelength diversity can be viewed as a generalized 3-D hologram in which one dimension has been synthesized by wavelength diversity. Such a generalized hologram contains not only spatial amplitude and phase data as in conventional holography but also spectral information and hence can yield better

resolution than the classical Rayleigh limit of the available aperture operating at the shortest wavelength of the spectral window used. This super-resolving property is further enhanced through an inherent suppression of the effects of object resonances and coherent noise in the retrieved image, the latter being so because frequency diversity tends to make the impulse response of the system unipolar resembling that of a non-coherent imaging system that is free of speckle and coherent noise artifacts<sup>15</sup>. Further enhancement of information content and resolution can be achieved by polarization diversity where the  $p$  space can be multiply accessed for different nonredundant polarizations of the illumination and the receivers and the resulting polarization diversity images added either coherently or non-coherently in order to achieve a degree of noise averaging as discussed elsewhere<sup>15</sup>.

The removal of several longstanding constraints on conventional longwave (microwave and acoustic) holography attained through the use of wavelength diversity as described here leads to a new class of imaging systems capable of converting spectral degrees of freedom into 3-D spatial image detail furnishing thereby true super-resolution. Wavelength diversity is applicable to the imaging of two classes of objects: perfectly reflecting objects of the type encountered in radar and sonar and weakly scattering objects of low or known dispersion of the type encountered in biology and medicine. The practical application of the concepts presented here to optical wavefield is presently under consideration. The availability of tunable dye lasers and electronic imaging devices suggest interesting possibilities of three dimensional wavelength diversity microscopy. Here one can conceive of an arrangement in which a minute semitransparent object with homogeneous or known dispersion is transilluminated by a collimated coherent light beam from a tunable dye laser which can also be made to provide a coherent reference point source in the immediate vicinity of the object. The resulting reference and the object scattered wavefields are intercepted by the photocathode of an electronic imaging device of known spectral response such as a vidicon. Because of the minute size of the object, the photocathode can easily be situated in the far field of the object. Thus nearly a lensless Fourier transform hologram recording arrangement results. The spatial frequency content in the resulting hologram is therefore expected to be sufficiently low to be resolved by a high resolution electronic imaging device. By recording and digitally storing the resulting detected hologram fringe pattern as a function of dye laser wavelength one can gain access to the 3-D Fourier space of the object since  $\bar{I}_{k_i}$  and  $\bar{I}_R$  for the recording geometry are precisely known.

A similar recording arrangement can be envisioned in the active coherent imaging of a distant reflecting object (active telescope) where the object can be made to furnish a reference point source situated on its surface like a wavelength independent stationary glint point or an intentionally placed retroreflector. Because in such an arrangement the reference and the object wavefields travel over the same path, atmospheric effects are expected to be minimized. The generation of an



object derived reference geometry in longwave (microwave and acoustic) wavelength diversity imaging has been described elsewhere<sup>20,27</sup>.

Finally it is worthwhile to note that since the scattering process is linear the multiaspect or multistatic frequency or wavelength response measurements referred to in this paper can be obtained also by measuring the multiaspect impulse response followed by Fourier transformation of the individual impulse responses measured<sup>19</sup>. This means that impulsive illumination can also be utilized. Because the impulse response of a linear system can be measured by using random noise excitation and cross-correlating the output with the input<sup>19</sup>, a possibility of using random noise (white light) illumination and cross-correlation detection techniques as a means for accessing the 3-D Fourier space of the object also emerges.

## REFERENCES

1. Schelkunoff, S.A., Bell Syst. Tech. J., 22, 80, (1943).
2. Anderson, A.P. and J.C. Bennet, Proc. IEE (letters), 64, 376, (1976).
3. DiFrancia, G.T., J. Opt. Soc. Am., 45, 497, (1955).
4. DiFrancia, G.T., J. Opt. Soc. Am., 59, 799, (1969).
5. Nassenstein, H., Optics Communications, 2, 231, (1970).
6. Wernecke, S.J. and L. D'Addario, IEEE Trans. on Computers, C-26, 351, (1977).
7. Lukosz, W., J. Opt. Soc. Am., 56, 1463, (1966).
8. Leith, E.N., Advances in Holography, 2, N. Farhat (Ed.), (M. Decker, New York. 1976).
9. Lukosz, W., J. Opt. Soc. Am., 57, 932, (1967).
10. Bojarski, N.N., Final Report, contract B000-19-73-C-0316, Naval Air Syst. Command, (1974).
11. Lewis, R.M., IEEE Trans. on Ant. and Prop., AP-17, 308, (1969).
12. Raz, S.R., IEEE Trans. on Ant. and Prop., AP-24, 66, (1976).
13. Meier, R.W., J. Opt. Soc. Am., 55, 987, (1965).
14. Smith, H.M., Principles of Holography, (Wiley-Interscience, New York, (1969).
15. Farhat, N.H. and C.K. Chan, in Optica Hoy Y Mañana, J. Bescos et. al. (eds.), (Sociedad Espanola De Optica, Madrid, 1978), 399.
16. Farhat, N.H., Ultrasonics Symposium Proceedings, IEEE Cat. No. 75 CHO 944-4SU, (1975).
17. Farhat, N.H., Proc. International Optical Computing Conference, IEEE Cat. No. 76-CH 1100-7C, (1976).
18. Farhat, N.H., Proc. IEEE (letters), 64, 379, (1976).
19. Farhat, N.H., J. Opt. Soc. Am., 67, 1015, (1977).
20. Farhat, N.H. and C.K. Chan, in Acoustical Imaging, A. Metherell (ed.), (Plenum, New York. 1980), 499.

21. Waters, W.M., Proc. IEEE (letters), 66, 609, (1978).
22. Chan C.K., Analytical and numerical studies of frequency swept imagery, Ph.D. Dissertation, Univ. of Pennsylvania, Philadelphia, (1978).
23. Stroke, G.W. and M. Halioua, Trans. Amer. Crystallographic Assoc., 12, 27, (1976).
24. Farhat, N.H., Univ. of Pennsylvania Report No. F1 Annual Report, AFOSR Grant No. 77-3256, July (1978).
25. Bracewell, R.N. and S.J. Wernecke, J. Opt. Soc. Am., 65, 1342, (1975).
26. Bracewell, R.N., Australian Journal of Physicas, 9, 198, (1956).
27. Farhat, N.H., C.K. Chan and T.H. Chu, Proc. AP-S/URSI, Symposium, Quebec, Canada (1980).

## APPENDIX III

### THE VIRTUAL FOURIER TRANSFORM AND ITS APPLICATION IN THREE DIMENSIONAL DISPLAY

#### ABSTRACT

In contrast to the well known and widely used instantaneous Fourier transforming property of the convergent lens in coherent (laser) light, the "Virtual Fourier Transform" (VFT) capability of the divergent lens is less widely known or used despite many advantages. We will review the principle of the VFT and discuss its advantages in certain applications. In particular a method for viewing the virtual Fourier transform of a two dimensional function with the naked eye using an ordinary point source will be presented. A scheme for three-dimensional image display based on a "Fourier domain projection theorem" utilizing varifocal VFT is described and a discussion of the properties of the displayed image given.

#### INTRODUCTION

Several sophisticated three dimensional (3-D) imaging techniques such as x-ray tomography<sup>1</sup>, electron microscopy<sup>2</sup>, crystallography<sup>2</sup>, wave-vector diversity imaging and inverse scattering<sup>3</sup>, involve measurements that give access to a finite volume in the 3-D Fourier space of a 3-D object function. A 3-D image of the original object can then be reconstructed by computing the inverse 3-D Fourier transform. The retrieved image normally represents the spatial distribution of a relevant parameter of the object such as absorption, reflectivity, scattering potential, etc.

Obviously, the required inverse transform can be performed digitally. Digital techniques however often preclude real-time operation particularly when the object being imaged is not simple but contains considerable resolvable intricate detail. More importantly, because of the inherent two dimensionality of CRT computer displays, direct true 3-D image display is not possible. Present day computer graphic displays are capable of displaying 3-D image detail either in separate cross-sections or slices, or in a computed perspective (isometric) view of the object, or in some instances stereoscopically where an illusion of a 3-D scene is created in the mind of the observer who is required usually to use special viewing glasses<sup>4,5</sup>.

Hybrid (opto-digital) computing techniques offer an alternate approach to 3-D image retrieval from 3-D Fourier space data. They furnish as shown in this paper the ability to display true 3-D image detail. The approach is based on "Fourier Domain Projection Theorems"<sup>2,3</sup> that are dual to "Spatial or Object Domain Projection Theorems" used in radio-astronomy<sup>6,7</sup> and tomography<sup>1</sup>. These theorems permit the reconstruction of 3-D image detail tomographically\* i.e. in slices from 2-D projections of the 3-D Fourier space data<sup>2,3</sup>. Although the required 2-D Fourier transform can be carried out digitally, the emphasis in this paper is on coherent optical techniques for performing the 2-D Fourier transform with particular attention to implementations that permit the execution of the necessary 2-D optical transforms of the various projection hologram sequentially in real-time. Specific attention is given to a technique that utilizes the virtual Fourier transform which permits the viewing of a virtual 3-D image in real-time.

#### FOURIER DOMAIN PROJECTION THEOREMS

There are two Fourier domain projection theorems. One leads to tomographic object reconstruction in parallel slices and is called the "weighted Fourier domain projection theorem"; the other leads to tomographic object reconstruction in meridional or central slices and can therefore be called the "meridional or central slice Fourier domain projection theorem".

We begin by considering a 3-D object function  $f(\vec{r})$  with  $\vec{r} = x\vec{I}_x + y\vec{I}_y + z\vec{I}_z$  being a position vector in object space. Let  $F(\vec{w})$  be the 3-D Fourier transform of  $f(\vec{r})$  defined by,

$$F(\vec{w}) = \int f(\vec{r}) e^{-j\vec{w} \cdot \vec{r}} d\vec{r} \quad (1)$$

where  $d\vec{r} = dx dy dz$  and  $\vec{w} = w_x\vec{I}_x + w_y\vec{I}_y + w_z\vec{I}_z$  is a position vector in the Fourier or spatial frequency domain.

Consider next the projection of  $F(\vec{w})$  on the  $w_x, w_y$  plane defined by,

$$F_p(w_x, w_y) = \int_{w_z} F(\vec{w}) dw_z \quad (2)$$

and combining eq. (1) and (2),

$$F_p(w_x, w_y) = \int_{w_z} \left\{ \iiint_{xyz} f(x, y, z) e^{-j(w_x x + w_y y + w_z z)} dx dy dz \right\} dw_z \quad (3)$$

\* From the Greek work Tomos meaning slice.

Integrating with respect to  $w_z$  first and assuming that the volume in  $\bar{w}$  space occupied by  $F(\bar{w})$  is sufficiently large we obtain,

$$F_p(w_x, w_y) = \int_x \int_y \int_z f(x, y, z) \delta(z) e^{-j(w_x x + w_y y)} dx dy dz \quad (4)$$

$$= \int_x \int_y f(x, y, 0) e^{-j(w_x x + w_y y)} dx dy \quad (5)$$

The 2-D Fourier domain projection  $F_p(w_x, w_y)$  and the central slice  $f(x, y, 0)$  through the object form thus a Fourier transform pair. This may be symbolically expressed as,

$$F_p(w_x, w_y) \leftrightarrow f(x, y, 0) \quad (6)$$

Other parallel slices through the object at  $z = z_n$ ,  $z_n$  being a constant describing the  $z$  coordinate of the  $n$ -th parallel slice, can in a similar manner be related to "weighted" Fourier domain projections of  $F(\bar{w})$  defined by,

$$F_{p,n}(w_x, w_y) = \int_{w_z} F(\bar{w}) e^{jz_n w_z} dw_z \quad (7)$$

Making use of eq. (1) and again performing the integration with respect to  $w_z$  first we obtain,

$$F_{p,n}(w_x, w_y) \leftrightarrow f(x, y, z_n) \quad (8)$$

which indicates that the weighted projection  $F_{p,n}(w_x, w_y)$  and the  $n$ -th parallel object slice  $f(x, y, z_n)$  form a Fourier transform pair.

Equation (6) is seen to be a special case of eq. (8) when  $z_n = 0$ .

Given the 3-D Fourier space data manifold  $F(\bar{w})$  one can digitally compute and display a set of "weighted projection holograms"  $F_{p,n}(w_x, w_y)$ .

A corresponding set of images of parallel slices or cross-sectional outlines of the 3-D object can then be retrieved via 2-D Fourier transform operations which can most conveniently be carried out optically from photographic transparency records of the weighted projection holograms displayed by the computer.

Returning to eqs. (1) and (2) one can also show that projections of  $F(\bar{w})$  on arbitrarily oriented planes other than the  $w_x, w_y$  plane chosen for eq. (2), yields "meridonal projection holograms" that are 2-D Fourier transforms of corresponding meridional (central) slices of the object. This is the "meridonal Fourier domain projection theorem". It furnishes the basis for angular multiplexing of the resulting meridonal projection holograms into a single composite hologram which can be used to form a 3-D image of the object in a manner similar to that in integral holography<sup>8</sup> which is increasingly being referred to as Cross holography\*.

### THE VIRTUAL FOURIER TRANSFORM

In contrast to the well known spatial Fourier transforming property<sup>9</sup> of the convergent lens widely used in coherent optical computing, the complementary virtual Fourier transform capability of a divergent lens<sup>10</sup> is less widely known or used despite many attractive features. This is surprising since the power spectrum associated with the VFT is a phenomenon that is frequently observed in daily life when one happens to look at a distant point source such as a street light through a fine mesh screen or the fine fabric of transparent curtain material. The spectrum of the screen transmittance appears then as a virtual image in the plane of the point source.

The VFT concept of the divergent lens is easily derived from the Fourier transform expression of the convergent lens. Figure 1 illustrates the well known process of forming a real Fourier transform with a convergent lens. The object transparency, with complex transmittance  $t(x_0, y_0)$ , is placed at a distance  $d$  in front of a convergent lens of focal length  $F$  and illuminated with a normally incident collimated laser beam. The complex field amplitude of the wavefield in the back focal plane, the transform plane, is given by the well known formula

$$T(x, y) = \frac{j}{\lambda F} e^{-jk \frac{d}{2F} [(1 - \frac{d}{F})(x^2 + y^2)]} \times \iint_{-\infty}^{\infty} t(x_0, y_0) e^{jk \frac{d}{F} (x x_0 + y y_0)} dx_0 dy_0 \quad (1)$$

in which the integral is recognized as the two dimensional Fourier transform of the object transmittance.  $T(x, y)$  becomes the exact Fourier transform of  $t(x_0, y_0)$  when  $d = F$  that is when the object transparency is placed in the Front focal plane of the lens. The power spectrum associated with the transform is real and can be projected on a screen placed in the back focal plane. It is also well known that a scaled version of the transform can be obtained in the back focal plane by placing the object transparency in the converging laser beam to the right of the lens<sup>9</sup>.

\* Named after Lloyd Cross the originator of integral holography.

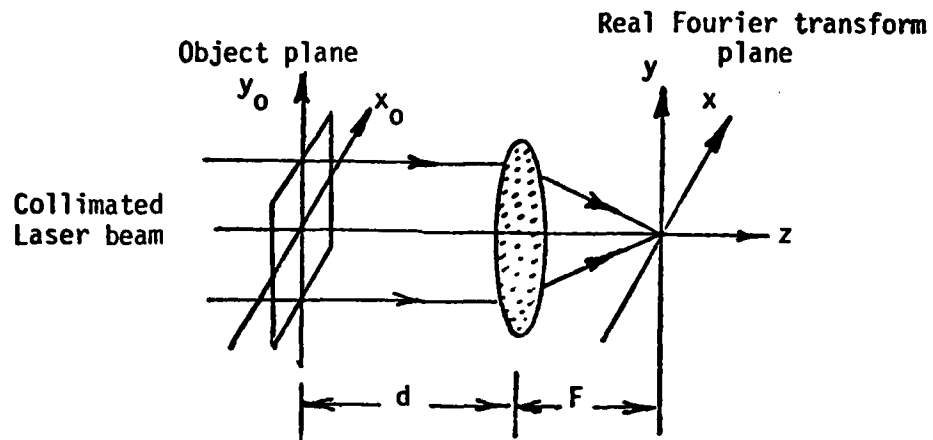


Fig. 1. Real Fourier transform formed with a convergent lens

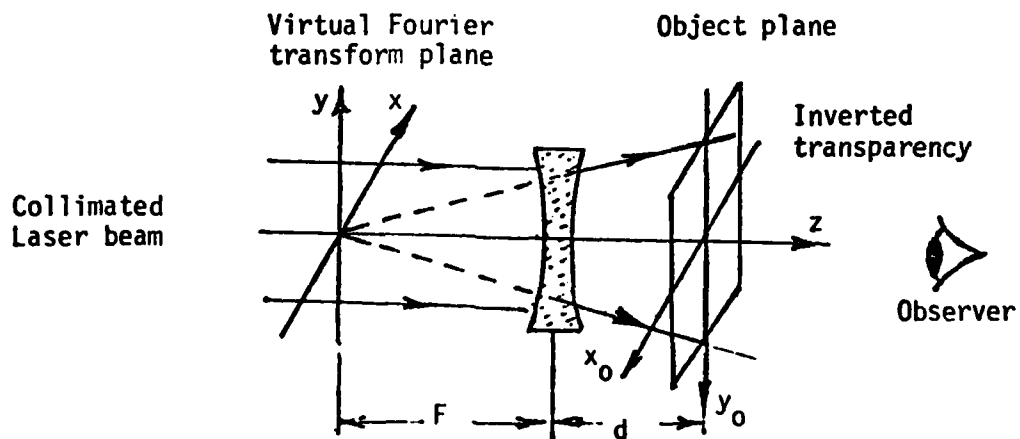


Fig. 2. Virtual Fourier transform formed with a divergent lens



Noting that eq. (1) does not change when we replace  $d$  by  $-d$ ,  $F$  by  $-F$ ,  $x_0$  and  $y_0$  by  $-x_0$  and  $-y_0$  respectively, we can arrive at the complementary VFT arrangement illustrated in Fig. 2. An inverted transparency  $t(x_0, y_0)$  is placed now in the divergent coherent beam to the right of the divergent lens (of focal length  $-F$ ) and a VFT given by eq. (1) is observed in the virtual focal plane of the lens. The same VFT can be seen by removing the divergent lens and replacing the laser beam with a point source placed at the origin of the VFT plane as depicted in Fig. 3. Thus a simple way of viewing the power spectrum associated with the VFT of a given diffracting screen (which is usually a Fourier transform hologram or a projection hologram of the type described above) is to hold the screen close to the eye and look through it at a distant bright point source. The point source used need not be derived from a laser. In fact it is preferable for safety purposes to use an LED or a spectrally filtered minute white light source such as a "grain-of-wheat" subminiature incandescent lamp or a miniature Christmas tree decorating lamp covered by a color or interference filter. This has the added advantage of furnishing a measure of control over the coherence properties of the wavefield impinging on the screen providing thereby a means for reducing coherent noise in the observed VFT and also, as will be discussed below, a means for coherent or noncoherent superposition of VFT's. As the distance of the point source from the diffracting screen is decreased in order to make it compatible with typical laboratory or optical bench dimensions, the size of the observed VFT decreased because of the change in the curvature of the wavefield illuminating the diffracting screen. To compensate for this effect it is necessary to reduce the size of the diffracting screen or transparency often to such a scale where viewing the VFT through the small available aperture becomes difficult. To overcome this limitation the displacement property of the Fourier transform can be utilized. A composite transparency containing an ordered or random array of reduced replicas of the transmittance function  $t(x_0, y_0)$  arranged side by side as illustrated in Fig. 4 is prepared. When such a composite transparency is viewed with the point source, the VFT's formed by the individual elements will overlap in the virtual Fourier plane. The VFT's are identical except for linear phase dependence on  $x, y$  which depends in each VFT on the central position of each element in the composite transparency. This leads to a desirable noise averaging effect and the appearance of fine checkered texture in the image detail. All this leads to an enhancement of the quality of the observed power spectrum. Both coherent and noncoherent superposition of the overlapping VFT's is possible using this scheme by varying the coherence area of the wavefield illuminating the composite transparency. When the coherence area is roughly equal to the size of the individual elements of the composite transparency noncoherent superposition results, while a coherence area equal or greater than the size of the composite transparency would yield coherent superposition.

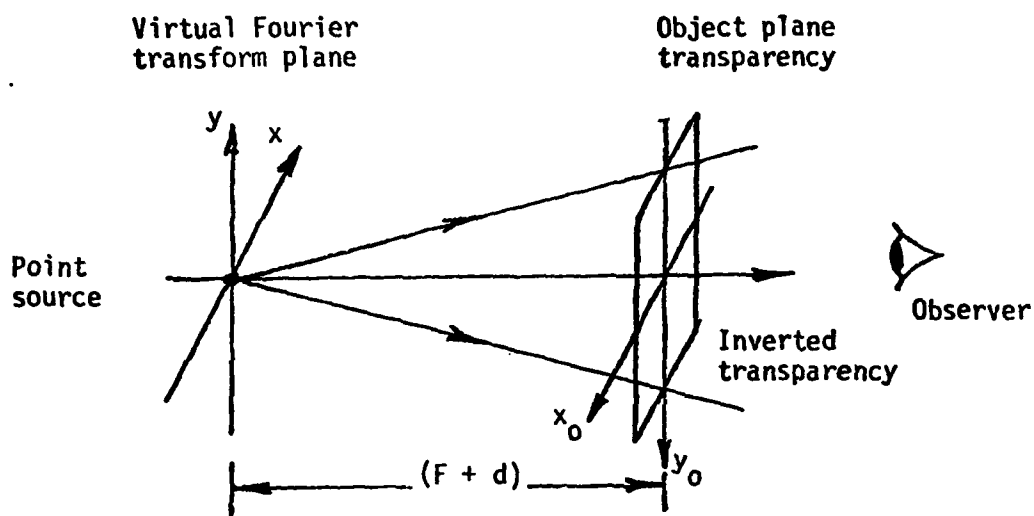


Fig. 3. Arrangement for viewing a virtual Fourier transform with a point source

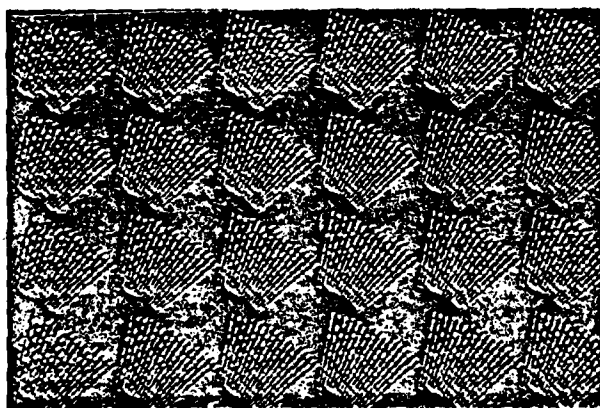


Fig. 4. A composite screen consisting of an ordered array of identical Fourier transform projection holograms.

## THREE DIMENSIONAL DISPLAY

The VFT concept and the "weighted Fourier domain projection theorem" discussed above can be combined in an attractive scheme for the reconstruction and display of a 3-D image from a series of weighted projection holograms corresponding to different parallel slices through the object. The scheme is based on viewing a series of weighted projection holograms sequentially in the proper order of the occurrence of their corresponding slices in the original object while displacing the point source axially for one hologram to next by an axial increment proportional to the spacings between adjacent object slices. In this fashion the reconstructed virtual images of the various slices are seen in depth at different VFT planes that are determined by the positions of the axially incremented point source. Repeated rapid execution of this procedure by displacing the point source back and forth leads the observer to see a virtual 3-D image tomographically in parallel slices or sections as he looks through the series of projection holograms passed rapidly, as in a motion picture film, in front of his eyes.

More specifically the scheme is based on preparing a series of  $N$  weighted Fourier domain projection holograms from the 3-D Fourier domain data  $F(\vec{w})$  of a given object  $f(\vec{r})$  as described in the preceding sections. Each of the projection holograms would correspond to a different parallel slice through the object. A composite transparency similar to that shown in Fig. 4 is formed for each projection hologram. In fact Fig. 4 is an example of a computer generated composite hologram containing an array of identical weighted projection holograms corresponding to one slice of the test object shown in Fig. 5. The test object chosen consisted of eight point scatterers arranged as shown. The 3-D Fourier space of this test object was accessed in a computer simulation of wavelength diversity imaging as described in a companion paper in this volume\*. The resulting computer generated Fourier space data manifold  $F(\vec{w})$  was used to compute three weighted projection holograms corresponding to the three planes  $R'_2 = 1m, 0, 1m$  of Fig. 5

containing the three different distributions of point scatterers. A composite array such as that of Fig. 4 was formed and displayed by the computer for each of the three projection holograms, each was photographed yielding a set of three projection hologram composite transparencies. Copies of these were then mounted on a rotating wheel as shown in Fig. 6 (a) and viewed with an axially scanned point source. Four sets of transparency copies of these three composite projection holograms were mounted in the order 1,2,3,2,1,2 ... on the periphery of a rotating wheel as shown in Fig. 6 (a). The wheel is driven by a computer controlled stepper motor. The axially scanned point source was produced by scanning a focused laser beam back and forth on a length of fine nylon thread with the aid of a deflecting mirror mounted on the shaft of a second computer controlled stepper motor as shown in Fig. 6 (b). The laser and optical bench arrangement for forming the scanned focused beam appear in the background of Fig. 6 (a). The computer controlled steppers enable precise positioning of the secondary point source on the scattering thread in synchronism with the hologram

\*See paper entitled "Holography, Wavelength Diversity Inverse Scattering" in this volume.

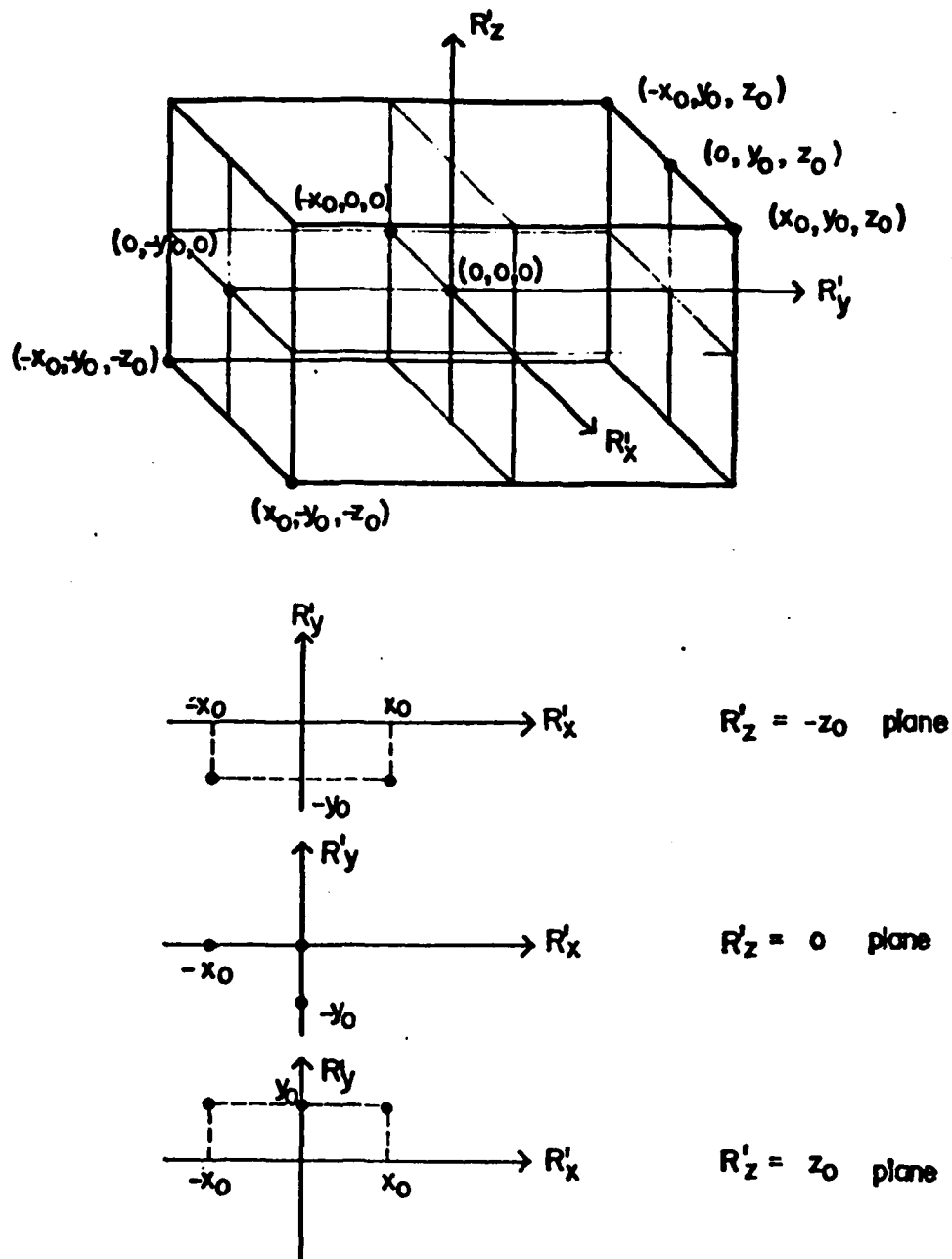
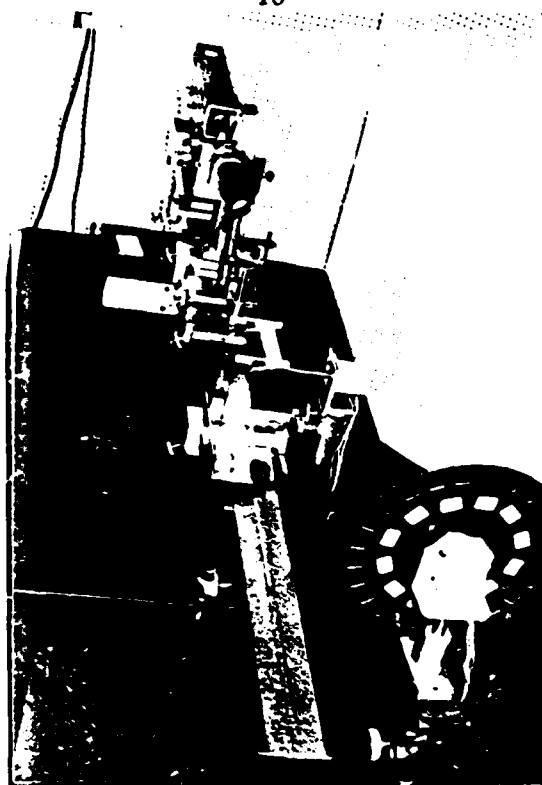
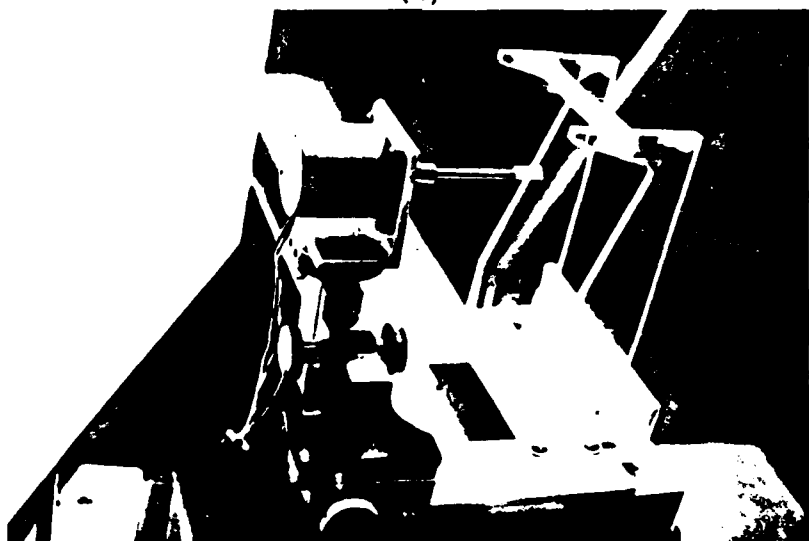


Fig. 5. A three-dimensional test object consisting of a set of eight point scatterers shown in isometric and  $R'_x$ - $R'_y$  plane views at  $R'_z = -z_0, 0, z_0$ .  $x_0 = y_0 = z_0 = 100$  cm.



(a)



(b)

Fig. 6. Quasi real-time three-dimensional image reconstruction and tomographic display in successive slices from a series of projection holograms mounted on rotating wheel seen in fore-front of (a); Detail of laser scanner used to produce linearly scanned point source is shown in (b).



(c)

(b)

(a)

Fig. 7. Photographs of three slices of the virtual 3-D image of the test object of Fig. 5 obtained by photographing the VFT's formed from corresponding Fourier domain projection holograms.

being viewed so that the VFTs are formed in their proper planes. A viewer looking at the axially displaced point source through each transparency mounted on the wheel as it passes in front of his eye will see a 3-D virtual image. Photographs of the three virtual images seen by an observer in this fashion are shown in Fig. 7. An opto-digital scheme for rapid real-time implementation of the procedure realized above is shown in Fig. 8. This scheme, presently under study, utilizes a rapid recyclable spatial light modulator (SLM) such as the Itek PROM in order to form VFT's of the projection holograms displayed by the computer in real-time.

### CONCLUSIONS

We have presented the basic principles of tomographic 3-D image display based on Fourier domain projection theorems. One possible implementation of the principle using the virtual Fourier transform and a series Fourier domain projection holograms has been described. There are several advantages for using the VFT rather than the real Fourier transform (RFT), the most important of which is the ease with which the position of the VFT plane can be moved axially by simply moving the position of the reconstruction point source. The VFT approach was adopted in the present study because it is much easier to move a point source rapidly than to move the display screen needed in the RFT approach. Furthermore focusing in the VFT approach is carried out by the observer while in the RFT approach it must be performed by the system. Other attractive features of the VFT are:

- (a) Simplicity - enables direct viewing of the power spectrum of a transparency or a hologram with a variety of simple point sources.
- (b) The scale of the observed VFT can be easily altered by changing the distance between the projection hologram transparency and the reconstruction point source.
- (c) Lower speckle noise and therefore higher reconstructed image quality can be attained by using nonlaser point sources in the reconstruction such as LED or miniature spectrally filtered incandescent lamps. Further reduction in speckle noise occurs when an array of the projection hologram rather than a single hologram is used and when the hologram is slightly vibrated or is in motion because of a noise averaging effect.
- (d) Coherent and noncoherent superposition of VFT's is possible by altering the coherence area of the reconstruction wavefield.
- (e) Because of the Fourier transform nature of the projection holograms utilized, the resolution requirements from the storage medium (photographic film or the CRT/SLM system of Fig. 8) are much lower than would be needed in the recording of a Fresnel hologram of the object as a means of 3-D image display. The 3-D image detail contained in the single Fresnel hologram is now distributed over a series of lower resolution projection holograms which are used to form the 3-D image sequentially in time in individual slices.

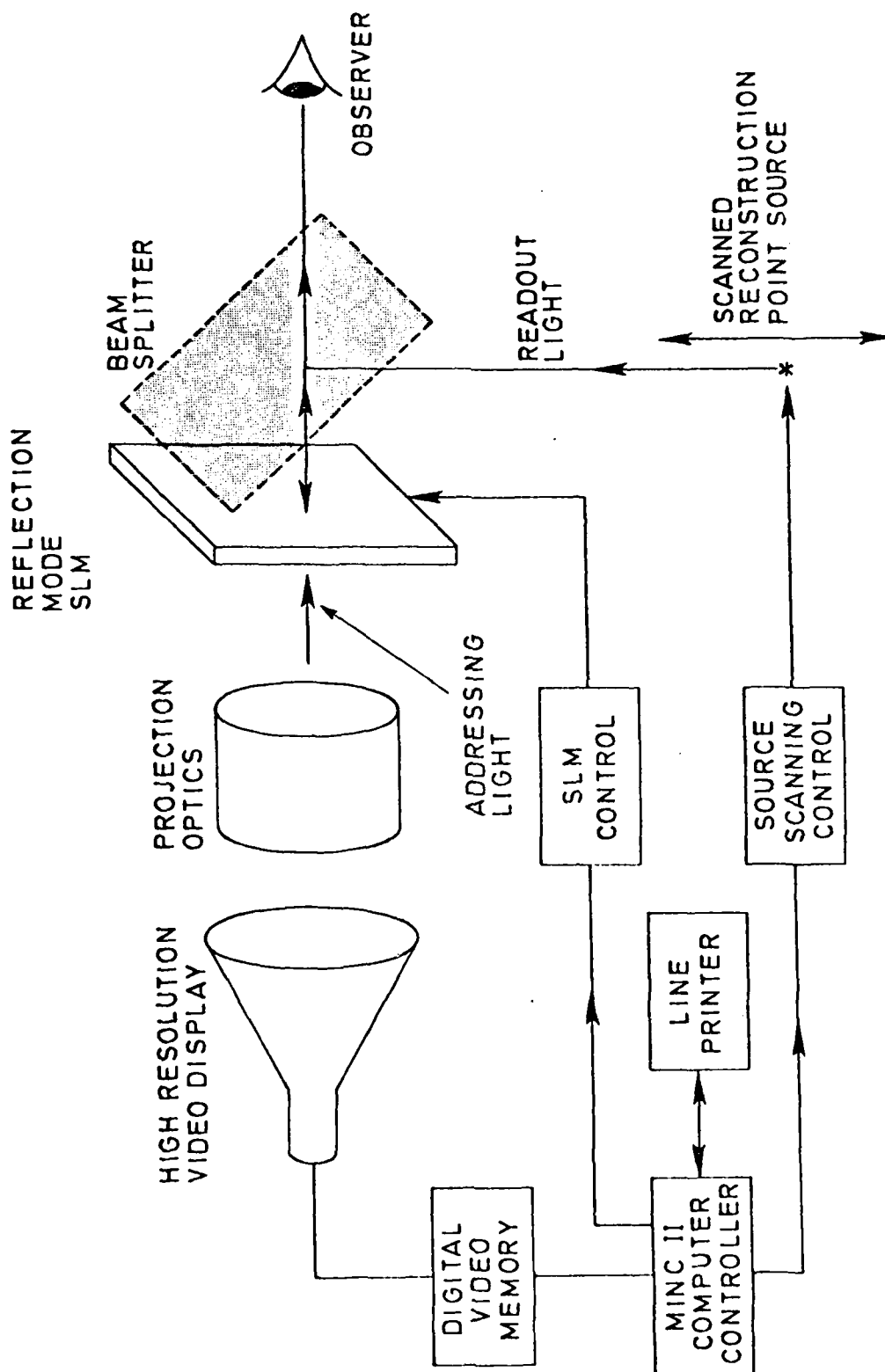


Fig. 8. Opto-digital scheme for the reconstruction and display of 3-D images using a recyclable spatial light modulator and a point source to view the VFT in real-time.



(f) Because 3-D image reconstruction is tomographic (in separate slices) there is no interference between the wavefields forming the various slices.

(g) Permits other forms of 3-D image display involving spatial or angular multiplexing in a fashion similar to integral holography.

## REFERENCES

1. H.H. Barret and M.Y. Chiu, *Optica Hoy Y Manãna*, J. Bescos et.al., (eds.) 136, (Proc. of ICO-11, Sociedad Española De Optica, 1978).
2. N.H. Farhat and C.K. Chan, *Acoustical Imaging*, 8, 499, A. Methere1 (ed.), (Plenum Press, New York, 1980).
3. G.W. Stroke and M. Halioua, *Trans. Amer. Crystallographic Assoc.*, 12, 27, (1976).
4. T. Okoshi, *Three-Dimensional Imaging Techniques*, (Academic Press, New York, 1976).
5. T. Okoshi, *Proc. IEEE*, 68, 548, (1980).
6. R.N. Bracewell, *Australian Journal of Physics*, 9, 148, (1956).
7. R.N. Bracewell and S.J. Wernecke, *J. Opt. Soc. Am.*, 65, 1342, (1975).
8. D.L. Vickers, *Lawerence Livermore Laboratory Report*, No. UCID-17035, (February 1976).
9. J.W. Goodman, *Introduction to Fourier Optics*, 83, (McGraw Hill, New York, 1968).
10. J. Knapp and M.F. Becker, *App. Optics*, 17, 1669, (1976).

APPENDIX IV

AN AUTOMATED FREQUENCY RESPONSE AND  
RADAR CROSS-SECTION MEASUREMENT FACILITY  
FOR MICROWAVE IMAGING

UNIVERSITY OF PENNSYLVANIA

THE MOORE SCHOOL OF ELECTRICAL ENGINEERING

AN AUTOMATED FREQUENCY RESPONSE AND RADAR CROSS-SECTION  
MEASUREMENT FACILITY FOR MICROWAVE IMAGING

CHARLES L. WERNER

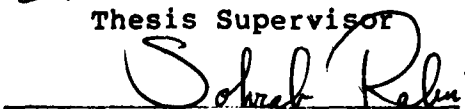
Presented to the faculty of the Moore School of Electrical  
Engineering (Department of Electrical Engineering &  
Science) in partial fulfillment of the requirements for the  
degree of Master of Science in Engineering.

Philadelphia, Pennsylvania

May 1980



Thesis Supervisor



Graduate Group Chairman

UNIVERSITY OF PENNSYLVANIA

THE MOORE SCHOOL OF ELECTRICAL ENGINEERING

AN AUTOMATED FREQUENCY RESPONSE AND RADAR CROSS-SECTION  
MEASUREMENT FACILITY FOR MICROWAVE IMAGING

ABSTRACT

This thesis investigates the development of a broadband microwave holographic imaging facility. Different methods for the correction of microwave target scatter data are discussed and implemented. A minicomputer automates all system functions including data acquisition, storage, calculation, and graphic display. The effects of range phase shift on holographic frequency diversity imaging is considered and techniques for the removal of this phase shift in a laboratory environment. The frequency dependent backscatter of several test targets is derived analytically and simulations done of the corresponding holograms. These holograms are compared to those measured experimentally. Finally both simulated and experimental holograms are optically reconstructed to yield target images using optical Fourier transforms and shown to be in excellent agreement.

Degree: Master of Science in Engineering for graduate work  
in electrical Engineering and Science

Date: May 1980

Charles L. Werner

Author

## ACKNOWLEDGEMENTS

I would like to extend my most sincere thanks to Dr. Nabil H. Farhat for making my studies at the University of Pennsylvania possible. His patience and wisdom were an inspiration for my research. I would also like to thank my parents for their love and understanding these many years. Finally I want to express appreciation to the Moore School for giving me the chance to study here.

## TABLE OF CONTENTS

I.....	INTRODUCTION	1
II.....	SYSTEM OPERATION AND ERROR REMOVAL	
2.1.....	Microwave sweeper operation	4
2.2.....	Network analyzer-computer interface	6
2.3.....	Implementation of the data aquisition system	9
2.4.....	System error correction	13
III.....	RANGE PHASE ANALYSIS	
3.1.....	The effects of range phase on imaging	27
3.2.....	Practical considerations for range phase removal	38
IV.....	SYSTEM IMPLEMENTATION OF SWEPT FREQUENCY IMAGING	
4.1.....	System repeatability	41
4.2.....	Computer control of target rotation	43
4.3.....	Sphere simulation	45
4.4.....	Simulation of frequency swept imaging	53
4.5.....	Experimental results	60
V.....	CONCLUSION	72
	BIBLIOGRAPHY	74
	Appendix I...Error Correction Programs and Utilities	
	Appendix II..Microwave imaging programs-acquisition and display	

## I INTRODUCTION

Frequency diversity imaging has been under study at the Electro-Optics and Microwave Optics laboratory of the Moore School Graduate Research Center.[1],[2],[3],[4] This study has established the theoretic feasibility of imaging objects by means of their multiaspect frequency response. For the purpose of experimentally studying frequency diversity imaging, an experimental measurement system has been assembled and installed in the Moore School anechoic chamber. In this thesis we will describe the automation of this measurement system and characterize its performance in the measurement of complex field amplitudes of scattered fields. A system block diagram fig.1.1, shows the major system components. The central element is the DEC MINC LSI 11/2 minicomputer. This computer performs several important functions. The MINC controls laboratory instrumentation via the IEEE-488 bus protocol standard. This allows the Hewlett-Packard 8620C microwave sweeper to be precisely tuned to any frequency in the 2.0 to 18.0 GHz range (fig.1.2). The computer collects data from the HP 8410B network analyzer through the four analog input channels available. These analog values are proportional to the amplitude in db and phase in the range  $(-\pi)$  to  $(+\pi)$  radians relative to the reference signal supplied to the network analyzer. The computer stores Experimental data on floppy discs. The available storage capacity is large, over 500,000 measurement pairs of complex field amplitude and

1



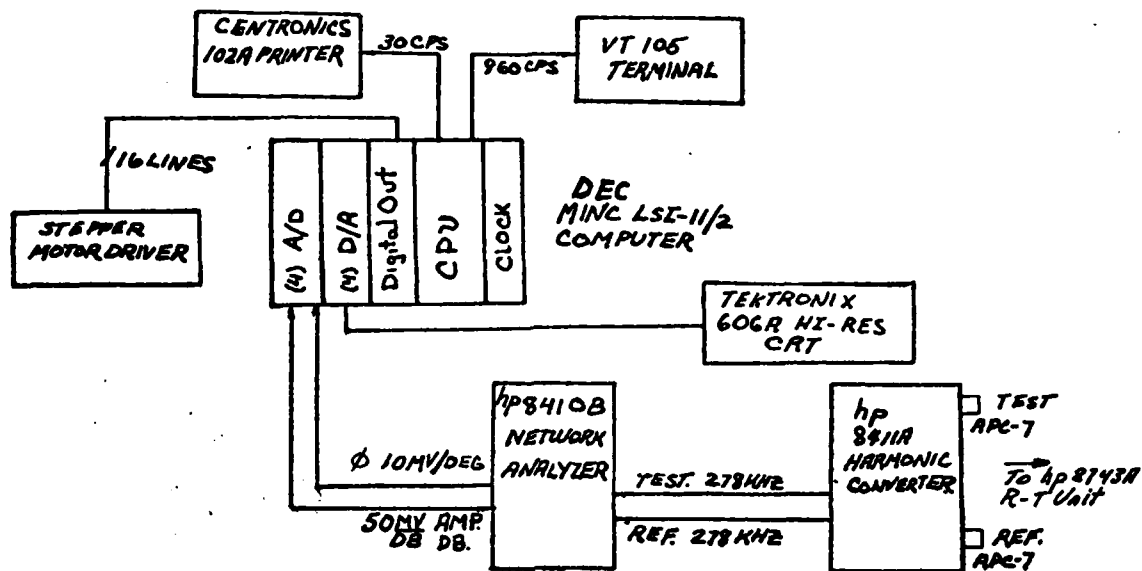


Fig. 1.1 System block diagram.



Fig. 1.2 HP 8620C microwave sweeper and HP 1410B network analyzer.

phase may be stored on a single disc. This data can be accessed for both processing and display on a Tektronix 606A high resolution CRT monitor. The disc system allows the MINC to operate under a sophisticated software system, DEC RT-11 V3.0B permitting programming in MINC BASIC, FORTRAN IV, and MACRO languages.

The processing capability of the system allows the removal of system response errors due to anechoic chamber clutter, antenna cross-coupling and receiver channel characteristics. The data may be processed for target range calculations and the removal of the phase shift due to the target range. In addition the collected data may be filtered to improve imaging and finally displayed on a high resolution Tektronix 606A X-Y CRT monitor using the MINC system D/A converter module.

The second part of this thesis will describe the simulation and actual operation of a holographic radar system verifying the theory of frequency diversity imaging. This is done using the system described in the first section. The scattering of various targets is derived and holograms using these results are generated for comparison with experimental data. Finally a system for the experimental measurement of the scattering for these targets is outlined and the results from this system compared to theory.

## II SYSTEM OPERATION AND ERROR REMOVAL

This chapter will cover the operation of the microwave backscatter data acquisition system. This will include actual interfacing information and an analysis of the types of errors encountered when making microwave measurements. The error correction techniques developed are later used in the experimental verification of the frequency diversity imaging theory.[4]

### 2.1 Microwave sweeper operation

The first task in the development of an automated data acquisition system is the implementation of a data communications link between the intelligent controller and instrumentation. The IEEE-488 bus protocol is utilized in this application for the transfer of data to the Hewlett-Packard 8620C microwave sweeper from the MINC LSI 11/2 computer. This bus is a high speed 8 bit wide bidirectional data path with 5 additional lines dedicated to control. Data is transferred in ASCII format over the bus. For example the number 1 is transmitted as the ASCII code for the character '1'. Certain sequences of characters make the sweeper perform different functions or enter different modes of operation via its IEEE-488 interface.

In order to set the frequency of the sweeper a number must be sent to the IEEE-488 interface in the range 1-10000. Each sweeper frequency band has been split into 10000 frequency points. The frequency of operation is controlled

by an internal analog voltage that varies between 0.0 and 10.0 volts. A D/A converter on the 8620C IEEE-488 interface changes the data transmitted from the MINC into the frequency controlling voltage. The correspondence between voltage and output frequency is essentially linear. In order to obtain the interpolating function for frequency versus control voltage; a microwave frequency counter was used to measure the voltage-frequency characteristic function. Using the MINC-BASIC program CALAB.BAS a least squares fit for both linear and quadratic functions was made on the frequency vs voltage data. This type of program is used for determining the best polynomial fit to the frequency-voltage characteristic of the sweeper. Sample output and program listings are in appendix I along with an explanation of program operation. The results from this work indicate that the quadratic fit was statistically superior for all bands on the microwave sweeper. The FORTRAN subroutine SWEEP was written which utilizes the quadratic interpolation polynomial for each of the four bands of the 8620C. This subroutine automatically calculates the control voltage and band to generate any frequency in the 2-18 GHz range and transmits the appropriate commands over the IEEE-488 bus. The variance of the frequency setting using the quadratic fit for the three bands are as follows: .6 MHz in the 2.0-6.3 GHz band; 1.2 MHz in the 6.3-12.0 GHz band; and 1.6 MHz in the 12.0-18.0 GHz band. For higher accuracy the sweeper may be phase

locked to the reference in a locking frequency counter yielding very high accuracy as precise as the frequency reference itself. The EIP 371 locking counter may be used in this application to lock the HP 8620C sweep oscillator to the correct frequency once it is within 20 MHz of the desired frequency. The auxiliary output of the HP 8620C supplies a sample of the signal generated by the fundamental 2.0-6.3 GHz oscillator module within the sweeper to the locking counter. Sweeper output on higher bands is this fundamental multiplied by a factor of 2 or 3 for the 6.3-12.0 and 12.0-18.00 GHz bands respectively. For example the locking frequency for a 10.0 GHz sweeper output on band 2 would be 5.0 GHz. In operation, subroutine SWEEP will set the frequency of the sweeper within 2.0 MHz of the desired frequency and subroutine SLOCK will be called to calculate the locking frequency; lock the HP 8620C and return to the main calling routine when lock will have occurred. Lock time varies from .1 to 3 seconds and resolution is 100 KHz. These subroutines are called whenever the sweeper must be set to a particular frequency or the sweeper must be placed in or be released from computer control.

## 2.2 Network analyzer-computer interface

The Hewlett-Packard 8410B network analyzer is the focus of the measurement capabilities of the microwave measurement system. It can make vector (amplitude and phase) measurements in the (.1-18.0)GHz range. The range of amplitude measurement is 80<sub>6</sub> db and phase may be measured

modulo ( $2\pi$ ). The system reference signal is fed from a 20db directional coupler to the HP8411A harmonic converter sampling head of the network analyzer. This reference is compared to the backscatter from the illuminated target; both in amplitude and phase. The reference signal amplitude is kept constant by leveling the sweeper with a feedback signal derived from its amplified output by means of a crystal detector. This allows the sweeper-TWT (Traveling Wave Tube) system to yield nearly constant output in the (2.0-16.5) GHz range; see fig.2.1. TWT power output is on the order of 1 watt over these frequencies.

The complex field amplitude measurements are available as analog voltages from the back panel of the 8410B. The outputs are proportional to amplitude and phase: 25 MV/db and 10 MV/DEGREE. These values are digitized by the MINC using its built in analog to digital conversion channels. The MINC A/D converters digitize voltages lying in the range of -5.12 to +5.12 volts to the range of 0-4096 yielding 12 bit resolution. If the signal is corrupted by noise; the user has the option of employing signal averaging to cancel the effects of noise uncorrelated to the received signal.

A difficulty encountered when measuring phase angle modulo ( $2\pi$ ) occurs when the phase is close to  $(+\pi)$  or  $(-\pi)$ . At this point a small change in the signal phase may cause the phase to flip between these two equivalent extremes rapidly. If a data sample is taken close to  $(+\pi)$  or  $(-\pi)$  it may be in transition between them and therefore incorrect.

Since such points occur infrequently in a typical measurement they may be ignored. ;their presence does not seriously hinder any holographic imaging due to the inherent redundancy and therefore noise immunity of the holographic reconstruction process.[5] If it is desired that these points be identified and removed it is necessary to estimate the mean and variance of the samples taken at each frequency point. At frequencies where the phase is flipping between  $(+\pi)$  and  $(-\pi)$ , the variance will be much larger than at other frequencies. The mean of the samples when this is occurring will be near zero. Hence to resolve the ambiguity problem it is necessary to decide if the variance exceeds a predetermined threshold when the mean in the neighborhood of zero. Two FORTRAN subroutines PHAMP and PHAMP2 which implement these algorithms are listed in appendix I.

Since such points occur infrequently in a typical measurement they may be ignored. ;their presence does not seriously hinder any holographic imaging due to the inherent redundancy and therefore noise immunity of the holographic reconstruction process.[5] If it is desired that these points be identified and removed it is necessary to estimate the mean and variance of the samples taken at each frequency point. At frequencies where the phase is flipping between  $(+\pi)$  and  $(-\pi)$ , the variance will be much larger than at other frequencies. The mean of the samples when this is occurring will be near zero. Hence to resolve the ambiguity problem it is necessary to decide if the variance exceeds a predetermined threshold when the mean in the neighborhood of zero. Two FORTRAN subroutines PHAMP and PHAMP2 which implement these algorithms are listed in appendix I.



### 2.3 Implementation of the data acquisition system

In an experimental environment it is important to be aware of the various types of errors inherent in the equipment and the experimental procedure adopted. Conditions and equipment always vary from theoretical ideals. A clear understanding of the error removal process leads to the development of practical implementations of theoretical concepts and enhancement of measurement accuracy unattainable otherwise.

Errors in complex field amplitude measurement may be caused by several factors. These may be grouped into two categories. Errors caused by the instruments themselves fall into the first class. Such factors as measurement variations caused by electronic noise, ,inaccurate A/D and logarithmic conversions, and inaccuracy and instability in the microwave source make up this category. The second group of errors is caused by the test set, antennas , cables, connectors, amplifier, and room clutter. All these factors interact with each other in the microwave region and are the significant cause of error in microwave measurements. Little can be done about the first class of errors since they are inherent in the characteristics of the equipment used. The second group of errors can be removed through the use of automated measurement of system parameters in the frequency range of interest. These errors can be removed from any measurements of scattering objects by digital processing and the results stored for later recall. This

essentially provides an automated and improved version of the conventional two antenna radar cross-section measurement technique [6] ;in which a microwave bridge is balanced in the absence of the target and the degree of imbalance is measured when the target is introduced into the microwave field.

Let us look at the first class of errors more closely since these errors will set the ultimate performance limits on the system. The characteristics of the signal source are important in this regard. In this case the signal source is a Hewlett-Packard 8620C microwave sweeper. Since the sweeper is not phase locked frequency and stability problems exist. The carrier also has significant FM noise which appears as phase noise in the scattered signal. The phase shift of the scattered signal as a function of frequency for small frequency variations is given by:

$$\Delta\theta = \Delta k \cdot R \quad (2.1)$$

where  $k=(2\pi/\lambda)$  and  $R$  is the path length. For  $R$  greater than a few tens of meters ,the FM noise on the signal source causes measurable variations in the phase of the scattered signal. The stability of a synthesizer is required for the implementation of a holographic radar system when target ranges are in terms of kilometers.

Another limit on the ultimate accuracy of the system is the resolution of the A/D conversions and the accuracy of the network analyzer. Given the 2.2MV resolution of the MINC A/D converter and the network analyzer analog output of

50 MV/db, the system can resolve .048 db steps. This resolution limit restricts the minimum signal to system error ratio. If the error signal consisting of clutter, antenna coupling, system directivity and noise exceeds the scattered target signal the resolution of the target signal suffers. For example, if the system error signal and target scattered signal are of equal intensity, then a 1 db change in the scattered signal causes a .53 db change in the total received signal vector. When the system error is 13 db above the scattered signal it becomes impossible to resolve a 1 db change in the target signal given the resolution capabilities of the system. This difficulty is further compounded by errors in the network analyzer. These too are amplified when the clutter exceeds the target scatter signal. In fig.2.1 is a plot of the minimum system resolution in order to detect a 1 db change in the target return signal versus the system error signal to scattered signal level in db. In fig.2.2 is plotted the target signal resolution versus the noise to signal level in db. When the system error is 20 db below the target signal then the resolution of the target scatter signal is very close to the ultimate resolution, .048db. Clutter is the component of the received signal not scattered by the target but that signal that is the result of coupling between antennas and signal scattered by the anechoic chamber walls. As the clutter/signal ratio increases the target scatter signal resolution decreases exponentially. Clutter may be reduced

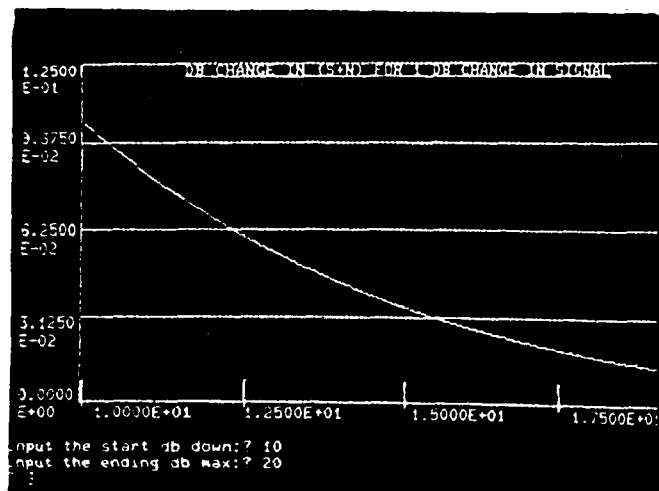


Fig. 2.1 The required resolution in db for a data acquisition system to detect a 1 db change in the desired signal vs. signal/error -signal ratio.

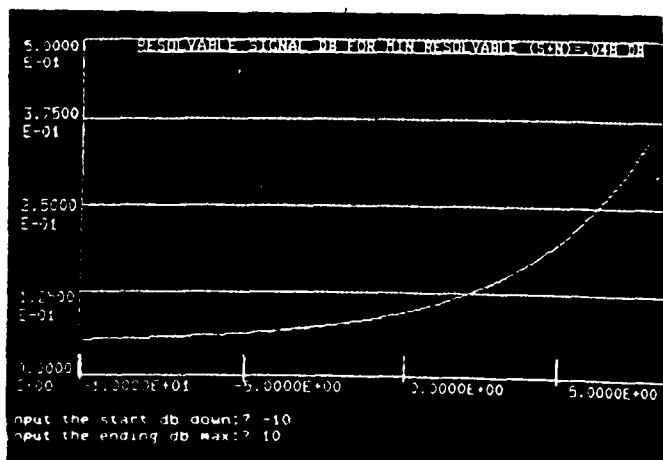


Fig. 2.2 Minimum change in desired signal level detectable versus signal/error signal level given .048 db system data acquisition resolution.

by improving the isolation between the transmitter and receiving antennas with the introduction of absorbing foam panels such as Emerson and Cummings' Ecosorb panels between the antennas.

#### 2.4 System error correction

Turning next to the second class of errors; those directly measurable and therefore removable; define the following quantities which are functions of frequency :

- I(f) -- Isolation of reference to test channels
- T(f) -- Transfer characteristic of system
- A(f) -- Attenuator characteristic
- A<sub>1</sub>(f) -- Antenna system characteristic
- S(f) -- Corrected backscatter for target
- C<sub>1</sub>(f) -- Uncorrected antenna clutter and coupling
- C<sub>2</sub>(f) -- Corrected antenna clutter and cross-coupling  
(uncorrected for antenna system response)
- C(f) -- Corrected antenna clutter and coupling
- R<sub>1</sub>(f) -- uncorrected reference target backscatter
- R<sub>2</sub>(f) -- Corrected reference target data  
(uncorrected for antenna system response)
- R(f) -- Corrected reference target data

Several possible techniques exist for the removal of system errors. The particular technique is dependent on the relative signal levels involved, the accuracy desired, ease of implementation, and computational speed. The first technique described here is similar to that used by Weir et al .[7]

The first step in the correction procedure measures the transfer function of an attenuator  $A(f)$  as a function of frequency. The equipment setup for this procedure is shown in fig. 2.3. The two ports of the reflection-transmission unit connected through a precision HP 11605A flexible coaxial arm. The MINC then steps the sweeper to a number of frequency points and stores the system response (log amplitude and phase vs. frequency) in memory. When this completed the attenuator is placed in series with the arm and another set of measurements is made at the same frequency points as before. the system response characteristic is subtracted from the combined attenuator plus system response measurement made on the second sweep. An example of this procedure is shown in fig 2.4. Computer subroutine PAD performs this operation. It is listed in appendix I along with all other computer program listings and output pertaining to system response measurement and removal.

The next step in the calibration process is measurement of the reference to test channel isolation  $I(f)$ . This characteristic is dependent on the directivity of the network analyzer harmonic converter, and the reflection transmission unit. For the Hewlett-Packard 8411A harmonic converter the isolation is greater than 50 db. In this measurement the ports of the reflection-transmission unit are terminated in the cables used for the later target scatter measurement. These coaxial cables are terminated in

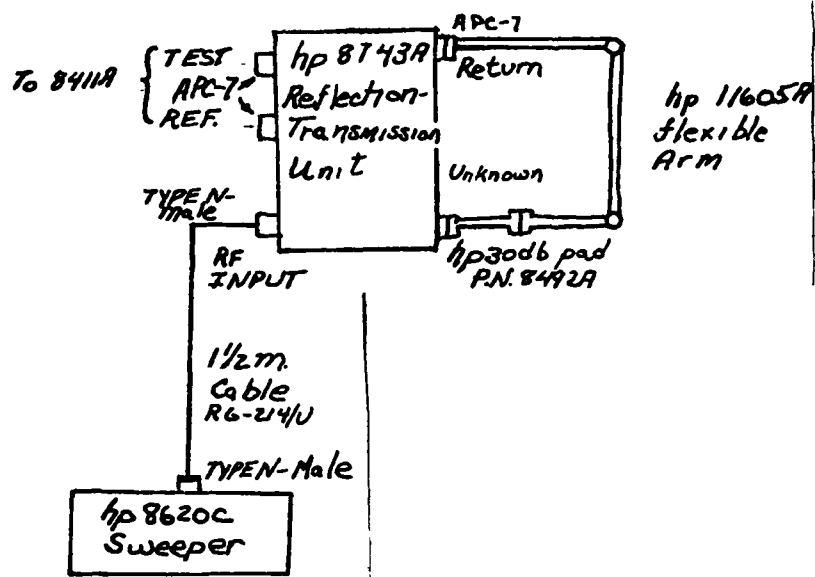


Fig. 2.3 Equipment setup for attenuator measurement.

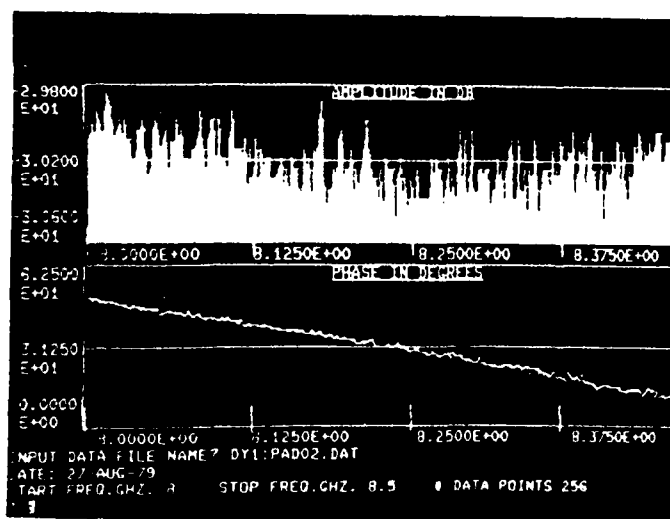


Fig. 2.4 30 db attenuator characteristic for 8.0-8.5 GHz.

50 ohm resistive loads as shown in fig.2.5. The results of a typical run are shown in fig.2.6. Computer subroutine IST automates this stage in the correction procedure. As can be seen the coupled signal is well in the noise of the system and would not affect later scatter data. If the isolation effect is ignored later calculation would be simplified greatly; but is included here to be consistent with the procedure outlined in the literature.[7]

The next stage in generating the data for correction of scatter data is measurement of the system transfer function  $T(f)$ . This consists of the characteristics of the traveling wave tube amplifier, system cables and connectors. This is done by connecting the cable from the transmitting antenna to the receiving antenna cable in fig.2.6 and placing the 30 db attenuator characterized previously in the line to avoid damage to the harmonic converter. The raw measurement  $MT(f)$  is a combination of several factors:

$$MT(f) = T(f) * A(f) + I(f) \quad (2.2)$$

Solving for  $T(f)$ :

$$T(f) = (MT(f) - I(f)) / A(f) \quad (2.2a)$$

The equipment setup for this procedure is shown in fig 2.7 and typical uncorrected and corrected transfer function data in fig.2.8 and 2.9.

Measurement of the antenna cross-coupling and room clutter is the next step in the correction process. In this procedure shown in fig.2.7b, the target is removed from the anechoic chamber and the antennas pointed to the target



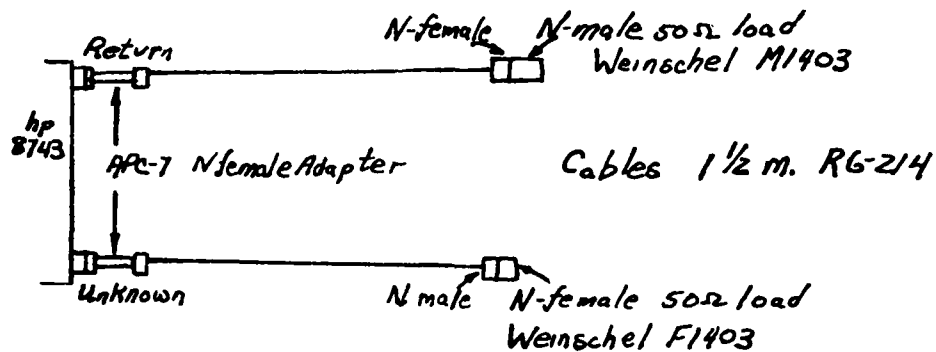


Fig. 2.5 System configuration for measuring isolation between reference and unknown ports.

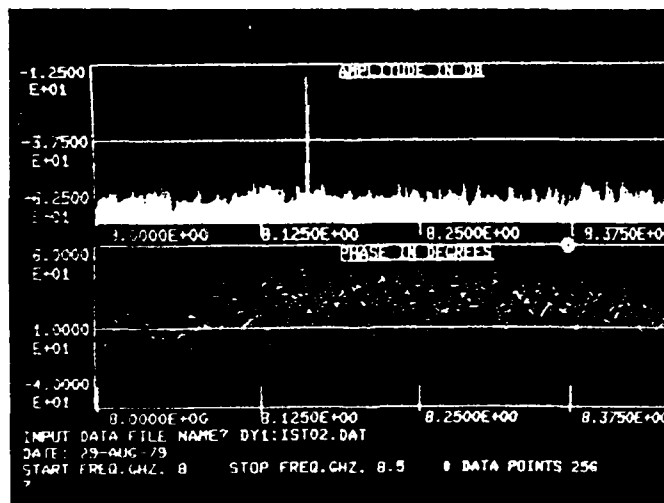
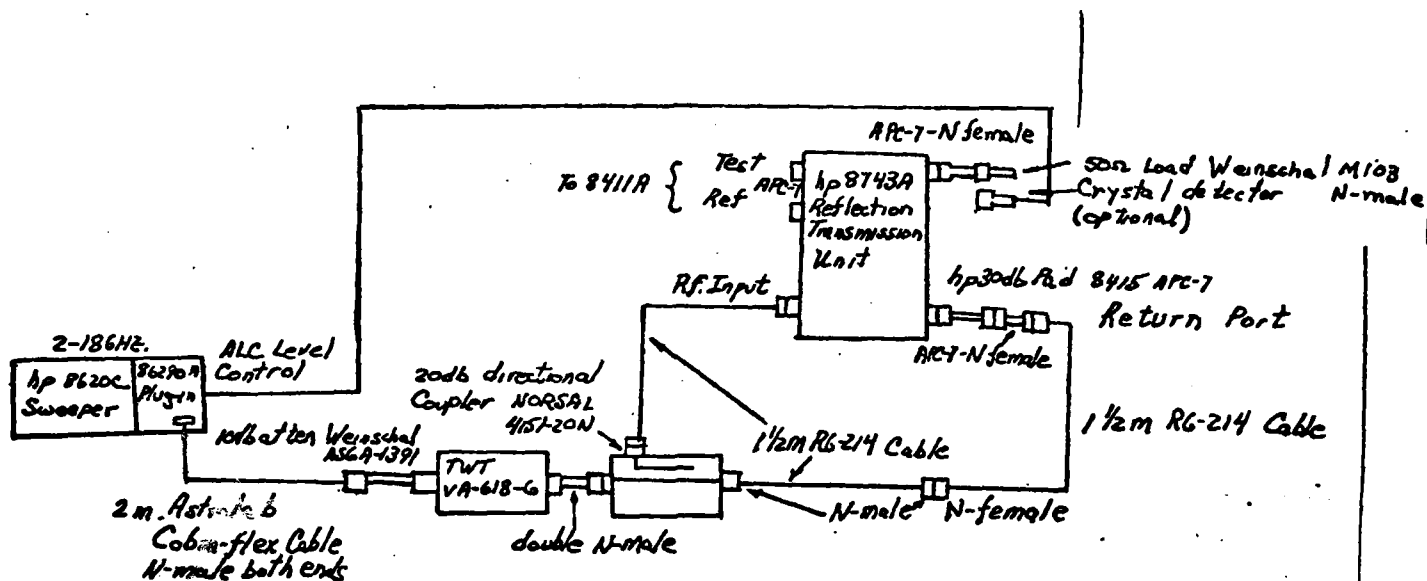
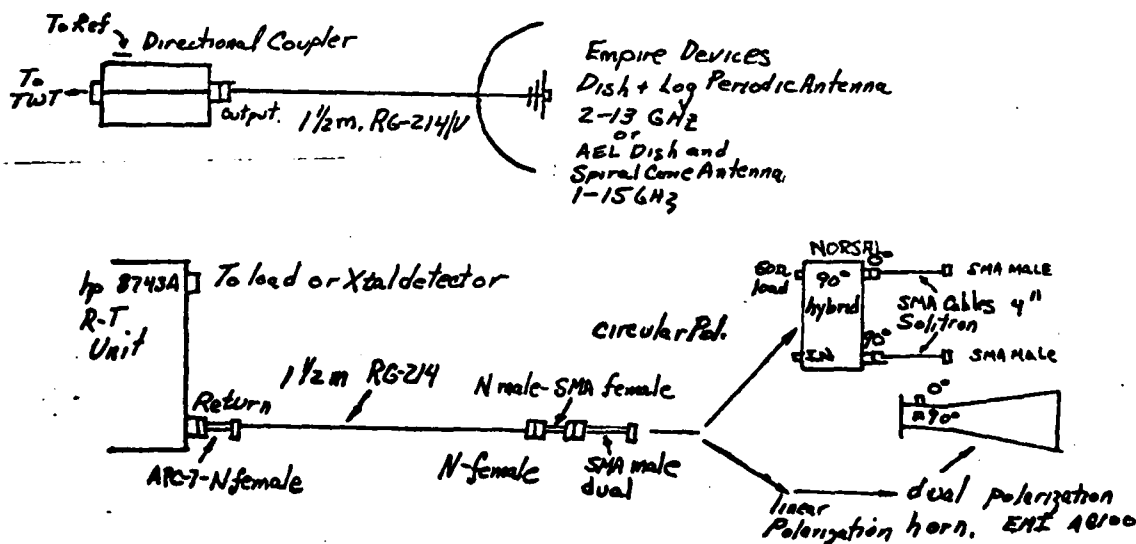


Fig. 2.6 Isolation between ports of reflection-transmission unit; 8.0-8.5 GHz.

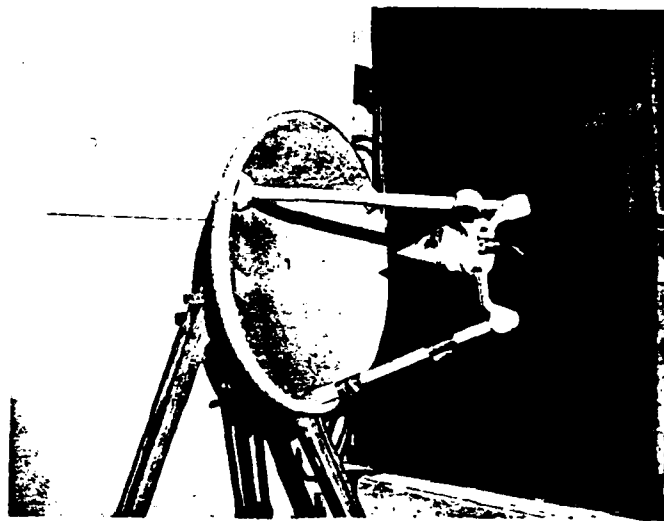


(a)

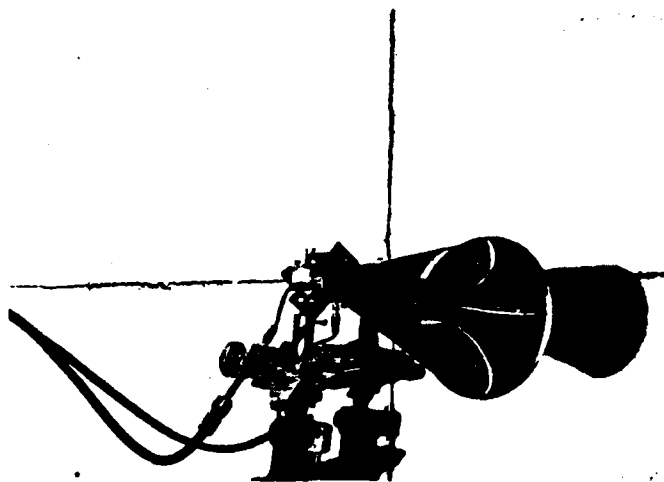


(b)

Fig. 2.7 a) System configuration for transfer characteristic measurement. b) Connection to antennas for scattering and clutter measurement. c) Transmitting antenna with spiral AEL antenna and parabolic dish. d) Receiving dual polarization horn ; EMI A6100 with Norsal 90 hybrid.



(c)



(d)

Fig. 2.7 (contd.) a) system configuration for transfer characteristic measurement. b) Connection to antennas for scattering and clutter measurement c) Transmitting antenna with spiral AEL antenna and parabolic dish. d) Receiving dual polarization horn; EMI A6100 with Norsal 90 hybrid.

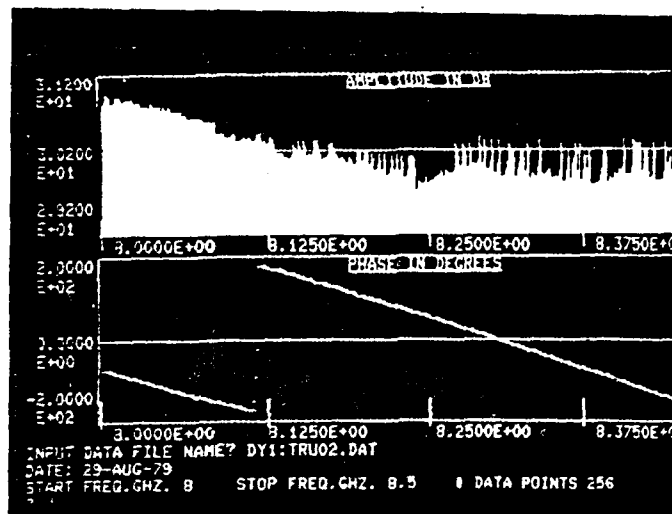


Fig. 2.8 Uncorrected transfer characteristic of system; 8.0-8.5 GHz.

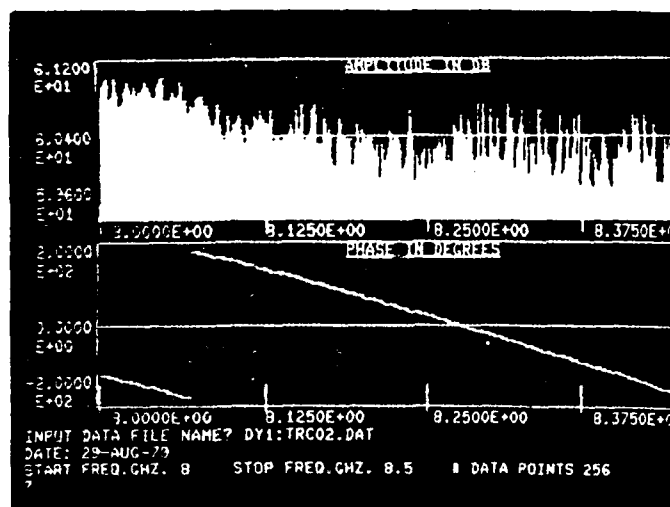


Fig. 2.9 Transfer characteristic corrected for attenuator response; 8.0-8.5 GHz.

location. A high gain parabolic dish antenna is used for illumination of the target since the narrow beam pattern of the antenna places most of the radiated power on the target area. A smaller dual polarization horn is used for receiving in order to sample a small area of the scattered field. The uncorrected clutter  $C1(f)$  is given by:

$$C1(f) = C2(f) * T(f) + I(f) \quad (2.3)$$

Solving for the corrected clutter and coupling:

$$C2(f) = (C1(f) - I(f)) / T(f) \quad (2.3a)$$

Subroutine ANTEN does the system clutter and coupling removal. Examples of the uncorrected and corrected clutter  $C1(f)$  and  $C2(f)$  are shown in figs. 2.10 and 2.11. The corrected clutter represents the actual signal reflected from the anechoic chamber walls and that signal coupled between the antennas with the system response removed.

These subroutines: PAD, IST, TRANS, and ANTEN, were combined into a program SYSRES. Data from each of these subroutines may be stored on disc for later recall or display. Theoretically if the system is not disturbed then the system response will remain constant. Then only the target data need be recorded in any run for a new corrected backscatter measurement.

The transfer function of the system and the range clutter- antenna cross coupling data are utilized the the next step of the error correction process. A reference object of known constant cross section is measured and the result stored. This data includes all the errors previously

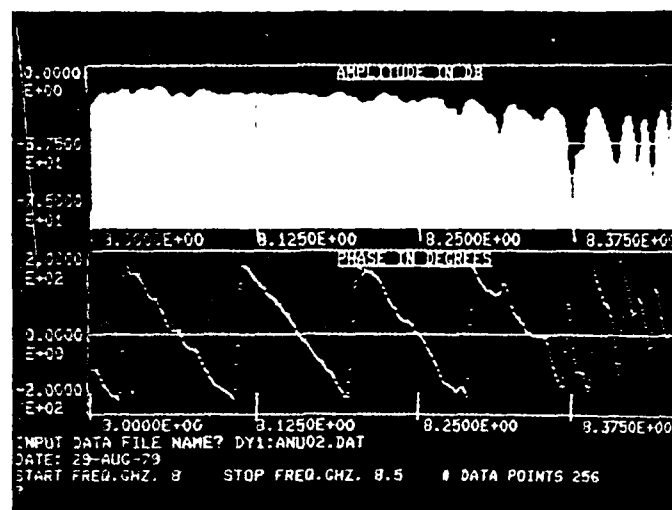


Fig. 2.10 Uncorrected system clutter; 8.0-8.5 GHz.

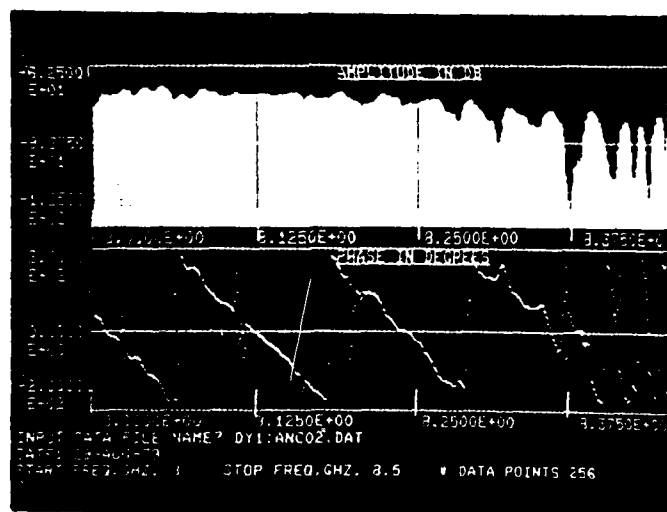


Fig. 2.11 System clutter corrected for transfer function; 8.0-8.5 GHz.

described but also takes into account the antenna system variations as a function of frequency:

$$R_1(f) = C_2(f) * T(f) + I(f) + R_2(f) * T(f) \quad (2.4)$$

Here  $C_2(f)$  and  $R_2(f)$  contain the antenna system response multiplying the actual values of corrected reference target and system clutter data.

$$R_2(f) = R(f) * A_1(f) \quad (2.5)$$

$$C_2(f) = C(f) * A_1(f) \quad (2.6)$$

This response  $A_1(f)$  takes into account the varying amount of power received and transmitted as a function of frequency in the antenna system. If the reference target is chosen to have a constant cross section and linear phase over the frequency range of interest then  $R(f)$  is of constant amplitude and linear phase. Solving for  $R_2(f)$ :

$$R_2(f) = (R_1(f) - I(f) - C_1(f)) / T(f) \quad (2.7)$$

This leaves  $R_2(f)$  proportional to  $A_1(f)$  shifted by a linear phase corresponding to the reference target range.

When the actual target is measured; it is corrected for system errors as was the reference target data and this result is divided the corrected reference target data to yield the final target scatter data.

$$S_2(f) = (S_1(f) - I(f) - C_1(f)) / T(f) \quad (2.8)$$

$$S(f) = S_2(f) / R_2(f) \quad (2.9)$$

This technique may be simplified considerably in the laboratory environment given the signal to noise ratio is greater than 10 db for the scattered signals. In this case only multiplicative errors remain and the additive errors

are masked by the high target scatter signal amplitude.

Hence:

$$\begin{aligned} I(f), C_1(f) &\rightarrow 0 \\ R_1(f) &= R_2(f) * T(f) \end{aligned} \quad (2.10)$$

and therefore:

$$S(f) = S_1(f) / R_1(f) \quad (2.11)$$

Weir and his group have reported that this technique has reduced equivalent range clutter to -45 db below 1 sq. meter.

There remains one source of error in the scattered signal measurement that cannot be removed by calculation. This error comes from multipath scattering from the object. The target scatters power in all directions. Some of this signal may be reflected off the walls or floor of the anechoic chamber. The signals reflected off the walls is over 48 db down from the incident wave amplitude in the 6.0-12.0 GHz range. However if the target is small in cross section; on the order of 100 sq. cm.; then it is possible for the walls (on the order of 100 000 sq. cm. ) to contribute a significant component to the received signal.

In order to analyze the effect of the multipath scattering, let the directly received signal be written:

$$S_o(t) = A \cos(\omega t + \psi) \quad (2.12)$$

and the indirectly received signal:

$$S_i(t) = B \cos(\omega t + \psi + \theta) \quad (2.13)$$

Then the total received signal is given by:

$$S_r(t) = (A^2 + 2AB \cos \theta + B^2) \cos(\omega t + \psi + \tan^{-1} \left( \frac{-B \sin \theta}{A + B \cos \theta} \right)) \quad (2.14)$$



Since theta is a function of the indirect path length differences and frequency, it will lead to a periodic variation in the amplitude of the scattered signal. As an example; if the paths differ in length by 1 meter then the amplitude oscillations will occur every 300 MHz given all other factors remain constant.

A series of programs was written to test these various techniques of error removal. They differ in the only in the error removal technique employed; not in file storage or display formats nor in range calculation and removal to be described. These programs used together:

- 1) Measure and correct the reference target data with files of transfer function and clutter data generated by SYSRES.
- 2) Measure and correct the target data and finally take the corrected reference target data and remove the antenna system response from the target data.
- 3) Alternately for high SNR; calculate the correct scattered target signal directly using the reference target data.
- 4) Calculate and remove phase shift due to range from the target signal after error correction

These programs are briefly described and differ in the mentioned categories:

SPHERE-Reads transfer function and clutter data files generated by SYSRES; takes the reference or object data and corrects for errors in the

equipment.

SPHER2-Measures clutter and reference target data.

It then subtracts clutter and divides the target data by the reference target transfer function.

SPHER3-Measures reference target and object signals ignoring clutter, and divides the object data by the reference target complex field amplitude data.

In order to implement the complete error correction process program SPHERE would be run twice; once for the reference target and then again for the test object. This data would be stored for later retrieval. Program SPHER3 would read these files and process them such that the test object complex field data would be divided by the reference target data. For high SNR cases; program SPHER3 alone would be run: first measuring the reference target and then the test target and finally dividing them yielding the final result. Listings and a more complete description of program operation is given in the program appendix I.

### III RANGE PHASE SHIFT ANALYSIS

This chapter contains an analysis of the effects on the phase shift due to target range on coherent imaging of a target. It includes a discussion of some of the available techniques for the removal of this phase shift and the required performance of these systems based on bandwidth and signal to noise ratio.

#### 3.1 The effects of range phase on imaging

As previously described by Farhat and Chan ;[4]; the scattered field of the scattering target is given by:

$$\psi(k, R_t, R_r) = \frac{jk}{2\pi(R_t + R_r)} e^{-jk(\vec{R}_t + \vec{R}_r)} \int_{-\infty}^{\infty} U(\vec{r}) e^{-jk(\vec{R}_t + \vec{R}_r) \cdot \vec{r}} d\vec{r} \quad (3.1)$$

Where  $\vec{R}_t$  and  $\vec{R}_r$  are the vectors from the receiving and transmitting antennas to the target respectively and  $k$  is the wave vector of the illuminating wave. In this case the integration is over the extent of the object. The integral term is independent of the range of the target. While the term preceeding the integral is target independent and contains range information. The argument of the complex exponential is a linear phase function of frequency.

In the single receiver-transmitter pair arrangement; shown in fig.3.1, the spatial frequency domain ( $\vec{p}$  space) data is collected in a plane perpendicular to the axis of rotation. In this case the multiplication of the range phase factor leads to the convolution of the transforms of the the range and target functions in the spatial domain. The real part of the range frequency domain function is a

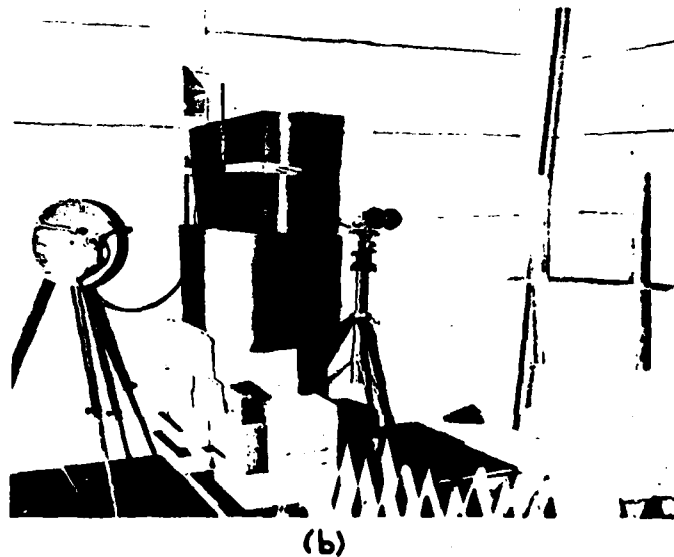
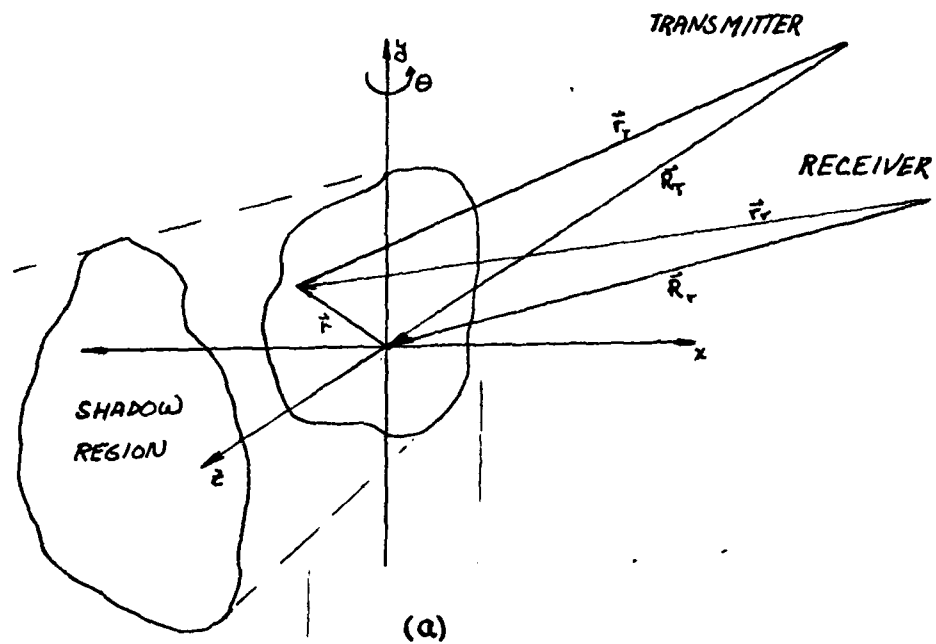


Fig. 2.12 a) Target and antenna placement relative to target considered in analysis. b) Experimental configuration in anechoic chamber; note target on rotating pedestal in forefront.

radially symmetric sinusoidal function:

$$R\{e^{-j k(R_T + R_r)}\} = \cos k(R_T + R_r) \quad (3.2)$$

This transforms to a circular ring of radius  $(R_T + R_r)$ . This indicates that each point of the reconstructed image is convolved with this circular ring pattern; seriously degrading the target image. In fact any error in the removal of phase will distort the image in this manner. The effect of removing the range phase factor is equivalent to the focusing of the system on the target.

There are several other reasons for the removal of the factor:

$$\frac{j k}{2\pi(R_T + R_r)} e^{-j k(R_T + R_r)} \quad (3.3)$$

from the received data. If the data is discrete then the considerations of aliasing and sufficient data sampling rate are introduced. When the sampling rate in the frequency domain is  $(f)$  then the maximum target range before aliasing will occur is  $(c/4 * f)$ . However if the phase factor is removed and the target is of smaller dimension  $L$  than the range, then the sampling rate in the frequency domain need only be sufficient to prevent aliasing over the dimensions of the object :

$$\Delta f \leq \frac{c}{4L} \quad (3.4)$$

This allows the entire resolution capability of the system to be placed on the target itself greatly reducing the data

volume.

Another reason for the removal of this phase factor term can be seen in systems involving multiple receiver-transmitter pairs. For each pair  $(\tilde{R}_i)$  and  $(\tilde{R}_j)$  is different and in order for the data to be coherent all phase centers must be equal for an image to be formed.

Several methods have been suggested for the removal of the range phase factor. [4] In all cases it is required that the range removal technique be accurate to within  $(\lambda/5)$  for there not to be serious image degradation. It is important to investigate the constraints on the ranging system parameters necessary to attain the required accuracy.

From the scaling theorem in Fourier analysis; a signal cannot be both of narrow bandwidth and short duration.[8]

$$af(at) \rightarrow F\left(\frac{\omega}{a}\right) \quad (3.5)$$

We define the duration and the bandwidth of the signal in the following manner: [ ]

$$(\Delta t)^2 = \frac{1}{E} \int_{-\infty}^{\infty} t^2 |f(t)|^2 dt \quad (a) \quad (\Delta \omega)^2 = \frac{1}{2\pi E} \int_{-\infty}^{\infty} \omega^2 |F(\omega)|^2 d\omega \quad (b) \quad (3.6a,b)$$

where:

$$E = \int_{-\infty}^{\infty} |f(t)|^2 dt = \frac{1}{2\pi} \int_{-\infty}^{\infty} |F(\omega)|^2 d\omega \quad (3.6c)$$

is the signal energy. Then if:

$$\lim_{|t| \rightarrow \infty} \sqrt{t} f(t) = 0 \quad (3.6d)$$

When applied to signals scattered by a target this may be translated to range uncertainty:

$$\Delta R \Delta f \geq \frac{c}{4\pi} \quad (3.7)$$

This represents a limit when the durations of the signal pairs are as previously defined. However it may be possible to improve the range resolution given that the signal to noise ratio is greater than 10 db.

Consider a sinusoid in narrow band gaussian noise:

$$r(t) = A \cos \omega t + n_c(t) \cos \omega t - n_s(t) \sin \omega t \quad (3.8)$$

$$n(t) = n_c(t) \cos \omega t - n_s(t) \sin \omega t$$

where  $n(t)$  is the noise signal and  $n_s(t)$  and  $n_c(t)$  are the quadrature components of the noise signal. The amplitude and phase may be expressed as:[9]

$$|r(t)| = \sqrt{(A + n_c(t))^2 + n_s(t)^2} \quad (3.9a)$$

$$\text{Arg}(r(t)) = \tan^{-1} \left\{ \frac{n_s(t)}{A + n_c(t)} \right\} \quad (3.9b)$$

Since the noise is gaussian  $n_c(t)$  and  $n_s(t)$  are gaussian. Assuming that the SNR is high the phase may be approximated by:

$$\text{Arg}(r(t)) = \tan^{-1} \left\{ \frac{n_s(t)}{A} \right\} \approx \frac{n_s(t)}{A} \quad (3.10)$$

Also since the noise is white  $n_s(t)$  may be related to the bandwidth of the receiving system.

$$\sigma_{n_s}^2 = 2N_b B \quad (3.11)$$

where  $(\sigma_{n_s}^2)$  is the variance of the  $n_s(t)$  quadrature phase component. The probability density of the phase may be written as:

$$f(\theta) = \frac{A}{\sqrt{2N_b B}} e^{-A^2 \theta^2 / 4N_b B} = N(0, \frac{\sigma_{n_s}^2}{A^2}) \quad (3.12)$$

This leads to an interesting result; the variance of the

phase is the inverse of the SNR:

$$\sigma_\phi^2 = \frac{\sigma_{\phi^2}^2}{A^2} = \frac{1}{\text{SNR}} \quad (3.13)$$

Translating this result to an uncertainty relationship the phase uncertainty may be expressed:

$$\Delta \omega \Delta t \geq \sqrt{\frac{8NB}{A}} \quad (3.14)$$

The uncertainty in phase is the product of the time and frequency uncertainties. This leads to an expression for the range resolution as a function of the SNR.

$$\Delta f \Delta R \geq \frac{c}{2\pi\sqrt{\text{SNR}}} \quad (3.15)$$

Wide band ranging systems measure range by calculating the propagation delay of the signal. In one such system a high speed code is transmitted. The received signal is correlated with the original coded signal in a delay locked loop. The value of the control signal in the loop is proportional to the target range. Obviously the resolution is only as good as the the period of one of the code bits(chips). Other wide band systems use other signals for ranging(chirps,walsh functions) to obtain high range resolution. [10], [11], [12]

The system implemented here at the Graduate Research center of the Moore school is a coherent amplitude-phase measurement facility. Ranging techniques that may be integrated into this system are therefore of special interest. The phase of a point scatterer is a linear function the frequency. This directly corresponds to the



phase factor preceeding the scattering integral in eq ( ). If the target consists of multiple scattering centers; then each of these will be represented as a delta function in the in the reconstructed image. This suggests a technique using Fourier analysis to determine range. First place the reference target in the microwave field and measure the phase/amplitude response over as wide a frequency range as possible. Then inverse transform this one dimensional collection of data. This will transform to essentially a delta function occurring at the time corresponding to the propagation delay. This will occur when the target has a single scattering center such as a sphere. Even when the object is more complex the inverse transform will be centered around the transit time. In this Fourier technique for range determination the resolution ( $\Delta x$ ) is inversely related to the frequency sweep width.

$$\Delta x = \frac{c}{2 \Delta f} \quad (3.16)$$

The factor of 1/2 results from the fact that the range is half the signal propagation path length.

A factor to be considered is that different scattering centers are visible from different receiver positions. It is imperative that all when several receivers are used simultaneously that all choose the same scattering center as the phase center for range removal. If the various phase centers do not coincide, the fringes of the hologram will be skewed. The data sets from each of the receivers will be brought into alignment using an adaptive

AD-A090 838

MOORE SCHOOL OF ELECTRICAL ENGINEERING PHILADELPHIA PA  
SUPER-RESOLUTION IMAGERY BY FREQUENCY SWEEPING. (U)  
AUG 80 N H FARHAT, C WERNER

F/6 17/9

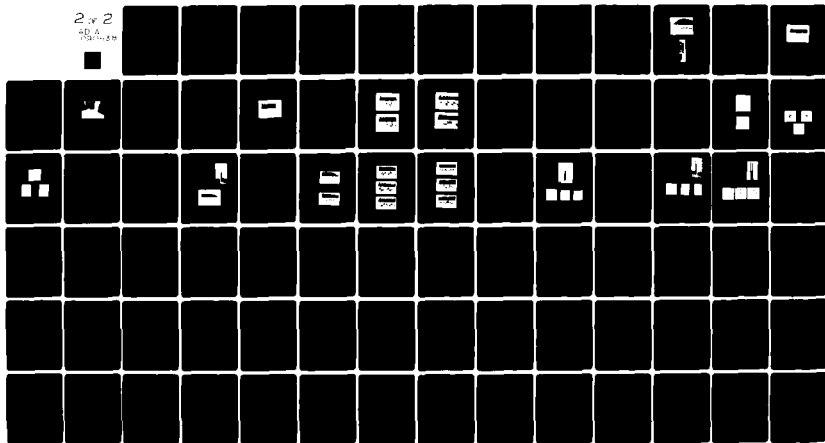
AFOSR-77-3256

UNCLASSIFIED

AFOSR-TR-80-1068

NL

2 of 2  
AD-A090 838



END  
DATE  
FILMED  
12-80  
DTIC

Information is lost in the hologram if the phase centers for the scan lines are separated.

When this process is automated the sweep is done by measuring the response at discrete frequency points. The amplitude and phase are stored at N frequency points in the sweep range. The range at which aliasing will occur is given by:

$$R_{\text{alias}} = \frac{c}{4 \Delta f} \quad (3.17)$$

This system exhibits processing gain ; a quality of all systems which spread a baseband signal into a wide spectrum. For this system the processing gain is a function of the number of measurements and the sweep width.

$$G_{\text{gain}} = \frac{\Delta f}{f_{\text{stepsize}}} = n \quad (3.18)$$

$$G_{\text{gain db}} = 10 \log_{10} n$$

As an example, for 256 measurement points, this would give 24 db of processing gain.

A set of subroutines was written to test this range removal technique. In one of them , RANGE, the range of the strongest scattering center is calculated and in the other ,RANCOR, the phase factor is calculated and removed from the target data. These subroutines are used in programs SPHERE, SPHER2 ,and, SPHER3.

The time domain equivalent of this technique is fitting a linear trend to the phase signal from the network analyzer. Since the phase signal is modulo (2 $\pi$ ); this means

estimating the frequency of a ramp waveform; either using a least squares approximation or implementing the equivalent of a phase locked loop. The slope of the ramp waveform is proportional to the range of the target. The accuracy to which the range may be determined depends on the sweep width, the target structure and the noise in the system. If the sweep is wide, then there will be more data with which to estimate the slope. Noise in the data will obviously interfere with the estimation process as will as any phase shifts due to the target structure.

Another type of system for generating a reference signal utilizes a Target Derived Reference. This system has been extensively studied at the Electro-Optics and Microwave Optics laboratory. [13] A brief review of the ideas developed to date in this regard are given below. The complex exponential in the integral term of scattered signal remains constant when the target is small relative to the illuminating signal wavelength.

$$\psi(\vec{p}) = \int_{-\infty}^{\infty} U(\vec{r}) e^{-j\vec{p} \cdot \vec{r}} d\vec{r} \approx e^{-j\vec{p} \cdot \vec{r}} \int_{-\infty}^{\infty} U(\vec{r}) d\vec{r} \quad (3.19)$$

This is true if  $(L_{\infty})$  is sufficiently small such that  $(\vec{p} \cdot \vec{r} \ll 1)$ . In this case the integral value approaches a constant multiplied by a linear phase; i.e. a point scatterer. It will only occur when the target dimensions are less than a tenth wavelength of the illuminating signal, placing it in the Rayleigh scattering region. The TDR signal is mixed harmonically with a phase locked scattered

estimating the frequency of a ramp waveform; either using a least squares approximation or implementing the equivalent of a phase locked loop. The slope of the ramp waveform is proportional to the range of the target. The accuracy to which the range may be determined depends on the sweep width, the target structure and the noise in the system. If the sweep is wide, then there will be more data with which to estimate the slope. Noise in the data will obviously interfere with the estimation process as will as any phase shifts due to the target structure.

Another type of system for generating a reference signal utilizes a Target Derived Reference. This system has been extensively studied at the Electro-Optics and Microwave Optics laboratory. [13] A brief review of the ideas developed to date in this regard are given below. The complex exponential in the integral term of scattered signal remains constant when the target is small relative to the illuminating signal wavelength.

$$\psi(\vec{p}) = \int_{-\infty}^{\infty} U(\vec{r}) e^{-j\vec{p} \cdot \vec{r}} d\vec{r} \approx e^{-j\vec{p} \cdot \vec{r}} \int_{-\infty}^{\infty} U(\vec{r}) d\vec{r} \quad (3.19)$$

This is true if  $(L_{\infty})$  is sufficiently small such that  $(\vec{p} \cdot \vec{r} \ll 1)$ . In this case the integral value approaches a constant multiplied by a linear phase; i.e. a point scatterer. It will only occur when the target dimensions are less than a tenth wavelength of the illuminating signal, placing it in the Rayleigh scattering region. The TDR signal is mixed harmonically with a phase locked scattered

signal at the imaging frequency. here the two signal sources are phase locked by a phase synchronizer. The high frequency sweeper acts as the slave signal source. These two signals simultaneously illuminate the target. Harmonic mixing of the suitably limited TDR and imaging signals will yield the desired phase corrected data.

Another technique which is useful for ranging is the frequency displaced reference method. Here the carrier is displaced ( $\Delta f$ ). It is important that the object not contribute to the phase shift; hence the displacement must satisfy the following condition:

$$\Delta f \ll \frac{2c}{L} \quad (3.20)$$

In this case the target structure will not contribute to the net phase shift. The range to the target phase center is given by:

$$R = \frac{\Delta \phi c}{\Delta f 2\pi} \quad (3.21)$$

$c$  - speed of light

Where ( $\Delta \phi$ ) is the change in phase for the carrier and displace carrier signals respectively. If the frequency shift is small then the phase shift will not be large. The resolution of the system then is directly related to the SNR in the receiver channel since the accuracy to which the phase may be measured is a function of the channel noise. If the displacement is large then the phase shift is increased and the SNR requirements on the signal for a specific resolution is decreased. This relationship may be expressed:

$$R_{\text{resolution}} \cdot \frac{c}{\Delta f 2\pi} = \frac{\sqrt{2N.B}}{4\pi A \cdot \Delta f} c \quad 3.22$$

The factor of 2 comes about due to the phase uncertainty existing in both the carrier and displaced carrier signals.

An alternate method for implementation of the displaced frequency ranging system is a swept frequency chirp system. The ranging signal frequency is given by :

$$f(t) = f_0 (1 + \alpha t) \quad \text{where } \alpha = \frac{f_1 - f_0}{T} \quad 3.23$$

T- Sweep period

$f_0$ - Initial frequency for sweep

$f_1$ - final frequency

The scattered signal from the target is given by:

$$f_s(t) = f_0 + \frac{d\phi}{dt} - \frac{f_0}{c} (R_T + R_r) \quad (3.24)$$

where  $(d\phi/dt)$  is the change in frequency due to the target structure. The range of the target may then be simply calculated using a frequency counter and sweep time T and sweep width  $(f_1 - f_0)$ . This method could be used in an analog imaging system.

Other Target Derived Reference systems simulate the low frequency reference carrier by measuring the change in phase of the imaging frequency over a narrow band. Over this small band the phase shift is assumed to be linear. In one system a series measurements is made for each frequency point. The first displaced down by a small amount,  $(\Delta f)$ ; the second at  $f$ ; and the final measurement at  $(f + \Delta f)$ . Phase and amplitude are measured at each frequency and processed to obtain the target range. In a similar system the three

signals are transmitted simultaneously by amplitude modulation of the carrier. These systems are presently under intense investigation by other workers at the Electro-Optics and Microwave Optics Laboratory of the Moore School.

### 3.2 Practical considerations for range phase removal

Several factors influence which of these systems would be of value in a long range imaging radar system versus a controlled laboratory environment. The distribution of the reference signal for complex field amplitude measurement makes implementation of system requiring a central reference difficult to implement. Techniques are being considered in the E.O. laboaraty for reference distribution using fiber optic that might remove this limitation. Reference distribution is accomplished in the lab readily since the distances are small.

Typical transmitter-receiver pattern arrangements might be the Wells array [14], an orthagonal pattern of receivers and transmitters, a circular array of receivers with central transmitter or a random array. Each combination of receiver and transmitter contributes another line in the frequency domain 3D data volume. For this reason it is advantageous that all combinations of the receivers and transmitters are utilized for data collection. Reference signal distribution difficulty therefore leaves the TDR systems as the only practical alternatives for long range imaging systems. The AM TDR system eliminates



reference distribution by transmitting the reference signal along with the imaging signal and automatically corrects for the target range. TDR systems have the additional advantage that they have immunity to turbulence and inhomogeneities in the propagation medium since both the reference and imaging signals follow the same path.

There are several considerations for determining the best TDR system. Narrow band systems yield only a weighted average of the range to the phase center of the object while wide band system can resolve individual scatters on the target body. A wide band system could adaptively choose one of the scattering centers for the phase reference of the system. A narrow band system could not do this, and any error would introduce image distortion. The narrow band systems have the advantage of automatically correcting the target data for the range phase factor.

For the laboratory imaging experiments a TDR system would not yield the correct phase factor since in this arrangement the object rotates about an axis and the correct phase factor would be a constant, representing the phase shift to the axis of rotation, not the target. The TDR system looks only at the range to the strongest specular reflector on the target surface.

If movement of the target is utilized for aperture synthesis then only one receiver-transmitter pair is required for 3-D imaging and the adaptive system is not required.

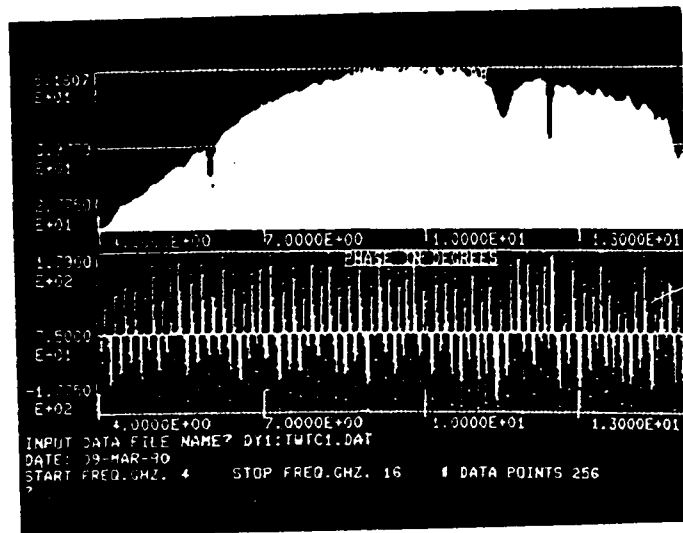
Knowledge of the placement of the data in the 3-D frequency domain volume is necessary for the reconstruction of the hologram. The azimuth and elevation angle of the target can be obtained from a conventional radar located at a central location where the data processing and reconstruction is taking place.

#### IV SYSTEM IMPLEMENTATION OF SWEEPED FREQUENCY IMAGING

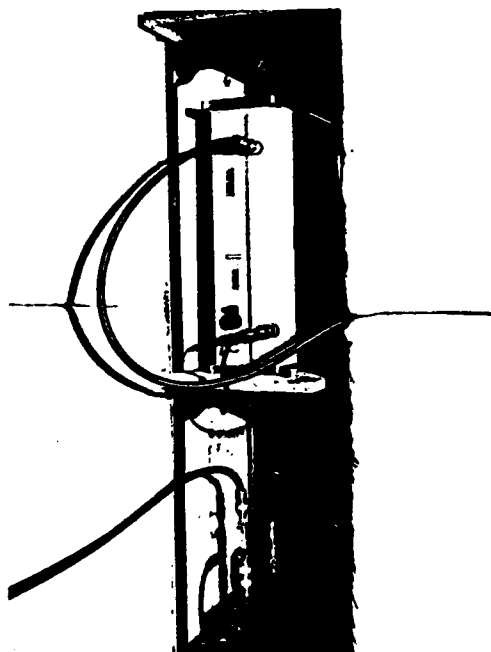
This section of the thesis will describe the research that was done in order to obtain a clear understanding of system performance. Following this will be a section of the thesis devoted to the experimental verification of the swept frequency imaging theory.[ ] The theory is applied in the simulation of the experiments performed.

##### 4.1 System repeatability

An important parameter of system performance is the repeatability of an experimental measurement. The frequency range over which this possible for the equipment used indicates the bandwidth for which imaging is possible. There are several feedback loops in the system which allow it to track variations in the transmitted signal level. The traveling wave tube amplifier characteristic is shown in fig.4.1. This plot is on a logarithmic scale, indicating that the TWT amplifier gain drops off exponentially below 7.0 GHz and above 15.0 GHz. This measurement was done by first measuring the system response(cables, connectors,attenuator) less the TWT amplifier and then subtracting this response from the TWT amplifier plus system data. A sample of the amplifier output is sampled using a 20 db directional coupler and this is fed to the RF input of the HP 8743A reflection-transmission (R-T) unit. A crystal detector at the 'unknown' port of the R-T unit rectifies a portion of this signal. The detector output is brought to the external signal leveling input of the HP 8620C sweeper.



(a)



(b)

Fig. 4.1 a) Traveling Wave Tube amplifier gain characteristic in db; 4.0-16.0 GHz. b) Varian VA 618G TWT amplifier (bottom) and HP 8743A reflection-transmission unit (top).

The leveling circuit of the sweeper can level the output over a 20 db range. In addition the AGC in the HP 8410B network analyzer can track the reference signal amplitude over a 40 db dynamic range. System performance may be seen in fig.4.2 for a cylindrical target 7 meters distant from the receiving and transmitting antennas. Two consecutive measurements of the target were made and the results divided. The ideal response would be 0 db flat amplitude and 0 degree phase difference over the entire frequency sweep. With few exceptions due to phase noise at the (+/- ) transition point, the system has the desired repeatability in the 5.5 to 16.0 GHz range. Below 4.5 GHz there are phase errors due to insufficient reference power whereas above 15 GHz errors come about due to the low amplitude of the received signal. Noise may be cancelled by taking multiple measurements and finding the mean. These results indicate the useful data can be recorded in the 5.5-16.0 GHz range

#### 4.2 Computer control of target rotation

When implementing a frequency diversity system with just one pair of receiving and transmitting antennas, the target must then be rotated in the electromagnetic field and the scattering measured for different rotation angles. The target used in the experimental system rotates on a stepper motor driven pedestal. The column of the pedestal is 1 1/2 meters in length and is made of styrofoam material with minimal cross section. A stepper motor controls table rotation precisely. In order for the pedestal to rotate one

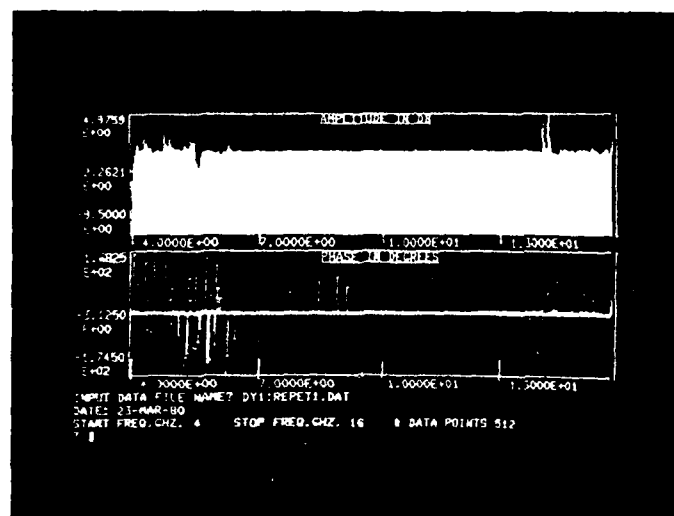


Fig. 4.2 System repeatability for two consecutive scattering measurements of a 80 cm long cylinder 7 cm in diameter; 4.0-16.0 GHz.

revolution the motor must be stepped 10 000 times. The motor is under direct computer control using the digital output port the MINC. A FORTRAN subroutine STEP2 was written for control of the stepper motor. It calculates the number of steps required for a specified angular rotation and moves the table clockwise or counter clockwise based on the direction parameters passed in the subroutine call. The stepper and pedestal are shown in fig.4.3.

### 4.3 Sphere Simulation

For the calibration of a radar system a reference target is required. The most commonly used reference target is the conducting sphere since its high degree of symmetry does not favor any particular polarization for the incident illumination. Both the bistatic and monostatic scattering of a metallic sphere was simulated.

The general solution for the plane wave electro-magnetic scattering of the sphere was first done by Mie in 1908.[15],[16] In the far field approximation, the scattered field is given by:

$$E_s(A, r, \theta, \phi) = E \frac{e^{ikr}}{kr} \left[ \cos \phi S_1(\theta) \hat{\theta} - \sin \phi S_2(\theta) \hat{\phi} \right] \quad (4.1)$$

where

$$S_1(\theta) = \sum_{n=1}^{\infty} (-1)^{n+1} \left[ A_n \frac{P'_n(\cos \theta)}{\sin \theta} + i B_n \frac{d}{d\theta} \left\{ P'_n(\cos \theta) \right\} \right] \quad (4.2)$$

and

$$S_2(\theta) = \sum_{n=1}^{\infty} (-1)^{n+1} \left[ A_n \frac{d}{d\theta} \left\{ \frac{P'_n(\cos \theta)}{\sin \theta} \right\} + i B_n \frac{P'_n(\cos \theta)}{\sin \theta} \right]$$

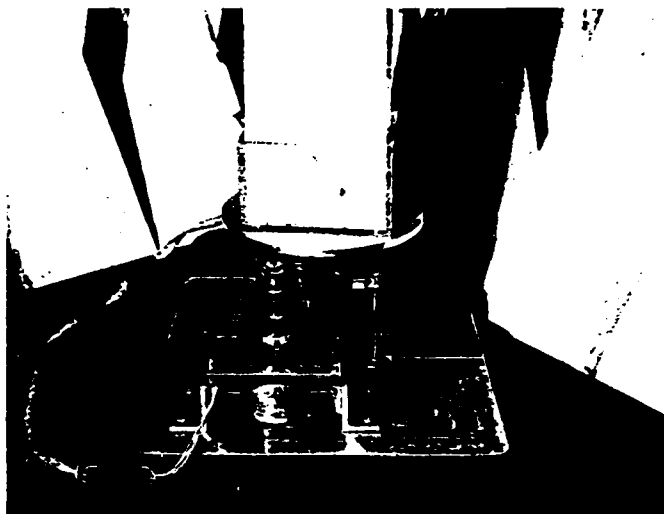


Fig. 4.3 Stepper motor and rotating pedestal.



$S_1(\theta)$  and  $S_2(\theta)$  are called the complex far field amplitudes for the  $(\hat{\theta})$  and  $(\hat{\phi})$  polarizations respectively. The quantity in the square brackets of eq. 4.1 is called the scattering function.

$$F(\theta, \phi) = \cos \phi S_1(\theta) \hat{\theta} - \sin \phi S_2(\theta) \hat{\phi} \quad (4.4)$$

The scattering cross section in any arbitrary polarization  $(\hat{\eta})$  for an incident wave polarized in the  $(\hat{\tau})$  direction may be written:

$$\sigma_n(\theta, \phi) = \frac{4\pi}{k^2} |F(\theta, \phi)|^2 |\hat{\tau} \cdot \hat{\eta}|^2 \quad (4.5)$$

Where  $(\hat{\eta})$  is the polarization of the incident wave and  $(\hat{\tau})$  is the polarization vector of the receiving system. For the perfectly conducting sphere the coefficients  $A_n$  and  $B_n$  are:

$$A_n = -(-i)^n \frac{2n+1}{n(n+1)} \frac{J_n(k_0 a)}{h_n'(k_0 a)} \quad (4.6a)$$

$$B_n = (-i)^n \frac{2n+1}{n(n+1)} \frac{[k_0 a J_n(k_0 a)]'}{[k_0 a h_n'(k_0 a)]'} \quad (4.6b)$$

$j_n(k_0 a)$  - Spherical Bessel function

$h_n'(k_0 a)$  - Spherical Hankel function

$P_n^1(x)$  - Associated Legendre function

$k_0$  - Wave number of incident wave

$a$  - Sphere radius

The prime on the expression for  $B_n$  denotes differentiation with respect to  $(k_0 a)$ .

Polynomial approximations exist for the Mie series exact solution.[15] Different polynomials are used for the three frequency regions for scattering. These are: low

frequency or Rayleigh region  $(k,a) < .4$  ; the resonance region  $.4 < (k,a) < 20$  ; and finally the high frequency or physical optics region  $(k,a) > 20$ . Two programs BISCAT and SPSCAT implement both bistatic and monostatic cases in the three frequency regions. Fig.4.4 shows the monostatic scattering of the sphere as calculated. This is exactly the same answer for the scattering of the sphere as the exact solution. The horizontal axis is in terms of the dimensionless quantity  $(k,a)$ . Figure 4.5 a,b,c and d show the bistatic scattering of the metallic sphere of bistatic angles of  $30^\circ, 60^\circ, 90^\circ$ , and  $120^\circ$  degrees. Note that the approximation are only valid in the range:

$$\delta < \theta' < \pi - \delta \quad (4.7)$$

where

$$\delta = O\left(\frac{1}{k,a}\right)$$

which leads to the discontinuities for small  $(k,a)$  at large bistatic angles. BASIC programs BIDISP and SDISP generate the graphs for the sphere simulations. These programs are in appendix II.

An important result from these simulations is that at high frequencies the scattered signal is of constant amplitude and linear phase irrespective of the bistatic scattering angle. The only exception to this is the forward scattering case when  $(\theta)$  equals  $(\pi)$ , where the cross section grows without bound as  $k$  increases. This indicates that the only portion of the sphere that is scattering for large  $(k,a)$  is the front face closest to both the receiver and transmitter; and therefore a ray optics approximation

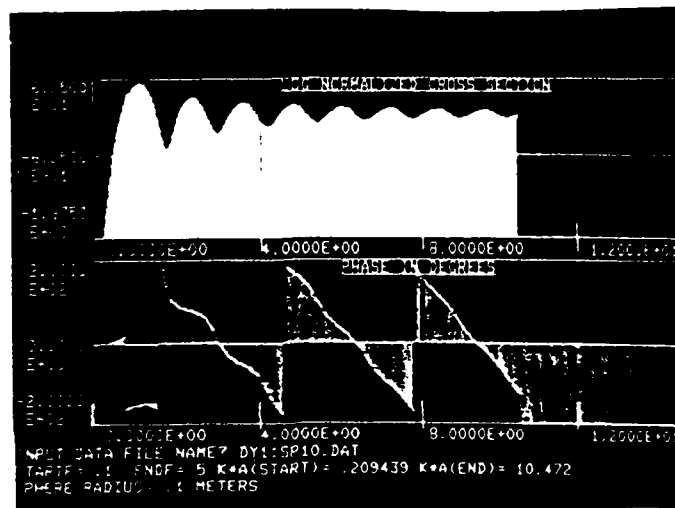
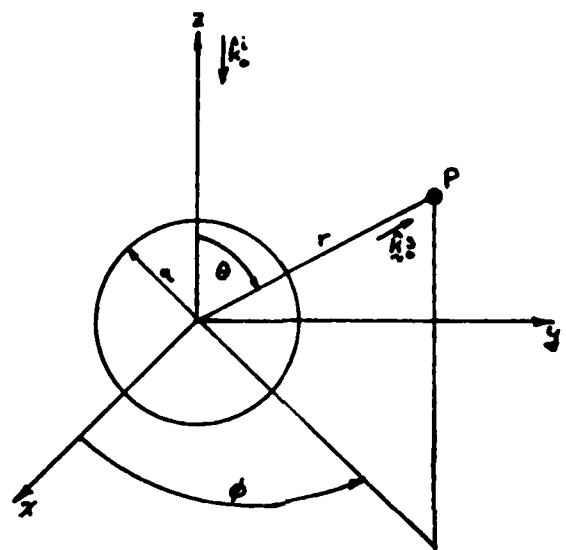
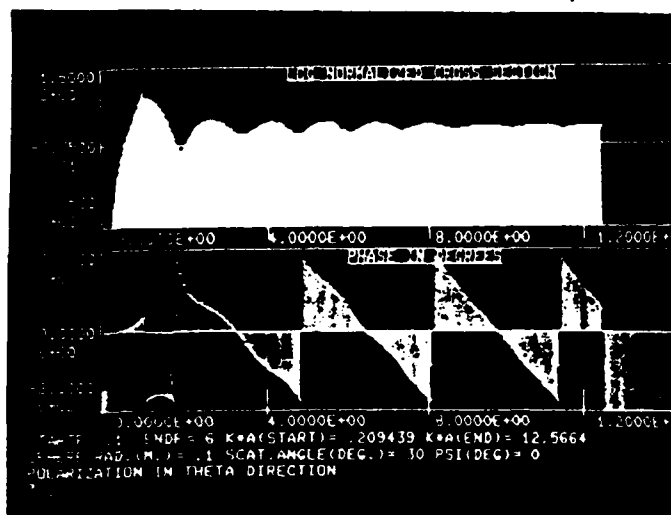


Fig. 4.4 Monostatic scattering for the perfectly conducting sphere. (k a) varies from .2 to 10.5 which corresponds to the scattering of a 20 cm. diameter sphere in the frequency range of .1 to 5.0 GHz. Log normalized cross section:  $\log(\quad)$ .

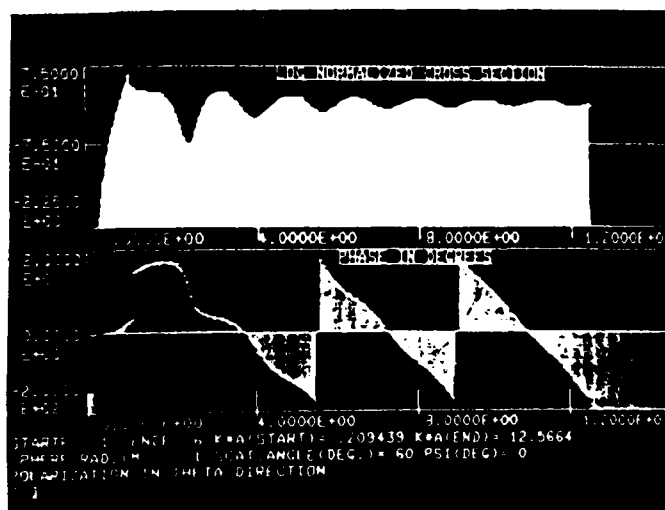


(a)

Fig. 4.5 Bistatic scattering of a 20 cm. diameter conducting sphere in the frequency range .1 to 6.0 GHz;  $.2 < (k \cdot a) < 12.6$ ; polarization of the receiver equal to scattered wave polarization. a) Geometry for scattering expression. b) Bistatic angle  $30^\circ$ . c) Bistatic angle  $60^\circ$ . d) Bistatic angle  $89^\circ$ . e) Bistatic angle  $120^\circ$ .

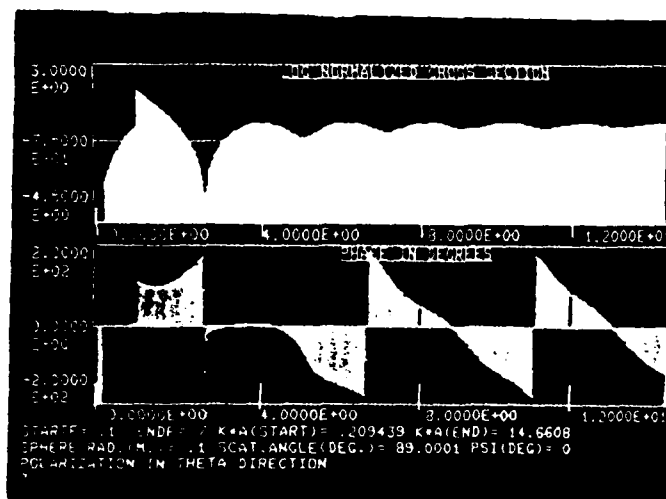


(b)

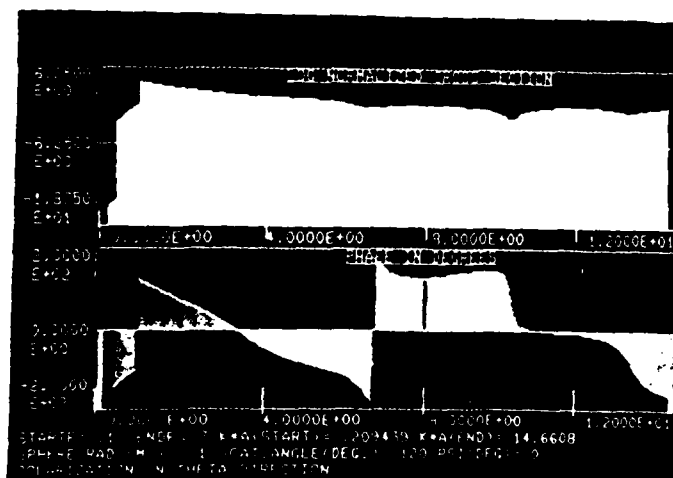


(c)

Fig. 4.5 (contd.) Bistatic scattering of a 20 cm. diameter conducting sphere in the frequency range .1 to 6.0 GHz;  $.2 < (k \cdot a) < 12.6$ ; polarization of the receiver equal to the scattered wave polarization. a) Geometry for scattering expression. b) Bistatic angle  $30^\circ$ . c) Bistatic angle  $60^\circ$ . d) Bistatic angle  $89^\circ$ . e) Bistatic angle  $120^\circ$ .



(d)



(e)

Fig. 4.5 (contd.) Bistatic scattering of a 20 cm. diameter conducting sphere in the frequency range .1 to 6.0 GHz;  $.2 < (k, a) < 12.6$ ; polarization of the receiver equal to the scattered wave polarization. a) Geometry for scattering expression. b) Bistatic angle 30°. c) Bistatic angle 60°. d) Bistatic angle 89°. e) Bistatic angle 120°.

may be applied to find the scattered field.

$$S_1(\theta) = S_2(\theta) = -\frac{1}{2} k_0 a e^{-i2k_0 a \cos \theta/2} \quad (4.8)$$

for the bistatic case. In the monostatic case this reduces to:

$$F(\theta) = -\frac{1}{2} k_0 a e^{-i2k_0 a} \quad (4.9)$$

For targets with features larger than a few wavelengths in size resonance effects become minimal.

Another possible reference target is the long cylinder ( $l \gg a$ ). The scattering of the cylinder in the high frequency region when it is oriented vertically yields an answer similar to that of the sphere. For  $(ka) > 5$  where  $a$  is the cylinder radius, resonance effects disappear and the copolarized scattered field is given by: [15]

$$E_s = E_i \left( \sqrt{\frac{1 + \cos \theta/2}{2}} \right) \exp \{ i k_0 2a \cos \theta/2 \} \quad (4.10)$$

$$r = (R_T + R_R)$$

The equation for the scattering of the cylinder is used for the computer simulations of frequency swept holography.

#### 4.4 Simulation of frequency swept imaging

A series of frequency swept hologram simulations were done of targets that would later be imaged experimentally. The basic arrangement consists of separate receiving and transmitting antennas which measure the scattering of a target that rotates about an axis. The center of rotation is chosen as the phase center of the imaging system. For this configuration the frequency domain data lies in a plane

perpendicular to the axis of rotation. Therefore the transforms of the holograms will be slices in this plane. The first object hologram simulated was comprised of two cylinders equidistant from the rotational axis. This target is shown in fig.4.6. Approximations for the various distances were derived:

$$r_1 \approx r - \frac{r}{2} \sin(\frac{\phi}{2} - \theta) \quad (4.11a)$$

$$r_2 \approx r + \frac{r}{2} \sin(\frac{\phi}{2} - \theta) \quad (4.11b)$$

$$x_1 \approx r + \frac{r}{2} \sin(\frac{\phi}{2} + \theta) \quad (4.11c)$$

$$x_2 \approx r - \frac{r}{2} \sin(\frac{\phi}{2} + \theta) \quad (4.11d)$$

the waves striking cylinders C1 and C2 are given by:

$$E_{c1} = E_0 e^{-i k_0 (\vec{x}_1)} \quad (4.12a)$$

$$E_{c2} = E_0 e^{-i k_0 (\vec{x}_2)} \quad (4.12b)$$

The scattered waves from the two cylinders including the cylinder response then follows:

$$E_{sc1} = E_{c1} \sqrt{\frac{a \cos \phi_1}{z(Rr)}} e^{-i k_0 (r_1 - 2a \cos \frac{\phi}{2})} \quad (4.13a)$$

$$E_{sc2} = E_{c2} \sqrt{\frac{a \cos \phi_2}{z(Rr)}} e^{-i k_0 (r_2 - 2a \cos \frac{\phi}{2})} \quad (4.13b)$$

This is further simplified by combining terms :

$$E_s = 2 E_0 e^{i k_0 (2a \cos \frac{\phi}{2})} \sqrt{\frac{a \cos \phi}{z(Rr)}} \left\{ \cos k_0 l \cos \frac{\phi}{2} \sin \theta \right\} \quad (4.14 b)$$

Finally take the real part of this function for display:

$$R(E_s) = C \cdot \cos(2 k_0 a \cos \frac{\phi}{2}) \cos(k_0 l \cos \frac{\phi}{2} \sin \theta) \quad (4.14b)$$

This was done for a two cylinder target with cylinders 5 cm.



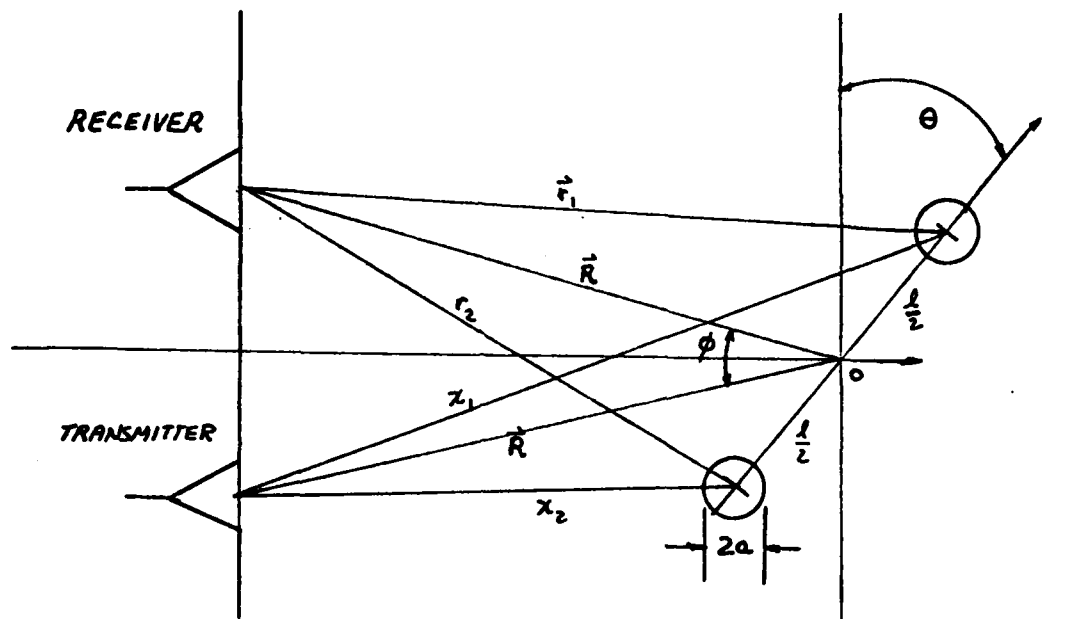
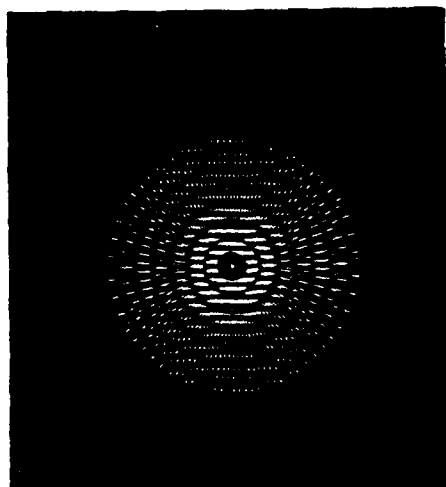


Fig. 4.6 Bistatic scattering of two cylinder target.

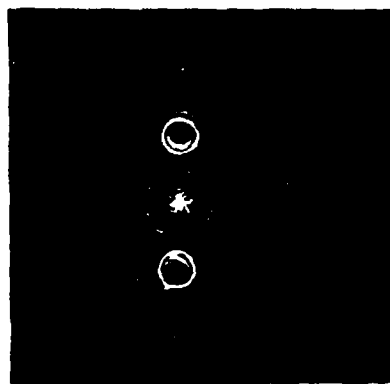
in radius ,separated by 25 cm. using program CYLIN. The results were displayed by program CDISP on a Tektronix 606A CRT display. CDISP gives the option of varying the gray scale compression of the hologram either logarithmically or by constant multiplication. These programs are listed in appendix II. The resultant hologram and the reconstructions obtained through Fourier transformation on the optical bench appear in figs.4.7 a,b The hologram simulated a sweep from 2.0 to 18.0 GHz in 64 frequency steps. The target in the simulation rotated 360 degrees in 128 steps.

Another target simulated which did not have the symmetry of the first target was comprised of two cylinders both mounted to one side of the rotational axis, as shown in fig.4.8. Two simulations were done of this target with varying diameter cylinders. In the first case 7 cm radius cylinders were used. The hologram for this case and the Fourier transform reconstructions are shown in figs.4.8 b,c,d. For the second simulation the target was two cylinders 3.5 cm in radius. In both cases the cylinders were located 10 cm from the center of rotation and the simulation was for a 2.0 to 18.0 GHz sweep. The hologram and the transformed images are shown in figs.4.9 a,b,c. The two cylinder off axis target was simulated by first calculating the copolarized scattered field for a single cylinder:

$$\vec{E}_s = 2\vec{E}_i e^{i\mathbf{k} \cdot \mathbf{r}_0} e^{-i\mathbf{k} \cdot \mathbf{r}_0} \quad (4.15)$$



(a)



(b)

Fig. 4.7 a) Simulation Hologram of two cylinder target; 10 cm. diameter, 25 cm. apart. Frequency range: 2.0-18.0 GHz; 128 lines, 64 points/line. b) Optical Fourier transform of hologram.

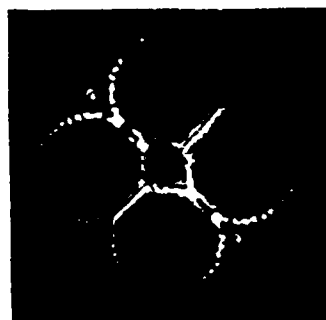
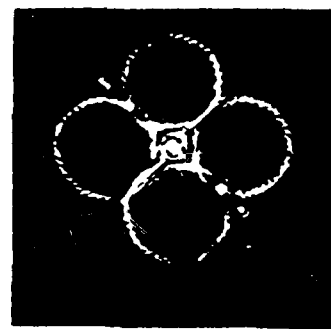
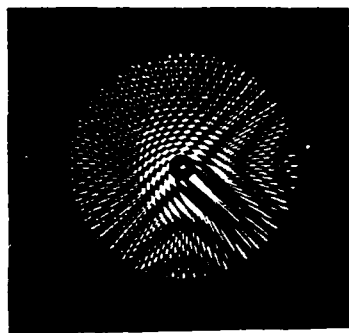
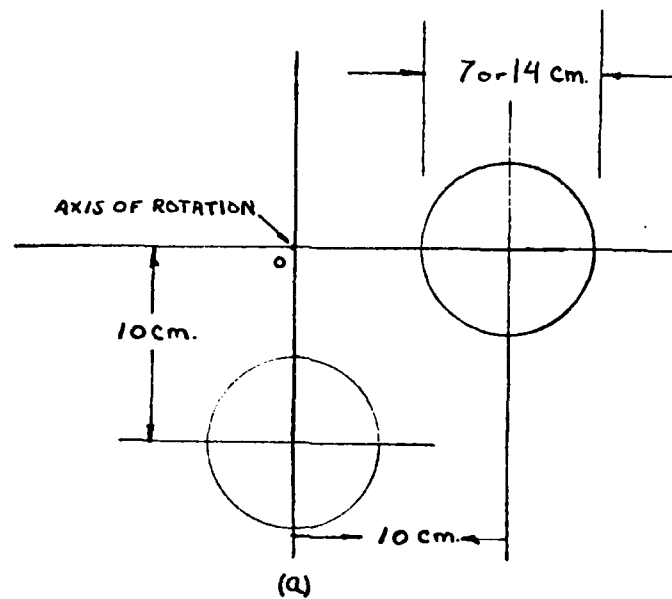
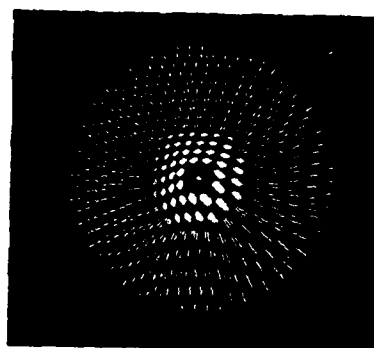
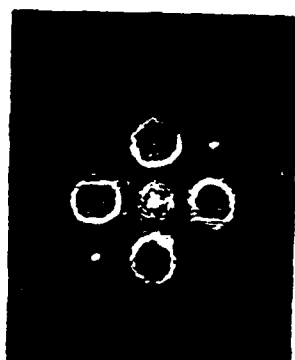


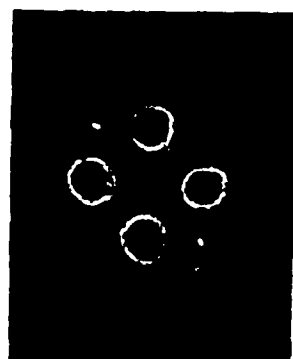
Fig. 4.8 a) Geometry of two cylinder off-axis target. b) Hologram simulation two cylinder off-axis target; 2.0-18.0 GHz; 64 points/line; 128 lines. b) Transform with zero order term. c) Transform with zero order removed.



(a)



(b)



(c)

Fig. 4.9 a) Hologram simulation of off-axis two cylinder target with cylinders 7 cm. in diameter; 2.0-18.0 GHz b) Optical Fourier transform with zero order. c) Transform with zero order term removed.

taking the real part:

$$\begin{aligned} R\{E_s\} &= 2E_0 \{ \cos k_z z a \cos k_z l \sin \theta + \sin k_z z a \sin k_z l \sin \theta \} \quad (4.15a) \\ &= 2E_0 \cos(k_z z a - k_z l \sin \theta) \end{aligned}$$

For the two cylinder off axis target, one cylinder is at  $(\theta)=0^\circ$  and the other at  $(\theta)=90^\circ$ , therefore the scattered field is given by:

$$R\{E_s\} = C \cdot \{ \cos(k_z z a - k_z l \sin \theta) + \cos(k_z z a - k_z l \cos \theta) \} \quad (4.16)$$

In general for an arbitrary set of circular scatterers of radius  $a$  and distance  $l$  from the origin; the scattered field may be written:

$$R\{E_s\} = \sum_n \cos \{ k_z z a_n - k_z l_n \sin(\theta + \theta_n) \} \quad (4.17)$$

This gives the capability to simulate the scattering of any target given that it can be decomposed into  $N$  spherical scattering centers.

#### 4.6 Experimental results

An experimental system for the implementation of swept frequency imaging was setup in the anechoic chamber at the Graduate Research Center in the Moore School. The frequency range for these experiments was from 6.3 to 16.0 GHz in 64 discrete steps. The targets were rotated 360 degrees in 128 steps. These holograms were then identical in form to the simulations previously done.

The system for error correction and range phase shift removal was that used for high signal to noise ratio signals. The reference target was a cylinder positioned so

that its front face was located on the axis of rotation as in fig.4.10. A plot of system response is shown in fig.4.11. This data represents the combined characteristics of the antennas, amplifier, cables and clutter. In addition it contains the linear phase shift that is the range phase factor. As an example for the two cylinder target shown in 4.12 the raw data, magnitude and phase is shown in fig.4.13. Figure 4.14 shows how this data has been corrected for range phase and system response. This data was generated using the Fortran program SPHER3.

The experimental properties of the two cylinder target were studied extensively. Both the scattering as a function of frequency for a specific orientation of the target and the scattering as a function of angular rotation at specific frequencies was obtained. In figs. 4.15 a,b,c are shown the corrected frequency response of the target for orientations of  $45^\circ$ ,  $90^\circ$  and  $135^\circ$  degrees.

Another computer program ANTPAT was written to obtain the radiation pattern of an arbitrary target or antenna. In the two cylinder case the pattern was measured at 5.0, 10.0 and 15.0 GHz. Note that when the cylinders are collinear all that is seen is the front surface specular reflection of the one cylinder hence the pattern of a point scatterer in the vicinity of  $0^\circ$  degrees. These patterns are shown in figs.4.16 a,b,c. At high frequencies the lobe spacing is much closer than at low frequencies, consistent with the theoretical result for the pattern. To see this examine the

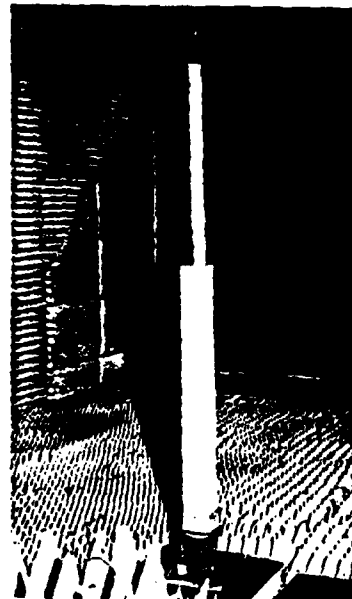
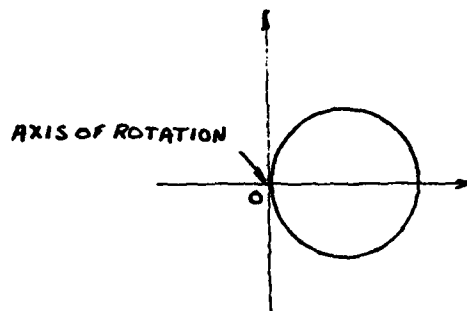


Fig. 4.10 Reference target on pedestal; 80 cm. long cylinder, 7 cm. in diameter.

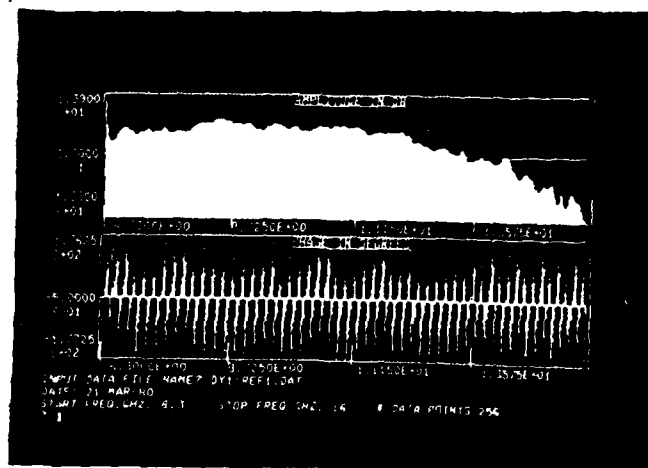


Fig. 4.11 Reference target response including system response and range phase shift; 6.3-16.0 GHz.



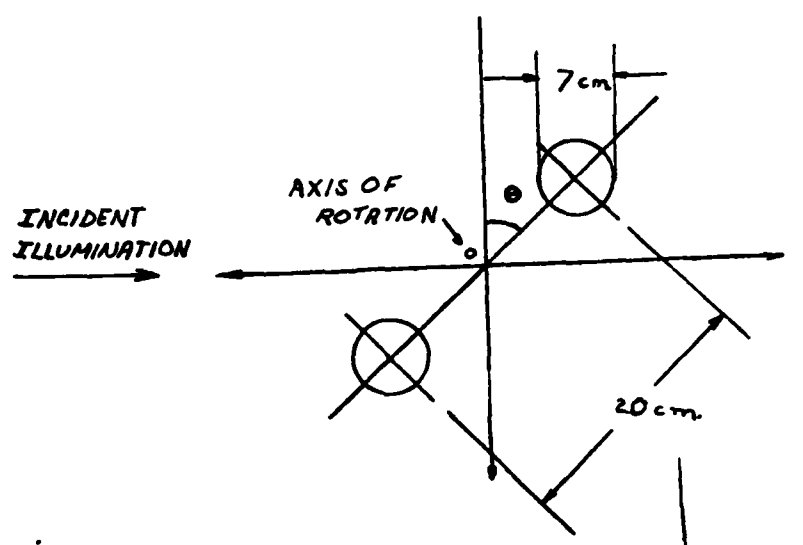


Fig. 4.12 Two cylinder target geometry.

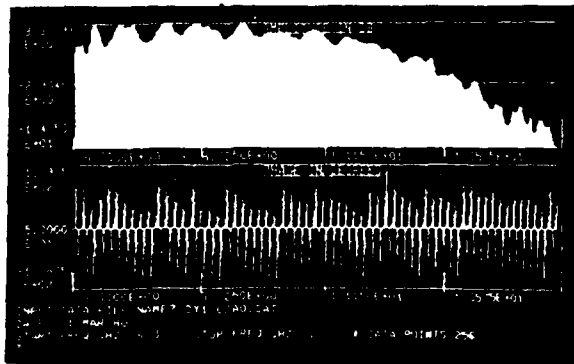


Fig. 4.13 Uncorrected scatter data for symmetrical two cylinder target ;  $(\theta) = 0^\circ$  , 6.3-16.0 GHz.

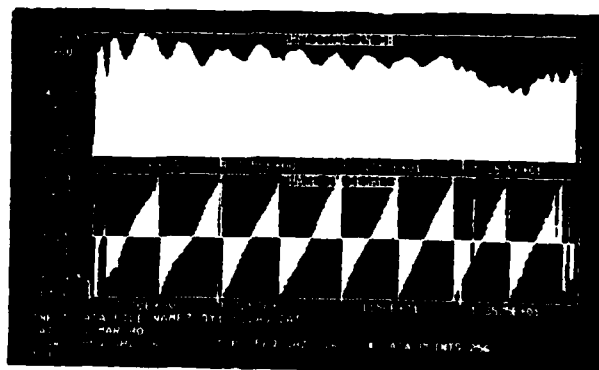
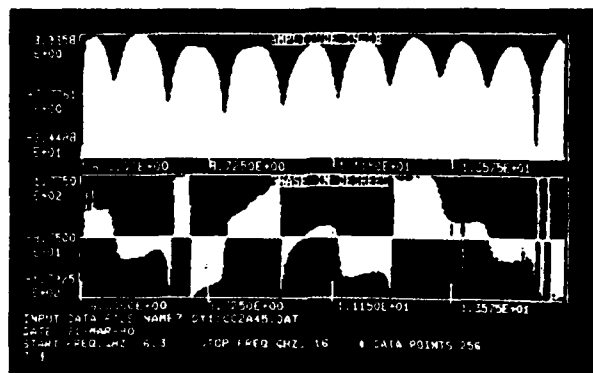
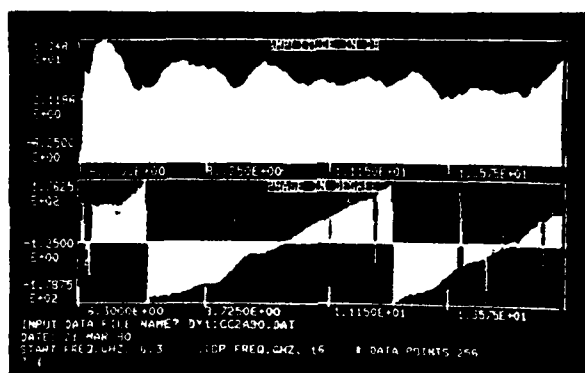


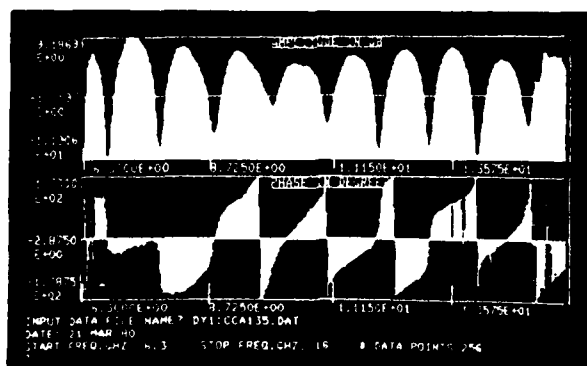
Fig. 4.14 Corrected two cylinder target data using system response of Fig. 4.11.



(a)

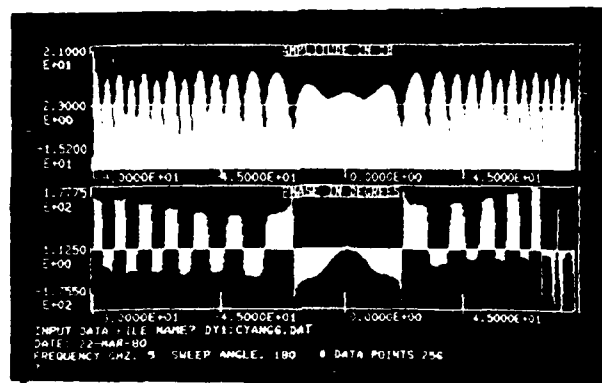


(b)

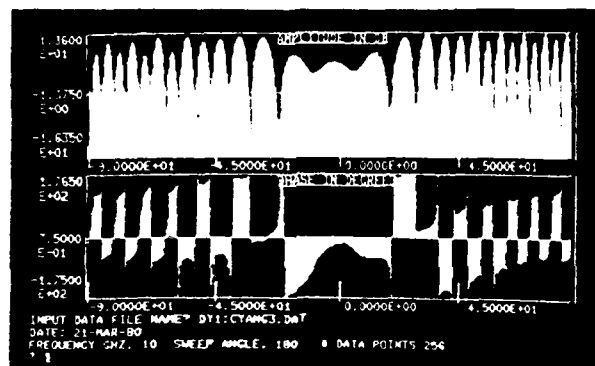


(c)

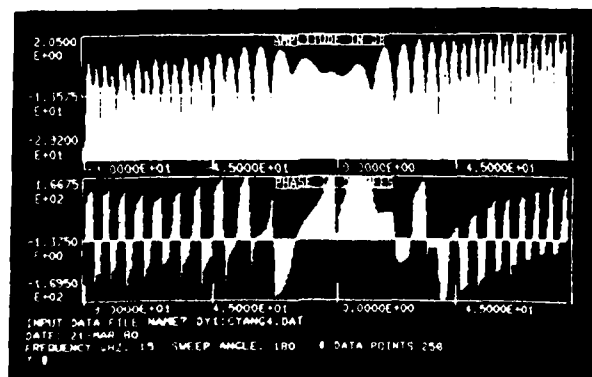
Fig. 4.15 a) Corrected two cylinder symmetrical target response; 6.3-16.0 GHz,  $(\theta) = 45^\circ$ . b)  $(\theta) = 90^\circ$ . c)  $(\theta) = 135^\circ$ .



(a)



(b)



(c)

Fig. 4.16 Scattering pattern of two cylinder target of Fig. 4.12 at different frequencies as a function target rotation angle. a) 5.0 GHz. b) 10.0 GHz. c) 15.0 GHz.

expression for the monostatic scattering of the symmetrical two cylinder target:

$$E_s = C \cdot \{ e^{i k_z 2a} \cdot \cos k_z l \cdot \sin \theta \} \quad (4.18)$$

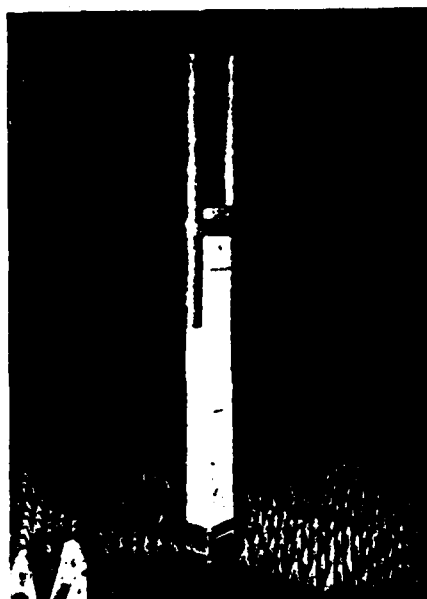
The expression for the scattering of the target at a given frequency as a function of angular rotation may be written:

$$E_s(k_z = k_z) = C \cdot \cos k_z l \sin \theta \quad C - \text{constant} \quad (4.19)$$

As for the swept frequency response;  $l \sin(\theta)$  remains constant, and the hence the swept frequency response is sinusoidal with period dependent on  $(k_z)$  and  $l$ .

The final test for the system was the generation of actual holograms. The first target measured was the two cylinder target shown in fig.4.17a. The cylinders are of aluminum, 80 cm. in length and 7 cm. in diameter. The real part of the corrected swept frequency data in the range 6.3 to 16.0 GHz was stored and displayed on the CRT. The targets were rotated 360 degrees in 128 steps yielding a total of 8192 points in the hologram (64 points/line \* 128 lines). The center of the hologram is at 0 HZ with radial distance directly proportional to frequency. An example is shown in fig.4.17b and the reconstructions in figs.4.17c and d. These Fourier transforms were done optically. [17]

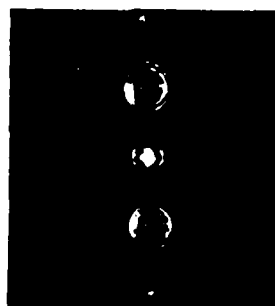
This procedure was followed for other targets not having the symmetry of the first object used. The target type was the same as the simulations done previously. The



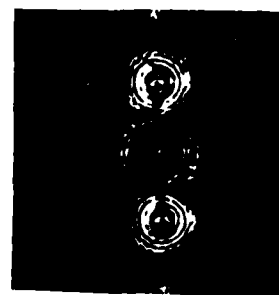
(a)



(b)



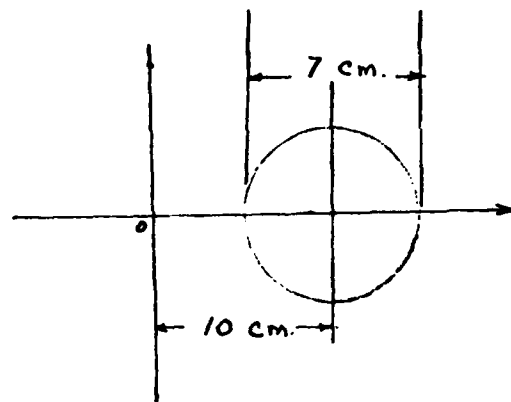
(c)



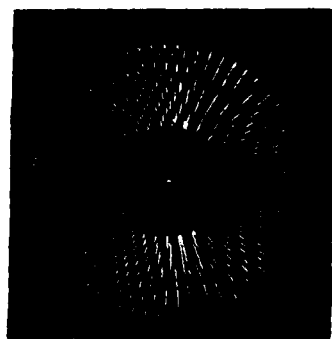
(d)

Fig. 4.17 a) Two cylinder target in anechoic chamber on rotating pedestal. b) Hologram of target measured between 5.3 and 16 GHz corrected for range and system response; 128 lines, 64 points/line. c) Optical Fourier transform of hologram. c) Optical Fourier transform without zero order term.

first of these was a single cylinder mounted off axis as shown in fig.4.18a. This cylinder was the same as the others used and the frequency range and angular sweep were identical to that of the two cylinder target. The hologram and reconstructions are shown in figs.4.18 b,c,d. The final target was the two off axis cylinder target pictured in fig.4.19a. The frequency diversity hologram and transforms are in figs.4.19 b,c,d.



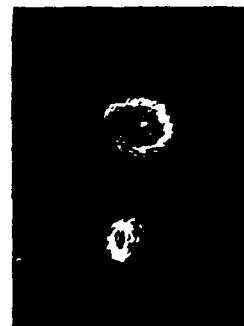
(a)



(b)



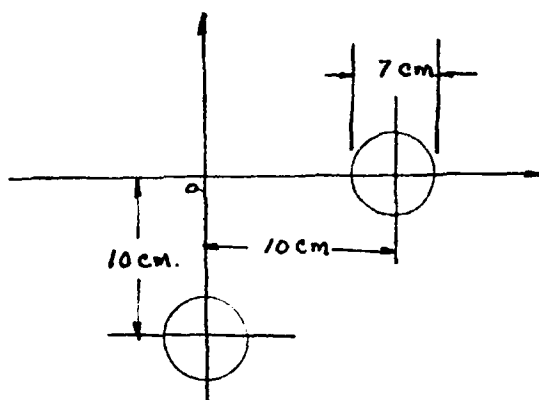
(c)



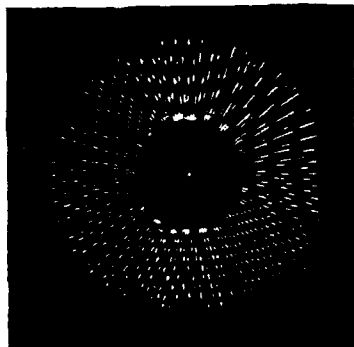
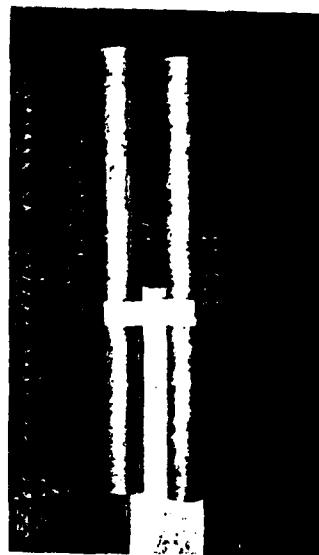
(d)

Fig. 4.18 a) Single cylinder off-axis target and position in anechoic chamber. b) Experimental hologram of target; 6.3-16 GHz; 128 lines, 64 points/line; corrected for range and system response. c) Optical Fourier transform of hologram. d) Optical Fourier transform without zero order term.

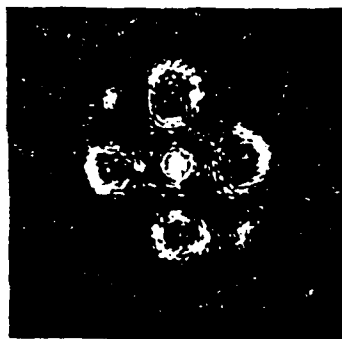




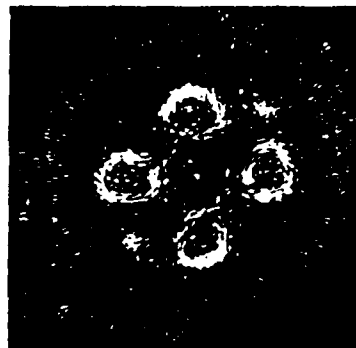
(a)



(b)



(c)



(d)

Fig. 4.19 a) Two cylinder off-axis target geometry and position in anechoic chamber. corrected for range and system response. c) Optical Fourier transform of hologram. d) Optical Fourier transform without zero order term.

## V Conclusion

This thesis has described an automated swept frequency measuring system. This system may be used for radar cross section measurement, antenna pattern measurement and swept frequency holography. The system has a useful range of 5.0-17.0 GHz in which amplitude and phase of the scattered microwaves from targets in the anechoic chamber of the Graduate Research Center may be recorded and stored. A DEC MINC LSI-11/2 completely automates the data acquisition process. A complete error correction algorithm was implemented using the data storage and processing capabilities of the minicomputer.

The effect of range phase shift on swept frequency holograms was investigated and various techniques for its removal were investigated. It is believed that a TDR system for range phase removal is required for implementation of a practical radar system. This system must have extremely high resolution for coherent imaging. The relationship between TDR system bandwidth, receiver channel bandwidth and resolution was derived:

$$\text{Resolution} = \frac{\sigma_0 c}{\Delta f 2\pi} = \frac{\sqrt{2 N_s B} c}{4\pi A \Delta f} \quad 322$$

where  $(\Delta f)$  is the imaging bandwidth,  $(R)$  the range uncertainty,  $B$  the receiver channel bandwidth and  $N_s$  the noise power spectral density.

Simulations were performed for the scattering of various radar targets which include the conducting sphere,

## V Conclusion

This thesis has described an automated swept frequency measuring system. This system may be used for radar cross section measurement, antenna pattern measurement and swept frequency holography. The system has a useful range of 5.0-17.0 GHz in which amplitude and phase of the scattered microwaves from targets in the anechoic chamber of the Graduate Research Center may be recorded and stored. A DEC MINC LSI-11/2 completely automates the data acquisition process. A complete error correction algorithm was implemented using the data storage and processing capabilities of the minicomputer.

The effect of range phase shift on swept frequency holograms was investigated and various techniques for its removal were investigated. It is believed that a TDR system for range phase removal is required for implementation of a practical radar system. This system must have extremely high resolution for coherent imaging. The relationship between TDR system bandwidth, receiver channel bandwidth and resolution was derived:

$$\text{Resolution} = \frac{\sigma_0 c}{\Delta f 2\pi} = \frac{\sqrt{2N} B c}{4\pi A \Delta f} \quad 322$$

where  $(\Delta f)$  is the imaging bandwidth,  $(R)$  the range uncertainty,  $B$  the receiver channel bandwidth and  $N$  the noise power spectral density.

Simulations were performed for the scattering of various radar targets which include the conducting sphere,

infinite cylinder and combinations of these. The holograms recorded from these analytical results reconstruct the targets extremely well and set a goal for practical system performance. An expression was derived for the scattering of N spherical/cylindrical cylinders in a plane passing through their centers:

$$R\{E_s\} = \sum_n \cos\{kz a_n - k l_n \sin(\theta + \theta_n)\} \quad (4.17)$$

where l is the distance from the axis of rotation ( $\theta_n$ ) the angle relative to some reference for the target angular position and a the target radius.

Finally experimental swept frequency holograms were generated using a rotating pedestal under computer control to scan the target in one dimension. The experiments done indicate the feasibility of implementing a practical holographic radar system. The holograms obtained for various targets agree well with theory even though the error correction and range phase shift removal techniques used were robust in nature. It is believed that better images are possible given that the error correction techniques previously outlined are implemented.

Further work can be done in testing the TDR techniques for their suitability for an imaging system. The system may also be expanded to include scanning in the ( ) direction to give true 3-D imaging capability. This may be implemented by adding a stepper motor controlled azimuthal scanner to the top of the rotating column.

infinite cylinder and combinations of these. The holograms recorded from these analytical results reconstruct the targets extremely well and set a goal for practical system performance. An expression was derived for the scattering of N spherical/cylindrical cylinders in a plane passing through their centers:

$$R\{E_s\} = \sum_n \cos\{kz a_n - k l_n \sin(\theta + \theta_n)\} \quad (4.17)$$

where  $l$  is the distance from the axis of rotation ( $\theta_n$ ) the angle relative to some reference for the target angular position and  $a$  the target radius.

Finally experimental swept frequency holograms were generated using a rotating pedestal under computer control to scan the target in one dimension. The experiments done indicate the feasibility of implementing a practical holographic radar system. The holograms obtained for various targets agree well with theory even though the error correction and range phase shift removal techniques used were robust in nature. It is believed that better images are possible given that the error correction techniques previously outlined are implemented.

Further work can be done in testing the TDR techniques for their suitability for an imaging system. The system may also be expanded to include scanning in the ( ) direction to give true 3-D imaging capability. This may be implemented by adding a stepper motor controlled azimuthal scanner to the top of the rotating column.

# BIBLIOGRAPHY

- [1] N.H. Farhat, 'Frequency Synthesized Imaging Apertures', Proceedings of the 1976 International Optical Computing Conference, IEEE Cat. No. 76 CH 1100-7c, 1976
- [2] N.H. Farhat, 'Principles of Broadband Coherent Imaging', J. Opt. Soc of Am., Vol.67, pp. 1015-1021, Aug. 1977.
- [3] N.H. Farhat, 'Microwave Holographic Imaging-Prospects for a Real time Camera', Proc. SPIE Technical Symposium, Vol. 180, Real-Time Signal Processing II, 1979.
- [4] N.H. Farhat and C.K. Chan, "Three Dimensional Imaging by Wave Vector Diversity", Presented at 8 Symposium on Acoustical Imaging; Key Biscayne, Fla. May 29-June 2 1978.
- [5] Robert J. Collier, C.B. Burckhardt and L.H. Lin, Optical Holography. New York: Academic Press, 1971.
- [6] J.S. Hollis, T.J. Lyon and L. Clayton, Microwave Antenna Measurements. Atlanta, Georgia: Scientific Atlanta, 1970
- [7] William B. Weir, LLOYD A. Robinson, Don Parker, "Broadband Automated Radar Cross Section Measurements", IEEE Transactions on Antennas and Propagation. Vol. 12 pp. 780-784, Nov. 1974.
- [8] Athanasios Papoulis, Signal Analysis. New York: McGraw-Hill, 1977.
- [9] John B. Thomas, An Introduction to Statistical Communication Theory. New York: John Wiley & Sons, 1969.
- [10] Advisory Group for Aerospace Research and Development: "Spread Spectrum Communications", U.S. Department of Commerce. AD-766-914, July 1973.
- [11] Henning F. Harmuth, Sequency Theory, Foundations and Applications. New York: Academic Press, 1977.
- [12] Athanasios Papoulis, Systems and Transforms with Applications in Optics. New York: McGraw-Hill, 1968.
- [13] CHI Keung Chan, "Analytical and Numerical Studies of

# BIBLIOGRAPHY

- [1] N.H. Farhat, 'Frequency Synthesized Imaging Apertures', Proceedings of the 1976 International Optical Computing Conference, IEEE Cat. No. 76 CH 1100-7c, 1976
- [2] N.H. Farhat, 'Principles of Broadband Coherent Imaging', J. Opt. Soc of Am., Vol.67, pp. 1015-1021, Aug. 1977.
- [3] N.H. Farhat, 'Microwave Holographic Imaging-Prospects for a Real time Camera', Proc. SPIE Technical Symposium, Vol. 180, Real-Time Signal Processing II, 1979.
- [4] N.H. Farhat and C.K. Chan, "Three Dimensional Imaging by Wave Vector Diversity", Presented at 8 Symposium on Acoustical Imaging; Key Biscayne, Fla. May 29-June 2 1978.
- [5] Robert J. Collier, C.B. Burckhardt and L.H. Lin, Optical Holography. New York: Academic Press, 1971.
- [6] J.S. Hollis, T.J. Lyon and L. Clayton, Microwave Antenna Measurements. Atlanta, Georgia: Scientific Atlanta, 1970
- [7] William B. Weir, LLOYD A. Robinson, Don Parker, "Broadband Automated Radar Cross Section Measurements", IEEE Transactions on Antennas and Propagation. Vol. 12 pp. 780-784, Nov. 1974.
- [8] Athanasios Papoulis, Signal Analysis. New York: McGraw-Hill, 1977.
- [9] John B. Thomas, An Introduction to Statistical Communication Theory. New York: John Wiley & Sons, 1969.
- [10] Advisory Group for Aerospace Research and Development: "Spread Spectrum Communications", U.S. Department of Commerce. AD-766-914, July 1973.
- [11] Henning F. Harmuth, Sequency Theory, Foundations and Applications. New York: Academic Press, 1977.
- [12] Athanasios Papoulis, Systems and Transforms with Applications in Optics. New York: McGraw-Hill, 1968.
- [13] CHI Keung Chan, "Analytical and Numerical Studies of

Frequency Swept Imaging", Phd. Thesis. Department of Electrical Engineering; University of Pennsylvania, 1978.

- [14] W.H. Wells, "Acoustical Imaging with Linear Transducer Arrays", Acoustical Holography, Vol. 2, A.F. Melherall and L.Larmaore, (Eds.) New York: Plenum, 1970.
- [15] G.T. Ruck, Radar Cross Section Handbook. New York: Plenum, 1970.
- [16] G. Mie, "Beitrage zur Optik truber Median speziell Kolloidaler Metallosungen", Ann. Phys. 25:377 1908.
- [17] J.W. Goodman, Introduction to Fourier Optics. New York: McGraw-Hill, 1968.



**APPENDIX I**

```

620 PRINT B2,B1,B0
630 PRINT \ PRINT
640 PRINT 'DO YOU WANT TO TEST THE DATA'
650 INPUT A$ \ IF A$='N' THEN GO TO 1020
660 PRINT 'THIS IS A TEST OF THE PREDICTION CAPABILITIES OF THE INTERPOLAT
670 PRINT 'FUNCTIONS. INPUT THE VOLTAGE IN MILLIVOLTS. TO TERMINATE ENTER
680 PRINT 'NUMBER GREATER THAN 1000.'
690 SEND 'M1' \ A1
700 PRINT \ PRINT
710 PRINT 'INPUT THE VOLTAGE IN MV.'
720 INPUT A \ IF A>9999 THEN GO TO 820
730 A$='V'+STR$(A)+'E'+CHR$(13)+CHR$(10)
740 SEND(A$.4)
750 F1=B0-B1*A-B2*A^2
760 F=SEND(C)
770 PRINT \ PRINT 'QUADRATIC FIT: F1
780 PRINT 'LINEAR FIT: TAB(14),F
790 PRINT
800 GO TO 710
810 PRINT \ PRINT
820 PRINT \ PRINT 'THIS PART OF THE PROGRAM WILL GENERATE THE ENTERED FRE
830 PRINT 'THE RANGE IS FROM 2.005-17.970 GHZ. ENTER 0 TO TERMINATE.'
840 PRINT 'WIT RETURN FOR QUADRATIC FIT'
850 INPUT 'INPUT FREQUENCY IN GHZ'
860 PRINT
870 INPUT F \ IF F=0 THEN GO TO 1020
880 V=(F-C)/M
890 V1=(-B1+SOR(B1^2-4*B2*(B0-F)))/(2*B2)
900 IF INT(10*V1)-10=INT(V1)>5 THEN V=V1+1
910 IF INT(10*V1)-10=INT(V1)>5 THEN V=V1+1
920 V1=INT(V1)
930 PRINT
940 V=INT(V)
950 A$='V'+STR$(V)+'E'+CHR$(13)+CHR$(10)
960 SEND(A$.4) \ PRINT 'FREQUENCY GENERATED FROM LINEAR FIT'
970 A$='V'+STR$(V1)+'E'+CHR$(13)+CHR$(10)
980 INPUT Z$
990 SEND(A$.4)
1000 PRINT 'FREQUENCY GENERATED FROM QUADRATIC FIT' \ PRINT
1010 GO TO 850
1020 CLOSE #1
1030 S=0 \ S1=0
1040 FOR I=1 TO 25
1050 S=S+(B1)-(M*A(I)+C))^2
1060 S1=S1*(B1)-(B0+B1*A(I)+B2*A(I)^2))^2
1070 NEXT I
1080 S=S/25 \ S1=S1/25
1090 PRINT \ PRINT 'STANDARD DEVIATION FOR THE LINEAR FIT: SOR(S), 'OH
1100 PRINT \ PRINT 'STANDARD DEVIATION FOR THE QUADRATIC FIT: SOR(S1), '
1110 END

```

```

10 DIM A(25),B(25)
20 PRINT 'THIS PROGRAM WILL CALABRATE THE MICROWAVE SHEEPER' \ PRINT
30 PRINT 'ENTER NEW DATA (V OR N)'
40 INPUT D$
50 IF D$='V' THEN GO TO 120
60 PRINT 'WHAT FILE NAME?' \ INPUT Z$
70 OPEN Z$ FOR INPUT AS FILE #1
80 FOR L=1 TO 25
90 INPUT #1,A(L),B(L)
100 NEXT L
110 GO TO 240
120 SEND 'M1' \ A1
130 PRINT 'WHAT FILE NAME?' \ INPUT Z$
140 OPEN Z$ FOR OUTPUT AS FILE #1
150 FOR I=1 TO 25
160 A(I)=500+375*(I-1)
170 C$='V'+STR$(A(I))+'E'+CHR$(13)+CHR$(10)
180 PRINT 'COMMAND: 'C$
190 SEND(C$.4)
200 PRINT 'INPUT THE COUNTER FREQUENCY'
210 INPUT B(I)
220 PRINT #1,A(I) \ PRINT #1,B(I)
230 NEXT I
240 V1=0 \ V2=0 \ C=0 \ N1=0 \ N2=0
250 FOR I=1 TO 25
260 N1=N1+A(I) \ N2=N2+B(I) \ V1=V1+A(I)^2 \ V2=V2+B(I)^2 \ C=C+A(I)*B(I)
270 NEXT I
280 FOR J=1 TO 25 \ PRINT A(J),B(J) \ NEXT J
290 PRINT 'CONTINUE FOR GRAPH (RETURN)' \ INPUT Z$
300 DISPLAY+CLEAR
310 GRAPH('LINES,BRANDS',25,A(1),B(1))
320 LABEL('LINEAR LINE', 'SHEEPER CALABRATION ****',1)
330 PRINT 'CONTINUE (RETURN)' \ INPUT Z$
340 DISPLAY+CLEAR
350 N1=N1/25 \ N2=N2/25 \ C=C/25 \ V1=V1/25 \ V2=V2/25
360 PRINT 'M1', 'M2', 'V1', 'V2', 'C'
370 PRINT N1,N2,V1,V2,C
380 M=(C-N1*N2)/(V1-N1^2)
390 PRINT \ PRINT
400 PRINT 'SLOPE='M
410 PRINT
420 C=N2-M*N1
430 PRINT 'INTERCEPT='C
440 N=25
450 Z1=0 \ Z2=0 \ Z3=0 \ Z4=0 \ V1=0 \ V2=0 \ V3=0
460 FOR I=1 TO 25
470 Z1=Z1+A(I) \ Z2=Z2+A(I)^2 \ Z3=Z3+A(I)^3 \ Z4=Z4+A(I)^4
480 V1=V1+B(I) \ V2=V2+B(I)*B(I) \ V3=V3+B(I)^2*B(I)
490 NEXT I
500 PRINT 'Z1', 'Z2', 'Z3', 'Z4'
510 PRINT Z1,Z2,Z3,Z4
520 PRINT \ PRINT
530 PRINT 'V1', 'V2', 'V3'
540 PRINT V1,V2,V3
550 PRINT \ PRINT
560 D$=(Z2+Z4-Z3^2)-Z1*(Z1+Z4-Z2+Z3)+Z2*(Z1+Z3-Z2^2)
570 B0=V1*(Z2+Z4-Z3^2)-V2*(Z1+Z4-Z2+Z3)+V3*(Z1+Z3-Z2^2)
580 B1=N1*(V2+Z4-V3*Z3)-V1*(Z1+Z4-Z2+Z3)+Z2*(Z1+Z3-Z2^2)
590 B2=N1*(Z2+V3-Z3*V2)-Z1*(Z1+V3-Z2+V2)+V1*(Z1+Z3-Z2^2)
600 B0=B0/D \ B1=B1/D \ B2=B2/D
610 PRINT 'B2', 'B1', 'B0'

```

0001      PORTMAN IV      V02 1-1      THU 09-AUG-79 00:36:32      PAGE 001

PROGRAM SYSES  
VERSION 1 2  
THIS PROGRAM WILL GENERATE THE SYSTEM RESPONSE USING THE  
SUBROUTINES FOR PAD, ISOLATION, TRANSFER FUNCTION AND  
ANTENNA RESPONSE GENERATION AND REMOVAL. THE END RESULT IS A  
FILE WITH NORMALIZED INTEGERS WITH THE SYSTEM RESPONSE FILES  
ARE GENERATED AT EACH STEP YIELDING A MODULAR PROCEDURE IN  
THIS PROCESS. HENCE A COMPONENT OF THE SYSTEM COULD BE  
CHANGED WITH OUT HAVING TO START FROM THE BEGINNING. FOR  
EXAMPLE A DIFFERENT ANTENNA COULD BE SUBSTITUTED AND THE  
SYSTEM RESPONSE COULD BE MEASURED WITHOUT HAVING TO START  
FROM THE BEGINNING WITH THE MEASUREMENT OF THE PAD  
CHARACTERISTICS

COMMON/PADA/IAMPAD, IPH4, IFLAG, FSTART, FEND, STEP, NPOINT, NSAMP  
COMMON/ISTA/IAMP2, IPH2, IFLAG2, NSAMP2  
COMMON/TRANSA/IAMP3, IPH3, IFLAG3, NSAMP3, IAMP4, IPH4  
COMMON/ANTA/IAMP5, IPH5, IFLAG4, NSAMP4, IAMP6, IPH6

INTEGER IAMPAD(512), IPH4(512), IAMP2(512), IPH2(512), IAMP3(512)  
INTEGER IPH3(512), IAMP4(512), IPH4(512), IPH5(512), IAMP5(512)  
INTEGER IPH6(512), IAMP6(512)

BYTE A  
TYPE 900  
TYPE 801  
ACCEPT \*, IUNIT  
TYPE 907  
ACCEPT \*, IFLAG  
IF (IFLAG) 10, 10, 20  
TYPE 908  
ACCEPT \*, NSAMP  
CALL PAD  
TYPE 901  
ACCEPT 700, A  
IF (A EQ 'N') GO TO 200  
WRITE(IUNIT, 902)  
WRITE(IUNIT, 903)  
DO 100 K=1, NPOINT  
AMPLIT=FLOAT(IAMPAD(K))\* .05  
PHASE=FLOAT(IPH4(K))\* .25  
FREQ=FLOAT(IAMP(K-1))\*STEP  
WRITE(IUNIT, 800)K, FREQ, AMPLIT, PHASE  
CONTINUE  
TYPE 909  
ACCEPT \*, IFLAG2  
IF (IFLAG2) 210, 210, 220

0002      PORTMAN IV      V02 1-1      THU 09-AUG-79 00:36:32      PAGE 002

PROGRAM SYSES  
VERSION 1 2  
THIS PROGRAM WILL GENERATE THE SYSTEM RESPONSE USING THE  
SUBROUTINES FOR PAD, ISOLATION, TRANSFER FUNCTION AND  
ANTENNA RESPONSE GENERATION AND REMOVAL. THE END RESULT IS A  
FILE WITH NORMALIZED INTEGERS WITH THE SYSTEM RESPONSE FILES  
ARE GENERATED AT EACH STEP YIELDING A MODULAR PROCEDURE IN  
THIS PROCESS. HENCE A COMPONENT OF THE SYSTEM COULD BE  
CHANGED WITH OUT HAVING TO START FROM THE BEGINNING. FOR  
EXAMPLE A DIFFERENT ANTENNA COULD BE SUBSTITUTED AND THE  
SYSTEM RESPONSE COULD BE MEASURED WITHOUT HAVING TO START  
FROM THE BEGINNING WITH THE MEASUREMENT OF THE PAD  
CHARACTERISTICS

COMMON/PADA/IAMPAD, IPH4, IFLAG, FSTART, FEND, STEP, NPOINT, NSAMP  
COMMON/ISTA/IAMP2, IPH2, IFLAG2, NSAMP2  
COMMON/TRANSA/IAMP3, IPH3, IFLAG3, NSAMP3, IAMP4, IPH4  
COMMON/ANTA/IAMP5, IPH5, IFLAG4, NSAMP4, IAMP6, IPH6

INTEGER IAMPAD(512), IPH4(512), IAMP2(512), IPH2(512), IAMP3(512)  
INTEGER IPH3(512), IAMP4(512), IPH4(512), IPH5(512), IAMP5(512)  
INTEGER IPH6(512), IAMP6(512)

BYTE A  
TYPE 900  
TYPE 801  
ACCEPT \*, IUNIT  
TYPE 907  
ACCEPT \*, IFLAG  
IF (IFLAG) 10, 10, 20  
TYPE 908  
ACCEPT \*, NSAMP  
CALL PAD  
TYPE 901  
ACCEPT 700, A  
IF (A EQ 'N') GO TO 200  
WRITE(IUNIT, 902)  
WRITE(IUNIT, 903)  
DO 100 K=1, NPOINT  
AMPLIT=FLOAT(IAMPAD(K))\* .05  
PHASE=FLOAT(IPH4(K))\* .25  
FREQ=FLOAT(IAMP(K-1))\*STEP  
WRITE(IUNIT, 800)K, FREQ, AMPLIT, PHASE  
CONTINUE  
TYPE 909  
ACCEPT \*, IFLAG2  
IF (IFLAG2) 210, 210, 220

0039      ACCEPT 700, A  
0040      IF (A EQ 'N') GO TO 300  
0041      WRITE(IUNIT, 904)  
0042      WRITE(IUNIT, 802)FSTART, FEND, STEP, NPOINT  
0043      WRITE(IUNIT, 903)  
0044      DO 250 K=1, NPOINT  
0045      AMPLIT=FLOAT(IAMP2(K))\* .05  
0046      PHASE=FLOAT(IPH2(K))\* .25  
0047      FREQ=FLOAT(IPH2(K-1))\*STEP  
0048      FREQ=FLOAT(IPH2(K-1))\*STEP  
0049      WRITE(IUNIT, 800)K, FREQ, AMPLIT, PHASE  
0050      CONTINUE  
0051      TYPE 910  
0052      ACCEPT \*, IFLAG3  
0053      IF (IFLAG3) 310, 310, 320  
0054      TYPE 908  
0055      ACCEPT \*, NSAMP3  
0056      CALL TRANS  
0057      TYPE 901  
0058      ACCEPT 700, A  
0059      IF (A EQ 'N') GO TO 400  
0060      WRITE(IUNIT, 912)  
0061      WRITE(IUNIT, 802)FSTART, FEND, STEP, NPOINT  
0062      WRITE(IUNIT, 903)  
0063      DO 330 K=1, NPOINT  
0064      AMPLIT=FLOAT(IAMP3(K))\* .05  
0065      PHASE=FLOAT(IPH3(K))\* .25  
0066      FREQ=FLOAT(IPH3(K-1))\*STEP  
0067      FREQ=FLOAT(IPH3(K-1))\*STEP  
0068      WRITE(IUNIT, 800)K, FREQ, AMPLIT, PHASE  
0069      CONTINUE  
0070      WRITE(IUNIT, 905)  
0071      WRITE(IUNIT, 802)FSTART, FEND, STEP, NPOINT  
0072      WRITE(IUNIT, 903)  
0073      DO 350 K=1, NPOINT  
0074      AMPLIT=FLOAT(IAMP4(K))\* .05  
0075      PHASE=FLOAT(IPH4(K))\* .25  
0076      FREQ=FLOAT(IPH4(K-1))\*STEP  
0077      FREQ=FLOAT(IPH4(K-1))\*STEP  
0078      WRITE(IUNIT, 800)K, FREQ, AMPLIT, PHASE  
0079      CONTINUE  
0080      TYPE 911  
0081      ACCEPT \*, IFLAG4  
0082      IF (IFLAG4) 410, 410, 420  
0083      TYPE 908  
0084      ACCEPT \*, NSAMP4  
0085      CALL ANTEN  
0086      TYPE 901  
0087      ACCEPT 700, A  
0088      IF (A EQ 'N') GO TO 500  
0089      WRITE(IUNIT, 913)  
0090      WRITE(IUNIT, 802)FSTART, FEND, STEP, NPOINT  
0091      WRITE(IUNIT, 903)  
0092      V02 1-1      THU 09-AUG-79 00:36:32  
0093      DO 430 K=1, NPOINT  
0094      AMPLIT=FLOAT(IAMP5(K))\* .05  
0095      PHASE=FLOAT(IPH5(K))\* .25  
0096      FREQ=FLOAT(IPH5(K-1))\*STEP  
0097      FREQ=FLOAT(IPH5(K-1))\*STEP  
0098      WRITE(IUNIT, 800)K, FREQ, AMPLIT, PHASE  
0099      CONTINUE  
0100      WRITE(IUNIT, 906)  
0101      WRITE(IUNIT, 802)FSTART, FEND, STEP, NPOINT  
0102      WRITE(IUNIT, 903)  
0103      DO 450 K=1, NPOINT  
0104      AMPLIT=FLOAT(IAMP6(K))\* .05

PAGE 003

COMMON BLOCK /PADA		/ SIZE = 004022 ( 1033.		WORDS)	
NAME	TYPE	OFFSET	NAME	TYPE	OFFSET
AMPAD	I+2	000000	IPHA	I+2	002000
ESTART	R+4	004002	FEND	R+4	004006
			STEP	R+4	004012

THIS ROUTINE WILL GENERATE THE CHARACTERISTIC OF THE PAD USED IN THE DETERMINATION OF THE SYSTEM RESPONSE IN THE FREQUENCY DIVERSITY IMAGING SYSTEM. IT INVOLVES PLACING THE FLEXIBLE ARM WITH THE REFLECTION TRANSMISSION UNIT WITH THE ARM CONNECTED FROM THE UNKNOWN TO THE TRANSMISSION RETURN PORT WITH A 6 DB PAD IN SERIES WITH THE ARM. THE PRECISION APC-7



```

1 'SERIES', ' ' AND CONNECT FROM THE UNKNOWN TO THE RETURN',
2 PART ON THE NETWORK ANALYZER',
FORMAT('///11', 'CONNECT THE DESIRED PAD IN SERIES WITH THE',
1 ' & DB PAD')
0068 906 FORMAT('///9', 'ENTER THE OLD PAD RESPONSE FILE NAME ' )
0069 906
END

```

```

FORTRAN IV STORAGE MAP FOR PROGRAM UNIT PAD
LOCAL VARIABLES, PSECT DATA, SIZE = 000044 ( 18 WORDS)
NAME TYPE OFFSET NAME TYPE OFFSET NAME TYPE OFFSET
FREQ R=4 000024 1A 1=2 000030 1P 1=2 000032
K 1=2 000022

```

```

COMMON BLOCK /PADA /, SIZE = 004022 ( 1033 WORDS)
NAME TYPE OFFSET NAME TYPE OFFSET NAME TYPE OFFSET
IAMPAD 1=2 000000 1PHA 1=2 002000 1FLAG 1=2 004000
FSTART R=4 004002 FEND R=4 004006 STEP R=4 004012
NPOINT 1=2 004016 NSAMP 1=2 004020

```

#### LOCAL AND COMMON ARRAYS

```

NAME TYPE SECTION OFFSET -----SIZE----- DIMENSIONS
IAMPAD 1=2 PADA 000000 002000 ( 512 ) (512)
1PHA 1=2 PADA 002000 002000 ( 512 ) (512)

```

#### SUBROUTINES, FUNCTIONS, STATEMENT AND PROCESSOR-DEFINED FUNCTIONS.

```

NAME TYPE NAME TYPE NAME TYPE NAME TYPE NAME TYPE
ASSIGN R=4 CLOSE R=4 FLOAT R=4 PHAMP2 R=4 SWEEP R=4

```

```

FORTRAN IV V02 1-1 THU 09-AUG-79 00 57:36 PAGE 001
SUBROUTINE 1ST
VERSION 1 3
THIS SUBROUTINE WILL MEASURE THE ISOLATION BETWEEN THE TWO
CHANNELS OF THE NETWORK ANALYZER. THE FREQUENCY RANGE AND
THE NUMBER OF STEPS WILL BE PASSED THROUGH COMMON BLOCK
PADA. THE OUTPUT WILL BE THROUGH COMMON BLOCK ISTA. THE
CARLES TO BE USED IN THE ACTUAL MEASUREMENT OF THE IMA-ING
SYSTEM ARE TERMINATED IN THEIR CHARACTERISTIC IMPEDANCE AND
THE MAGNITUDE AND PHASE OF THE LEAKAGE SIGNAL ARE MEASURED
AT THE SAME GAIN OF THE N/A FRONT PANEL AS THE SYSTEM
MEASUREMENTS
IAMP2 ARRAY WITH AMPLITUDE OF LEAKED SIGNAL
1PHA2 ARRAY WITH PHASE OF LEAKED SIGNAL
1FLAG2 FLAG FOR OLD OR NEW DATA 0=>GENERATE NEW DATA
1=> READ OLD DATA
NSAMP2 NUMBER OF SAMPLE POINTS TAKEN AT EACH FREQUENCY
COMMON/PADA/IAMPAD, 1PHA, 1FLAG, FSTART, FEND, STEP, NPOINT, NSAMP
COMMON/ISTA/IAMP2, 1PHA2, 1FLAG2, NSAMP2
INTEGER IAMPAD(512), 1PHA(512), IAMP2(512), 1PHA2(512)
1P(1FLAG2) 100, 100, 500
TYPE '000'
PAUSE
CALL SWEPT(1, FSTART, 1, 4)
DO 200 K=1, NPOINT
FREQ = FSTART + FLOAT(K-1)*STEP
CALL SWEPT(1, FREQ, 1, 4)
CALL PHAMP2(1A, 1P, NSAMP2)
IAMP2(K) = 1A - 2048
1PHA2(K) = 1P - 2048
CONTINUE
CALL SWEPT(10, FSTART, 1, 4)
TYPE '001'
CALL ASSON(12, -1, 'NEW', 'NC', 1, 1)
WRITE(12, *) FSTART
WRITE(12, *) FEND
WRITE(12, *) NPOINT
DO 300 K=1, NPOINT
WRITE(12, *) IAMP2(K)
WRITE(12, *) 1PHA2(K)
CONTINUE
CALL CLOSE(12)
DO 700 TO 700
TYPE '002'
TYPE '003'
CALL ASSON(12, -1, 'OLD', 'NC', 1, 1)
READ(12, *) FSTART
READ(12, *) FEND
FORTRAN IV V02 1-1 THU 09-AUG-79 00 57:36 PAGE 002
READ(12, *) NPOINT
STEP = (FEND - FSTART) / FLOAT(NPOINT)
DO 600 K=1, NPOINT
READ(12, *) IAMP2(K)
READ(12, *) 1PHA2(K)
CONTINUE
0001 C
0002 C
0003 C
0004 C
0005 C
0006 C
0007 C
0008 C
0009 C
0010 C
0011 C
0012 C
0013 C
0014 C
0015 C
0016 C
0017 C
0018 C
0019 C
0020 C
0021 C
0022 C
0023 C
0024 C
0025 C
0026 C
0027 C
0028 C
0029 C
0030 C
0031 C
0032 C
0033 C
0034 C
0035 C
0036 C
0037 C
0038 C

```

```

0001
FORTTRAN IV V02 I-1 THU 09-AUG-79 01.03.11 PAGE 001
SUBROUTINE TRANS
VERSION 1 3
THIS SUBROUTINE WILL FIND THE TRANSFER FUNCTION OF THE CABLES
AND THE NETWORK ANALYZER SYSTEM THE ISOLATION AND PAD
CHARACTERISTICS ARE PASSED THROUGH COMMON TO THIS ROUTINE
AT THAT POINT THE CABLES FROM THE TRANSMITTING AND RECEIVING
ANTENNAS ARE CONNECTED TOGETHER THROUGH A PAD WHOSE RESPONSE
IS ALREADY KNOWN THE TRANSFER CHARACTERISTIC IS THEN CAL-
CULATED AND STORED
IAMP3 ARRAY CONTAINING UNCORRECTED TRANSFER CHARACTERISTICS
AMPLITUDE
IPH3 ARRAY CONTAINING UNCORRECTED TRANSFER
CHARACTERISTIC PHASE
IAMP4 ARRAY CONTAINING CORRECTED AMP TRANS CHAR
IPHA ARRAY CONTAINING CORRECTED TRANS PHASE CHAR
NSAMP3 NUMBER OF SAMPLES AT EACH FREQUENCY POINT
IFLAG3 FLAG FOR OLD OR NEW DATA 0=>NEW 1=>OLD DATA
T/R=(C+PAG)/R
T RECEIVER CHANNEL SIGNAL
R REFERENCE CHANNEL SIGNAL
C NETWORK ANALYZER REFERENCE-TO-RECEIVER CHANNEL
ISOLATION
P PAD CHARACTERISTIC
O FREQUENCY CHARACTERISTICS(TRANSFER FUNCTION) OF
THE RECEIVER CHANNEL AND ITS CABLE
CORRECT THIS FOR THE REFERENCE TO RECEIVER CHANNEL ISOLATION
AND THE PAD FREQUENCY CHARACTERISTICS
C/R => M1 MEASUREMENT OF REFERENCE TO RECEIVER ISOLATION
OVER REFERENCE
(C+PAO) => M2 MEASUREMENT OF TRANSFER FUNCTION PLUS PAD AND
ISOLATION
G/R=(M2-M1)/P SUBTRACT PAD AND ISOLATION RESPONSES
AND STONE
COMMON/PADA/IAMPAD, IPHA, IFLAG, FSTART, FEND, STEP, NPOINT, NSAMP
COMMON/ISTA/IAMP2, IPH2, IFLAG2, NSAMP2
COMMON/TRANS/IAMP3, IPH3, IFLAG3, NSAMP3, IAMP4, IPH4
INTEGER IAMPAD(512), IPHA(512), IAMP2(512), IPH2(512), IAMP3(512),
IPH3(512), IAMP4(512), IPH4(512)
IF (IFLAG3) 100, 100, 500
TYPE 900
TYPE 901
FORTTRAN IV V02 I-1 THU 09-AUG-79 01.03.11 PAGE 002
PAUSE CALL SNEEP(1,FSTART,1,4)
DEQ=3.1415926/180
0001

```

```

0001  FORTTRAN IV      V02 1-1      THU 09-AUG-79 01.03.11      PAGE 001
SUBROUTINE TRANS
VERSION 1.3

C THIS SUBROUTINE WILL FIND THE TRANSFER FUNCTION OF THE CABLES
C AND THE NETWORK ANALYZER SYSTEM THE ISOLATION AND PAD
C CHARACTERISTICS ARE PASSED THROUGH COMMON TO THIS ROUTINE
C AT THAT POINT THE CABLES FROM THE TRANSMITTING AND RECEIVING
C ANTENNAS ARE CONNECTED TOGETHER THROUGH A PAD WHOSE RESPONSE
C IS ALREADY KNOWN THE TRANSFER CHARACTERISTIC IS THEN CAL-
C CULATED AND STORED
C IAMP3  ARRAY CONTAINING UNCORRECTED TRANSFER CHARACTERISTICS
C AMPITUDE
C IPH3  ARRAY CONTAINING UNCORRECTED TRANSFER
C CHARACTERISTIC PHASE
C IAMP4  ARRAY CONTAINING CORRECTED AMP TRANS CHAR
C IPH4  ARRAY CONTAINING CORRECTED TRANS PHASE CHAR
C NSAMP3  NUMBER OF SAMPLES AT EACH FREQUENCY POINT
C IFLAG3  FLAG FOR OLD OR NEW DATA 0=NEW 1=OLD DATA
C T/R=(C+P*G)/R
C T  RECEIVER CHANNEL SIGNAL
C R  REFERENCE CHANNEL SIGNAL
C C  NETWORK ANALYZER REFERENCE-TO-RECEIVER CHANNEL
C ISOLATION
C P  PAD CHARACTERISTIC
C O  FREQUENCY CHARACTERISTICS(TRANSFER FUNCTION) OF
C THE RECEIVER CHANNEL AND ITS CABLE
C CORRECT THIS FOR THE REFERENCE TO RECEIVER CHANNEL ISOLATION
C AND THE PAD FREQUENCY CHARACTERISTICS
C C/R => M1  MEASUREMENT OF REFERENCE TO RECEIVER ISOLATION
C OVER REFERENCE
C (C+P*0) => M2  MEASUREMENT OF TRANSFER FUNCTION PLUS PAD AND
C ISOLATION
C G/R=(M2-M1)/P  SUBTRACT PAD AND ISOLATION RESPONSES
C AND STORE
C COMMON/PAD/IAMPAD,IPHA,IFLAG,FSTART,FEND,STEP,NPOINT,NSAMP
C COMMON/1STA/IAMP2,IPH2,IFLAG2,NSAMP2
C COMMON/TRANSA/IAMP3,IPH3,IFLAG3,NSAMP3,IAMP4,IPH4
C INTEGER IAMPAD(512),IPHA(512),IAMP2(512),IPH2(512),IAMP3(512),
C IPH3(512),IAMP4(512),IPH4(512)
C
C IF (IFLAG3) 100,100,500
C TYPE 900
C TYPE 901
0006  FORTTRAN IV      V02 1-1      THU 09-AUG-79 01.03.11      PAGE 002
0007  PAUSE
0008  CALL SWEET(1,FSTART,1,4)
0009  DEG=3.1415926/180.
0010
0011

```

```

0001
FORTTRAN IV V02 I-1 THU 09-AUG-79 01.03.11 PAGE 001
SUBROUTINE TRANS
VERSION 1 3
THIS SUBROUTINE WILL FIND THE TRANSFER FUNCTION OF THE CABLES
AND THE NETWORK ANALYZER SYSTEM THE ISOLATION AND PAD
CHARACTERISTICS ARE PASSED THROUGH COMMON TO THIS ROUTINE
AT THAT POINT THE CABLES FROM THE TRANSMITTING AND RECEIVING
ANTENNAS ARE CONNECTED TOGETHER THROUGH A PAD WHOSE RESPONSE
IS ALREADY KNOWN THE TRANSFER CHARACTERISTIC IS THEN CAL-
CULATED AND STORED
IAMP3 ARRAY CONTAINING UNCORRECTED TRANSFER CHARACTERISTICS
AMPLITUDE
IPH3 ARRAY CONTAINING UNCORRECTED TRANSFER
CHARACTERISTIC PHASE
IAMP4 ARRAY CONTAINING CORRECTED AMP TRANS CHAR
IPHA ARRAY CONTAINING CORRECTED TRANS PHASE CHAR
NSAMP3 NUMBER OF SAMPLES AT EACH FREQUENCY POINT
IFLAG3 FLAG FOR OLD OR NEW DATA 0=>NEW 1=>OLD DATA
T/R=(C+PAG)/R
T RECEIVER CHANNEL SIGNAL
R REFERENCE CHANNEL SIGNAL
C NETWORK ANALYZER REFERENCE-TO-RECEIVER CHANNEL
ISOLATION
P PAD CHARACTERISTIC
O FREQUENCY CHARACTERISTICS(TRANSFER FUNCTION) OF
THE RECEIVER CHANNEL AND ITS CABLE
CORRECT THIS FOR THE REFERENCE TO RECEIVER CHANNEL ISOLATION
AND THE PAD FREQUENCY CHARACTERISTICS
C/R => M1 MEASUREMENT OF REFERENCE TO RECEIVER ISOLATION
OVER REFERENCE
(C+PAQ) => M2 MEASUREMENT OF TRANSFER FUNCTION PLUS PAD AND
ISOLATION
G/R=(M2-M1)/P SUBTRACT PAD AND ISOLATION RESPONSES
AND STONE
COMMON/PADA/IAMPAD, IPHA, IFLAG, FSTART, FEND, STEP, NPOINT, NSAMP
COMMON/ISTA/IAMP2, IPH2, IFLAG2, NSAMP2
COMMON/TRANS/IAMP3, IPH3, IFLAG3, NSAMP3, IAMP4, IPH4
INTEGER IAMPAD(512), IPHA(512), IAMP2(512), IPH2(512), IAMP3(512),
IPH3(512), IAMP4(512), IPH4(512)
IF (IFLAG3) 100, 100, 500
TYPE 900
TYPE 901
FORTTRAN IV V02 I-1 THU 09-AUG-79 01.03.11 PAGE 002
PAUSE
CALL SNEEP(1,FSTART,1,4)
DEQ=3.1415926/180
0001

```







```

0073      READ(12,*) IAMP5(K)
0074      READ(12,*) IPH5(K)
0075      CONTINUE
0076      CALL CLOSE(12)
0077      TYPE 903
0078      CALL ASSIGN(12,*,1,'OLD','NC',1)
0079      READ(12,*) FSTART
0080      READ(12,*) FEND
0081      READ(12,*) NPOINT
0082      DO 650 K=1,NPOINT
0083      READ(12,*) IAMP6(K)
0084      READ(12,*) IPH6(K)
0085      CONTINUE
0086      CALL CLOSE(12)
0087      RETURN
0088      C
0089      C
0090      C
0091      C
0092      C
0093      C
0094      C

```

```

0095      C
0096      C
0097      C
0098      C
0099      C
0100      C
0101      C
0102      C
0103      C
0104      C
0105      C
0106      C
0107      C
0108      C
0109      C
0110      C
0111      C
0112      C
0113      C
0114      C
0115      C
0116      C
0117      C
0118      C
0119      C
0120      C
0121      C
0122      C
0123      C
0124      C
0125      C
0126      C
0127      C
0128      C
0129      C
0130      C
0131      C
0132      C
0133      C
0134      C
0135      C
0136      C
0137      C
0138      C
0139      C
0140      C
0141      C
0142      C
0143      C
0144      C
0145      C
0146      C
0147      C
0148      C
0149      C
0150      C
0151      C
0152      C
0153      C
0154      C
0155      C
0156      C
0157      C
0158      C
0159      C
0160      C
0161      C
0162      C
0163      C
0164      C
0165      C
0166      C
0167      C
0168      C
0169      C
0170      C
0171      C
0172      C
0173      C
0174      C
0175      C
0176      C
0177      C
0178      C
0179      C
0180      C
0181      C
0182      C
0183      C
0184      C
0185      C
0186      C
0187      C
0188      C
0189      C
0190      C
0191      C
0192      C
0193      C
0194      C
0195      C
0196      C
0197      C
0198      C
0199      C
0200      C
0201      C
0202      C
0203      C
0204      C
0205      C
0206      C
0207      C
0208      C
0209      C
0210      C
0211      C
0212      C
0213      C
0214      C
0215      C
0216      C
0217      C
0218      C
0219      C
0220      C
0221      C
0222      C
0223      C
0224      C
0225      C
0226      C
0227      C
0228      C
0229      C
0230      C
0231      C
0232      C
0233      C
0234      C
0235      C
0236      C
0237      C
0238      C
0239      C
0240      C
0241      C
0242      C
0243      C
0244      C
0245      C
0246      C
0247      C
0248      C
0249      C
0250      C
0251      C
0252      C
0253      C
0254      C
0255      C
0256      C
0257      C
0258      C
0259      C
0260      C
0261      C
0262      C
0263      C
0264      C
0265      C
0266      C
0267      C
0268      C
0269      C
0270      C
0271      C
0272      C
0273      C
0274      C
0275      C
0276      C
0277      C
0278      C
0279      C
0280      C
0281      C
0282      C
0283      C
0284      C
0285      C
0286      C
0287      C
0288      C
0289      C
0290      C
0291      C
0292      C
0293      C
0294      C
0295      C
0296      C
0297      C
0298      C
0299      C
0300      C
0301      C
0302      C
0303      C
0304      C
0305      C
0306      C
0307      C
0308      C
0309      C
0310      C
0311      C
0312      C
0313      C
0314      C
0315      C
0316      C
0317      C
0318      C
0319      C
0320      C
0321      C
0322      C
0323      C
0324      C
0325      C
0326      C
0327      C
0328      C
0329      C
0330      C
0331      C
0332      C
0333      C
0334      C
0335      C
0336      C
0337      C
0338      C
0339      C
0340      C
0341      C
0342      C
0343      C
0344      C
0345      C
0346      C
0347      C
0348      C
0349      C
0350      C
0351      C
0352      C
0353      C
0354      C
0355      C
0356      C
0357      C
0358      C
0359      C
0360      C
0361      C
0362      C
0363      C
0364      C
0365      C
0366      C
0367      C
0368      C
0369      C
0370      C
0371      C
0372      C
0373      C
0374      C
0375      C
0376      C
0377      C
0378      C
0379      C
0380      C
0381      C
0382      C
0383      C
0384      C
0385      C
0386      C
0387      C
0388      C
0389      C
0390      C
0391      C
0392      C
0393      C
0394      C
0395      C
0396      C
0397      C
0398      C
0399      C
0400      C
0401      C
0402      C
0403      C
0404      C
0405      C
0406      C
0407      C
0408      C
0409      C
0410      C
0411      C
0412      C
0413      C
0414      C
0415      C
0416      C
0417      C
0418      C
0419      C
0420      C
0421      C
0422      C
0423      C
0424      C
0425      C
0426      C
0427      C
0428      C
0429      C
0430      C
0431      C
0432      C
0433      C
0434      C
0435      C
0436      C
0437      C
0438      C
0439      C
0440      C
0441      C
0442      C
0443      C
0444      C
0445      C
0446      C
0447      C
0448      C
0449      C
0450      C
0451      C
0452      C
0453      C
0454      C
0455      C
0456      C
0457      C
0458      C
0459      C
0460      C
0461      C
0462      C
0463      C
0464      C
0465      C
0466      C
0467      C
0468      C
0469      C
0470      C
0471      C
0472      C
0473      C
0474      C
0475      C
0476      C
0477      C
0478      C
0479      C
0480      C
0481      C
0482      C
0483      C
0484      C
0485      C
0486      C
0487      C
0488      C
0489      C
0490      C
0491      C
0492      C
0493      C
0494      C
0495      C
0496      C
0497      C
0498      C
0499      C
0500      C
0501      C
0502      C
0503      C
0504      C
0505      C
0506      C
0507      C
0508      C
0509      C
0510      C
0511      C
0512      C
0513      C
0514      C
0515      C
0516      C
0517      C
0518      C
0519      C
0520      C
0521      C
0522      C
0523      C
0524      C
0525      C
0526      C
0527      C
0528      C
0529      C
0530      C
0531      C
0532      C
0533      C
0534      C
0535      C
0536      C
0537      C
0538      C
0539      C
0540      C
0541      C
0542      C
0543      C
0544      C
0545      C
0546      C
0547      C
0548      C
0549      C
0550      C
0551      C
0552      C
0553      C
0554      C
0555      C
0556      C
0557      C
0558      C
0559      C
0560      C
0561      C
0562      C
0563      C
0564      C
0565      C
0566      C
0567      C
0568      C
0569      C
0570      C
0571      C
0572      C
0573      C
0574      C
0575      C
0576      C
0577      C
0578      C
0579      C
0580      C
0581      C
0582      C
0583      C
0584      C
0585      C
0586      C
0587      C
0588      C
0589      C
0590      C
0591      C
0592      C
0593      C
0594      C
0595      C
0596      C
0597      C
0598      C
0599      C
0600      C
0601      C
0602      C
0603      C
0604      C
0605      C
0606      C
0607      C
0608      C
0609      C
0610      C
0611      C
0612      C
0613      C
0614      C
0615      C
0616      C
0617      C
0618      C
0619      C
0620      C
0621      C
0622      C
0623      C
0624      C
0625      C
0626      C
0627      C
0628      C
0629      C
0630      C
0631      C
0632      C
0633      C
0634      C
0635      C
0636      C
0637      C
0638      C
0639      C
0640      C
0641      C
0642      C
0643      C
0644      C
0645      C
0646      C
0647      C
0648      C
0649      C
0650      C
0651      C
0652      C
0653      C
0654      C
0655      C
0656      C
0657      C
0658      C
0659      C
0660      C
0661      C
0662      C
0663      C
0664      C
0665      C
0666      C
0667      C
0668      C
0669      C
0670      C
0671      C
0672      C
0673      C
0674      C
0675      C
0676      C
0677      C
0678      C
0679      C
0680      C
0681      C
0682      C
0683      C
0684      C
0685      C
0686      C
0687      C
0688      C
0689      C
0690      C
0691      C
0692      C
0693      C
0694      C
0695      C
0696      C
0697      C
0698      C
0699      C
0700      C
0701      C
0702      C
0703      C
0704      C
0705      C
0706      C
0707      C
0708      C
0709      C
0710      C
0711      C
0712      C
0713      C
0714      C
0715      C
0716      C
0717      C
0718      C
0719      C
0720      C
0721      C
0722      C
0723      C
0724      C
0725      C
0726      C
0727      C
0728      C
0729      C
0730      C
0731      C
0732      C
0733      C
0734      C
0735      C
0736      C
0737      C
0738      C
0739      C
0740      C
0741      C
0742      C
0743      C
0744      C
0745      C
0746      C
0747      C
0748      C
0749      C
0750      C
0751      C
0752      C
0753      C
0754      C
0755      C
0756      C
0757      C
0758      C
0759      C
0760      C
0761      C
0762      C
0763      C
0764      C
0765      C
0766      C
0767      C
0768      C
0769      C
0770      C
0771      C
0772      C
0773      C
0774      C
0775      C
0776      C
0777      C
0778      C
0779      C
0780      C
0781      C
0782      C
0783      C
0784      C
0785      C
0786      C
0787      C
0788      C
0789      C
0790      C
0791      C
0792      C
0793      C
0794      C
0795      C
0796      C
0797      C
0798      C
0799      C
0800      C
0801      C
0802      C
0803      C
0804      C
0805      C
0806      C
0807      C
0808      C
0809      C
0810      C
0811      C
0812      C
0813      C
0814      C
0815      C
0816      C
0817      C
0818      C
0819      C
0820      C
0821      C
0822      C
0823      C
0824      C
0825      C
0826      C
0827      C
0828      C
0829      C
0830      C
0831      C
0832      C
0833      C
0834      C
0835      C
0836      C
0837      C
0838      C
0839      C
0840      C
0841      C
0842      C
0843      C
0844      C
0845      C
0846      C
0847      C
0848      C
0849      C
0850      C
0851      C
0852      C
0853      C
0854      C
0855      C
0856      C
0857      C
0858      C
0859      C
0860      C
0861      C
0862      C
0863      C
0864      C
0865      C
0866      C
0867      C
0868      C
0869      C
0870      C
0871      C
0872      C
0873      C
0874      C
0875      C
0876      C
0877      C
0878      C
0879      C
0880      C
0881      C
0882      C
0883      C
0884      C
0885      C
0886      C
0887      C
0888      C
0889      C
0890      C
0891      C
0892      C
0893      C
0894      C
0895      C
0896      C
0897      C
0898      C
0899      C
0900      C
0901      C
0902      C
0903      C
0904      C
0905      C
0906      C
0907      C
0908      C
0909      C
0910      C
0911      C
0912      C
0913      C
0914      C
0915      C
0916      C
0917      C
0918      C
0919      C
0920      C
0921      C
0922      C
0923      C
0924      C
0925      C
0926      C
0927      C
0928      C
0929      C
0930      C
0931      C
0932      C
0933      C
0934      C
0935      C
0936      C
0937      C
0938      C
0939      C
0940      C
0941      C
0942      C
0943      C
0944      C
0945      C
0946      C
0947      C
0948      C
0949      C
0950      C
0951      C
0952      C
0953      C
0954      C
0955      C
0956      C
0957      C
0958      C
0959      C
0960      C
0961      C
0962      C
0963      C
0964      C
0965      C
0966      C
0967      C
0968      C
0969      C
0970      C
0971      C
0972      C
0973      C
0974      C
0975      C
0976      C
0977      C
0978      C
0979      C
0980      C
0981      C
0982      C
0983      C
0984      C
0985      C
0986      C
0987      C
0988      C
0989      C
0990      C
0991      C
0992      C
0993      C
0994      C
0995      C
0996      C
0997      C
0998      C
0999      C
1000      C

```

```

FORTRAN IV STORAGE MAP FOR PROGRAM UNIT ANTEN
LOCAL VARIABLES, PSECT $DATA, SIZE = 000216 ( 71. WORDS)

```

NAME	TYPE	OFFSET	NAME	TYPE	OFFSET	NAME	TYPE	OFFSET
AAAT	R=4	000110	AAATX	R=4	000124	AAATY	R=4	000130
ADAB	R=4	000100	ADABT	R=4	000074	ADABTM	R=4	000154
AIST	R=4	000104	AISTX	R=4	000114	AISTY	R=4	000120
AREP	R=4	000160	AREPX	R=4	000150	AREPY	R=4	000154
ATEMP	R=4	000140	ATEMPX	R=4	000060	ATEMPY	R=4	000064
IA	I=2	000050	IP	I=2	000052	K	I=2	000042
PANT	R=4	000070	PI	R=4	000054	PIST	R=4	000064
PRES	R=4	000164	PTEMP	R=4	000144			

```

COMMON BLOCK /PADA /, SIZE = 004022 ( 1033. WORDS)

```

NAME	TYPE	OFFSET	NAME	TYPE	OFFSET	NAME	TYPE	OFFSET
IAMPAD	I=2	000000	IPHA	I=2	002000	IFLAG	I=2	004000
FSTART	R=4	004002	FEND	R=4	004006	STEP	R=4	004012

```

NPOINT I=2 004016 NSAMP I=2 004020

```

```

COMMON BLOCK /ISTA /, SIZE = 004004 ( 1026. WORDS)

```

NAME	TYPE	OFFSET	NAME	TYPE	OFFSET	NAME	TYPE	OFFSET
IAMP2	I=2	000000	IPH2	I=2	002000	IFLAG2	I=2	004000

```

NSAMP2 I=2 004002

```

```

COMMON BLOCK /TRANSAL, SIZE = 010004 ( 2050. WORDS)

```

NAME	TYPE	OFFSET	NAME	TYPE	OFFSET	NAME	TYPE	OFFSET
IAMP3	I=2	000000	IPH3	I=2	002000	IFLAG3	I=2	004000

NAME	TYPE	OFFSET	NAME	TYPE	OFFSET	NAME	TYPE	OFFSET
NSAMP3	I=2	004002	IAMP4	I=2	004004	IPH4	I=2	006004

```

COMMON BLOCK /ANTA /, SIZE = 010004 ( 2050. WORDS)

```

NAME	TYPE	OFFSET	NAME	TYPE	OFFSET	NAME	TYPE	OFFSET
IAMP5	I=2	000000	IPH5	I=2	002000	IFLAG5	I=2	004000

NAME	TYPE	OFFSET	NAME	TYPE	OFFSET	NAME	TYPE	OFFSET
NSAMP4	I=2	004002	IAMP6	I=2	004004	IPH6	I=2	006004

```

LOCAL AND COMMON ARRAYS:

```

```

NAME TYPE SECTION OFFSET SIZE DIMENSIONS

```

NAME	TYPE	SECTION	OFFSET	SIZE	DIMENSIONS
IAMPAD	I=2	PADA	000000	002000	( 512 ) ( 512 )
IAMP2	I=2	ISTA	000000	002000	( 512 ) ( 512 )
IAMP3	I=2	TRANSAL	000000	002000	( 512 ) ( 512 )
IAMP4	I=2	TRANSAL	004004	002000	( 512 ) ( 512 )
IAMP5	I=2	ANTA	000000	002000	( 512 ) ( 512 )
IAMP6	I=2	ANTA	004004	002000	( 512 ) ( 512 )
IPHA	I=2	PADA	002000	002000	( 512 ) ( 512 )
IPH2	I=2	ISTA	002000	002000	( 512 ) ( 512 )
IPH3	I=2	TRANSAL	002000	002000	( 512 ) ( 512 )

NAME	TYPE	SECTION	OFFSET	SIZE	DIMENSIONS
IPHA	I=2	TRANSAL	004004	002000	( 512 ) ( 512 )

NAME	TYPE	SECTION	OFFSET	SIZE	DIMENSIONS
IPH5	I=2	ANTA	002000	002000	( 512 ) ( 512 )

NAME	TYPE	SECTION	OFFSET	SIZE	DIMENSIONS
IPH6	I=2	ANTA	004004	002000	( 512 ) ( 512 )

```

FORTRAN IV STORAGE MAP FOR PROGRAM UNIT ANTEN
SUBROUTINES, FUNCTIONS, STATEMENT AND PROCESSED-DEFINED FUNCTIONS

```

NAME	TYPE	NAME	TYPE	NAME	TYPE	NAME	TYPE
ALOG10	R=4	ASSIGN	R=4	ATAN2	R=4	COS	R=4
FLOAT	R=4	IFIX	I=2	PHANP2	R=4	SIN	R=4
SLEEP	R=4						



WRITE(20,\*)FEND  
DO 460 K=1,NPOINT  
WRITE(20,\*)OBJAT(K)  
WRITE(20,\*)OBJP(K)  
CONTINUE  
CALL CLOSE(20)

THIS SECTION WILL DISPLAY THE DATA

CONTINUE  
FORMAT STATEMENTS

FORMAT(10X,'ENTER THE FILE NAME FOR THE RANGE  
1 CORRECTED DATA')

FORMAT(10X,'ENTER THE FILE NAME FOR THE CORRECTED DATA (Y OR N)')  
FORMAT(10X,'DO YOU WANT TO STORE THE CORRECTED DATA (Y OR N)')

FORMAT(10X,'\*\*\*\*\* PROGRAM SPHERE \*\*\*\*\*')  
FORMAT(10X,'DO YOU WANT TO STORE THE RANGE CORRECTED  
1 DATA (Y OR N) ?')

FORMAT(10X,'THIS SECTION WILL GENERATE CORRECTED SPHERE DATA  
1 FROM " EXPERIMENTAL DATA")

FORMAT(10X,'PRINT THE UNCORRECTED DATA (Y OR N) :')  
FORMAT(10X,'\*\*\*\*\* UNCORRECTED SPHERE DATA \*\*\*\*\*')  
FORMAT(10X,'STARTING FREQUENCY GHZ :',IP015,7/15X,  
1 ENDING FREQUENCY IN GHZ :',IP015,7/15X,'FREQUENCY STEP MHZ :',  
2 IP015,7/15X,'NUMBER OF STEPS :',17)

FORMAT(10X,'POINT #',5X,'FREQUENCY',7X,  
1 AMPLITUDE DB :',5X,'PHASE DEGREES',1X,75(' '),IP015,7)  
FORMAT(10X,17,5X,IP015,7,3X,IP015,7)  
FORMAT(10X,'\*\*\*\*\* CORRECTED EXPERIMENTAL SPHERE  
1 DATA \*\*\*\*\*')

FORMAT(10X,'\*\*\*\*\* EXPERIMENTAL SPHERE DATA CORRECTED  
1 FOR RANGE \*\*\*\*\*')

FORMAT(10X,'ENTER LOGICAL UNIT NUMBER FOR OUTPUT (7=2  
1 TERMINAL)')

FORMAT(10X,'CALCULATED RANGE TO THE TARGET= ',IP015,7,  
1 METERS)

FORMAT(10X,'ENTER THE RANGE CALCULATION FLAG',1X,2'DIRECT  
1 MEASUREMENT',2X,2'FOURIER ANALYSIS',1X,2'INPUT FLAG')

FORMAT(10X,'PRINT SPHERE DATA CORRECTED FOR SYSTEM RESPONSE  
1 (Y OR N)')

FORMAT(10X,'PRINT SPHERE DATA CORRECTED FOR RANGE (Y OR N) :')  
FORMAT(10X,1000)

STOP \*\*\*\*\* END OF PROGRAM \*\*\*\*\*

FORTRAN IV 0001

LOCAL VARIABLES, PSECT \$DATA, SIZE = 000066 ( 27 WORDS)

NAME TYPE OFFSET NAME TYPE OFFSET

A L=1 000026 AMPLIT R=4 000036 FREQ R=4 000046

I=01 1=2 000052 K 1=2 000034 PHASE R=4 000042

STEP R=4 000030

NAME TYPE SECTION OFFSET SIZE DIMENSIONS

LOCAL AND COMMON ARRAYS:

NAME TYPE SECTION OFFSET SIZE DIMENSIONS

COMMON BLOCK /SYSTA /, SIZE = 010012 ( 2053 WORDS)

NAME TYPE OFFSET NAME TYPE OFFSET

TRANA 1=2 000000 TRANP 1=2 002000 CLUTA 1=2 004000

CLUTP 1=2 006000 FSTART R=4 010000 FEND R=4 010004

NPOINT 1=2 010010



THIS SUBROUTINE WILL OBTAIN DATA FOR AN OBJECT OVER THE FREQ RANGE SET WITH THE NUMBER OF POINTS SPECIFIED.

```

COMMON/OBJ/OBJA,OBJP,NSAMP2
COMMON/SYSTA/TRANA,TRANP,CLUTA,CLUTP,FSTART,FEND,NPOINT
INTEGER OBJA(512),OBJP(512),NPOINT
INTEGER TRANA(512),TRANP(512),CLUTA(512),CLUTP(512)
STEP=(FEND-FSTART)/FLOAT(NPOINT)
CALL SWEPT(1,FSTART,1.4)
DO 100 K=1,NPOINT
  FREQ=FSTART+FLOAT(K-1)*STEP
  CALL PHAMP2(1A,IP,NSAMP2)
  OBJA(K)=1A-2048
  OBJP(K)=IP-2048
CONTINUE
CALL SWEPT(1,FSTART,1.4)
RETURN
END
100

```

FORTRAN IV STORAGE MAP FOR PROGRAM UNIT OBJDAT  
LOCAL VARIABLES: PSECT SDATA, SIZE = 000026 ( 11. WORDS)

NAME	TYPE	OFFSET	NAME	TYPE	OFFSET
FREQ	R=4	000014	1A	I=2	000020
K	I=2	000012	STEP	R=4	000006

COMMON BLOCK /OBJ /, SIZE = 004002 ( 1025 WORDS)

NAME	TYPE	OFFSET	NAME	TYPE	OFFSET
OBJA	I=2	000000	OBJP	I=2	002000
NSAMP2	I=2	004000			

COMMON BLOCK /SYSTA /, SIZE = 010012 ( 2053 WORDS)

NAME	TYPE	OFFSET	NAME	TYPE	OFFSET
TRANA	I=2	000000	TRANP	I=2	002000
CLUTA	I=2	006000	FSTART	R=4	010000
FEND	R=4	010004			

NPOINT I=2 010010

LOCAL AND COMMON ARRAYS:

NAME	TYPE	SECTION	OFFSET	SIZE	DIMENSIONS
CLUTA	I=2	SYSTA	004000	002000 ( 512 )	( 512 )
CLUTP	I=2	SYSTA	006000	002000 ( 512 )	( 512 )
OBJA	I=2	OBJ	000000	002000 ( 512 )	( 512 )

THIS SUBROUTINE WILL TAKE THE DATA THAT WAS TAKEN FROM SPHATD AND CORRECT IT WITH THE DATA FROM SUBROUTINE SYSPIN, WHICH IS THE SYSTEM RESPONSE.

```

VERSION 1.1 7-OCT-79
COMMON/OBJ/OBJA,OBJP,NSAMP2
COMMON/SYSTA/TRANA,TRANP,CLUTA,CLUTP,FSTART,FEND,NPOINT
INTEGER OBJA(512),OBJP(512),TRANA(512),TRANP(512)
INTEGER CLUTA(512),CLUTP(512),NPOINT,NSAMP2
*****
SUBTRACT ANTENNA CLUTTER FROM OBJECT DATA THIS CLUTTER DATA MUST NOT!!! BE CORRECTED FOR THE SYSTEM TRANSFER FUNCTION
*****
THE NEXT STEP IS TO DIVIDE BY THE TRANSFER CHARACTERISTIC OF THE SYSTEM IN ARRAYS TRANA(AMPLITUDE) AND TRANP(FREQ).
*****
PI=3.1415926
DED=PI/180
DO 100 K=1,NPOINT
  CDBAMP=FLOAT(CLUTA(K))* 05
  CLPH=FLOAT(CLUTP(K))* 25*DEG
  TRAMP=FLOAT(TRANA(K))* 05
  TRPH=FLOAT(TRANP(K))* 25*DEG
  ODBAMP=FLOAT(OBJA(K))* 05
  OBJPH=FLOAT(OBJP(K))* 25*DEG
*****
CDBAMP=>CLUTTER IN DBM
CLPH=>CLUTTER PHASE IN RADIAN
TRAMP=>TRANSFER CHARACTERISTIC IN DBM
TRPH=>PHASE OF TRANSFER CHARACTERISTIC IN RADIAN
ODBAMP=>OBJECT AMPLITUDE IN DBM
OBJPH=>PHASE OF OBJECT DATA IN RADIAN
OBJAMP=>OBJECT AMPLITUDE IN MILLIWATTS
CLAMP=>CLUTTER AMPLITUDE IN MILLIWATTS
*****
CLAMP=10.**(CDBAMP/10.)
OBJAMP=10.**(ODBAMP/10.)
*****
CLCOS=>REAL PART OF CLUTTER
CLCSIN=>IMAGINARY PART OF CLUTTER
OBJCOS=>REAL PART OF OBJECT DATA
OBJJSIN=>IMAGINARY PART OF OBJECT DATA
*****

```

```

PI=3.1415926
DED=PI/180
DO 100 K=1,NPOINT

```

```

CDBAMP=FLOAT(CLUTA(K))* 05
CLPH=FLOAT(CLUTP(K))* 25*DEG
TRAMP=FLOAT(TRANA(K))* 05
TRPH=FLOAT(TRANP(K))* 25*DEG
ODBAMP=FLOAT(OBJA(K))* 05
OBJPH=FLOAT(OBJP(K))* 25*DEG

```

CDBAMP=>CLUTTER IN DBM  
CLPH=>CLUTTER PHASE IN RADIAN  
TRAMP=>TRANSFER CHARACTERISTIC IN DBM  
TRPH=>PHASE OF TRANSFER CHARACTERISTIC IN RADIAN  
ODBAMP=>OBJECT AMPLITUDE IN DBM  
OBJPH=>PHASE OF OBJECT DATA IN RADIAN  
OBJAMP=>OBJECT AMPLITUDE IN MILLIWATTS  
CLAMP=>CLUTTER AMPLITUDE IN MILLIWATTS

```

CLAMP=10.**(CDBAMP/10.)
OBJAMP=10.**(ODBAMP/10.)

```

CLCOS=>REAL PART OF CLUTTER  
CLCSIN=>IMAGINARY PART OF CLUTTER  
OBJCOS=>REAL PART OF OBJECT DATA  
OBJJSIN=>IMAGINARY PART OF OBJECT DATA

```

OBJCOS=OBJAMP*COS(OBJPH)
OBJJSIN=OBJAMP*SIN(OBJPH)
CLCOS=CLAMP*COS(CLPH)

```

0001 SUBROUTINE RANGE  
0002 C  
0003 C  
0004 C  
0005 C  
0006 C  
0007 C  
0008 C  
0009 C  
0010 C  
0011 C  
0012 C  
0013 C  
0014 C  
0015 C  
0016 C  
0017 C  
0018 C  
0019 C  
0020 C  
0021 C  
0022 C  
0023 C  
0024 C  
0025 C  
0026 C  
0027 C  
0028 C  
0029 C  
0030 C  
0031 C  
0032 C  
0033 C  
0034 C  
0035 C  
0036 C  
0037 C

CLSN=CLAMP\*SIN(CLPH)  
\*\*\*\*\*  
TEMPOS=REAL PART OF OBJECT-CLUTTER  
TEMPSIN=IMAGINARY PART OF OBJECT-CLUTTER  
ATEMP=MAGNITUDE IN DBM OF (OBJECT-CLUTTER)  
PTEMP=PHASE OF OBJECT-CLUTTER  
ADRES=MAGNITUDE OF RESULT(ATEMP/TRAMP) DIVIDE BY TRANSFER  
CHARACTERISTIC IN DBM  
PRES=PHASE OF RESULT((OBJECT-CLUTTER)/TRANSFER)  
\*\*\*\*\*  
\*\*\*\*\* SUBTRACT CLUTTER FROM OBJECT DATA \*\*\*\*\*  
TEMCOS=OBJCOS-CLCOS  
TEMSIN=OBJSIN-CLSN  
\*\*\*\*\*  
\*\*\*\*\* CONVERT BACK TO PHASOR FORM \*\*\*\*\*  
PTEMP=ATAN2(TEMSIN,TEMCOS)  
ATEMP=SQRT(TEMSIN\*\*2+TEMCOS\*\*2)  
\*\*\*\*\*  
\*\*\*\*\* DIVIDE BY TRANSFER CHARACTERISTIC \*\*\*\*\*  
ADSTEM=10.\*LOG10(ATEMP)  
ADRES=ADSTEM-TDBAMP  
PRES=(PTEMP-TRPH)  
IF(PRES GT.PI)PRES=PRES-2.\*PI  
IF(PRES LT.-PI)PRES=PRES+2.\*PI  
\*\*\*\*\*  
\*\*\*\*\* REPLACE DATA INTO INTEGER ARRAY \*\*\*\*\*  
OBJA(K)=IFIX(20.\*ADRES)  
OBJP(K)=IFIX((PRES/DEG)\*4.)  
CONTINUE  
RETURN  
END

0001 SUBROUTINE RANGE  
0002 C  
0003 C  
0004 C  
0005 C  
0006 C  
0007 C  
0008 C  
0009 C  
0010 C  
0011 C  
0012 C  
0013 C  
0014 C  
0015 C  
0016 C  
0017 C  
0018 C  
0019 C  
0020 C  
0021 C  
0022 C  
0023 C  
0024 C  
0025 C  
0026 C  
0027 C  
0028 C  
0029 C  
0030 C  
0031 C  
0032 C  
0033 C  
0034 C  
0035 C  
0036 C  
0037 C

COMMON /RANGE1/DIST,IRFLAG,UNIT  
COMMON /OBJ/OBJA,OBJP,NSAMP2  
COMMON /SYSTA/TRANA,TRANP,CLUTA,CLUTP,FSTART,FEND,NPOINT  
INTEGER OBJA(512),OBJP(512),TRANA(512),TRANP(512)  
INTEGER CLUTA(512),CLUTP(512),NPOINT,NSAMP2,IRFLAG  
REAL PWR(512),C.PI  
DATA C/2.997925E+08/.PI/3.1415926/  
IF (IRFLAG NE.1) GO TO 200  
\*\*\*\*\* THIS SECTION FOR DIRECT RANGE INPUT \*\*\*\*\*  
TYPE 900  
ACCEPT \*.DIST  
GO TO 1000  
IF (IRFLAG NE.2) GO TO 1000  
\*\*\*\*\* THIS SECTION FOR FOURIER TRANSFORM METHOD FOR RANGE \*\*\*\*\*  
AMULT=ALOG(FLOAT(NPOINT))/ALOG(2.)  
IF (ABS(AMULT-IFIX(AMULT))- .001) 300,300,400  
N=2.\*IFIX(AMULT\*.01)  
GO TO 500  
N=2.\*IFIX(AMULT\*.1)  
GO TO 400  
N=2.\*IFIX(AMULT\*.5)  
GO TO 300  
TYPE \*.N  
\*\*\*\*\* ZERO OUT CLUTA AND CLUTP ARRAYS FOR LATER USE \*\*\*\*\*  
DO 510 K=1,512  
CLUTAI(K)=0  
CLUTPI(K)=0  
CONTINUE  
\*\*\*\*\* FIND SCALE FACTOR \*\*\*\*\*  
AMX=0  
DO 550 K=1,NPOINT  
AMP=10.\*FLOAT(OBJA(K)\*.05)/10.)  
AMX=AMX+AMP  
CONTINUE  
AMX=6.\*(AMX/FLOAT(NPOINT))  
SCALE=32576./AMX  
TYPE \*.SCALE FACTOR  
DO 600 K=1,NPOINT

0001 SUBROUTINE RANGE  
0002 C  
0003 C  
0004 C  
0005 C  
0006 C  
0007 C  
0008 C  
0009 C  
0010 C  
0011 C  
0012 C  
0013 C  
0014 C  
0015 C  
0016 C  
0017 C  
0018 C  
0019 C  
0020 C  
0021 C  
0022 C  
0023 C  
0024 C  
0025 C  
0026 C  
0027 C  
0028 C  
0029 C  
0030 C  
0031 C  
0032 C  
0033 C  
0034 C  
0035 C  
0036 C  
0037 C

CLSN=CLAMP\*SIN(CLPH)  
\*\*\*\*\*  
TEMPOS=REAL PART OF OBJECT-CLUTTER  
TEMPSIN=IMAGINARY PART OF OBJECT-CLUTTER  
ATEMP=MAGNITUDE IN DBM OF (OBJECT-CLUTTER)  
PTEMP=PHASE OF OBJECT-CLUTTER  
ADRES=MAGNITUDE OF RESULT(ATEMP/TRAMP) DIVIDE BY TRANSFER  
CHARACTERISTIC IN DBM  
PRES=PHASE OF RESULT((OBJECT-CLUTTER)/TRANSFER)  
\*\*\*\*\*  
\*\*\*\*\* SUBTRACT CLUTTER FROM OBJECT DATA \*\*\*\*\*  
TEMCOS=OBJCOS-CLCOS  
TEMSIN=OBJSIN-CLSN  
\*\*\*\*\*  
\*\*\*\*\* CONVERT BACK TO PHASOR FORM \*\*\*\*\*  
PTEMP=ATAN2(TEMSIN,TEMCOS)  
ATEMP=SQRT(TEMSIN\*\*2+TEMCOS\*\*2)  
\*\*\*\*\*  
\*\*\*\*\* DIVIDE BY TRANSFER CHARACTERISTIC \*\*\*\*\*  
ADSTEM=10.\*LOG10(ATEMP)  
ADRES=ADSTEM-TDBAMP  
PRES=(PTEMP-TRPH)  
IF(PRES GT.PI)PRES=PRES-2.\*PI  
IF(PRES LT.-PI)PRES=PRES+2.\*PI  
\*\*\*\*\*  
\*\*\*\*\* REPLACE DATA INTO INTEGER ARRAY \*\*\*\*\*  
OBJA(K)=IFIX(20.\*ADRES)  
OBJP(K)=IFIX((PRES/DEG)\*4.)  
CONTINUE  
RETURN  
END

0001 SUBROUTINE RANGE  
0002 C  
0003 C  
0004 C  
0005 C  
0006 C  
0007 C  
0008 C  
0009 C  
0010 C  
0011 C  
0012 C  
0013 C  
0014 C  
0015 C  
0016 C  
0017 C  
0018 C  
0019 C  
0020 C  
0021 C  
0022 C  
0023 C  
0024 C  
0025 C  
0026 C  
0027 C  
0028 C  
0029 C  
0030 C  
0031 C  
0032 C  
0033 C  
0034 C  
0035 C  
0036 C  
0037 C

CLSN=CLAMP\*SIN(CLPH)  
\*\*\*\*\*  
TEMPOS=REAL PART OF OBJECT-CLUTTER  
TEMPSIN=IMAGINARY PART OF OBJECT-CLUTTER  
ATEMP=MAGNITUDE IN DBM OF (OBJECT-CLUTTER)  
PTEMP=PHASE OF OBJECT-CLUTTER  
ADRES=MAGNITUDE OF RESULT(ATEMP/TRAMP) DIVIDE BY TRANSFER  
CHARACTERISTIC IN DBM  
PRES=PHASE OF RESULT((OBJECT-CLUTTER)/TRANSFER)  
\*\*\*\*\*  
\*\*\*\*\* SUBTRACT CLUTTER FROM OBJECT DATA \*\*\*\*\*  
TEMCOS=OBJCOS-CLCOS  
TEMSIN=OBJSIN-CLSN  
\*\*\*\*\*  
\*\*\*\*\* CONVERT BACK TO PHASOR FORM \*\*\*\*\*  
PTEMP=ATAN2(TEMSIN,TEMCOS)  
ATEMP=SQRT(TEMSIN\*\*2+TEMCOS\*\*2)  
\*\*\*\*\*  
\*\*\*\*\* DIVIDE BY TRANSFER CHARACTERISTIC \*\*\*\*\*  
ADSTEM=10.\*LOG10(ATEMP)  
ADRES=ADSTEM-TDBAMP  
PRES=(PTEMP-TRPH)  
IF(PRES GT.PI)PRES=PRES-2.\*PI  
IF(PRES LT.-PI)PRES=PRES+2.\*PI  
\*\*\*\*\*  
\*\*\*\*\* REPLACE DATA INTO INTEGER ARRAY \*\*\*\*\*  
OBJA(K)=IFIX(20.\*ADRES)  
OBJP(K)=IFIX((PRES/DEG)\*4.)  
CONTINUE  
RETURN  
END

```

0038 AM=SCALE*10**((AMDB/10.))
0039 AM=AMCOS(PHASE)
0040 AMI=AMOSIN(PHASE)
0041 IF(ABS(AM)) GE 32676) AMR=SIGN(32676,AMR)
0043 IF(ABS(AMI)) GE 32676) AMI=SIGN(32676,AMI)
C
C ***** REUSE CLUTA AND CLUTP ARRAYS FOR FOURIER TRANSFORM *****
C
0045 CLUTA(K)=IFIX(AMR)
0046 CLUTP(I)=IFIX(AMI)
0047 CONTINUE
0049 CALL FFT(FEEDPOR,N,CLUTA,CLUTP,1,ISCALE)
0049 CALL POWRSP(N,CLUTA,CLUTP,PHR)
0050 ALIAS=C/14*(FEED-FSTART)/FLOAT(N)*1.E9)
0051 RESC=(FEED-FSTART)*2*1.E9)
0052 WRITE(IUNIT,9011)ALIAS,RES
C
C ***** FIND MAXIMUM ENERGY POINT AND RANGE *****
C
0053 AMPHAX=0
0054 DO 800 K=1, (N/2)
0055 IF (AMPHAX-PMR(K)) 750, 750, 800
0056 AMPHAX=PMR(K)
0057 PMAX=K
0058 CONTINUE
0059 DIST=MAX-RES
0060 RETURN
0061 9011 FORMAT('//////////ENTER THE DISTANCE TO THE OBJECT IN METERS. ')
0062 10011 FORMAT('////////// ALIASING RANGE (METERS): ',IPOS,7)
0063 10012 RESOLUTION (METERS): ',IPOS,7)
END

```

```

FORTRAN IV
LOCAL VARIABLES: PSECT 9DATA, SIZE = 004156 ( 1079 WORDS)
NAME TYPE OFFSET NAME TYPE OFFSET NAME TYPE OFFSET
ALIAS R+4 004104 AM R+4 004064 AMDB R+4 004060
AMI R+4 004074 AMP R+4 004044 AMPHAX R+4 004114
AMP R+4 004070 AMULT R+4 004030 AMI R+4 004040
C R+4 004000 IERROR I+2 004100 ISCALE I+2 004102
K I+2 004036 PMAX I+2 004120 N I+2 004034
PHASE R+4 004054 PI R+4 004004 RES R+4 004110
SCALE R+4 004050

```

```

COMMON BLOCK /RANGE1/, SIZE = 000010 ( 4 WORDS)
NAME TYPE OFFSET NAME TYPE OFFSET
DIST R+4 000000 IIRFLAG I+2 000004 IUNIT I+2 000006
COMMON BLOCK /OBJ /, SIZE = 004002 ( 1025 WORDS)
NAME TYPE OFFSET NAME TYPE OFFSET

```

```

FORTRAN IV
SUBROUTINE RANCOR
VERSION 1.3 7-OCT-79
THIS SUBROUTINE WILL CORRECT THE OBJECT DATE FOR RANGE
COMMON/RANGE)/DIST,IIRFLAG,IUNIT
COMMON/OBJ/OBJA,OBJP,NSAMP2
COMMON/SYSTA/TRANA,TRANP,CLUTA,CLUTP,FSTART,FEND,NPOINT
INTEGER IIRFLAG,OBJA,OBJP,NSAMP2,TRANA(512)
INTEGER TRANP(512),CLUTA(512),CLUTP(512),NPOINT
REAL*4 DIST,FSTART,FEND,PATH,KSTART,KFREQ,PI,C,KDELTA
DATA PI/3.1415926/C/2.997925E+08/
C
C PATH=2*DIST
C KSTART=2*PI*(FSTART*1.E+09)/C
C FDELTA=(FEND-FSTART)/FLOAT(NPOINT)
C KDELTA=2*PI*(FDELTA*1.E+09)/C
C KFREQ=KSTART
C TPOI=2*PI
C RAD=PI/180
C DEG=180/PI
C DO 100 K=1,NPOINT
C PHASE=-(PATH*KFREQ)
C PHADAT=FLOAT(OBJP(K))*23-RAD
C PHEN=PHADAT-PHASE
C PHEN=MOD(PHEN,TPOI)
C IF (PHEN GT PI) PHEN=PHEN-TPOI
C IF (PHEN LT -PI) PHEN=PHEN+TPOI
C OBJP(K)=IFIX(PHEN*DEG*4.)
C KFREQ=KFREQ+KDELTA
C CONTINUE
C RETURN
C END

```

```

FORTRAN IV
LOCAL VARIABLES: PSECT 9DATA, SIZE = 000104 ( 34 WORDS)
NAME TYPE OFFSET NAME TYPE OFFSET NAME TYPE OFFSET
C R+4 000006 DEG R+4 000050 FDELTA R+4 000034
K I+2 000034 KDELTA R+4 000030 KFREQ R+4 000024
KSTART R+4 000020 PATH R+4 000014 PHADAT R+4 000032
PHASE R+4 000056 PHEN R+4 000046 PI R+4 000002
RAD R+4 000044 TPOI R+4 000040
COMMON BLOCK /RANGE1/, SIZE = 000010 ( 4 WORDS)
NAME TYPE OFFSET NAME TYPE OFFSET NAME TYPE OFFSET

```



```

0001      PROGRAM SPHER2
0002      VERSION 1.0 30-NOV-79
0003      THIS PROGRAM WILL TAKE EXPERIMENTAL DATA FOR THE SPHERE
0004      AND CORRECT IT FOR THE SYSTEM RESPONSE. IT WILL PRINT
0005      BOTH THE CORRECTED AND UNCORRECTED DATA AND FINALLY DISPLAY
0006      IT ON THE HIGH RESOLUTION CRT
0007      ALSO IT DESIRED IT WILL GENERATE IF DESIRED ANALYTICAL
0008      DATA FOR THE SPHERE AND STORE IT IN A FILE. IT WILL ALSO
0009      PRINT THIS DATA IF DESIRED TO A FILE AND ALSO DISPLAY IT ON
0010      THE HIGH RESOLUTION CRT MONITOR.
0011      COMMON/RANGE1/DIST,IRFLAG,IUNIT
0012      COMMON/OBJ/OBJA,OBJP,NSAMP2
0013      COMMON/SYSTA/TRANA,TRANP,CLUTA,CLUTP,FSTART,FEND,NPOINT
0014      INTEGER OBJA(512),OBJP(512),TRANA(512)
0015      INTEGER TRANP(512),CLUTA(512),CLUTP(512),NPOINT,NSAMP2
0016      BYTE A
0017
0018      TYPE 900
0019      ACCEPT *,IUNIT
0020
0021      THIS SECTION WILL GENERATE CORRECTED SPHERE DATA FROM
0022      EXPERIMENTAL DATA
0023
0024      TYPE 902
0025      CALL S751
0026      STEP=(FEND-FSTART)/FLOAT(NPOINT)
0027      TYPE *,PRINT THE SYSTEM RESPONSE DATA (Y OR N)
0028      ACCEPT I'000,A
0029      IF (A EQ 'N') GO TO 100
0030      WRITE(IUNIT,917)
0031      WRITE(IUNIT,905)FSTART,FEND,STEP,NPOINT
0032      DO 20 K=1,NPOINT
0033      AMPLIT=FLOAT(TRANA(K))* .05
0034      PHASE=FLOAT(TRANP(K))* .25
0035      FREQ=FSTART+FLOAT(K-1)*STEP
0036      WRITE(IUNIT,907)K,FREQ,AMPLIT,PHASE
0037      CONTINUE
0038
0039      WRITE(IUNIT,918)
0040      WRITE(IUNIT,905)FSTART,FEND,STEP,NPOINT
0041      WRITE(IUNIT,906)
0042      DO 30 K=1,NPOINT
0043      AMPLIT=FLOAT(CLUTA(K))* .05
0044      FREQ=FSTART+FLOAT(K-1)*STEP
0045      PHASE=FLOAT(CLUTP(K))* .25
0046
0047      WRITE(IUNIT,907)K,FREQ,AMPLIT,PHASE
0048      CONTINUE
0049      CALL SHEEP(10,....)

```

```

0038      TYPE 903
0039      ACCEPT I'000,A
0040      IF (A EQ 'N') GO TO 220
0041      WRITE(IUNIT,904)
0042      WRITE(IUNIT,905)FSTART,FEND,STEP,NPOINT
0043      WRITE(IUNIT,906)
0044      DO 210 K=1,NPOINT
0045      AMPLIT=FLOAT(OBJA(K))* .05
0046      PHASE=FLOAT(OBJP(K))* .25
0047      FREQ=FSTART+FLOAT(K-1)*STEP
0048      WRITE(IUNIT,907)K,FREQ,AMPLIT,PHASE
0049      CONTINUE
0050      CALL CORREC
0051
0052      HERE LIST THE CORRECTED SPHERE DATA
0053
0054      TYPE 915
0055      ACCEPT I'000,A
0056      IF (A EQ 'N') GO TO 280
0057      WRITE(IUNIT,909)
0058      WRITE(IUNIT,905)FSTART,FEND,STEP,NPOINT
0059      WRITE(IUNIT,906)
0060      DO 277 K=1,NPOINT
0061      INDI=K
0062      AMPLIT=FLOAT(OBJA(K))* .05
0063      PHASE=FLOAT(OBJP(K))* .25
0064      FREQ=FSTART+FLOAT(INDI-1)*STEP
0065      WRITE(IUNIT,907)K,FREQ,AMPLIT,PHASE
0066      CONTINUE
0067
0068      THIS SECTION WILL STORE THE CORRECTED DATA FOR SYSTEM RESPONSE
0069
0070      TYPE 902
0071      ACCEPT I'000,A
0072      IF (A EQ 'N') GO TO 400
0073      CALL ASSIGN(20,-1,'NEW','NC',)
0074      WRITE(20,*)FSTART
0075      WRITE(20,*)FEND
0076      WRITE(20,*)NPOINT
0077      DO 310 K=1,NPOINT
0078      WRITE(20,*)OBJA(K)
0079      WRITE(20,*)OBJP(K)
0080      CONTINUE
0081      CALL CLOSE(20)
0082
0083      THIS SECTION WILL CORRECT FOR RANGE
0084
0085      TYPE 914
0086      ACCEPT *,IRFLAG
0087      CALL RANGE
0088
0089      TYPE 913,DIST
0090      CALL RANCOR
0091      TYPE 916
0092      ACCEPT I'000,A
0093      IF (A EQ 'N') GO TO 470
0094      WRITE(IUNIT,913)DIST
0095      WRITE(IUNIT,911)
0096      WRITE(IUNIT,905)FSTART,FEND,STEP,NPOINT

```



FORTRAN IV002 1-1

SUBROUTINE SYS1  
VERSION 1.0 29-NOV-79

PAGE 001

THIS SUBROUTINE WILL READ IN THE SYSTEM RESPONSE FILES  
AND PLACE THEM IN A COMMON BLOCK TO BE PASSED TO OTHER  
ROUTINES

COMMON /SYSTA/ TRANA, TRAMP, CLUTA, CLUTP, FSTART, FEND, NPOINT

BYTE C

INTEGER TRANA(512), TRAMP(512), CLUTA(512), CLUTP(512), NPOINT

TYPE 900

TYPE \*, 'OLD OR NEW DATA (1=NEW, 0=OLD)'

ACCEPT \*, FLAG

IF (FLAG) 50, 50, 10

TYPE \*, 'ENTER THE STARTING FREQ IN GHZ: '

ACCEPT \*, FSTART

TYPE \*, 'ENTER THE ENDING FREQ IN GHZ: '

ACCEPT \*, FEND

TYPE \*, 'ENTER THE NUMBER OF FREQ POINTS: '

ACCEPT \*, NPOINT

TYPE \*, 'ENTER THE NUMBER OF SAMPLES AT EACH FREQ: '

ACCEPT \*, NSAMP2

TYPE \*, 'SET UP REFLECTING PLANE FOR TRANSFER FUNCTION MEASUREMENT'

PAUSE '\*\*\*\*\* HIT RETURN TO PROCEED \*\*\*\*\*'

CALL SHDAT(TRANA, TRAMP, FSTART, FEND, NPOINT, NSAMP2)

TYPE \*, 'SET UP FOR CLUTTER MEASUREMENT'

PAUSE '\*\*\*\*\* HIT RETURN TO PROCEED \*\*\*\*\*'

CALL SHDAT(CLUTA, CLUTP, FSTART, FEND, NPOINT, NSAMP2)

TYPE \*, 'STORE DATA ON DISC? (Y OR N)'

ACCEPT 900, C

IF (C EQ 'N') GOTO 300

TYPE 901

CALL ASSIGN(12, -1, 'NEW', 'NC', 1)

WRITE(12, \*) FSTART

WRITE(12, \*) FEND

WRITE(12, \*) NPOINT

DO 30 F=1, NPOINT

WRITE(12, \*) TRANA(K)

WRITE(12, \*) TRAMP(K)

CONTINUE

CALL CLOSE(12)

TYPE 902

CALL ASSIGN(12, -1, 'NEW', 'NC', 1)

WRITE(12, \*) FSTART

WRITE(12, \*) FEND

WRITE(12, \*) NPOINT

DO 40 F=1, NPOINT

WRITE(12, \*) CLUTA(K)

WRITE(12, \*) CLUTP(K)

CONTINUE

CALL CLOSE(12)

GO TO 300

TYPE 901

0049 CALL ASSIGN(12, -1, 'OLD', 'NC', 1)  
0050 READ(12, \*) FSTART  
0051 READ(12, \*) FEND  
0052 READ(12, \*) NPOINT  
0053 DO 100 K=1, NPOINT  
0054 READ(12, \*) TRANA(K)  
0055 READ(12, \*) TRAMP(K)  
0056 CONTINUE  
0057 CALL CLOSE(12)  
0058 TYPE 902  
0059 CALL ASSIGN(12, -1, 'OLD', 'NC', 1)  
0060 READ(12, \*) FSTART  
0061 READ(12, \*) FEND  
0062 READ(12, \*) NPOINT  
0063 DO 200 K=1, NPOINT  
0064 READ(12, \*) CLUTA(K)  
0065 READ(12, \*) CLUTP(K)  
0066 CONTINUE  
0067 CALL CLOSE(12)  
0068 RETURN  
0069 800  
0070 900  
0071 901  
0072 902  
0073 END

LOCAL VARIABLES. PSECT \$DATA, SIZE = 000044 ( 18 WORDS)

NAME TYPE OFFSET NAME TYPE OFFSET NAME TYPE OFFSET

C L+1 000022 FLAQ R+4 000024 K I+2 000032

NSAMP2 I+2 000030

COMMON BLOCK /SYSTA /, SIZE = 010012 ( 2053 WORDS)

NAME TYPE OFFSET NAME TYPE OFFSET NAME TYPE OFFSET

TRANA I+2 000000 TRAMP I+2 002000 CLUTA I+2 004000

CLUTP I+2 006000 FSTART R+4 010000 FEND R+4 010004

NPOINT I+2 010010

LOCAL AND COMMON ARRAYS:

NAME TYPE SECTION OFFSET -----SIZE----- DIMENSIONS

CLUTA I+2 SYSTA 004000 002000 ( 512 ) ( 512 )

CLUTP I+2 SYSTA 006000 002000 ( 512 ) ( 512 )

TRANA I+2 SYSTA 000000 002000 ( 512 ) ( 512 )

TRAMP I+2 SYSTA 002000 002000 ( 512 ) ( 512 )

SUBROUTINES, FUNCTIONS, STATEMENT AND PROCESSOR-DEFINED FUNCTIONS.

NAME TYPE NAME TYPE NAME TYPE NAME TYPE NAME TYPE

ASSIGN R+4 CLOSE R+4 .SHDAT R+4

FORTRAN IWS2 1-1 FRI 30-NOV-79 00 25 58 PAGE 001

PROGRAM SPHER3

VERSION 1.0 30-NOV-79

THIS PROGRAM WILL TAKE EXPERIMENTAL DATA FOR THE SPHERE  
AND CORRECT IT FOR THE SYSTEM RESPONSE. IT WILL PRINT  
BOTH THE CORRECTED AND UNCORRECTED DATA AND FINALLY DISPLAY  
IT ON THE HIGH RESOLUTION CRT.

ALSO IT DESIGNS IT WILL GENERATE IF DESIRED ANALYTICAL  
DATA FOR THE SPHERE AND STORE IT IN A FILE. IT WILL ALSO  
PRINT THIS DATA IF DESIRED TO A FILE AND ALSO DISPLAY IT ON  
THE HIGH RESOLUTION CRT MONITOR.

COMMON/RANGE1/01ST,IRFLAG,IUNIT  
COMMON/OBJ/OBJA,OBJP,NSAMP2

COMMON/SYSTA/TRANA,TRANP,CLUTA,CLUTP,FSTART,FEND,NPOINT

INTEGER OBJA(512),OBJP(512),TRANA(512)  
INTEGER TRANP(512),CLUTA(512),CLUTP(512),NPOINT,NSAMP2  
BYTE A

TYPE 900  
TYPE 912  
ACCEPT \*,IUNIT

THIS SECTION WILL GENERATE CORRECTED SPHERE DATA FROM  
EXPERIMENTAL DATA

TYPE 902  
CALL SYS2  
STEP=(FEND-FSTART)/FLOAT(NPOINT)  
TYPE \*,PRINT THE SYSTEM RESPONSE DATA (Y OR N),  
ACCEPT 1000,A  
IF (A EQ 'N') GO TO 100

WRITE(IUNIT,917)  
WRITE(IUNIT,905)FSTART,FEND,STEP,NPOINT  
WRITE(IUNIT,906)  
DO 20 K=1,NPOINT  
AMPLIT=FLOAT(TRANA(K))\*05  
PHASE=FLOAT(TRANP(K))\*25  
FREQ=FSTART+FLOAT(K-1)\*STEP  
WRITE(IUNIT,907)K,FREQ,AMPLIT,PHASE  
CONTINUE

CALL SWEEP(10,....)  
TYPE 903  
ACCEPT 1000,A  
IF (A EQ 'N') GO TO 220  
WRITE(IUNIT,904)  
WRITE(IUNIT,905)FSTART,FEND,STEP,NPOINT  
WRITE(IUNIT,906)

DO 210 K=1,NPOINT  
AMPLIT=FLOAT(OBJA(K))\*05  
PHASE=FLOAT(OBJP(K))\*25  
FREQ=FSTART+FLOAT(K-1)\*STEP  
WRITE(IUNIT,907)K,FREQ,AMPLIT,PHASE  
CONTINUE  
CALL CORDAT

HERE LIST THE CORRECTED SPHERE DATA

TYPE 915  
ACCEPT 1000,A  
IF (A EQ 'N') GO TO 280  
WRITE(IUNIT,909)  
WRITE(IUNIT,905)FSTART,FEND,STEP,NPOINT  
WRITE(IUNIT,906)  
DO 277 K=1,NPOINT  
INDI=K  
AMPLIT=FLOAT(OBJA(K))\*05  
PHASE=FLOAT(OBJP(K))\*25  
FREQ=FSTART+FLOAT(INDI-1)\*STEP  
WRITE(IUNIT,907)K,FREQ,AMPLIT,PHASE  
CONTINUE  
CONTINUE

THIS SECTION WILL STORE THE CORRECTED DATA FOR SYSTEM RESPONSE

TYPE 902  
ACCEPT 1000,A  
IF (A EQ 'N') GO TO 400  
TYPE 901  
CALL ASSIGN(20,,-1,'NEW','NC',)  
WRITE(20,\*)FSTART  
WRITE(20,\*)FEND  
WRITE(20,\*)NPOINT  
DO 310 K=1,NPOINT  
WRITE(20,\*)OBJA(K)  
WRITE(20,\*)OBJP(K)  
CONTINUE  
CALL CLOSE(20)

THIS SECTION WILL CORRECT FOR RANGE

TYPE 914  
ACCEPT \*,IRFLAG  
CALL RANGE  
TYPE 913,DIST  
CALL RANGOR  
TYPE 916  
ACCEPT 1000,A  
IF (A EQ 'N') GO TO 470  
WRITE(IUNIT,913)DIST

WRITE(IUNIT,911)  
WRITE(IUNIT,905)FSTART,FEND,STEP,NPOINT  
WRITE(IUNIT,906)  
DO 410 K=1,NPOINT  
INDI=K  
AMPLIT=FLOAT(OBJA(K))\*05  
PHASE=FLOAT(OBJP(K))\*25  
FREQ=FSTART+FLOAT(INDI-1)\*STEP

مجلس

0048 901 FORMAT('///S', 'ENTER THE TRANSFER FUNCTION FILE NAME. ')

0049 END

LOCAL VARIABLES. PSECT \$DATA, SIZE = 000030 ( 12 WORDS)

NAME TYPE OFFSET NAME TYPE OFFSET NAME TYPE OFFSET

C L\*1 000012 FLAG R\*4 000014 K I\*2 000022

NSAMP2 I\*2 000020

COMMON BLOCK /SYSTA /, SIZE = 010012 ( 2053 WORDS)

NAME TYPE OFFSET NAME TYPE OFFSET NAME TYPE OFFSET

TRANA I\*2 000000 TRAMP I\*2 002000 CLUTA I\*2 004000

CLUTP I\*2 006000 FSTART R\*4 010000 FEND R\*4 010004

NPOINT I\*2 010010

LOCAL AND COMMON ARRAYS:

NAME TYPE SECTION OFFSET NAME TYPE OFFSET NAME TYPE OFFSET

CLUTA I\*2 SYSTA 004000 002000 ( 512 ) ( 512 )

CLUTP I\*2 SYSTA 006000 002000 ( 512 ) ( 512 )

TRANA I\*2 SYSTA 000000 002000 ( 512 ) ( 512 )

TRAMP I\*2 SYSTA 002000 002000 ( 512 ) ( 512 )

SUBROUTINES, FUNCTIONS, STATEMENT AND PROCESSOR-DEFINED FUNCTIONS.

NAME TYPE NAME TYPE NAME TYPE NAME TYPE NAME TYPE

ASSIGN R\*4 CLOSE R\*4 SNDAT R\*4

FORTRAN IUV02 1-1 FRI 30-NOV-79 00:20:30 PAGE 001

SUBROUTINE SYS2

VERSION 1.0 29-NOV-79

THIS SUBROUTINE WILL READ IN THE SYSTEM RESPONSE FILES

AND PLACE THEM IN A COMMON BLOCK TO BE PASSED TO OTHER

ROUTINES

COMMON /SYSTA/ TRANA, TRAMP, CLUTA, CLUTP, FSTART, FEND, NPOINT

BYTE

INTEGER TRANA(512), TRAMP(512), CLUTA(512), CLUTP(512), NPOINT

TYPE 900

TYPE \*, 'OLD OR NEW DATA (1=NEW, 0=OLD)'

IF (FLAG) 50, 50, 10

TYPE \*, 'ENTER THE STARTING FREQ IN GHZ: '

ACCEPT \*, FSTART

TYPE \*, 'ENTER THE ENDING FREQ IN GHZ: '

ACCEPT \*, FEND

TYPE \*, 'ENTER THE NUMBER OF FREQ. POINTS: '

ACCEPT \*, NPOINT

TYPE \*, 'ENTER THE NUMBER OF SAMPLES AT EACH FREQ. '

ACCEPT \*, NSAMP2

TYPE \*, 'SET UP REFLECTING PLANE FOR TRANSFER FUNCTION MEASUREMENT'

PAUSE '\*\*\*\* HIT RETURN TO PROCEED \*\*\*\*'

CALL SHRT( TRANA, TRAMP, FSTART, FEND, NPOINT, NSAMP2 )

TYPE \*, 'STORE DATA ON DISC (Y OR N)'

ACCEPT 800, C

IF (C.EQ. 'N') GOTO 300

TYPE 901

CALL ASSIGN(12, -1, 'NEW', 'NC', 1, 1)

WRITE(12, \*) FSTART

WRITE(12, \*) FEND

WRITE(12, \*) NPOINT

DO 30 K=1, NPOINT

WRITE(12, \*) TRANA(K)

WRITE(12, \*) TRAMP(K)

CONTINUE

CALL CLOSE(12)

GO TO 300

TYPE 901

CALL ASSIGN(12, -1, 'OLD', 'NC', 1, 1)

READ(12, \*) FSTART

READ(12, \*) FEND

READ(12, \*) NPOINT

DO 100 K=1, NPOINT

READ(12, \*) TRANA(K)

READ(12, \*) TRAMP(K)

CONTINUE

CALL CLOSE(12)

RETURN

FORMAT (A1)

FORMAT('///11, '\*\*\*\* SUBROUTINE SYS2P OBTAINS THE SYSTEM RESPONSE

1 FILES \*\*\*\*')

Info: This document is a copy of the original document  
FROM G001 (CONTAINED IN 000)

```

FOSTRAN 1-1  FRI 30-NOV-79 10:10:36  PAGE 001
0001  SUBROUTINE SUDAT(OBJA,OBJP,FSTART,FEND,NPOINT,NSAMP2)
      C
      C
      C  THIS SUBROUTINE WILL OBTAIN DATA FOR AN OBJECT OVER THE FREQ
      C  RANGE SET WITH THE NUMBER OF POINTS SPECIFIED.
      C

```

```

0002 INTEGER OB,JA(512),OB,JP(512),NPOINT,NSAMP2
0003 INTEGER TRANA(512),TRANP(512),CLUTA(512),CLUTP(512)
0004
0005 STEP=(FEND-FSTART)/FLOAT(NPOINT)
0006 CALL SLEEP(1,FSTART,1,4)
0007 DO 100 K=1,NPOINT
0008   FREQ=FSTART+FLOAT(K-1)*STEP
0009   CALL SLEEP(1,FREQ,1,4)
0010   CALL PHAMP2(1A,1P,NSAMP2)
0011   OB,JA(K)=1A-2048
0012   OB,JP(K)=1P-2048
0013 CONTINUE
0014 CALL SLEEP(1,FSTART,1,4)
0015 RETURN
0016 END

```

LOCAL VARIABLES, PSECT #DATA, SIZE = 010040 ( 2064, WORDS)											
NAME	TYPE	OFFSET	NAME	TYPE	OFFSET	NAME	TYPE	OFFSET	NAME	TYPE	OFFSET
FEND	R#4	000006	FREQ	R#4	010026	FSTART	R#4	000004			
IA	I#2	010032	IP	I#2	010034	K	I#2	010024			
NPOINT	I#2	000010	NSAMP2	I#2	000012	STEP	R#4	010020			

**LOCAL AND COMMON ARRAYS:**

NAME	TYPE	SECTION	OFFSET	-----SIZE-----	DIMENSIONS
CLUTP	I*2	\$DATA	004014	002000 (	512) (512)
CLUTP	I*2	\$DATA	006014	002000 (	512) (512)
OB-PA	I*2	\$DATA	002000	002000 (	512) (512)
OB-PA	I*2	\$DATA	000002	002000 (	512) (512)
TRANA	I*2	\$DATA	000014	002000 (	512) (512)
TRANA	I*2	\$DATA	002014	002000 (	512) (512)

**SUBROUTINES, FUNCTIONS, STATEMENT AND PROCESSOR-DEFINED FUNCTIONS.**

NAME	TYPE	NAME	TYPE	NAME	TYPE	NAME	TYPE
NAME	TYPE	NAME	TYPE	NAME	TYPE	NAME	TYPE

Float	R#4	PHAMP2	R#4	SHEEP	R#4
-------	-----	--------	-----	-------	-----

EORTPAN 1W02 1-1 FRI 30-NOV-79 00:21:16 . PAGE 001  
 0001 SUBROUTINE CORDAT  
 C THIS SUBROUTINE WILL TAKE THE DATA THAT WAS TAKEN FROM  
 C SPHDATA AND CORRECT IT WITH THE DATA FROM SUBROUTINE  
 C SYSPIN, WHICH IS THE SYSTEM RESPONSE.

0002 VERSION 1.0 30-NOV-79  
COMMON/OBJ/OBJA.OBJP.NSAMP2  
0003 COMMON/SYSTA/TRANA.TRAMP.CLUTA.CLUTP.FSTART.FEND.NPOINT

```

C
0004 INTEGER OBJA(512),OBJBP(512),TRANA(512),TRANP(512)
0005 INTEGER CLUTA(512),CLUTBP(512),NP(NT,NSAMP2)
C
C *****
C SUBTRACT ANTENNA CLUTTER FROM OBJECT DATA. THIS CLUTTER DATA
C MUST NOT!!! BE CORRECTED FOR THE SYSTEM TRANSFER FUNCTION
C
C THE NEXT STEP IS TO DIVIDE BY THE TRANSFER CHARACTERISTIC
C OF THE SYSTEM IN ARRAYS TRANA(AMPLITUDE) AND TRANP(PHASE).
C *****
C

```

```

0006 PI=3.1415926
0007 DEG=PI/180
0008 DO 100 K=1, NPOINT
0009   TDEG=FLOAT(TRANP(K))* .05
0010   TDEG=FLOAT(TRANP(K))* .25*DEG
0011   ODBPM=FLOAT(OBJA(K))* .05
0012   ODBPM=FLOAT(OBJA(K))* .25*DEG

```

```

*****
C      TDBAMP=TRANSFER CHARACTERISTIC IN DBM
C      TDPHN=PHASE OF TRANSFER CHARACTERISTIC IN RADIANS
C      *****
C      ***** DIVIDE BY TRANSFER CHARACTERISTIC *****
C      *****

```

```
00013 ADDRESS=DDRAMP-TDRAMP
00014 PRES=(O8.PH-T8PH)
00015 IF (PRES GT. P1) PRES=PRES-2.*PI
00016 IF (PRES LT. -PI) PRES=PRES+2.*PI
```

```

C ***** REPLACE DATA INTO INTEGER ARRAY *****
C

```

```
00019 OB_JA(K)=IFIX(20 *ADRES)
00020 OB_P(K)=IFIX((PRES/DEG)*4.)
00021 CONTINUE
00022 RETURN
00023 END
```

LOCAL VARIABLES: DSCT INDATA SIZE = 000044 / 27 WORDS)

NAME	TYPE	OFFSET	NAME	TYPE	OFFSET
------	------	--------	------	------	--------

ADRES R+4	000044	DEQ	R+4	000016	K	1+2	000022
-----------	--------	-----	-----	--------	---	-----	--------

08.1PM	R+4	000040	00BAMP	R+4	000034	P!	R+4	000012
--------	-----	--------	--------	-----	--------	----	-----	--------

PRES	R#4	000050	TDBAMP	R#4	000024	TRPM	R#4	000030
------	-----	--------	--------	-----	--------	------	-----	--------

100

```

0001  C  FORTTRAN IV  V02 1-1  FRI 24-AUG-79 00:19:19
0002  C  SUBROUTINE PHAMP2(IAMP,IPHAS,NUM)
0003  C  THIS ROUTINE WILL TAKE NUM READINGS FROM A/D CHANNELS
0004  C  0 AND 1 0=>PHASE 1=>AMPLITUDE
0005  C  AMP=0
0006  C  DO 5 J=1,200
0007  C  PHAS=0
0008  C  DO 10 I=1,NUM
0009  C  IAMP=IADINP(0,1)
0010  C  IPHAS=IADINP(0,0)
0011  C  AMP=AMP+FLOAT(IAMP)
0012  C  PHAS=PHAS+FLOAT(IPHAS)
0013  C  DO 20 J=1,20
0014  C  CONTINUE
0015  C  IAMP=IFIX(IAMP/FLOAT(NUM))
0016  C  IPHAS=IFIX(IPHAS/FLOAT(NUM))
0017  C  RETURN
0018  C  END

```

```

0001  C  FORTTRAN IV  STORAGE MAP FOR PROGRAM UNIT PHAMP2
0002  C  LOCAL VARIABLES, PSECT 8DATA, SIZE = 000050 ( 20, WORDS)
0003  C
0004  C  NAME TYPE OFFSET NAME TYPE OFFSET
0005  C  AMP R=4 000006 IAMP I=2 000000 IAMP1 I=2 000022
0006  C  IPHAS I=2 000002 IPHAS1 I=2 000024 J I=2 000016
0007  C  I I=2 000020 NUM I=2 000004 PHAS R=4 000012
0008  C
0009  C  SUBROUTINES, FUNCTIONS, STATEMENT AND PROCESSOR-DEFINED FUNCTIONS.
0010  C
0011  C  NAME TYPE NAME TYPE NAME TYPE NAME TYPE
0012  C  FLOAT R=4 IADINP I=2 IFIX I=2

```

```

0001  C  FORTTRAN IV  V02 1-1  FRI 24-AUG-79 00:18:52
0002  C  SUBROUTINE SHEEP(MODE,FREQ,IBAND,IEEENO)
0003  C  MODE IS THE SHEEPER MODE 1-9. MODE 1 IS DISCRETE MODE FOR SETTING
0004  C  THE CN FREQUENCY. OTHER MODES ARE OUTLINED IN THE SHEEPER IEEE
0005  C  MANUAL.
0006  C  IF MODE=10 THEN THE PROGRAM WILL RESET THE INTERFACE
0007  C
0008  C  IBAND: IF IBAND=4 THEN FULL SHEEP 2-18 OHZ OTHERWISE THE
0009  C  PROGRAM WILL COMPUTE THE NECESSARY BAND
0010  C  INITIALIZE IBAND2 AND MODE1 TO ZERO IN THE MAIN LINE
0011  C
0012  C  BYTE CHD(17),MD(3),BND(3)
0013  C  DATA CHD(17)/"15"/,MD(3)/"15"/,BND(3)/"15"/
0014  C  DATA CHD(11)/"V"/,CHD(6)/"E"/,MD(11)/"W"/,BND(11)/"B"/
0015  C  IF (MODE=10) 3,2,3
0016  C  CALL IBIFC
0017  C  GO TO 2000
0018  C  IF (MODE=MODE1) 5,10,5
0019  C  ENCODE(1,1000,MD(2)) MODE
0020  C  CALL IBIFC
0021  C  CALL IBEREN
0022  C  CALL ISEND(MD,IEEENO)
0023  C  DO 8 ITER=1,500
0024  C  CONTINUE
0025  C  MODE1=MODE
0026  C  IF (IBAND=4) 25,20,25
0027  C  IF IBAND IS EQUAL TO 4 THEN TRANS
0028  C  GO TO 35
0029  C  IF (FREQ GE 2.00) AND (FREQ LT 6.05) IBAND1=1
0030  C  IF (FREQ GE 6.05) AND (FREQ LT 12.4) IBAND1=2
0031  C  IF (FREQ GE 12.4) AND (FREQ LT 18.0) IBAND1=3
0032  C  IF (IBAND2=IBAND1) 36,38,36
0033  C  ENCODE(1,1000,BND(2)) IBAND1
0034  C  CALL ISEND(BND,IEEENO)
0035  C  IBAND2=IBAND1
0036  C  GO TO (40,50,60,70),IBAND1
0037  C  B0=2.00022
0038  C  B1=4.18734E-04
0039  C  B2=1.27261E-10
0040  C  GO TO 80
0041  C  B0=5.99786
0042  C  B1=6.38009E-04
0043  C  B2=2.03858E-10
0044  C  GO TO 80
0045  C  B0=12.0018
0046  C  B1=5.98325E-04
0047  C  B2=9.44848E-11
0048  C  GO TO 80
0049  C  B0=1.99636
0050  C  B1=1.59929E-03
0051  C  B2=6.01267E-11
0052  C
0053  C  FORTTRAN IV  V02 1-1  FRI 24-AUG-79 00:18:52
0054  C  THESE CONSTANTS WERE DERIVED USING PROGRAM CALAB BAS ON
0055  C  AUG-24-1979

```



```

0045 C
0046 IV1=IFIX((B1+SORT(B1+2-4*B2*(B0-FREQ)))/(2*B2))
0047 EPCODE(4,1001,CND(2)) IV1
0048 CALL IBSEND(CND,,IEENO)
0049 DO 90 ITER=1,200
0050 CONTINUE
0051 FORMAT(11)
0052 RETURN
0053 END

FORTRAN IV STORAGE MAP FOR PROGRAM UNIT SHEEP
LOCAL VARIABLES: PSECT DATA, SIZE = 000070 ( 28 WORDS)

NAME TYPE OFFSET NAME TYPE OFFSET
B0 R+4 000036 B1 R+4 000042 B2 R+4 000046
FREQ R+4 000002 IBAND I+2 000004 IBAND1 I+2 000032
IBAND2 I+2 000034 IEENO I+2 000006 ITER I+2 000030
IV1 I+2 000052 MODE I+2 000000 MODE1 I+2 000026

LOCAL AND COMMON ARRAYS:

NAME TYPE SECTION OFFSET SIZE-----DIMENSIONS
BND L+1 DATA 000022 000003 ( 2 ) (3)
CND L+1 DATA 000010 000007 ( 4 ) (7)
PID L+1 DATA 000017 000003 ( 2 ) (3)

SUBROUTINES, FUNCTIONS, STATEMENT AND PROCESSOR-DEFINED FUNCTIONS.

NAME TYPE NAME TYPE NAME TYPE NAME TYPE
IBIFC I+2 IBREN I+2 IBSEND I+2 IFIX I+2 SORT R+4

```

```

10 DIM A(500), B(500), F(500)
20 DIM B$(20)
30 PRINT 'INPUT DATA FILE NAME',
40 INPUT A$
50 PRINT 'DATE: ', DATE$
60 OPEN A$ FOR INPUT AS FILE #1
70 INPUT #1, B$
80 B$=SEG$(B$, 5, 20)
90 F1=VAL(B$)
100 INPUT #1, F2 \ INPUT #1, N
110 PRINT 'START FREQ. GHZ. ', F1, ' STOP FREQ. GHZ. ', F2, ' DATA POINTS ', N
120 FOR I=0 TO N-1
130 D=(F2-F1)/N
140 INPUT #1, A
150 A(I)=A*.05
160 INPUT #1, B
170 B(I)=B*.25
180 F(I)=F1+I*D
190 NEXT I
200 F(N-1)=F2
210 REGION('UPPER', 1)
220 REGION('LOWER', 2)
230 GRAPH('LINES', N, F(1), A(1), 1)
240 LABEL('UNDERLINE', N, F(1), B(1), 1)
250 GRAPH('LINES', N, F(1), B(1), 2)
260 LABEL('UNDERLINE', N, F(1), B(1), 2)
270 LINPUT 16
280 DISPLAY+CLEAR
290 CLOSE #1
300 GO TO 30
310 END

```

## APPENDIX II

```

FORTRAN IVU02 1-1   SUN 21-OCT-79 02:12:32   PAGE 001
PROGRAM BISCAT

C
00002 COMMON /SCT/ETHETA,FPSI,PSI
00003 COMMON S01,S02,SC1,SC2,KA,THETA
00004 COMPLEX S01,S02,SC1,SC2,ETHETA,FPSI,F
00005 REAL KA,KA,MAG(512),ANGLE(512),KAS,KAE,PSI,THETA
00006 BYTE ANS
00007 DATA C/2,997925E+10/

C
00008 TYPE *, 'ENTER SPHERE RADIUS (A) (CM) : '
00009 ACCEPT *,A
00010 TYPE *, 'ENTER STARTING FREQ (GHZ) : '
00011 ACCEPT *,FSTART
00012 TYPE *, 'ENTER ENDING FREQ (GHZ) : '
00013 ACCEPT *,FEND
00014 MAG=2*3.1415926*(1.0E+9/C)
00015 KAS=FSTART*HAYWA
00016 KAE=FEND*HAYWA
00017 TYPE *, 'ENTER SCATTERING ANGLE THETA (DEGREES) : '
00018 ACCEPT *,THETA
00019 THETA=THETA*3.1415926/180.0
00020 TYPE *, 'ENTER POLARIZATION SCATTERING ANGLE PSI (DEGREES) : '
00021 ACCEPT *,PSI
00022 PSI=PSI*3.1415926/180.0
00023 TYPE *, 'IN WHICH POLARIZATION CALCULATE FIELD (0=>THETA, 1=>PSI) : '
00024 ACCEPT *,IPOL
00025 TYPE *, 'ENTER NUMBER OF POINTS : '
00026 ACCEPT *,NUMPTS
00027 TYPE *, 'ENTER LOGICAL UNIT NUMBER FOR OUTPUT : '
00028 ACCEPT *,IUNIT
00029 WRITE (IUNIT,800)A,FSTART,KAS,FEND,KAE,NUMPTS,THETA*(S0/3.1415926)
00030 1,PSI*180/3.1415926
00031 IF (IPOL EQ 0) WRITE(IUNIT,810)
00032 IF (IPOL EQ 1) WRITE(IUNIT,811)
00034 WRITE(IUNIT,801)

C
00035 STEPK=(KAE-KAS)/NUMPTS
00036 FREQ=FSTART
00037 STEPM=(FEND-FSTART)/NUMPTS
00038 KA=KAS
00039 DO 100 I=1,NUMPTS
00040 N=I
00041 CALL BISCAT
00042 IF (IPOL EQ 0) F=FTHETA
00043 IF (IPOL EQ 1) F=FPSI
00044 AMP=COS(F)
00045 REA=REAL(F)
00046 CPM=AIMAG(F)
00047 ANG=ATAN2(CPM,REA)*(180/3.1415926)
00048 MAG(N)=AMP
00049 ANGLE(N)=ANG
00051 IF (AMP EQ 0.0) AMP=1.0E-35
00052

00054 WRITE (IUNIT,*,N,FREQ,KA,10*ALOG10(AMP),ANG)
00055 FREQ=FREQ+STEPM
00056 KA=KA+STEPM
00057 CONTINUE
00059 TYPE *, 'STORE DATA FOR DISPLAY (Y OR N) : '
100

```



FORTMAN IW002 1-1 SUBROUTINE BSCAT2 PAGE 001

THIS PROGRAM WILL CALCULATE THE SCATTERING CONSTANTS  
OF A PERFECTLY CONDUCTING SPHERE IN THE RANGE  
 $4 \leq VA < 1$  AS A FUNCTION OF BISTATIC ANGLE THETA  
SEE RADAR CROSS-SECTION HANDBOOK GEORGE T RUCK ED.  
PLENUM PRESS 1970.

COMMON S01, S02, SC1, SC2, KA, THETA  
COMPLEX S01, S02, SC1, SC2  
REAL KA, THETA

T1= 5+COS(THETA)

T2=( 3-(11.0/45.0)\*COS(THETA)+(1.0/12.0)\*COS(2\*THETA))\*KA\*\*2

T3=(1.0/120.0)\*(-11907.0/70.0)-(2531.0/105.0)\*COS(THETA)+  
1157.0/42.0)\*COS(2\*THETA)+(1.0/3.0)\*COS(3\*THETA))\*KA\*\*4

T4=KA\*\*6\*((1.0/6.0)\*(-4\*COS(THETA)-1)+(1.0/3.0)\*(-1+2\*COS(THETA))  
+KA\*\*2))

SC1R=KA\*\*3\*(T1-T2+T3)

SC1I=T4

SC1=CMPLX(SC1R, SC1I)

C1= 5+COS(THETA)+1

C2=( 3-(29.0/60.0)\*COS(THETA)-(1.0/18.0)\*COS(2\*THETA))\*KA\*\*2

C3=(1.0/60.0)\*(-11343.0/105.0)+(3769.0/280.0)\*COS(THETA)+  
1157.0/63.0)\*COS(2\*THETA)+(1.0/8.0)\*COS(3\*THETA))\*KA\*\*4

C4=KA\*\*6\*((1.0/6.0)\*(-4-COS(THETA))\*2\*(COS(THETA)+2)\*KA\*\*2)

SC2R=KA\*\*3\*(C1+C2+C3)

SC2I=C4

SC2=CMPLX(SC2R, SC2I)

RETURN

END

LOCAL VARIABLES: PSECT 9DATA, SIZE = 000110 ( 36. WORDS)

NAME	TYPE	OFFSET	NAME	TYPE	OFFSET
C1	R=4	000030	C2	R=4	000034
C4	R=4	000044	SC1I	R=4	000024
			SC1R	R=4	000020

FORTMAN IW002 1-1 SUBROUTINE BSCAT3 PAGE 001

THIS SUBROUTINE FINDS THE SCATTERING COEFFICIENTS SC1, SC2, SC1, SC2  
USING A POLYNOMIAL APPROXIMATION IN THE RESONANCE REGION  
FOR A PERFECTLY CONDUCTING SPHERE. RANGE 1<KA<20. KA=VA VECTOR  
A=RADIUS OF SPHERE THETA=BISTATIC SCATTERING ANGLE

COMMON S01, S02, SC1, SC2, KA, THETA  
COMPLEX S01, S02, SC1, SC2  
COMPLEX T1, T2, T3, T4, T5, T6, B1, B2, B3, CON  
COMPLEX CON1, CON2, CON3, CON4, C1, C2, C3, C4, C5, C6, C7, C9  
COMPLEX C11, C12, C13, C14, C15, XT, XTH  
COMPLEX CON5, CON6, CON7, CON8, CON9  
REAL KA, THETA  
CON=(0.0, 1.0)  
X=KA  
X3=X\*\*3  
XN3=1.0/X3  
XN23=X\*\*(-2.0/3.0)  
COST2=COS(THETA/2.0)  
SINT2=SIN(THETA/2.0)  
SINT=SIN(THETA)  
COST=COS(THETA)  
XT=CON\*THETA\*X  
XTH=XT  
PI=3.1415926  
PT=(PI-THETA)  
PTH=(PI-THETA)

P1=-2\*KA\*COST2

T1=(KA/2)\*CEXP(CON\*P1)

P2=-1.0/(2\*KA\*(COST2\*\*3))

T2=1.0\*CON\*P2

T3=(1.0/(4\*(KA\*\*2)))\*((SINT2\*\*2)/(COST2\*\*6))

S01=T1\*(T2-T3)

P4=-COST/(2\*KA\*(COST2\*\*3))

T4=(1.0\*CON\*P4)

T5=(1.0/(4\*(KA\*\*2)))\*((6.0\*COST)\*(SINT2\*\*2)/  
1\*(COST2\*\*6))

S02=T1\*(T4-T5)

\*\*\*\*\* CALCULATE CREEPING WAVE TERMS \*\*\*\*\*

X=KA

B1=CEXP(CON\*P1)

B2=-CON\*X3\*SQRT(X/(2\*PI\*SINT))

C1=B2\*B1

```

0038 CON1=( 933506,1,616911)
0039 C2=2 715175+(X*CON1)
0040 C
0041 P1=( 8750/(X*THETA)))
0042 C3=(1 0-CON*P1)
0043 CON2=( 700283, - 404308)
0044 CON3=( 141774, 081853)
0045 B2=PTM(X3)*CON2
0046 B3=PTM(X3)*CON3
0047 C4=CEXP(XTH-B2-B3)
0048 C5=CON*(1 0-CON*P1)
0049 B2=PTM(X3)*CON2
0050 B3=PTM(X3)*CON3
0051 C6=CEXP(XTH-B2-B3)
0052 T1=C2*((C3+C4)-(C5+C6))
0053 CON4=(1 032306,1,788036)
0054 CON5=(2 232697,-1,289048)
0055 CON6=( 141482, 081684)
0056 C7=1 991727+(X*CON3)*CON4
0057 B2=PTM(X3)*CON5
0058 B3=PTM(X3)*CON6
0059 C9=CEXP(XTH-B2-B3)
0060 B2=PTM(X3)*CON5
0061 B3=PTM(X3)*CON6
0062 C11=CEXP(XTH-B2-B3)
0063 T2=C7*((C3+C9)-(C5+C11))
0064 CON7=(1 607133,- 927879)
0065 CON8=( 060415, 057397)
0066 C12= 201776/(X*SINT)
0067 B2=PTM(X3)*CON7
0068 B3=PTM(X3)*CON8
0069 C13=CEXP(XTH-B2-B3)
0070 B2=PTM(X3)*CON7
0071 B3=PTM(X3)*CON8
0072 C14=CEXP(XTH-B2-B3)
0073 T3=C12*(C13-CON*C14)
0074 SC1=C1*(T1+T2+T3)
0075 C
0076 C
0077 C
0078 C
0079 C
0080 C
0081 C
0082 C
0083 C
0084 C
0085 C
0086 C
0087 C
0088 C
0089 C
0090 C
0091 C
0092 C
0093 C
0094 C
0095 C
0096 C
0097 C
0098 C
0099 C
0100 C
0101 C
0102 C
0103 C
0104 C
0105 C
0106 C
0107 C
0108 C
0109 C
0110 C
0111 C
0112 C
0113 C
0114 C
0115 C
0116 C
0117 C
0118 C
0119 C
0120 C
0121 C
0122 C
0123 C
0124 C
0125 C
0126 C
0127 C
0128 C
0129 C
0130 C
0131 C
0132 C
0133 C
0134 C
0135 C
0136 C
0137 C
0138 C
0139 C
0140 C
0141 C
0142 C
0143 C
0144 C
0145 C
0146 C
0147 C
0148 C
0149 C
0150 C
0151 C
0152 C
0153 C
0154 C
0155 C
0156 C
0157 C
0158 C
0159 C
0160 C
0161 C
0162 C
0163 C
0164 C
0165 C
0166 C
0167 C
0168 C
0169 C
0170 C
0171 C
0172 C
0173 C
0174 C
0175 C
0176 C
0177 C
0178 C
0179 C
0180 C
0181 C
0182 C
0183 C
0184 C
0185 C
0186 C
0187 C
0188 C
0189 C
0190 C
0191 C
0192 C
0193 C
0194 C
0195 C
0196 C
0197 C
0198 C
0199 C
0200 C
0201 C
0202 C
0203 C
0204 C
0205 C
0206 C
0207 C
0208 C
0209 C
0210 C
0211 C
0212 C
0213 C
0214 C
0215 C
0216 C
0217 C
0218 C
0219 C
0220 C
0221 C
0222 C
0223 C
0224 C
0225 C
0226 C
0227 C
0228 C
0229 C
0230 C
0231 C
0232 C
0233 C
0234 C
0235 C
0236 C
0237 C
0238 C
0239 C
0240 C
0241 C
0242 C
0243 C
0244 C
0245 C
0246 C
0247 C
0248 C
0249 C
0250 C
0251 C
0252 C
0253 C
0254 C
0255 C
0256 C
0257 C
0258 C
0259 C
0260 C
0261 C
0262 C
0263 C
0264 C
0265 C
0266 C
0267 C
0268 C
0269 C
0270 C
0271 C
0272 C
0273 C
0274 C
0275 C
0276 C
0277 C
0278 C
0279 C
0280 C
0281 C
0282 C
0283 C
0284 C
0285 C
0286 C
0287 C
0288 C
0289 C
0290 C
0291 C
0292 C
0293 C
0294 C
0295 C
0296 C
0297 C
0298 C
0299 C
0300 C
0301 C
0302 C
0303 C
0304 C
0305 C
0306 C
0307 C
0308 C
0309 C
0310 C
0311 C
0312 C
0313 C
0314 C
0315 C
0316 C
0317 C
0318 C
0319 C
0320 C
0321 C
0322 C
0323 C
0324 C
0325 C
0326 C
0327 C
0328 C
0329 C
0330 C
0331 C
0332 C
0333 C
0334 C
0335 C
0336 C
0337 C
0338 C
0339 C
0340 C
0341 C
0342 C
0343 C
0344 C
0345 C
0346 C
0347 C
0348 C
0349 C
0350 C
0351 C
0352 C
0353 C
0354 C
0355 C
0356 C
0357 C
0358 C
0359 C
0360 C
0361 C
0362 C
0363 C
0364 C
0365 C
0366 C
0367 C
0368 C
0369 C
0370 C
0371 C
0372 C
0373 C
0374 C
0375 C
0376 C
0377 C
0378 C
0379 C
0380 C
0381 C
0382 C
0383 C
0384 C
0385 C
0386 C
0387 C
0388 C
0389 C
0390 C
0391 C
0392 C
0393 C
0394 C
0395 C
0396 C
0397 C
0398 C
0399 C
0400 C
0401 C
0402 C
0403 C
0404 C
0405 C
0406 C
0407 C
0408 C
0409 C
0410 C
0411 C
0412 C
0413 C
0414 C
0415 C
0416 C
0417 C
0418 C
0419 C
0420 C
0421 C
0422 C
0423 C
0424 C
0425 C
0426 C
0427 C
0428 C
0429 C
0430 C
0431 C
0432 C
0433 C
0434 C
0435 C
0436 C
0437 C
0438 C
0439 C
0440 C
0441 C
0442 C
0443 C
0444 C
0445 C
0446 C
0447 C
0448 C
0449 C
0450 C
0451 C
0452 C
0453 C
0454 C
0455 C
0456 C
0457 C
0458 C
0459 C
0460 C
0461 C
0462 C
0463 C
0464 C
0465 C
0466 C
0467 C
0468 C
0469 C
0470 C
0471 C
0472 C
0473 C
0474 C
0475 C
0476 C
0477 C
0478 C
0479 C
0480 C
0481 C
0482 C
0483 C
0484 C
0485 C
0486 C
0487 C
0488 C
0489 C
0490 C
0491 C
0492 C
0493 C
0494 C
0495 C
0496 C
0497 C
0498 C
0499 C
0500 C
0501 C
0502 C
0503 C
0504 C
0505 C
0506 C
0507 C
0508 C
0509 C
0510 C
0511 C
0512 C
0513 C
0514 C
0515 C
0516 C
0517 C
0518 C
0519 C
0520 C
0521 C
0522 C
0523 C
0524 C
0525 C
0526 C
0527 C
0528 C
0529 C
0530 C
0531 C
0532 C
0533 C
0534 C
0535 C
0536 C
0537 C
0538 C
0539 C
0540 C
0541 C
0542 C
0543 C
0544 C
0545 C
0546 C
0547 C
0548 C
0549 C
0550 C
0551 C
0552 C
0553 C
0554 C
0555 C
0556 C
0557 C
0558 C
0559 C
0560 C
0561 C
0562 C
0563 C
0564 C
0565 C
0566 C
0567 C
0568 C
0569 C
0570 C
0571 C
0572 C
0573 C
0574 C
0575 C
0576 C
0577 C
0578 C
0579 C
0580 C
0581 C
0582 C
0583 C
0584 C
0585 C
0586 C
0587 C
0588 C
0589 C
0590 C
0591 C
0592 C
0593 C
0594 C
0595 C
0596 C
0597 C
0598 C
0599 C
0600 C
0601 C
0602 C
0603 C
0604 C
0605 C
0606 C
0607 C
0608 C
0609 C
0610 C
0611 C
0612 C
0613 C
0614 C
0615 C
0616 C
0617 C
0618 C
0619 C
0620 C
0621 C
0622 C
0623 C
0624 C
0625 C
0626 C
0627 C
0628 C
0629 C
0630 C
0631 C
0632 C
0633 C
0634 C
0635 C
0636 C
0637 C
0638 C
0639 C
0640 C
0641 C
0642 C
0643 C
0644 C
0645 C
0646 C
0647 C
0648 C
0649 C
0650 C
0651 C
0652 C
0653 C
0654 C
0655 C
0656 C
0657 C
0658 C
0659 C
0660 C
0661 C
0662 C
0663 C
0664 C
0665 C
0666 C
0667 C
0668 C
0669 C
0670 C
0671 C
0672 C
0673 C
0674 C
0675 C
0676 C
0677 C
0678 C
0679 C
0680 C
0681 C
0682 C
0683 C
0684 C
0685 C
0686 C
0687 C
0688 C
0689 C
0690 C
0691 C
0692 C
0693 C
0694 C
0695 C
0696 C
0697 C
0698 C
0699 C
0700 C
0701 C
0702 C
0703 C
0704 C
0705 C
0706 C
0707 C
0708 C
0709 C
0710 C
0711 C
0712 C
0713 C
0714 C
0715 C
0716 C
0717 C
0718 C
0719 C
0720 C
0721 C
0722 C
0723 C
0724 C
0725 C
0726 C
0727 C
0728 C
0729 C
0730 C
0731 C
0732 C
0733 C
0734 C
0735 C
0736 C
0737 C
0738 C
0739 C
0740 C
0741 C
0742 C
0743 C
0744 C
0745 C
0746 C
0747 C
0748 C
0749 C
0750 C
0751 C
0752 C
0753 C
0754 C
0755 C
0756 C
0757 C
0758 C
0759 C
0760 C
0761 C
0762 C
0763 C
0764 C
0765 C
0766 C
0767 C
0768 C
0769 C
0770 C
0771 C
0772 C
0773 C
0774 C
0775 C
0776 C
0777 C
0778 C
0779 C
0780 C
0781 C
0782 C
0783 C
0784 C
0785 C
0786 C
0787 C
0788 C
0789 C
0790 C
0791 C
0792 C
0793 C
0794 C
0795 C
0796 C
0797 C
0798 C
0799 C
0800 C
0801 C
0802 C
0803 C
0804 C
0805 C
0806 C
0807 C
0808 C
0809 C
0810 C
0811 C
0812 C
0813 C
0814 C
0815 C
0816 C
0817 C
0818 C
0819 C
0820 C
0821 C
0822 C
0823 C
0824 C
0825 C
0826 C
0827 C
0828 C
0829 C
0830 C
0831 C
0832 C
0833 C
0834 C
0835 C
0836 C
0837 C
0838 C
0839 C
0840 C
0841 C
0842 C
0843 C
0844 C
0845 C
0846 C
0847 C
0848 C
0849 C
0850 C
0851 C
0852 C
0853 C
0854 C
0855 C
0856 C
0857 C
0858 C
0859 C
0860 C
0861 C
0862 C
0863 C
0864 C
0865 C
0866 C
0867 C
0868 C
0869 C
0870 C
0871 C
0872 C
0873 C
0874 C
0875 C
0876 C
0877 C
0878 C
0879 C
0880 C
0881 C
0882 C
0883 C
0884 C
0885 C
0886 C
0887 C
0888 C
0889 C
0890 C
0891 C
0892 C
0893 C
0894 C
0895 C
0896 C
0897 C
0898 C
0899 C
0900 C
0901 C
0902 C
0903 C
0904 C
0905 C
0906 C
0907 C
0908 C
0909 C
0910 C
0911 C
0912 C
0913 C
0914 C
0915 C
0916 C
0917 C
0918 C
0919 C
0920 C
0921 C
0922 C
0923 C
0924 C
0925 C
0926 C
0927 C
0928 C
0929 C
0930 C
0931 C
0932 C
0933 C
0934 C
0935 C
0936 C
0937 C
0938 C
0939 C
0940 C
0941 C
0942 C
0943 C
0944 C
0945 C
0946 C
0947 C
0948 C
0949 C
0950 C
0951 C
0952 C
0953 C
0954 C
0955 C
0956 C
0957 C
0958 C
0959 C
0960 C
0961 C
0962 C
0963 C
0964 C
0965 C
0966 C
0967 C
0968 C
0969 C
0970 C
0971 C
0972 C
0973 C
0974 C
0975 C
0976 C
0977 C
0978 C
0979 C
0980 C
0981 C
0982 C
0983 C
0984 C
0985 C
0986 C
0987 C
0988 C
0989 C
0990 C
0991 C
0992 C
0993 C
0994 C
0995 C
0996 C
0997 C
0998 C
0999 C
1000 C

```

```

***** CALCULATE SECOND CREEPING WAVE TERM *****
C1=C1
P2= 339397/(X*SINT)

```

```

0076 T4=P2*(C4-CON*C6)
0077 P2= 173966/(X*SINT)
0078 T5=P2*(C9-CON*C11)
0079 CON9=(. 848747,1,470073)
0080 C15=1.614208+X*CON9
0081 T6=C15*((C3+C13)-(C5+C14))
0082 SC2=C1*(T4+T5+T6)
0083 RETURN
0084 END

```

LOCAL VARIABLES: PSECT \$DATA, SIZE = 000730 ( 236 WORDS)											
NAME	TYPE	OFFSET	NAME	TYPE	OFFSET	NAME	TYPE	OFFSET	NAME	TYPE	OFFSET
B1	C#8	000060	B2	C#8	000070	B3	C#8	000100			
CON	C#8	000110	CON1	C#8	000120	CON2	C#8	000150			
CON3	C#8	000140	CON4	C#8	000150	CON5	C#8	000150			
CON6	C#8	000360	CON7	C#8	000370	CON8	C#8	000400			
CON9	C#8	000410	COST	R#4	000454	COST2	R#4	000440			
C1	C#8	000160	C11	C#8	000260	C12	C#8	000270			
C13	C#8	000300	C14	C#8	000310	C15	C#8	000320			
C2	C#8	000170	C3	C#8	000200	C4	C#8	000210			
C5	C#8	000220	C6	C#8	000230	C7	C#8	000240			
C9	C#8	000250	P1	R#4	000460	PT	R#4	000464			
PTH	R#4	000470	P1	R#4	000474	P2	R#4	000500			
P4	R#4	000504	SINT	R#4	000450	SINT2	R#4	000444			
T1	C#8	000000	T2	C#8	000010	T3	C#8	000020			
T4	C#8	000030	T5	C#8	000040	T6	C#8	000050			
X	R#4	000420	X*CON9	R#4	000434	X*CON9	R#4	000430			
XT	C#8	000330	XTM	C#8	000340	X3	R#4	000424			
COMMON BLOCK / , SIZE = 000050 ( 20 WORDS)											
NAME	TYPE	OFFSET	NAME	TYPE	OFFSET	NAME	TYPE	OFFSET	NAME	TYPE	OFFSET
S01	C#8	000000	S02	C#8	000010	SC1	C#8	000020			
SC2	C#8	000030	KA	R#4	000040	THETA	R#4	000044			

SUBROUTINES, FUNCTIONS, STATEMENT AND PROCESSOR-DEFINED FUNCTIONS

NAME	TYPE	NAME	TYPE	NAME	TYPE	NAME	TYPE
CEIP	C=8	COS	R=4	SIN	R=4	SGRT	R=4
						TAN	R=4

FORTRAN IJW02 1-1 SIN 21-OCT-79 38:26:12 PAGE 001

0001 C SUBROUTINE BSCAT4

0002 C THIS SUBPROGRAM WILL CALCULATE BISTATIC SCATTERING

0003 C COEFFICIENTS FOR THE PERFECTLY CONDUCTING SPHERE. IN THE

0004 C RANGE KA/20

0005 C COMMON S01, S02, SC1, SC2, KA, THETA

0006 C COMPLEX S01, S02, SC1, SC2, C1

0007 C REAL KA, THETA

0008 C P1=2\*KA/COS(THETA/2)

0009 C C1=CMPLX(0.0, -PI)

0010 C SC1=-5\*KA\*CEIP(C1)

0011 C SC2=SC1

0012 C RETURN

0013 C END

0014 C LOCAL VARIABLES. PSECT SDATA, SIZE = 000024 ( 10. WORDS)

NAME	TYPE	OFFSET	NAME	TYPE	OFFSET	NAME	TYPE	OFFSET
C1	C=8	000000	P1	R=4	000010			

0015 C COMMON BLOCK / , SIZE = 000050 ( 20. WORDS)

NAME	TYPE	OFFSET	NAME	TYPE	OFFSET	NAME	TYPE	OFFSET
S01	C=8	000000	S02	C=8	000010	SC1	C=8	000020
SC2	C=8	000030	KA	R=4	000040	THETA	R=4	000044

0016 C SUPROUTINES, FUNCTIONS, STATEMENT AND PROCESSOR-DEFINED FUNCTIONS.

NAME	TYPE	NAME	TYPE	NAME	TYPE	NAME	TYPE
CEIP	C=8	CMPLX	C=8	COS	R=4		

FORTRAN IJW02 1-1 THU 18-OCT-79 00:04:05 PAGE 001

0001 C PROGRAM SPSCAT

0002 C COMMON KA, F

0003 C COMPLEX F

0004 C REAL KA, MAG(S12), ANGLE(S12), KAS, KAE

0005 C BYTE ANS

0006 C DATA C/2 9\*7925E+10/

0007 C TYPE \*, ENTER SPHERE RADIUS (A) (CM.):

0008 C ACCEPT \*, A

0009 C TYPE \*, ENTER STARTING FREQ (GHZ):

0010 C ACCEPT \*, FSTART

0011 C TYPE \*, ENTER ENDING FREQ (GHZ):

0012 C ACCEPT \*, FEND

0013 C MAV=2\*3.1415926\*(1.0E+9/C)

0014 C KAS=FSTART\*MAV\*KA

0015 C KAE=FEND\*MAV\*KA

0016 C TYPE \*, ENTER NUMBER OF POINTS

0017 C ACCEPT \*, NUMPTS

0018 C TYPE \*, ENTER LOGICAL UNIT NUMBER FOR OUTPUT

0019 C ACCEPT \*, IUNIT

0020 C WRITE (IUNIT, 800) A, FSTART, KAS, FEND, KAE, NUMPTS

0021 C WRITE (IUNIT, 801)

0022 C STEPK=(KAE-KAS)/NUMPTS

0023 C FREQ=FSTART

0024 C STEPP=(FEND-FSTART)/NUMPTS

0025 C KA=KAS

0026 C DO 100 I=1, NUMPTS

0027 C N=1

0028 C CALL SCAT

0029 C AMP=CAES(F)

0030 C REA=REAL(F)

0031 C CPT=AIMAG(F)

0032 C ANG=ATAN2(CPT, REA)\*(180/3.1415926)

0033 C MAG(N)=AMP

0034 C ANGLE(N)=ANG

0035 C WRITE (IUNIT, \*) N, FREQ, KA, 10\*ALOG10(AMP), ANG

0036 C FREQ=FREQ+STEPP

0037 C KA=KA+STEPP

0038 C CONTINUE

0039 C TYPE \*, STORE DATA FOR DISPLAY (Y OR N) :

0040 C ACCEPT 700, ANS

0041 C IF (ANS.EQ.'N') GO TO 1000

0042 C TYPE \*, ENTER THE NAME FOR DATA FILE:

0043 C TYPE \*

0044 C CALL ASSON(20, -1, 'NEW', 'NC', 1,)

0045 C WRITE (20, \*) NUMPTS

0046 C WRITE (20, \*) FSTART

0047 C WRITE (20, \*) FEND

0048 C WRITE (20, \*) A

0049 C WRITE (20, \*) KA

0050 C DO 200 I=1, NUMPTS

0051 C N=I

0052 C WRITE (20, \*) MAG(N)

0053 C WRITE (20, \*) ANGLE(N)







```

0047 TYPE *
0048 CALL ASSGN(15,-1,'OLD','NC',1)
0049 READ(15,*)FREQ
0050 READ(15,*)ANGLE
0051 READ(15,*)IN
0052 READ(15,*)NSAMP
0053 DO 600 J=1,N
0054 READ(15,*)AMP(J)
0055 READ(15,*)PHA(J)
0056 CONTINUE
0057 TYPE *, 'PRINT DATA? (Y/N)'
0058 ACCEPT 999,STRING
0059 IF(STRING.EQ.'Y')GO TO 800
0060 GO TO 900
0061 TYPE *, 'ENTER THE LOGIC UNIT NUMBER FOR OUTPUT'
0062 ACCEPT *,LUNIT
0063 ACCEPT *,LUNIT
0064 WRITE(UNIT,*)'***** ANTENNA PATTERN *****'
0065 WRITE(UNIT,*)'FREQ= ',FREQ
0066 WRITE(UNIT,*)'ANGLE= ',ANGLE
0067 WRITE(UNIT,*)'NUMBER OF POINTS= ',N
0068 WRITE(UNIT,*)'SAMPLES/POINT= ',NSAMP
0069 WRITE(UNIT,*)
0070 WRITE(UNIT,990)
0071 WRITE(UNIT,990)
0072 WRITE(UNIT,*)'POINT * ANGLE(DEG) AMPLITUDE(DB) PHASE(DEG)'
0073 WRITE(UNIT,990)
0074 DO 850 J=1,N
0075 ANGLE=(-ANGLE/2.0)*(ANGLE/(N-1))*(J-1)
0076 WRITE(UNIT,991),J,ANGLE(J)*.05,PHA(J)*.25
0077 CONTINUE
0078 850 CALL CLOSE(15)
0079 990 FORMAT(60,'*')
0080 991 FORMAT(11,16,3X,F7.2,6X,F7.2,10X,F7.2)
0081 992 FORMAT(A1)
0082 STOP '***** END OF PROGRAM *****'
0083 END

```

LOCAL VARIABLES, PSECT 9DATA, SIZE = 004114 ( 1062 WORDS)

NAME	TYPE	OFFSET	NAME	TYPE	OFFSET	NAME	TYPE	OFFSET
A	R=4	004044	ANGLE	R=4	004030	ANG1	R=4	004064
DTMETHA	R=4	004040	FREQ	R=4	004020	I	I=2	004050
IA	I=2	004054	IFLAG	I=2	004016	INDEX	I=2	004052
IP	I=2	004056	LUNIT	I=2	004062	J	I=2	004060
N	I=2	004024	NSAMP	I=2	004026	STRING	L=1	004014
THETA	R=4	004034						

LOCAL AND COMMON ARRAYS:

NAME	TYPE	SECTION	OFFSET	-----SIZE-----	DIMENSIONS
AMP	I=2	9DATA	000000	( 512 )	(512)
PHA	I=2	9DATA	002000	( 512 )	(512)

SUBROUTINES, FUNCTIONS, STATEMENT AND PROCESSOR-DEFINED FUNCTIONS:

NAME	TYPE	NAME	TYPE	NAME	TYPE	NAME	TYPE

```

FORTRAN IVV02.1-1
0001 PROGRAM CYLIN
0002
0003 AUTHOR C. WERNER FEB 19, 1980
0004
0005 THIS PROGRAM WILL GENERATE THE DATA FOR A SHEET FREQUENCY
0006 HOLOGRAM FOR TWO CYLINDERS OF INFINITE LENGTH.
0007
0008 INTEGER SYSA(512), SYSP(512), TARA(512), TARP(512)
0009 BYTE NAME(20)
0010 REAL L,KSTEP,KSTART,K1
0011
0012 TYPE *, '***** CYLINDER SIMULATION *****'
0013 TYPE *, 'ENTER CYLINDER RADIUS IN CM.'
0014 ACCEPT *,A
0015 TYPE *, 'ENTER THE DISTANCE BETWEEN THE CYLINDERS IN CM.'
0016 ACCEPT *,L
0017 TYPE *, 'ENTER THE SHEEP START FREQUENCY IN GHZ.'
0018 ACCEPT *,FREQIN
0019 TYPE *, 'ENTER THE SHEEP ENDING FREQUENCY IN GHZ.'
0020 ACCEPT *,FSTOP
0021 TYPE *, 'ENTER THE NUMBER OF LINES IN THE HOLOGRAM.'
0022 ACCEPT *,NLINES
0023 TYPE *, 'ENTER THE ANGULAR SHEEP FOR THE HOLOGRAM IN DEGREES.'
0024 ACCEPT *,THETA
0025 TYPE *, 'ENTER THE NUMBER OF POINTS PER LINE'
0026 ACCEPT *,NPTS
0027
0028 TYPE *, 'ENTER FILENAME FOR DATA'
0029 TYPE *,
0030 CALL GTLIN(NAME,'?')
0031 OPEN(UNIT=15,NAME=NAME,TYPE='NEW',ACCESS='SEQUENTIAL',
0032 IFORM='UNFORMATTED')
0033 WRITE (15) FREQIN,FSTOP,NLINES,THETA,NPTS
0034 DTMETHA=(THETA/NLINES)*(3.1415926/180.0)
0035 KSTEP=((FSTOP-FREQIN)/NPTS)*(2*3.1415926/2.997E+11)
0036 DO 400 K=1,NLINES
0037 ANGLE=(K-1)*DTMETHA
0038 STHETA=SIN(ANGLE)
0039 DO 200 J=1,NPTS
0040 K1=KSTEP*(J-1)+KSTART
0041 SIG=COS(2*K1*A)*COS(K1*L*STHETA)
0042 IVAL=IFIX(200*SIG)
0043 WRITE(15)IVAL
0044 CONTINUE
0045 200 CONTINUE
0046 400 CLOSE(UNIT=15)
0047 STOP '***** END PROGRAM *****'
0048 END

```

LOCAL VARIABLES, PSECT 9DATA, SIZE = 010136 ( 2095 WORDS)

FORTRAN IV02 1-1 THU 21-FEB-80 05:03:15 PAGE 001  
PROGRAM CYPEP

AUTHOR C WERNER 21-AUG-80

THIS PROGRAM WILL FIND THE FREQUENCY SHEET HOLOGRAM OF  
A TARGET WITH VERTICAL SYMMETRY. THE FREQUENCY RANGE  
WILL BE BETWEEN FBEGIN AND FSTOP WITH NPTS FREQUENCY PTS.  
THE ANGLE RANGE WILL BE THETA WITH NLINES IN THAT ANGULAR  
SHEEP. THE REAL PART OF THE SCATTERED FIELD WILL BE SCALED  
FOR DISPLAY BY PROGRAM CDISP. THE TARGET WILL BE CORRECTED  
FOR SYSTEM RESPONSE AND RANGE BY USE OF A REFERENCE TARGET

INTEGER REFA(128), REFP(128), TARA(128), TARP(128)  
BYTE NAME(20)

TYPE \*, '\*\*\*\*\* 2D FREQUENCY SHEET HOLOGRAM \*\*\*\*\*'  
ACCEPT \*, FBEGIN  
TYPE \*, 'ENTER STARTING FREQUENCY GHZ.'  
ACCEPT \*, FSTOP  
TYPE \*, 'ENTER THE NUMBER OF FREQUENCY POINTS (<128).'  
ACCEPT \*, NPTS  
TYPE \*, 'ENTER ANGULAR SHEEP IN DEGREES.'  
ACCEPT \*, THETA  
TYPE \*, 'ENTER THE NUMBER OF LINES.'  
ACCEPT \*, NLINES  
TYPE \*, 'ENTER THE NUMBER OF SAMPLES/FREQUENCY POINT.'  
ACCEPT \*, NSAMP  
TYPE \*, 'ENTER THE NAME OF THE FILE FOR DATA STORAGE.'  
TYPE \*,  
CALL GTLINE(NAME, '?')  
OPEN(UNIT=15, NAME=NAME, TYPE='NEW', ACCESS='SEQUENTIAL',  
FORM='UNFORMATTED')  
WRITE(15) FBEGIN, FSTOP, NLINES, THETA, NPTS  
DTHETA=(THETA/NLINES)\*(3.141526/180.)

GET SYSTEM RESPONSE

TYPE \*, '\*\*\*\*\* PLACE REFERENCE TARGET IN THE FIELD \*\*\*\*\*'  
PAUSE '\*\*\* HIT RETURN TO CONTINUE \*\*\*'  
CALL SHDAT(REF, REFP, FBEGIN, FSTOP, NPTS, NSAMP)

GET SCALE FACTOR FOR DISPLAY

TYPE \*, '\*\*\*\*\* PLACE IMAGE TARGET IN THE FIELD \*\*\*\*\*'  
PAUSE '\*\*\* HIT RETURN TO CONTINUE \*\*\*'  
CALL SHDAT(TARA, TARP, FBEGIN, FSTOP, NPTS, NSAMP)  
RADC= 25\*3.141526/180.05  
APP=0  
DO 10 K=1, NPTS

TARA(K)=TARA(K)-REFP(K)

00033 TARP(K)=TARP(K)-REFP(K)  
00034 IF (TARP(K) GT 720) TARP(K)=TARP(K)-1440  
00036 IF (TARP(K) LT -720) TARP(K)=TARP(K)+1440  
00038 AMP=AMP\*(TARA(K)\*.05)  
00039 CONTINUE  
10  
00040 AMP=AMP/NPTS  
00041 TYPE \*, 'AVERAGE AMPLITUDE IN DB: ', AMP  
00042 TYPE \*, 'ENTER DYNAMIC RANGE FOR DISPLAY IN DB: '  
00043 ACCEPT \*, DENORM  
00044 AMAX=(DBNORM/2)  
00045 AMIN=-AMAX  
00046 AMAX=10.0\*(AMAX/10.0)  
00047 AMIN=10.0\*(AMIN/10.0)  
00049 TYPE \*, 'AMAX: ', AMAX  
00049 TYPE \*, 'AMIN: ', AMIN  
00050 SCALE=(200.0\*(2.0\*\*5))/(AMAX-AMIN)  
00050 TYPE \*, 'SCALE FACTOR FOR DATA: ', SCALE  
C  
C  
C COLLECT HOLOGRAM DATA  
DO 500 J=1, NLINES  
CALL SHDAT(TARA, TARP, FBEGIN, FSTOP, NPTS, NSAMP)  
DO 100 K=1, NPTS  
TARA(K)=TARA(K)-REFP(K)  
TARP(K)=TARP(K)-REFP(K)  
IF (TARP(K) GT 720) TARP(K)=TARP(K)-1440  
IF (TARP(K) LT -720) TARP(K)=TARP(K)+1440  
RNDNM=10.0\*(1.0\*(TARA(K)\*.05)-AMP)/(10.0\*(COS(TARP(K)\*RADC)  
12=12+RNDNM\*SCALE)  
TYPE \*, K, 12  
WRITE(15) 12  
100  
CONTINUE  
00064 CALL STEP2(DTHETA, 0)  
00065 CONTINUE  
500  
CLOSE(UNIT=15)  
STOP '\*\*\* END OF PROGRAM \*\*\*'  
END  
00069

LOCAL VARIABLES, PSECT \$DATA, SIZE = 002154 ( 566 WORDS)  
NAME TYPE OFFSET NAME TYPE OFFSET NAME TYPE OFFSET  
AMAX R+4 002110 AMIN R+4 002114 AMAX R+4 002100  
AMIN R+4 002104 AMP R+4 002066 DBNORM R+4 002074  
DTHETA R+4 002056 FBEGIN R+4 002034 FSTOP R+4 002040  
12 I+2 002132 J I+2 002124 K I+2 002072  
NLINES I+2 002052 NPTS I+2 002044 NSAMP I+2 002034  
RADC R+4 002062 RNDNM R+4 002126 SCALE R+4 002120  
THETA R+4 002046

LOCAL AND COMMON ARRAYS:

NAME	TYPE	SECTION	OFFSET	SIZE	DIMENSIONS
NAME	L+1	\$DATA	002000	000024 ( 10 )	( 20 )
REFP	I+2	\$DATA	000000	000400 ( 128 )	( 128 )
TARA	I+2	\$DATA	000400	000400 ( 128 )	( 128 )
TARP	I+2	\$DATA	001000	000400 ( 128 )	( 128 )

UNCLASSIFIED//FOR OFFICIAL USE ONLY  
FROM 0001 TO 0002

```

0001  FORTRAN IWO2 1-1      SAT 23-FEB-80 01:31:06      PAGE 001
0002  PROGRAM CDISP
0003  C
0004  C
0005  C
0006  C
0007  C
0008  C
0009  C
0010  C
0011  C
0012  C
0013  C
0014  C
0015  C
0016  C
0017  C
0018  C
0019  C
0020  C
0021  C
0022  C
0023  C
0024  C
0025  C
0026  C
0027  C
0028  C
0029  C
0030  C
0031  C
0032  C
0033  C
0034  C
0035  C
0036  C
0037  C
0038  C
0039  C
0040  C
0041  C
0042  C
0043  C
0044  C
0045  C
0046  C
0047  C
0048  C
0049  C
0050  C
0051  C
0052  C
0053  C
0054  C
0055  C
0056  C
0057  C
0058  C
0059  C
0060  C
0061  C
0062  C
0063  C
0064  C
0065  C
0066  C
0067  C
0068  C
0069  C
0070  C
0071  C
0072  C
0073  C
0074  C
0075  C
0076  C
0077  C
0078  C
0079  C
0080  C
0081  C
0082  C
0083  C
0084  C
0085  C
0086  C
0087  C
0088  C
0089  C
0090  C
0091  C
0092  C
0093  C
0094  C
0095  C
0096  C
0097  C
0098  C
0099  C
0100  C
0101  C
0102  C
0103  C
0104  C
0105  C
0106  C
0107  C
0108  C
0109  C
0110  C
0111  C
0112  C
0113  C
0114  C
0115  C
0116  C
0117  C
0118  C
0119  C
0120  C
0121  C
0122  C
0123  C
0124  C
0125  C
0126  C
0127  C
0128  C
0129  C
0130  C
0131  C
0132  C
0133  C
0134  C
0135  C
0136  C
0137  C
0138  C
0139  C
0140  C
0141  C
0142  C
0143  C
0144  C
0145  C
0146  C
0147  C
0148  C
0149  C
0150  C
0151  C
0152  C
0153  C
0154  C
0155  C
0156  C
0157  C
0158  C
0159  C
0160  C
0161  C
0162  C
0163  C
0164  C
0165  C
0166  C
0167  C
0168  C
0169  C
0170  C
0171  C
0172  C
0173  C
0174  C
0175  C
0176  C
0177  C
0178  C
0179  C
0180  C
0181  C
0182  C
0183  C
0184  C
0185  C
0186  C
0187  C
0188  C
0189  C
0190  C
0191  C
0192  C
0193  C
0194  C
0195  C
0196  C
0197  C
0198  C
0199  C
0200  C
0201  C
0202  C
0203  C
0204  C
0205  C
0206  C
0207  C
0208  C
0209  C
0210  C
0211  C
0212  C
0213  C
0214  C
0215  C
0216  C
0217  C
0218  C
0219  C
0220  C
0221  C
0222  C
0223  C
0224  C
0225  C
0226  C
0227  C
0228  C
0229  C
0230  C
0231  C
0232  C
0233  C
0234  C
0235  C
0236  C
0237  C
0238  C
0239  C
0240  C
0241  C
0242  C
0243  C
0244  C
0245  C
0246  C
0247  C
0248  C
0249  C
0250  C
0251  C
0252  C
0253  C
0254  C
0255  C
0256  C
0257  C
0258  C
0259  C
0260  C
0261  C
0262  C
0263  C
0264  C
0265  C
0266  C
0267  C
0268  C
0269  C
0270  C
0271  C
0272  C
0273  C
0274  C
0275  C
0276  C
0277  C
0278  C
0279  C
0280  C
0281  C
0282  C
0283  C
0284  C
0285  C
0286  C
0287  C
0288  C
0289  C
0290  C
0291  C
0292  C
0293  C
0294  C
0295  C
0296  C
0297  C
0298  C
0299  C
0300  C
0301  C
0302  C
0303  C
0304  C
0305  C
0306  C
0307  C
0308  C
0309  C
0310  C
0311  C
0312  C
0313  C
0314  C
0315  C
0316  C
0317  C
0318  C
0319  C
0320  C
0321  C
0322  C
0323  C
0324  C
0325  C
0326  C
0327  C
0328  C
0329  C
0330  C
0331  C
0332  C
0333  C
0334  C
0335  C
0336  C
0337  C
0338  C
0339  C
0340  C
0341  C
0342  C
0343  C
0344  C
0345  C
0346  C
0347  C
0348  C
0349  C
0350  C
0351  C
0352  C
0353  C
0354  C
0355  C
0356  C
0357  C
0358  C
0359  C
0360  C
0361  C
0362  C
0363  C
0364  C
0365  C
0366  C
0367  C
0368  C
0369  C
0370  C
0371  C
0372  C
0373  C
0374  C
0375  C
0376  C
0377  C
0378  C
0379  C
0380  C
0381  C
0382  C
0383  C
0384  C
0385  C
0386  C
0387  C
0388  C
0389  C
0390  C
0391  C
0392  C
0393  C
0394  C
0395  C
0396  C
0397  C
0398  C
0399  C
0400  C
0401  C
0402  C
0403  C
0404  C
0405  C
0406  C
0407  C
0408  C
0409  C
0410  C
0411  C
0412  C
0413  C
0414  C
0415  C
0416  C
0417  C
0418  C
0419  C
0420  C
0421  C
0422  C
0423  C
0424  C
0425  C
0426  C
0427  C
0428  C
0429  C
0430  C
0431  C
0432  C
0433  C
0434  C
0435  C
0436  C
0437  C
0438  C
0439  C
0440  C
0441  C
0442  C
0443  C
0444  C
0445  C
0446  C
0447  C
0448  C
0449  C
0450  C
0451  C
0452  C
0453  C
0454  C
0455  C
0456  C
0457  C
0458  C
0459  C
0460  C
0461  C
0462  C
0463  C
0464  C
0465  C
0466  C
0467  C
0468  C
0469  C
0470  C
0471  C
0472  C
0473  C
0474  C
0475  C
0476  C
0477  C
0478  C
0479  C
0480  C
0481  C
0482  C
0483  C
0484  C
0485  C
0486  C
0487  C
0488  C
0489  C
0490  C
0491  C
0492  C
0493  C
0494  C
0495  C
0496  C
0497  C
0498  C
0499  C
0500  C
0501  C
0502  C
0503  C
0504  C
0505  C
0506  C
0507  C
0508  C
0509  C
0510  C
0511  C
0512  C
0513  C
0514  C
0515  C
0516  C
0517  C
0518  C
0519  C
0520  C
0521  C
0522  C
0523  C
0524  C
0525  C
0526  C
0527  C
0528  C
0529  C
0530  C
0531  C
0532  C
0533  C
0534  C
0535  C
0536  C
0537  C
0538  C
0539  C
0540  C
0541  C
0542  C
0543  C
0544  C
0545  C
0546  C
0547  C
0548  C
0549  C
0550  C
0551  C
0552  C
0553  C
0554  C
0555  C
0556  C
0557  C
0558  C
0559  C
0560  C
0561  C
0562  C
0563  C
0564  C
0565  C
0566  C
0567  C
0568  C
0569  C
0570  C
0571  C
0572  C
0573  C
0574  C
0575  C
0576  C
0577  C
0578  C
0579  C
0580 
```



**DATE**  
**ILME**